

**Inorganic polyphosphates metabolism
studies in hypervirulent *Klebsiella
pneumoniae* strains**

Tesis

**Entregada A La
Universidad De Chile
En Cumplimiento Parcial De Los Requisitos
Para Optar Al Grado De**

**Doctor en Ciencias mención en
Microbiología**

Facultad De Ciencias

Por

**Diego Andrés Rojas Muñoz
Diciembre, 2023**

**Director de Tesis Dr: Francisco Chávez
Co-Director de Tesis Dr: Nicolás Guiliani**

FACULTAD DE CIENCIAS
UNIVERSIDAD DE CHILE
INFORME DE APROBACIÓN
TESIS DE DOCTORADO

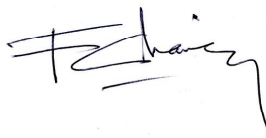
Se informa a la Escuela de Postgrado de la Facultad de Ciencias que la Tesis de Doctorado presentada por el candidato.

Diego Andrés Rojas Muñoz

Ha sido aprobada por la comisión de Evaluación de la tesis como requisito para optar al grado de Doctor en Ciencias mención Microbiología, en el examen de Defensa Privada de Tesis rendido el día

Director de Tesis:

Dr. Francisco Chávez



Co-Director de Tesis

Dr. Nicolás Guiliani



Comisión de Evaluación de la Tesis

Dr. Roberto Vidal

Dra. Monica Imaray

Dr. Sergio Alvarez

Para mi amada esposa Katherine

y mis hijos, Agustín y Laura

Resumen biográfico

Nací el 16 de febrero de 1993. Hijo del medio de mi amado padre José Bruno y mi amada madre Jenny. Mi padre fue quien primeramente me inspiró en el gusto por la ciencia. Me hacía imaginarme como sería vivir dentro de un auto de juguete. Desde ahí, el mundo de lo que no podemos ver con nuestros ojos me llamó la atención. Fui un alumno destacado en Biología en el colegio y decidí estudiar Pedagogía en Biología, pues me daba mucha satisfacción enseñar a otros aquello que comencé a conocer. En mis estudios de pedagogía, decidí perfeccionarme más en el área de la microbiología y luego de tres años postulé al programa de doctorado. A finales del 2021 me integré a trabajar en el laboratorio de comunicación bacteriana con el profesor Nicolás Guiliani y posteriormente en el Laboratorio Sysmicro con el profesor Francisco Chávez. Agradezco a Dios por guiarme hasta este momento de mi formación, y ser parte de ambos laboratorios junto a cada persona que he podido conocer.

Agradecimientos

Quiero partir dando gracias a Dios quien me ha guiado hasta esta parte de mi vida, en la que no solo he podido aprender más sobre microbiología, sino que también me ha permitido pasar tiempo junto a mi familia. Mis hijos me han acompañado en todo este proceso y junto a mi esposa Katherine, han sido un apoyo fundamental. Gracias por su amor y paciencia. A mi madre, por su constante apoyo tanto emocional como material. A mi padre, por su dedicación a enseñarme desde muy pequeño y trasmitirme el gusto por la ciencia sin quererlo. A mis hermanos por su apoyo y a mis Hermanos en la Fe, quienes han sido una fuente de consejo y sabiduría para enfrentar la ansiedad, el temor, la desesperanza. Al Dr. Camilo Toncio, quien me guio en mi formación de pregrado y me motivo a estudiar el doctorado y especialmente a la Dra. Mabel Catalán, quien impulso mi formación y preparación en el laboratorio tanto en mi tesis de pregrado, así como en lo laboral. Gracias por tu amistad, consejos, retos y sabiduría (es mejor tener amigos que plata). Agradezco al Dr. Nicolas Guliani por aceptarme en su laboratorio quien, además, por diferentes circunstancias me guio a trabajar con el Dr. Francisco Chávez, quien ha sido una persona muy especial para mí. Siempre recuerdo su consejo, “la familia es primero”. A mis compañeros de laboratorio, Mauricio, que fue una pieza fundamental en el inicio de mi tesis, a Diego San Martin por su dedicación en el trabajo de laboratorio. A Nicole Molina por su incansable trabajo para que todos nosotros tengamos lo necesario. A Jorge Vielma, Antonia Ramos, la Ian, compañeros del estrecho lab.

Índice

<i>LIST OF FIGURES</i>	VIII
<i>LIST OF TABLES</i>	X
<i>LIST OF ABBREVIATIONS</i>	XI
<i>Resumen</i>	XIII
<i>Abstract</i>	XV
<i>1. Introduction</i>	1
1.1 <i>Klebsiella pneumoniae</i>: a serious threat to human health	1
1.2 Hypervirulent <i>K. pneumoniae</i>	4
1.2.1 Risk Factors	5
1.2.2 Pathogenesis.....	6
1.2.3 Capsule	8
1.2.4 Lipopolysaccharides	12
1.2.5 Fimbriae (Types I and III).....	13
1.2.6 Siderophores	15
1.2.7 Colibactin.....	18
1.3 <i>Dictyostelium discoideum</i> as a Host-Pathogen Interaction Model	19
1.4 Paradigm Shift – The Post-Antibiotic Era	23
1.5 Inorganic Polyphosphate and Virulence	24
1.6 <i>Klebsiella pneumoniae</i> and polyphosphate	29
1.7 Problem Statement	29
<i>Hypothesis</i>	31
<i>General Objective</i>	31
Specific Objectives.....	31
<i>2. Materials and methods</i>	32
2.1 Strains, plasmids, and growth conditions	32
2.2 Culture Conditions of <i>D. discoideum</i>	34
2.3 Genetic manipulation of <i>K. pneumoniae</i> SGH10	35
2.4 Proteomic profile	37
2.4.1 Protein Extraction.....	37
2.4.2 Mass spectrometry preparation.....	37
2.4.3 Liquid Chromatography – Tandem Mass Spectrometry	38

2.4.4 Protein Identification.....	38
2.4.5 Protein Quantification LFQ (Free Label Quantification)	39
2.5 Calculation of the z-score.....	41
2.6 Growth curve.....	41
2.7 Quantification of polyP under nutrient deprivation.....	42
2.8 Capsule production quantification	42
2.9 Low-speed centrifugation of bacteria	43
2.10 Quantification of Biofilm Biomass and EPS using Confocal Microscopy.....	43
2.11 Scanning electron microscopy.....	44
2.12 Predation resistance assay	45
2.13 Social Development Assays	46
2.14 Phagocytosis assays.....	47
3. Results	48
3.1 Generation of mutants in the polyphosphate (polyP) metabolism in the hypervirulent strain <i>Klebsiella pneumoniae</i> SGH10.....	48
3.2 Mutants lacking genes involved in PolyP synthesis and degradation preserve the viability.....	53
3.3 PPK1 is essential for polyP accumulation in the SGH10 strain.....	53
3.4 Altered mucus and amount of capsule in mutants in polyP metabolism	59
3.5 PPK1 plays a crucial role in biofilm formation.	64
3.6 PPK1 is essential for HV <i>K. pneumoniae</i> virulence in <i>D. discoideum</i>	70
3.7 Global Proteomic Profiling Reveals Key Proteins Involved in Virulence in <i>Klebsiella pneumoniae</i> SGH10	80
4. Discussion.....	91
5. Conclusions	102
6. Bibliographic references	103
7. Annexes	116

LIST OF FIGURES

Figure 1:	Characterized virulence factors in classical and hypervirulent strains of <i>K. pneumoniae</i>	7
Figure 2:	Capsular polysaccharide synthesis pathway dependent on the Wzy pathway	11
Figure 3:	The social development of <i>Dictyostelium discoideum</i>	22
Figure 4:	Structure and general metabolism of polyP in bacteria	28
Figure 5:	Mutant development workflow	36
Figure 6:	Diagram of the workflow used in protein identification	40
Figure 7:	Workflow in mutant development	52
Figure 8:	Growth curve in rich medium	55
Figure 9:	Growth curve in minimal medium	56
Figure 10:	Nutritional downshift	57
Figure 11:	PolyP accumulation in nutrient deprivation	58
Figure 12:	Mucus production in polyP metabolism mutants	61
Figure 13:	Capsule production	62
Figure 14:	Scanning electron microscopy	63
Figure 15:	Biofilm Formation	66
Figure 16:	EbbaBiolight 680	67
Figure 17:	Confocal microscopy for biofilm observation	68
Figure 18:	Macrocolony biofilm	69
Figure 19:	Predation resistance assay.	74
Figure 20:	Social development assay	75
Figure 21:	Number of fruiting bodies on the third day	76
Figure 22:	Development social progress	77
Figure 23:	Timelapse of phagocytosis	78
Figure 24:	Fluorescence quantification	79
Figure 25:	Principal Component Analysis	83

Figure 26:	Volcano plot of the differentially expressed proteins from the comparison of each of the comparisons made	85
Figure 27:	Heatmap of virulence factors	86
Figure 28:	Network of curated interactions between proteins involved in the virulence of <i>Klebsiella pneumoniae</i>	87
Figure 29:	The chordplot graph illustrates protein-protein interactions categorized based on the VFDB database	88
Figure 30:	Colistin resistance assessment of SGH10 strains, $\Delta ppk1$, Δppx , $\Delta ppk1$ - Δppx	89
Figure 31:	The Z-score plot of the global relative abundance of each of the proteins associated with virulence factors	90

LIST OF TABLES

Table 1:	Strains and plasmids used in this study	32
Table 2:	List of primers used for generating mutants	34
Table 3:	Number of quantifiable proteins and DEPs (Differential Expression Proteins) obtained for each of the global proteomic profiling comparisons	85

LIST OF ABBREVIATIONS

ATP	Adenosine Triphosphate
cAMP	cyclic adenosine monophosphate
CG23	Clonal group 23
cKp	Classical <i>K. pneumoniae</i>
CPS	Capsule
DAPI	4',6-diamidino-2-phenylindole
DC	Dendritic cells
DEP	differential expression of proteins
DNA	Desoxyribonucleic Acid
DTT	Dithiothreitol
EPS	Extracellular Polymeric Substance
ESBLs	Extended-Spectrum Beta-Lactamases
fAR1	formyl peptide receptor 1
FDR	False Discovery Rate
GDP	Guanosine diphosphate
GFP	Green Fluorescent Protein
GTP	Guanosine Triphosphate
HEPES	4-(2-hydroxyethyl)-1-piperazineethanesulfonic acid
hvKp	hypervirulent <i>Klebsiella pneumoniae</i>
K ₂ HPO ₄	Dipotassium Phosphate
Kdo	Keto-Deoxyoctulosonate
KOH	Potassium Hydroxide
LB	Luria-Bertani
LC-	
MS/MS	Liquid Chromatography-Tandem Mass Spectrometry
LPS	Lipopolysaccharide
MDR	multidrug-resistant strains
MgSO ₄	Magnesium Sulfate
MOI	Multiplicity of Infection
MOPS	3-(N-morpholino)propane sulfonic acid
NaCl	Sodium Chloride
OD	Optical Density
PASEF	Parallel Accumulation-Serial Fragmentation
PBS	Phosphate-Buffered Saline
polyP	Inorganic polyphosphates
PPK	polyphosphate kinases

PPX	exopolyphosphatase
PTM	post-translational modifications
RNA	Ribonucleic Acid
SEM	Scanning Electron Microscopy
T1F	type 1 fimbriae
T3F	type 3 fimbriae
timsTOF	trapped ion mobility spectrometry-time of flight
TLR	Toll-like Receptor
UHPLC	Ultra-High-Performance Liquid Chromatography
Und-PP	Undecaprenyl Pyrophosphate

Resumen

La aparición de cepas hipervirulentas de *Klebsiella pneumoniae* (hvKp) representa una amenaza significativa para la salud pública debido a sus altas tasas de mortalidad y propensión a causar infecciones graves adquiridas en la comunidad en individuos por lo demás sanos. La capacidad de hvKp para formar biopelículas y producir una cápsula protectora contribuye a su mayor virulencia y plantea desafíos significativos para el tratamiento efectivo con antibióticos. Por lo tanto, comprender los mecanismos moleculares subyacentes a la virulencia y formación de biopelículas de hvKp es crucial para desarrollar nuevas estrategias terapéuticas. La polifosfato quinasa 1 (PPK1) es una enzima responsable de la síntesis de polifosfato inorgánico y desempeña un papel vital en la regulación de varios procesos fisiológicos en bacterias. En este estudio, investigamos el impacto de la mutación de PPK1 en la formación de biopelículas y cápsulas, así como en los rasgos de virulencia en hvKp utilizando la ameba *Dictyostelium discoideum* como modelo hospedador. Encontramos que el mutante de PPK1 presentaba una formación de biopelículas y cápsulas deteriorada y mostraba una virulencia atenuada en *D. discoideum* en comparación con la cepa de tipo salvaje. Para obtener una mejor comprensión del mecanismo molecular subyacente, realizamos un análisis proteómico del mutante de PPK1 y la cepa de tipo salvaje. Los resultados revelaron que el mutante de PPK1 tenía una expresión diferencial de proteínas (DEP) involucradas en la síntesis de cápsulas (Wzi - Ugd), formación de biopelículas (MrkC-D-H), síntesis del precursor de la colibactina genotoxina (ClbB), así como proteínas asociadas con la síntesis y modificación del lípido A (LpxC - PagP). Estos hallazgos proteómicos corroboran las observaciones fenotípicas

e indican que la mutación de PPK1 está asociada con una formación deteriorada de biopelículas y cápsulas, así como una virulencia atenuada en *K. pneumoniae* hipervirulenta. En general, nuestro estudio destaca la importancia de la síntesis de polifosfato en la regulación de la síntesis de capsula, formación de biopelículas y virulencia en *K. pneumoniae*, y proporciona información sobre posibles objetivos terapéuticos para el tratamiento de infecciones por *K. pneumoniae*.

Abstract

The emergence of hypervirulent *Klebsiella pneumoniae* (hvKp) strains poses a significant threat to public health due to their high mortality rates and propensity to cause severe community-acquired infections in otherwise healthy individuals. The ability of hvKp to form biofilms and produce a protective capsule contributes to its enhanced virulence and poses significant challenges for effective antibiotic treatment. Therefore, understanding the molecular mechanisms underlying hvKp virulence and biofilm formation is crucial for developing new therapeutic strategies. Polyphosphate Kinase 1 (PPK1) is an enzyme responsible for inorganic polyphosphate synthesis and plays a vital role in regulating various physiological processes in bacteria. In this study, we investigated the impact of PPK1 mutation on the biofilm and capsule formation, as well as virulence traits, in hvKp using *Dictyostelium discoideum* amoeba as a model host. We found that the PPK1 mutant was impaired in biofilm and capsule formation and showed attenuated virulence in *D. discoideum* compared to the wild-type strain. We performed a proteomic analysis of the PPK1 mutant and wild-type strain to gain further insight into the underlying molecular mechanism. The results revealed that the PPK1 mutant had a differential expression of proteins (DEP) involved in capsule synthesis (Wzi - Ugd), biofilm formation (MrkC-D-H), synthesis of the colibactin genotoxin precursor (ClibB), as well as proteins associated with the synthesis and modification of lipid A (LpxC - PagP). These proteomic findings corroborate the phenotypic observations and indicate that the PPK1 mutation is associated with impaired biofilm and capsule formation and attenuated virulence in hypervirulent *K. pneumoniae*. Overall, our study highlights the

importance of polyphosphate synthesis in regulating capsule synthesis, biofilm formation, and virulence in *K. pneumoniae*, providing insights into potential therapeutic targets for the treatment of *K. pneumoniae* infections.

1. Introduction

1.1 *Klebsiella pneumoniae*: a serious threat to human health

Klebsiella pneumoniae was first described in 1882 by Karl Friedländer, who analyzed lung samples from patients who died of pneumonia (Friedlaender, 1882). This Gram-negative bacillus belongs to the Enterobacteriaceae family. It is non-motile, typically encapsulated, forming mucoid colonies on agar plates. It is considered a commensal microorganism, colonizing the gastrointestinal tract and respiratory mucosa as a part of the commensal microbiota (Joseph et al., 2021). However, it can also cause opportunistic intrahospital infections and infections in immunocompetent community members (Chen et al., 2023).

The average genome size is around 5 to 6 Mbp, with a core genome of approximately 1,700 genes and a pangenome exceeding 100,000 genes (Wyres et al., 2020). It is widely distributed in the environment, including surface water, drinking water, wastewater, industrial effluents, soil, plants, and wild and domesticated animals. Nevertheless, it is especially prevalent on the mucosal surfaces of mammals, such as the nasopharyngeal epithelium, mouth, and gastrointestinal tract (Paczosa and Meccas, 2016).

Given its ubiquity, environmental isolates are reported to be similar to those found in clinical settings. They can express various virulence factors related to serum resistance, clinically important capsular polysaccharides, type I and III fimbriae, and siderophores.

This suggests that environmentally sourced *K. pneumoniae* may affect public health (Podschun et al., 2001).

Classical *K. pneumoniae* strains (cKp) are often acquired in hospital environments as opportunistic pathogens, causing a range of complications that arise as secondary to the underlying disease in immunocompromised patients or those with existing barrier breakdown (e.g., intravascular devices, endotracheal tubes, or surgical wounds) (Martin and Bachman, 2018). Due to the widespread use of antimicrobials in recent decades, there has been a concerning increase in the acquisition of resistance to a broad range of antibiotics, leading to the emergence of multidrug-resistant strains (MDR-KP) (Magiorakos et al., 2012). These variants originate from classical strains and result from acquiring two main types of resistance. The first involves the expression of Extended-Spectrum Beta-Lactamases (ESBLs), providing resistance to third-generation cephalosporins and monobactams. ESBLs are serine β -lactamases belonging to Ambler's class A, including sulfhydryl variable β -lactamase (SHV), Temoniera β -lactamase (TEM), and cefotaxime-M β -lactamase (CTX-M) (Karaikos and Giamarellou, 2020). They are frequently associated with epidemic outbreaks in hospital settings. In the late 1970s, the first beta-lactamases for ampicillin (SHV-1 and TEM-1) were described. In the early 1980s, SHV-2, capable of hydrolyzing third-generation cephalosporins, was reported (Knothe et al., 1983), increasing its affinity for cefotaxime 350-fold compared to SHV-1 (Kliebe et al., 1985). In the late 1980s, CTX-M was described, which emerged independently of SHV and TEM, resulting from environmental transfer from *Kluyvera spp.*, conferring high-level resistance to cefuroxime, cefotaxime and cefepime (Calbo and

Garau, 2015). The second type of resistance is due to the expression of carbapenemases, endowing *K. pneumoniae* with resistance to all available beta-lactam antibiotics, including carbapenems, a group of antibiotics used to treat multidrug-resistant bacteria that produce ESBLs. The first carbapenemase was reported in North Carolina, USA, in 1996 (Archibald et al., 1997), and it was identified as KPC (Yigit et al., 2001). Currently, additional carbapenemases such as MBL, NDM-1, IMP, and VIM have been described in other species of the Enterobacteriaceae family. Strains carrying KPC-2 and three have successfully spread and caused severe infectious diseases (such as pneumonia, bacteremia, or meningitis) in critical care units in hospitals worldwide, often with mortality rates exceeding 40% (Tzouveleki et al., 2012; De Oliveira et al., 2020).

In Chile, the epidemiological report from the Ministry of Health (MINSAL) in 2018 placed *K. pneumoniae* as one of the leading pathogens causing urinary tract infections, mainly associated with permanent urinary catheters, surpassing *Escherichia coli* UPEC. It also ranked high as the causative agent of persistent infections in surgical wounds, bacteremias (resulting from parenteral nutrition, central venous catheters, and hemodialysis), pneumonia associated with invasive mechanical ventilation, and central nervous system infections. Furthermore, 12 epidemic outbreaks of carbapenemase-producing multidrug-resistant *K. pneumoniae* (KPC and NMD) and ESBL were reported in different public hospitals (Informe IAAS, 2018).

Considering the recent COVID-19 pandemic, numerous studies reported co-infections by opportunistic pathogens like *K. pneumoniae* in intubated patients in the ICU,

associated with severe acute respiratory syndrome due to COVID-19 (Forcelledo et al., 2020; Montrucchio et al., 2020; Tiri et al., 2020; Arcari et al., 2021; Hosoda et al., 2021). This was facilitated by the high-intensity care required, the prone position that involves 4-5 healthcare workers, prolonged patient contact, and other factors (Forcelledo et al., 2020; Tiri et al., 2020).

For all these reasons, *K. pneumoniae* is one of the six pathogens of the ESKAPE group, recognized in 2008 by the Infectious Diseases Society of America (IDSA) (Rice, 2008), and is part of the critically important group for the study of new antimicrobial strategies as announced by the World Health Organization (Tacconelli et al., 2018). It has developed resistance mechanisms against oxazolidinones, lipopeptides, macrolides, fluoroquinolones, tetracyclines, beta-lactam combinations, and antibiotics that are the last line of defense, including carbapenems, glycopeptides, and polymyxins (De Oliveira et al., 2020).

1.2 Hypervirulent *K. pneumoniae*

In 1985, Taiwan reported seven patients who presented with pyogenic liver abscesses associated with septic endophthalmitis, followed by blindness. The causative agent was a new variant of *K. pneumoniae*, belonging to the clonal group CG23, which had not been described until then (Liu et al., 1986). This new strain is considered hypervirulent (hv) due to its ability to infect healthy individuals of any age and the tendency of infected patients to present with multiple sites of infection and develop subsequent metastatic

spread, an unusual occurrence for other members of the Enterobacteriaceae family (Russo and Marr, 2019). The hallmark clinical syndrome is a hepatic abscess without biliary tract disease. However, the hypervirulent *Klebsiella pneumoniae* (hvKp) strain, can infect nearly every part of the body, including bacteremia, meningitis, necrotizing fasciitis, and abscesses in various organs, with mortality rates as high as 50% (Gonzalez-Ferrer et al., 2021). Generally, hvKp strains are not associated with resistance determinants (except for resistance to ampicillin due to blaSHV), and their survival strategy is determined mainly by their ability to evade the immune response through hyperexpression and elongation of the length of the capsular polysaccharide, which conceals molecular recognition patterns from immune cells, such as fimbriae and lipopolysaccharide (LPS) (Fung et al., 2011; Xu et al., 2021)

1.2.1 Risk Factors

Most reports have focused on countries in Asia with a "preference" for this ethnic group, possibly due to the higher circulation of these strains in these geographical areas, as well as a possible genetic susceptibility to hvKp infections (Russo and Marr, 2019). More studies are needed to confirm the latter conclusion. It was also observed that patients with diabetes mellitus had more severe metastatic infections, such as endophthalmitis and necrotizing fasciitis (Huang et al., 2002; Phd et al., 2012). Possible explanations for these observations include that glucose promotes capsule expression, which could facilitate bacteria escaping immune recognition. In addition, diabetes-related complications affecting the circulatory system due to vascular integrity loss could promote the metastasis

of hvKp strains and defects in neutrophil recruitment in the innate immune response (Berbudi et al., 2020). This is particularly relevant in Western countries, including Chile, where the percentage of diabetic adults reaches 11% of the population (Sapunar Z., 2016). Other associated risk factors have been reported, such as gender, with a slight likelihood that men are more susceptible to hvKp infections (Russo and Marr, 2019). However, hvKp strains can infect immunocompetent individuals regardless of gender, age, or previous health conditions.

1.2.2 Pathogenesis

For some pathogens, the best strategy for survival and propagation is to mount a strong offensive, including toxin secretion systems, as seen in the case of *Salmonella enterica* (Wagner and Hensel, 2011; Troxell, 2018). For *K. pneumoniae*, its strategy for success is based on defense, presenting mechanisms to evade the immune response, compete with the commensal intestinal microbiota for a niche, obtain nutrients and iron, and promote tolerance to antimicrobial chemotherapy, thus contributing to pathogenesis (Paczosa and Meccas, 2016). For this purpose, hvKp strains have a series of virulence factors, many of which are shared with cKp strains, enabling a successful infection in immunocompetent patients. The most studied factors include the capsule, siderophores, fimbriae, LPS, and colibactin (Fig. 1).

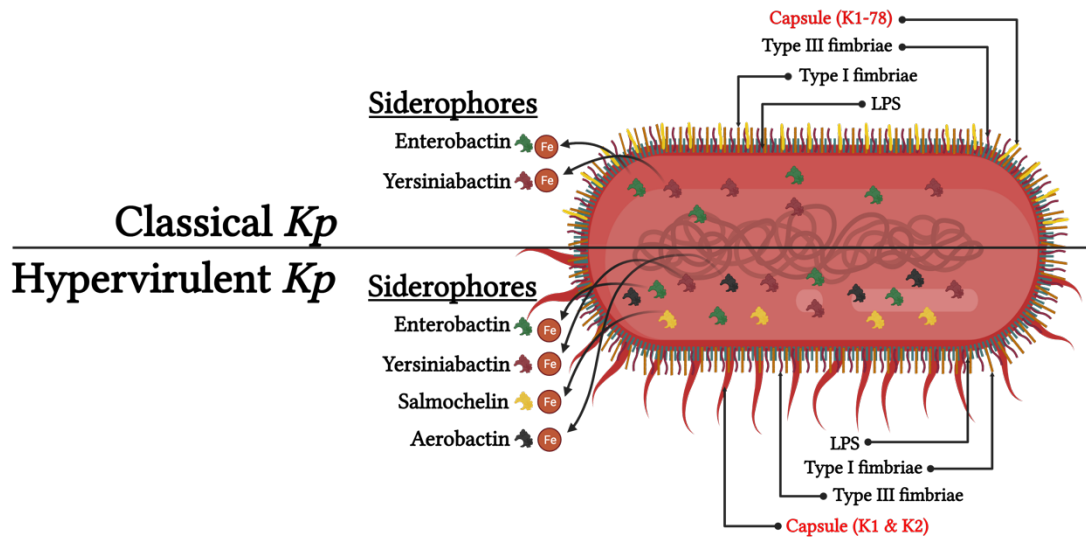


Figure 1. Well-characterized virulence factors in classical and hypervirulent *K. pneumoniae* (hvKp) strains include the capsule, LPS, fimbriae (type 1 and type 3), and siderophores. Capsules vary in serotypes (K1 to K78) and are associated with increased pathogenicity. Both strain types produce LPS with different O-antigen serotypes. They also have adhesive structures (type 1 and type 3 fimbriae) and secrete siderophores for iron scavenging. Most strains make enterobactin, while yersiniabactin is produced by half of the classical strains and most hypervirulent strains. Salmochelin and aerobactin are common in hypervirulent strains, with aerobactin being highly expressed. modified from (Paczosa and Mecsas, 2016).

1.2.3 Capsule

Most *K. pneumoniae* strains express a polysaccharide capsule that shields the bacterium from desiccation, phage predation, protists, and immune system action. Nevertheless, hvKp strains exhibit a significant increase in polysaccharide capsule synthesis, both in quantity and length, promoting the characteristic hypermucoviscous (HMV) phenotype found in most hvKp strains. Over 130 types of K capsules have been identified (Wyres et al., 2016; Walker et al., 2020), with K1 and K2 types generally being more virulent and predominantly present in hvKp strains (Martin and Bachman, 2018). The K1 type consists of a trisaccharide of fucose, glucose, and glucuronic acid (Patro and Rathinavelan, 2019). The acetylation of C2-OH (or C3-OH) in fucose in the K1 CPS may assist *K. pneumoniae* in evading phagocytosis (Wu et al., 2008; Hsu et al., 2011). The hyperexpression of the capsule shields *K. pneumoniae* from opsonization and phagocytosis by innate immune cells (macrophages, neutrophils, dendritic cells (DC) by obstructing binding and internalization compared to non-hypervirulent strains (Wang et al., 2017b; Zhu et al., 2021).

The capsule produced by *K. pneumoniae* is synthesized via a Wzy-dependent pathway, which shares similarities with Group 1 capsule production in *E. coli* (Figure 2) (Palacios et al., 2018). The genes responsible for polysaccharide synthesis and export are encoded in the core genome, commencing with the biosynthesis of nucleotide sugar precursors specific to each strain's K type and the assembly of the repeating unit on the cytoplasmic face. This process involves particular glycosyltransferases encoded by genes like *wcaJ*. Subsequently, the specific repeating unit is recognized by the flippase Wzx,

with the initial sugar linked to undecaprenol-pyrophosphate (Und-PP), followed by transport to the periplasmic side. The co-polymerase Wzy facilitates the polymerization of the repeating unit. Finally, the proteins Wza (an outer-membrane translocon), Wzc (a tyrosine autokinase), and Wzb (a phosphatase) work in unison to transport the capsular polysaccharide to the bacterial surface and anchor it to the outer-membrane protein Wzi (Bertani and Ruiz, 2018). Sugar composition analysis indicates that K1 and K2 serotypes possess WcaJ and use glucose-Und-PP to initialize sugar (Patro and Rathinavelan, 2019). The diversity in capsule types arises from glycosyltransferase activities.

Specific proteins encoded in the virulence plasmid act upon this synthesis pathway to significantly increase CPS synthesis and regulate the length of the capsular polysaccharide. This is achieved through the *rpmADC* operon, whose protein products regulate the capsule synthesis pathway. RmpA has been reported to autoregulate the operon, RmpC promotes capsule synthesis, and recently, it was discovered that RmpD interacts with Wzc in the inner membrane, thereby enabling an increase in the length of the capsular polysaccharide (Ovchinnikova et al., 2023). This regulation underlies the HMV phenotype of most hvKp strains, characterized by forming a 5 mm filament when colonies are touched with a loop (Walker et al., 2020).

Capsule-deficient strains are significantly less virulent and more susceptible to immune system action (Tan et al., 2020). It has been reported that cKp strains lacking hyperexpression of capsular polysaccharides are readily internalized by macrophages, increasing intracellular load (Mina et al., 2024). This also promotes the M1 macrophage polarization marker CD86 and the expression of proinflammatory cytokines. In contrast,

hvKp strain 17ZR101 (K2) displayed a lower rate of internalization and intracellular load. This had been reported before, where the capsular polysaccharide can impair DC maturation and reduce DC-mediated production of pro-Th1 cytokines, such as IL-12 and TNF- α . This, in turn, results in the destructive function of immature DCs during *K. pneumoniae* antigen presentation, leading to reduced DC-mediated natural killer cell migration.

Consequently, this allows the bacteria to avoid host defenses and multiply more efficiently *in vivo*. However, clinical isolates without capsules, resulting from spontaneous mutations in genes such as *wzi*, *wza*, and *wzc*, have been shown to promote robust biofilm formation and invasion of bladder epithelial cells. This suggests capsule loss enhances persistence more than virulence and dissemination, providing a fitness advantage under specific infections such as urinary tract infections. It creates a reservoir for acute conditions that is also more tolerant to antimicrobials (Ernst et al., 2020). Interestingly, the same study described a single mutation in the *wzc* gene that conferred hypercapsulation to a KPC strain, which did not possess overactivating factors of CPS like the *rpmADC* operon, leading to increased virulence.

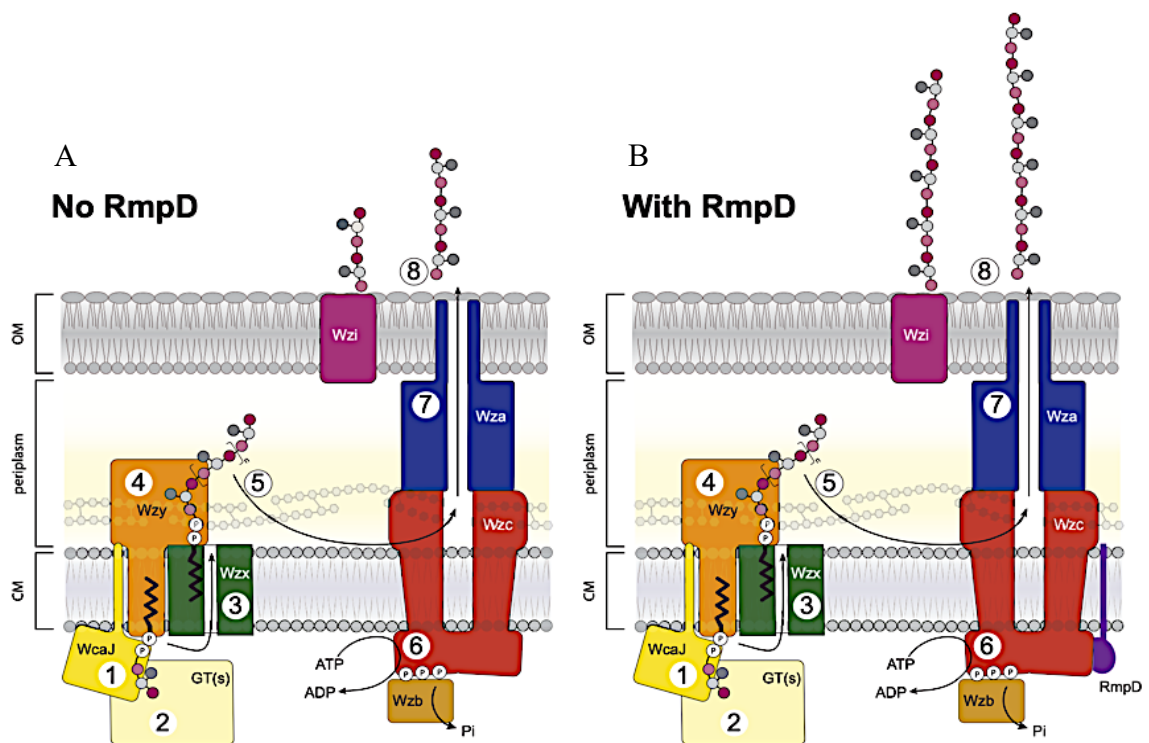


Figure 2. Capsular polysaccharide synthesis pathway dependent on the Wzy pathway. (A) CPS repeat unit synthesis begins with WcaJ phospho-glycosyltransferase on an undecaprenol phosphate acceptor, followed by the involvement of serotype-specific glycosyltransferases and export through Wzx, a member of the MOPS transporter family. A Wzy homolog performs polymerization, and translocation involves the complex of Wzc and Wza proteins. Wzc has dual roles in polymerization and translocation, regulated by reversible phosphorylation. Likely, direct interaction between Wzy and Wzc is necessary. (B) In the presence of RmpD, CPS chains likely elongate through interaction with Wzc, although this interaction's exact location and nature remain unknown (Ovchinnikova et al., 2023). with Wzc, although the exact location and nature of this interaction remain unknown. Modified figure from Ovchinnikova et al., 2023.

1.2.4 Lipopolysaccharides

The outer membrane of Gram-negative bacteria is highly asymmetric, composed of phospholipids facing the periplasm and lipopolysaccharide (LPS) facing the external side. Considered an endotoxin, LPS is a glycolipid consisting of three structural domains: Lipid A, the oligosaccharide core, and the O antigen, encoded by the *wb*, *waa*, and *lpx* genes, respectively (Martin and Bachman, 2018). Lipid A forms the hydrophobic portion of the outer membrane, and the core typically contains residues of 3-deoxy-D-manno-oct-2-ulosonic acid (Kdo), heptoses, and various hexoses (Patro and Rathinavelan, 2019). The O antigen is the first molecule encountered by the innate immune system. It is composed of a repetitive oligosaccharide comprising two to eight sugars. In specific serotypes, LPS protects bacterial cell against cationic antimicrobial peptides and the complement system (Russo and Marr, 2019).

Lipid A is a potent Toll-like Receptor 4 (TLR4) ligand, leading to a signaling cascade for activating the immune response mediated by neutrophils and macrophages (Lee et al., 2017). It has been documented that *K. pneumoniae* can modify the structure of its Lipid A to evade TLR4 recognition and mask Lipid A in the presence of the capsule (Bertani and Ruiz, 2018). Most immune system cells can recognize the conserved portion of Lipid A to trigger a chemotactic and phagocytic response. However, a study on the social amoeba *Dictyostelium discoideum* shows that the fAR1 receptor recognizes the core region of LPS and triggers chemotaxis and phagocytosis (Pan et al., 2018).

The O antigen has essential functions in protection against the complement, including preventing the binding of C1q to bacteria, inhibiting the subsequent activation of the complement pathway, and blocking the binding of C3b to avoid the formation of the membrane attack complex (Shankar-Sinha et al., 2004). Of the eight serotypes, O1 is usually associated with hvKp isolates with K1 and K2 capsule types (Follador et al., 2016). It has been reported that specific antibodies to O1 have differential effects depending on whether the capsule type is K1 or K2, suggesting that the structure of the capsular polysaccharide could affect the interaction with O-antigen antibodies, implying possible interactions between the capsule, the O antigen, and their respective targeted antibodies (Wantuch et al., 2023).

1.2.5 Fimbriae (Types I and III)

Bacterial biofilm formation is the primary lifestyle of bacteria in their natural state, serving as a successful strategy to thrive in niches exposed to various stressors. This is the most efficient means of transporting mobile genetic elements and is a critical aspect of bacterial virulence and persistence within the host, facilitated by fimbrial adhesins (Flemming et al., 2016).

There is a consensus in the literature regarding the ability of both classical and multidrug-resistant strains of *K. pneumoniae* to form biofilms in a variety of niches, especially among immunocompromised individuals (Wu et al., 2011; Vuotto et al., 2014; Wang et al., 2020b). The *fim* and *mrk* operons, responsible for encoding type I and type

III fimbriae, respectively, play a crucial role in the initial adhesion to both biotic and abiotic surfaces.

Type 1 fimbriae (T1F), encoded by the *fim* cluster, are thin, rigid, adhesive, thread-like surface appendages on the outer membrane. They primarily comprise repeating FimA subunits with an adhesin molecule, FimH, at the tip. These fimbriae extend beyond the capsule, mediating bacterial adhesion to mannose-containing structures on host cells or extracellular matrices via the adhesin FimH (Chen et al., 2011). T1F is essential for establishing urinary tract infections, although they do not affect *K. pneumoniae's* ability to colonize the intestine or infect the lung (Schembri et al., 2005).

T3F are characterized as appendages 2-4 nm wide and 0.5-2 μ m long. The gene *mrkA* encodes the major fimbrial subunit, which polymerizes to form the helical fimbrial shaft. The adhesive subunit, which can bind to collagen molecules, is encoded by *mrkD* and located at the tip of the fimbriae. Genes *mrkB*, *mrkC*, and *mrkF* encode the chaperone, usher, and scaffolding proteins responsible for fimbrial assembly and stabilization (Ares et al., 2017).

T3F mediates *in vitro* adhesion to epithelial cells, kidney, and lung tissues, likely in a mannose-resistant manner. While they significantly contribute to *K. pneumoniae* biofilm formation, they play no role in intestinal and pulmonary infections (Paczosa and Mecsas, 2016).

Both type 1 and type 3 fimbriae work complementary to enhance *K. pneumoniae* biofilm formation on urinary catheters. Besides type 1 fimbriae, type 3 fimbriae is another

essential colonization factor for biofilm-associated urinary infections due to indwelling urinary catheters.

Recently, a gene named *iroP* was identified in the virulence plasmid-encoded salmochelin operon (Chu et al., 2023a). This gene cross-regulates and suppresses promoter activity in the chromosomal type 3 fimbriae gene transcription. IroP itself is repressed by iron through the ferric uptake regulator. In iron-rich conditions, there is an increase in T3F expression, suppressing the hypermucoid capsule phenotype and promoting biofilm formation and cell adhesion. Conversely, under iron-poor conditions, a transcriptional switch occurs, leading to hypermucoid capsule production and repression of the *mrk* operon. This switch allows hvKp strains to regulate biofilm formation based on iron availability, favoring the gastrointestinal tract, where iron concentrations are higher due to the unabsorbed iron from the duodenum. During systemic circulation, where accessible iron sources are limited (10^{-24} M) (Hider, 2007), the hypermucoid capsule phenotype and low T3F predominate to aid dissemination. This regulatory network allows hvKp strains to alternate between an HMV phenotype and a phenotype with high T3F expression and basal capsule production, thus modulating their adhesion to various surfaces in different niches.

1.2.6 Siderophores

Iron is an essential element for microorganisms, required to carry out the metabolic functions necessary for their growth, proliferation, energy generation, respiration, and virulence. However, iron availability in the host's biological fluids is limited and strictly regulated as part of an innate defense system (Miethke and Marahiel, 2007). In response

to the limited availability of iron within mammalian hosts due to its sequestration by multiple iron-binding proteins, bacteria synthesize diminutive molecules capable of sequestering iron, referred to as siderophores. These siderophores are produced through non-ribosomal synthesis and are secreted into the extracellular space (Hider, 2007). They bind iron with high affinity and are transported back to the bacterial cell through specific receptors in the outer membrane. These receptors transport them to the periplasm, where siderophores combine with periplasmic proteins to facilitate their transport to the inner membrane. Finally, iron passes through a channel-mediated by an ABC transporter into the bacterial cytoplasm, where ferric iron is reduced to ferrous iron, making it accessible to the bacteria.

K. pneumoniae produces a prototypical siderophore found in the Enterobacteriaceae family called enterobactin, which exhibits the highest affinity for iron compared to any other known iron chelator (Holden et al., 2018). The genes required for enterobactin biosynthesis are carried on the chromosome in the *entABCDEF* gene cluster. In contrast, the *fepABCDG* gene cluster encodes the proteins responsible for its transport, with *fepA* encoding the specific uptake receptor. However, mammals secrete lipocalin 2, which blocks iron acquisition from enterobactin (Bachman et al., 2011). As a countermeasure, strains of *K. pneumoniae* with a tendency to cause clinical respiratory or pulmonary infections produce additional siderophores, such as yersiniabactin (a phenolate-type siderophore), whose synthesis pathway is encoded by *irp* genes as part of a pathogenicity island *ICEKp10*. It is predicted that the *ybt* and *fyu* genes encode the transporters required for the secretion of this siderophore, and the uptake receptor is

encoded by *ybtQ* (Lawlor et al., 2007). Additionally, there is salmochelin, a glycosylated form of enterobactin. The genes for salmochelin are encoded on a virulence plasmid in hvKp strains within the *iroA* gene cluster, *iroBCDE*. Transport of the iron-laden form is mediated by IroN (Chu et al., 2023a). As mentioned before, IroP has recently been described as an essential factor in the switch between biofilm and capsule formation, depending on the extracellular iron concentration.

Approximately 93% to 100% of hvKp strains synthesize aerobactin, with its genes encoded on the virulence plasmid (Liu et al., 2022). Aerobactin is a hydroxamate-based siderophore biosynthesized through the activity of four genes, *IucABCD*. The aerobactin transporter, *IutA*, is also carried on the same virulence plasmid that carries the *rmpADC* operon (Li et al., 2019). Aerobactin accounts for about 90% of the siderophore activity, and considering that hvKp strains increase siderophore activity by 6 to 10-fold compared to cKp strains, aerobactin has been considered a molecular marker of hvKp strains. In a study conducted by (Russo et al., 2015), it was demonstrated that the inability to produce aerobactin significantly decreased the virulence of hvKp in outbred CD1 mice after either pulmonary or subcutaneous challenge. In conclusion, molecular epidemiologic studies have shown that salmochelin, yersiniabactin, and aerobactin are more commonly present in hvKp strains than in cKp strains. Yersiniabactin is also present in cKp strains (22%), while salmochelin and aerobactin are specific to hvKp (Chen et al., 2023).

1.2.7 Colibactin

Colibactin is a genotoxic chemical compound synthesized by polyketide synthases, non-ribosomal peptide synthases, and hybrid enzymes encoded within a 54-kb genomic island designated as *pks* (Faïs et al., 2018). This compound is linked to severe genotoxicity. The biosynthetic genes for colibactin (*pks*) are within a mobile genetic element called *ICEKp10* in hvKp strains. This genetic element typically also contains genes responsible for yersiniabactin and microcin E492 synthesis. The assembly line for colibactin synthesis consists of 19 genes (*clbA* to *clbS*) within the 54-kilobase genomic island *pks* (Faïs et al., 2018). This machinery includes three non-ribosomal peptide megasynthases (NRPS: ClbH, ClbJ, ClbN), three polyketide megasynthases (PKS: ClbC, ClbI, ClbO), two hybrid NRPS/PKS megasynthases (ClbB, ClbK), and nine accessory, tailoring, and editing enzymes. *ICEKp10* is predominantly found in CG23 (K1 capsule type) hvKp strains but is less common in other hvKp strains (Choby et al., 2020). Colibactin induces DNA double-strand breaks, chromosome aberrations, and cell cycle arrest in the G2/M phase, significantly enhancing the bacterium's virulence (Lan et al., 2019).

HvKp K1 CG23 strains that produce colibactin (*pks*⁺) show a notable preference for the brain of BALB/c mice. Deletion of the *clbA* gene, which abolishes colibactin production, substantially impedes *K. pneumoniae* hypervirulence in the critical pathogenic steps leading to the development of meningitis, furthermore the infection caused by colibactin-producing *K. pneumoniae* escalates rapidly (Lu et al., 2017). Additionally, it has been identified that diabetes mellitus and the K1 and K20 capsular types are

independent risk factors associated with *pks*⁺ *K. pneumoniae* bloodstream infections (Lan et al., 2019). Furthermore, it has been demonstrated that *pks*⁺ hvKp strains promote intestinal colonization. The genomic island ICEKp10, which also encodes for Microcin E492, exhibits activity against Enterobacteriaceae, and its activity necessitates the binding of salmochelin, thereby facilitating the entry of microcin by the target bacteria. Hence, it is predicted that hvKp strains producing the combination of colibactin, microcin E492, and salmochelin would have a significant advantage in colonizing the competitive environment of the colon in immunocompetent patients (Russo and Marr, 2019).

1.3 *Dictyostelium discoideum* as a Host-Pathogen Interaction Model

Virulence is understood as the capacity of a microorganism to cause harm in a susceptible host (Casadevall and Pirofski, 2002). That is why every bacterium can be a potential pathogen, depending on the previous conditions of the host (Casadevall, 2017). Traditionally, virulence has been primarily studied in murine models (Paczosa and Mecsas, 2016). However, these models have significant drawbacks, such as the costly infrastructure required for maintenance, invasive sampling procedures, and the need to navigate a complex web of ethical considerations. These limitations hinder the cost-effective and statistically robust execution of high-throughput experiments (Marcoleta et al., 2018). To overcome these challenges, many research groups have turned to analyzing host-pathogen interactions in surrogate and non-vertebrate animal models (Kurz and Ewbank, 2007; Varas et al., 2017a, 2018). In this context, more adaptable infection models, where both the pathogen and the host are genetically manageable and where

interactions can be tracked through live-cell imaging, have significantly contributed to our understanding of the universal mechanisms underlying host-pathogen interactions.

The social amoeba *D. discoideum* has been validated as a robust model for pathogen-host interactions due to its unique lifestyle, ease of handling and manipulation in the laboratory, low maintenance costs, and the existence of an online database (dictyBase) (Kreppel, 2004; Bozzaro and Eichinger, 2011; Fey et al., 2013)

In its free-living state, *D. discoideum* feeds on environmental bacteria through phagocytosis using molecular pattern recognition mechanisms similar to those found in macrophages and neutrophils (Pan et al., 2018). Therefore, under laboratory conditions, it can be infected with various bacterial pathogens or libraries of mutants to search for virulence factors that could alter the amoeba's life cycle (Ifrid et al., 2022). Under nutrient-rich conditions, *D. discoideum* remains in a unicellular free-living state. However, in response to external signals such as nutrient depletion and population growth (Rijal et al., 2022), it initiates a process of differential gene expression that promotes the aggregation of over 10,000 amoebas into a central aggregation center mediated by cAMP streams. This aggregation is characterized by the polarization of amoebas toward the center, resembling streams of cells converging into a mound. This multicellular body transforms into a phototactic slug-like structure, and social development culminates by forming a mature fruiting body (Medina et al., 2019). Within the fruiting body, 80% of the amoebas concentrate in the spore-laden sorus, while 20% undergo programmed cell death to form a stalk of dead cells that support the sorus. This process typically takes 24 hours when *D.*

discoideum grows on a lawn of non-virulent bacteria. However, social development is delayed or results in morphological alterations when faced with virulent bacteria.

By quantifying different parameters such as phagocytosis plaque formation, resistance to phagocytosis, progress of social development, among others, it is possible to determine degrees of virulence attenuation as a result of the activity or prior treatment of bacteria with drugs, molecules of interest, or mutants, providing valuable information for further studies.

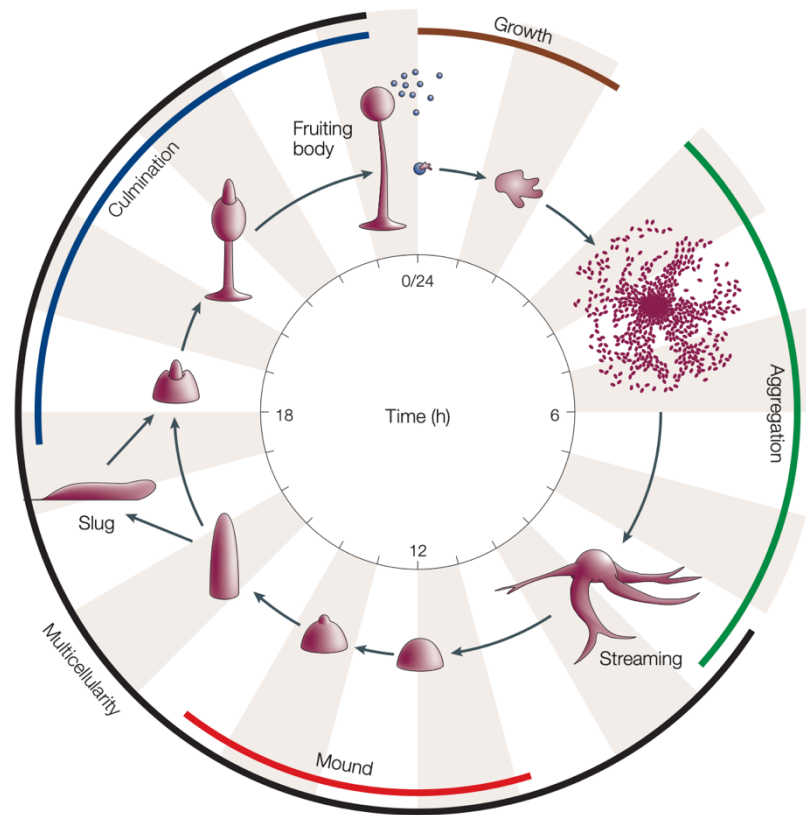


Figure 3. The social development of *Dictyostelium discoideum*. It begins with individual vegetative amoeba and culminates in forming a mature fruiting body. During this process, amoebas aggregate multicellularly due to chemotaxis toward cyclic AMP, forming a mound. As development progresses, the mound extends, and an anterior-posterior axis is established. Ultimately, culmination leads to the development of the fruiting body, which includes a sorus of spore cells on top of a stalk. The entire process, from the starvation of vegetative cells to the formation of the mature fruiting body, takes 24 hours (Chisholm and Firtel, 2004).

1.4 Paradigm Shift – The Post-Antibiotic Era

The emergence of MDR-KP strains worldwide in recent decades, coupled with the rise of hvKP strains, including those in Chile, has coincided with the slow development of an effective antibiotic pipeline. Furthermore, it is improbable, and in some cases, that merely increasing iterations based on classical chemical structures can yield innovative, safe, and effective antimicrobials suitable for our current context (Alanis, 2005). This has led to a new era known as the "post-antibiotic" era (Wang et al., 2020a). These have become ideal targets thanks to the knowledge gained about the molecular mechanisms and signaling pathways that regulate crucial bacterial processes (such as signal transduction, regulators, virulence, or bacterial membrane permeabilization). These new targets exert less selective pressure because their action doesn't aim to kill the bacteria directly. Instead, it seeks to disrupt key processes in bacterial pathogenesis, allowing the host's immune system, possibly in conjunction with antibiotics, to achieve clearance.

Particular interest has been placed on virulence factors as targets for developing new therapies because they mediate fundamental processes in pathogenesis, such as initial colonization, immune system evasion, and persistence in the host. Regarding *K. pneumoniae*, virulence traits vary according to the strain and the site of infection. For example, strains causing persistent urinary tract infections exhibit altered capsule expression, which promotes the expression of type I and III fimbriae for the colonization of epithelial cells and the formation of robust biofilms (Sahly et al., 2000; Struve and Krogfelt, 2003; Wilksch et al., 2011; Ernst et al., 2020). This is because the capsule masks

the fimbrial structures. On the other hand, the presence of the capsule as a virulence factor is crucial for hvKp strains with metastatic characteristics, enabling them to evade the immune system as they migrate through different host organs (Ernst et al., 2020). All of this supports the notion that the production of biofilms and capsules could be suitable targets in the design of anti-virulence drugs.

1.5 Inorganic Polyphosphate and Virulence

In recent decades, there has been a significant interest in studying and understanding inorganic polyphosphate (polyP) metabolism and its role in resistance to various types of stress and virulence. Early on, it was proposed that inorganic polyP synthesis in bacteria could serve as a novel cellular target for designing antivirulence drugs in *Pseudomonas aeruginosa* (Chávez et al., 2011). PolyP is a ubiquitous linear polymer with hundreds of orthophosphate residues (Pi) linked by phosphoanhydride bonds. It has been found in all three domains of life (Archaea, Bacteria, and Eukarya), with a primary focus on prokaryotes (Kornberg et al., 1999).

Key enzymes related to polyP metabolism in bacteria include polyphosphate kinases (PPK1 and PPK2) and exopolyphosphatase (PPX). PPK1 enzymes catalyze the reversible polymerization of the terminal phosphate of ATP or GTP into a polyP chain and the hydrolysis of a terminal phosphate group from the polyP chain, with exopolyphosphatases (PPX) being the primary hydrolytic enzymes (Baijal and Downey, 2021). PPK1 synthesizes polyP from ATP, while PPK2 preferentially catalyzes the reverse reaction, synthesizing GTP from GDP in a polyP-driven process (Zhang et al.,

2002). Although orthologs of PPK1 and PPK2 are present in many bacterial genomes, only a few eukaryotes, such as *D. discoideum* and yeast *Candida humicola*, have reported orthologs to PPK1 and PPK2 (Brown and Kornberg, 2008). PPX plays a crucial role in phosphate metabolism, particularly in maintaining the appropriate levels of PolyP by degrading it processively from its ends (Song et al., 2020). PolyP was initially described as a phosphate reservoir and a source of "high-energy" phosphate bonds to ATP. Further genetic and biochemical experiments with *ppk1* mutants in various bacteria have revealed additional roles for polyP (Brown and Kornberg, 2004; Varela et al., 2010). These roles include inhibiting RNA degradation, activating the Lon protease during the stringent response, and participating in membrane channel structure. Additionally, polyP provides resistance to stress factors such as heat, oxidants, osmotic challenges, antibiotics, and UV radiation, effectively acting as a primary ATP-independent chaperone (Gray et al., 2014; Gray and Jakob, 2015). PolyP has also been found to be associated with lipopolysaccharides (LPS), but its role in immune response activation remains unclear (Terashima-Hasegawa et al., 2019; Ito et al., 2020). Notably, a *Pseudomonas aeruginosa* PAO1 mutant lacking *ppk1* demonstrated impairments in motility, biofilm development, quorum sensing, virulence, and antibiotic resistance (Fraley et al., 2007a; Ortiz-Severín et al., 2015), emphasizing the significance of polyP synthesis as a valuable target for designing novel antimicrobials.

Disrupting the *ppk1* gene in various bacterial pathogens often results in cellular defects, particularly in their virulence towards the host, for instance, *Salmonella sp. Δppk1* mutants showed reduced acid tolerance and invasiveness in epithelial cells, along with

compromised survival within macrophage cells (Kim et al., 2002a; Varas et al., 2018). *Shigella flexneri*, the agent of bacillary dysentery, also exhibited reduced invasiveness for epithelial cells in the absence of *ppk1* (Kim et al., 2002b). In *Vibrio cholerae*, *ppk1*-null mutants displayed increased sensitivity to acid and defects in stationary-phase survival. Additionally, *ppk1*-null mutants of *Neisseria meningitidis* were susceptible to killing by human sera (Tinsley et al., 1993a). *Mycobacterium tuberculosis* was observed to accumulate extracellular polyP, inhibiting phagosome maturation in macrophages and *D. discoideum* (Rijal et al., 2020). Furthermore, reducing *ppk1* gene expression in *Mycobacterium tuberculosis* decreased the ability to colonize and survive in macrophages (Singh et al., 2013). Similarly, a $\Delta ppk1$ *Helicobacter pylori* strain exhibited compromised colonization in mice (S et al., 2005).

Pseudomonas aeruginosa PAO1 $\Delta ppk1$ mutants still retained approximately 20% of wild-type polyP levels due to the enzymatic activity of PPK2. PPK2 belongs to the large superfamily of P-loop kinases characterized by two conserved sequence motifs (Walker A and B), which bind the β and γ phosphates of ATP and Mg^{+} , respectively (Nocek et al., 2008). PPK2's enzymatic activity in *P. aeruginosa* differs significantly from PPK1 in two essential aspects. While PPK1 primarily synthesizes polyP from ATP, PPK2 primarily uses polyP to produce GTP at a rate 75 times greater than polyP synthesis from GTP. Moreover, PPK1 is specific to ATP, while PPK2 equally utilizes GTP and ATP during polyP synthesis (Neville et al., 2021)

Based on this evidence, the modulation of polyP metabolism emerges as a promising therapeutic target for altering the previously described virulence mechanisms. An antimicrobial drug targeting PPK proteins, especially PPK1, is expected to have a broad spectrum of activity due to the high degree of sequence conservation within this protein family across both Gram-positive and Gram-negative species (Tzeng and Kornberg, 1998; Müller et al., 2019) Furthermore since PPK enzymes lack orthologs in mammals, drugs targeting these proteins are unlikely to generate toxicity (Müller et al., 2019). Additionally, as PPK1 participates in cellular metabolism rather than performing an essential function, drugs targeting it are less likely to provoke resistance (Rashid et al., 2000a).

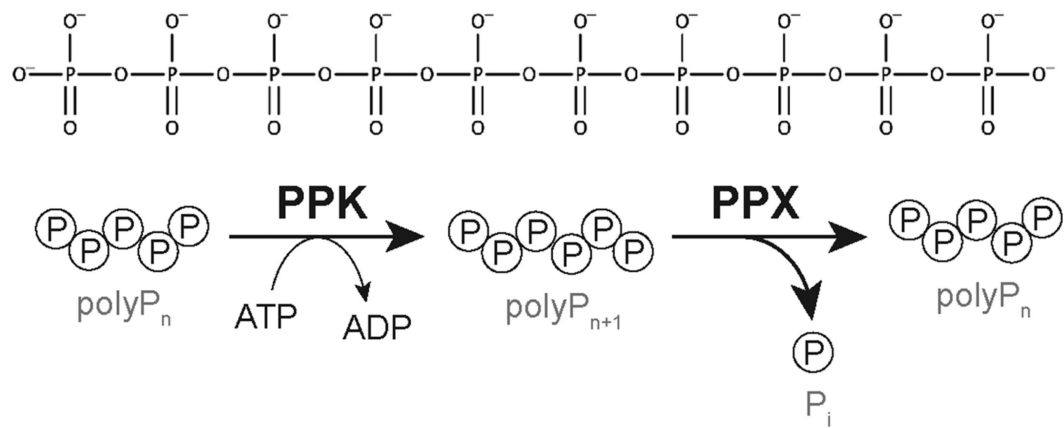


Figure 4. Structure and general metabolism of polyP in bacteria. PPK1 is a polyphosphokinase, and PPX is an exopolyphosphatase. The figure is taken and modified from Bowlin and Gray (2021).

1.6 *Klebsiella pneumoniae* and polyphosphate

There is substantial evidence highlighting the role of polyphosphate (polyP) in various organisms, including bacteria, unicellular eukaryotes, and humans (Suess and Gomer, 2016; Varas et al., 2018; Müller et al., 2019). In the context of *K. pneumoniae* and polyP metabolism, researchers have explored the effects of Gallein, a polyP synthesis inhibitor, and observed that it results in a concentration-dependent decrease in biofilm formation in MDR-KP (Roberge et al., 2021).

HvKp strains are well-known for their elevated virulence, characterized by biofilm formation and the production of a protective capsule, which significantly contribute to their pathogenicity. However, the exact mechanism through polyP metabolism and PPK1 influence hvKp virulence remains poorly understood. Therefore, uncovering the molecular basis of the interplay between polyP metabolism, PPK1, and hvKp virulence is crucial for developing novel therapeutic strategies against hvKp infections.

1.7 Problem Statement

Based on our advanced work and available data from the literature, in this thesis, we propose to study whether polyP metabolism is relevant to various virulence traits of hypervirulent *Klebsiella pneumoniae*. We aim to investigate how alterations in polyP metabolism may affect the expression of virulence factors, with a specific focus on cellular envelope macromolecules and biofilm formation. It is important to note that strain SGH10

has been identified as the most representative among hvKP CG23 strains and is a suitable model for studying their pathogenesis (Lam et al., 2018; Wyres et al., 2020).

Based on the following facts:

- *Klebsiella pneumoniae* seriously threatens human health, and novel strains have acquired hypervirulent and multiple antibiotic-resistant phenotypes.
- PolyP metabolism has not been studied in Hv *Klebsiella pneumoniae*.
- *K. pneumoniae* virulence can be conveniently studied in the surrogate host model *D. discoideum*.
- PolyP interacts with the capsule, and LPS is secreted to the extracellular environment by some bacteria.
- The presence of *ppk1-ppx* operons in *K. pneumoniae* SGH10

The following hypothesis arises.

Hypothesis

Inorganic polyphosphates are relevant for virulence by regulating the capsule and biofilm formation in the hypervirulent strain of *K. pneumoniae*. Consequently, the deletion of genes involved in their metabolism will result in a reduction of virulence in this strain.

General Objective

To evaluate the role of polyP in regulating and expressing virulence factors in hypervirulent strains of *Klebsiella pneumoniae* with particular emphasis on capsule and biofilm formation.

Specific Objectives

- I.** To develop knockout mutant strains of polyP synthesis and degradation genes in the *K. pneumoniae* SGH10 strain.
- II.** To characterize the molecular and cellular biology of wild-type *K. pneumoniae* SGH10 and their polyP metabolism mutant derivatives by comparing global proteomic profiling, hypermucoviscosity, capsule, and biofilm formation capabilities.
- III.** To evaluate the virulence and avoidance of phagocytosis phenotypes of hypervirulent *K. pneumoniae* polyP metabolism mutant strains.

2. Materials and methods

2.1 Strains, plasmids, and growth conditions

The details of the used strains, plasmids and primers can be found in Table 1 and 2. *Escherichia coli* and *Klebsiella pneumoniae* strains were grown routinely at 37°C in LB broth (10 g/L Tryptone, 5 g/L Yeast Extract, 5 g/L NaCl). For solid medium, 1.5% w/v agar was added. MOPS medium supplemented with 0.4% glucose and 0.1% K₂HPO₄ was used for the nutrient deprivation assay. For the macrobiofilm assays, LB agar without NaCl supplemented with Thioflavin S (40 µg/mL) or Congo Red (40 µg/mL) was used. 100 µg/mL Ampicillin or Carbenicillin, 50 µg/mL Kanamycin, or 10 µg/mL Tetracycline were used for antibiotic selection.

Table 1. Strains and plasmids used in this study.

Bacterial strain or plasmid	Genotype or comments	Source/Reference
<i>Klebsiella aerogenes</i> (KpgE) DBS0305928	Recommended strain for supporting the growth of <i>D. discoideum</i>	Dicty Stock Center
<i>Escherichia coli</i> S17 λpir	Laboratory strain typically used for cloning purposes	Laboratory Collection
<i>Klebsiella pneumoniae</i> SGH10	This strain was isolated from a patient's hepatic abscess in 2014 and was found to be hypermucoviscous and hypervirulent.	Andres Marcoleta's laboratory collection
<i>K. pneumoniae</i> SGH10 <i>Δppk1</i>	Null mutant for the gene that encodes the enzyme that synthesizes polyP	This work

<i>K. pneumoniae</i> SGH10 Δppx	Null mutant for the gene that encodes the enzyme that degrades polyP	This work
<i>K. pneumoniae</i> SGH10 $\Delta ppk1-\Delta ppx$	Double null mutant for the operon that metabolizes polyP.	This work
<i>K. pneumoniae</i> SGH10 $\Delta wcaJ$	Null mutant for the gene encoding the WcaJ glycosyltransferase that performs the first step in capsule polysaccharide synthesis. This strain was used as a control.	Andres Marcoleta's laboratory collection
pBBR1-GFP	Constitutive expression of the GFP protein, Kan ^r	Laboratory Collection
pR6KtetsacB	Vector used for the generation of gene deletions of interest. It contains a tetracycline resistance cassette and the gene to promote the second sacB recombination event	Laboratory collection of Yunn-Hwen Gan and Yahua Chen (Singapore).

Table 2. List of primers used for generating mutants.

PPK1_UP_F	TGACATGATTACGAATTCTGCATGAAAAACATCGTGGT
PPK1_UP_R	GGGGTGTATCGTTTAACCGCTCACACTCCGTTTTA
PPK1_DOWN_F	ACGGAGTGTGAGCGGTTAAACGATAACACCCCTCGGC
PPK1_DOWN_R	AAGCTTGCATGCCTGCAGGCGGCTACGAATATCCTGGT
PPX_UP_F	ACATGATTACGAATTCAGGATTCGCGCATTATTGAC
PPX_UP_R	GTTGATTGCCAGAGATTGTTCGAACCAAGGTCAACC
PPX_down_F	GACCTTGGTTCGAACAATCTCTGGCAATCAACCGAG
ppx_down_R	AAGCTTGCATGCCTGCAGGCCGGTCAAGCATCTGTATT
CTR_PPK1_Fw	CCGACGAATGAACAACCAG
CTR_PPK1_Rv	CAACGCCATAAAAATCAGG
CTR_PPX_Fw	TCAGTATTGTGGACCGTTTCC
CTR_PPX_Rv	CTACGCCCGGTTAAAAACAA
CTR_PoliP_Fw	CCGACGAATGAACAACCAG
CTR_PoliP_Rv	CTACGCCCGGTTAAAAACAA

2.2 Culture Conditions of *D. discoideum*

We obtained the *D. discoideum* strain AX4 (DBS0302402) from the Dicty Stock Center (Kreppel et al., 2004; Basu et al., 2013; Fey et al., 2013) and cultured them using standard protocols (Fey et al., 2007). Briefly, the *D. discoideum* strains were maintained at 23°C in SM medium containing 10 g/L glucose, 10 g/L peptone, 1 g/L yeast extract, 1 g/L MgSO₄ × 7H₂O, 1.9 g/L KH₂PO₄, 0.6 g/L K₂HPO₄, and 20 g/L agar. They were grown on a confluent lawn of *Klebsiella aerogenes* DBS0305928. Before the assays, amoebae were grown at 23°C with agitation (180 rpm) in liquid HL5 medium, which contained 14 g/L tryptone, 7 g/L yeast extract, 0.35 g/L Na₂HPO₄, 1.2 g/L KH₂PO₄, and 14 g/L glucose at pH 6.3. These cultures were axenic, meaning they were free of bacteria.

We harvested amoebae in the early exponential phase ($1-2 \times 10^6$ cells/mL) and centrifuged them at 2000 rpm for 5 min. Before the infection assays, we discarded the supernatant and washed the pellet three times using Soerensen buffer (2 g/L KH_2PO_4 , 0.36 g/L $\text{Na}_2\text{HPO}_4 \times 2 \text{H}_2\text{O}$, pH 6.0) or adjusted it to 1×10^6 cells/mL in HL5 medium for social development assays. We determined the number of viable amoeba cells by performing Trypan blue exclusion and counting in a Neubauer chamber. For the social development assay with *D. discoideum*, Agar N was used. For the predation resistance assay, Agar SM was used.

2.3 Genetic manipulation of *K. pneumoniae* SGH10

We followed the pipeline below to acquire mutant strains with a deleted gene of interest. First, we amplified ~1000 bp fragments upstream and downstream of the target gene from genomic DNA templates using Q5 high-fidelity DNA polymerase (New England Biolabs). We assembled them into the vector pR6KTet-SacB using NEBuilder® HiFi DNA Assembly Master Mix (New England Biolabs). The plasmids were then introduced into *K. pneumoniae* SGH10 through conjugation with the *E. coli* donor strain S17-1 λ pir. After selecting single cross-transconjugants in a medium containing Tetracycline (50 $\mu\text{g/ml}$), we eliminated the donor *Escherichia coli* by adding ampicillin (100 $\mu\text{g/ml}$). To counteract the selection of the *sacB* gene in the pR6KTet-sacB backbone, single tetracycline-resistant crosses were passaged in an LB medium without sodium chloride but supplemented with 20% sucrose. Successful deletion of the gene of interest was confirmed by selecting tetracycline-sensitive double crossovers via polymerase chain reaction. We also confirmed the mutant strains, including $\Delta ppk1$, Δppx , and $\Delta ppk1-\Delta ppx$,

through scar generation in the SGH10 genome by sequencing the fragments and matching them with the complete genome of the SGH10 WT (Figure 5).

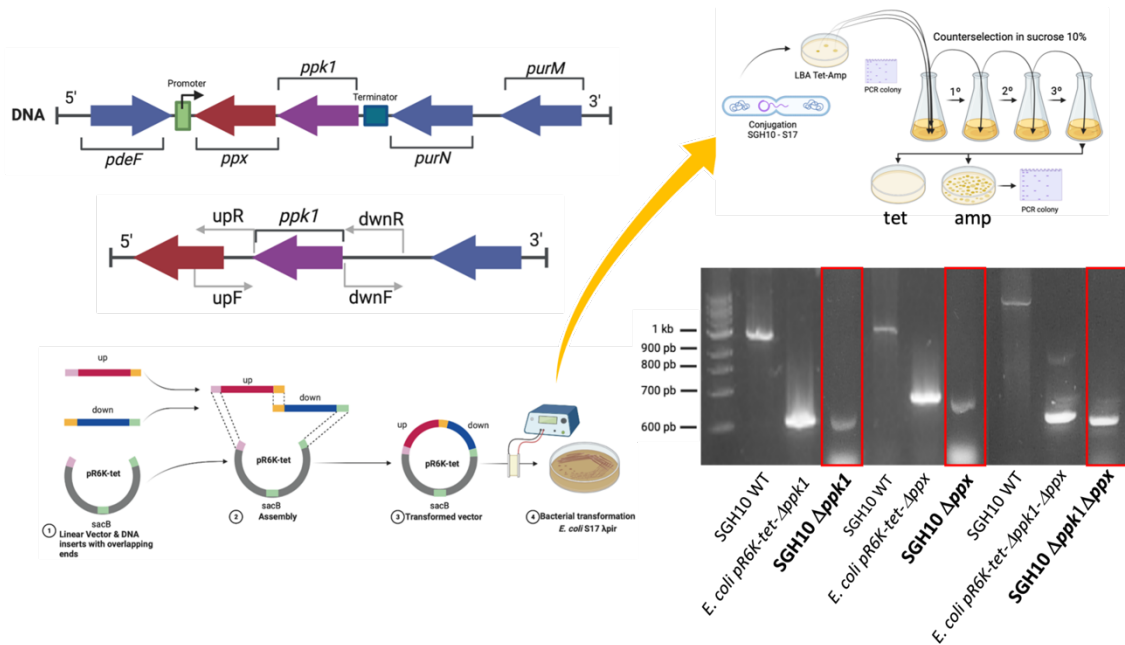


Figure 5. Mutant development workflow. Upstream and downstream fragments (~1000 bp) of the target gene were amplified from genomic DNA using Q5 high-fidelity DNA polymerase (NEB). These fragments were then assembled into the pR6KTet-SacB vector using NEBuilder® HiFi DNA Assembly Master Mix (NEB). The plasmids were introduced into *K. pneumoniae* SGH10 via conjugation with *E. coli* donor strain S17-1λpir. Tetracycline selection (50 μg/ml) was used to isolate single cross-transconjugants, then the donor *E. coli* was eliminated using ampicillin (100 μg/ml). To counteract the selection of the *sacB* gene, tetracycline-resistant crosses were passaged in an LB medium without sodium chloride but with 20% sucrose. Successful deletion of the target gene was confirmed by selecting tetracycline-sensitive double crossovers using PCR. Mutant strains ($\Delta ppk1$, Δppx , and $\Delta ppk1\text{-}\Delta ppx$) were validated by sequencing the fragments and comparing them with the complete genome of SGH10 WT.

2.4 Proteomic profile

2.4.1 Protein Extraction

Protease/phosphatase inhibitor (#1861284, Thermo Scientific) was added to each sample of protein at a 1X final concentration. Then, the samples were lyophilized and resuspended in 8M urea with 25 mM ammonium bicarbonate pH 8 and later, they were homogenized using ultrasound for 1 min with 10 s on/off pulses at an amplitude of 50% using a cold bath. Then, they were incubated on ice for 5 min and later centrifuged to remove debris at 21,000 x g for 10 min at 4°C. Samples were immediately quantified using the Qubit Protein Assay reagent (#Q33212, Invitrogen).

2.4.2 Mass spectrometry preparation

The resulting proteins were subjected to chloroform/methanol extraction. Then, they were equilibrated at room temperature for 10 min, centrifuged at 16,000 x g for 15 min at 4°C, and discarded the supernatant. The resulting pellet was washed 3 times with cold 80% acetone. Subsequently, the protein pellet was dried in a rotary concentrator.

Samples were resuspended in 30 µL 8M Urea and 25 mM ammonium bicarbonate. Then, they were reduced with DTT to a final concentration of 20 mM in 25 mM ammonium bicarbonate and incubated for 1 hour at room temperature. They were then alkylated by adding iodoacetamide to a final concentration of 20 mM in 25 mM ammonium bicarbonate and incubated for 1 hour in the dark at room temperature. Subsequently, the samples are diluted 8 times with 25 mM ammonium bicarbonate.

Digestion was performed with sequencing grade Trypsin (#V5071, Promega) in a 1:50 ratio of protease: protein (mass/mass) and incubated for 16 h at 37°C. Digestion was stopped by pH adding 10% formic acid. Then, the samples were subjected to Clean Up Sep-Pak C18 Spin Columns (Waters), according to the supplier's instructions. Subsequently, the clean peptides were dried in a rotary concentrator at 1000 rpm overnight at 10°C.

2.4.3 Liquid Chromatography – Tandem Mass Spectrometry

Two hundred ng of the peptides obtained in the previous step were injected into a nanoElute nanoUHPLC (Bruker Daltonics) coupled to a timsTOF Pro mass spectrometer (“Trapped Ion Mobility Spectrometry – Quadrupole Time Of Flight Mass Spectrometer,” Bruker Daltonics) using an Aurora column. UHPLC (25cm x 75µm ID, 1.6µm C18, IonOpticks, Australia). Liquid chromatography was performed using a 90-minute gradient of 2% to 35% buffer B (0.1% Formic Ac. - Acetonitrile). The collection of results was performed using the TimsControl 2.0 software (Bruker Daltonics) under 10 PASEF cycles, with a mass range of 100-1,700 m/z, capillary ionization of 1,500 V, and a temperature of 180°C, TOF frequency 10 KHz at a resolution of 50,000 FWHM.

2.4.4 Protein Identification

The data obtained were analyzed with the MSFragger 3.5 software (Kong et al., 2017) through the Fragpipe v18.0 platform (<https://fragpipe.nesvilab.org/>) using the "default" workflow in a data analysis server consisting of 48 cores and 512 Gb of RAM. Mass

tolerance parameters of 50 ppm were used, using monoisotopic masses and 0.05 Da fragment ions. Among the digestion options, trypsin was used as the enzyme, specific digestion mode and a maximum of two cleavages per peptide (“missed cleavages per peptides”). The following were used as post-translational modifications (PTM): Cysteine carbamidomethylation, as fixed PTM: Methionine oxidation (M), N-terminal acetylation, Asparagine and Glutamine (NQ) deamination, as variable PTMs. The database used for identification was the standard proteome of *Klebsiella pneumoniae* subsp. *pneumoniae* (strain SGH10) (5,126 total entries). The FDR estimate was included using a decoy database. As a filter, an FDR \geq 1% and 1 minimum unique peptide per protein were used for identification.

2.4.5 Protein Quantification LFQ (Free Label Quantification)

The columns corresponding to the Uniprot access codes and intensity values were selected using the protein identification results. Data were concatenated and missing values in the intensity columns were imputed. The resulting matrix was subjected to normalization by medians. Differential expression proteins were determined by applying a T-Test with a Benjamini-Horschberg multiple correction test (adjusted p-value < 0.05). DEPs (Differentially Expressed Proteins) were identified between the comparisons: $\Delta ppk1$ vs. WT, Δppx vs. WT and $\Delta ppk1$ - Δppx vs. WT.

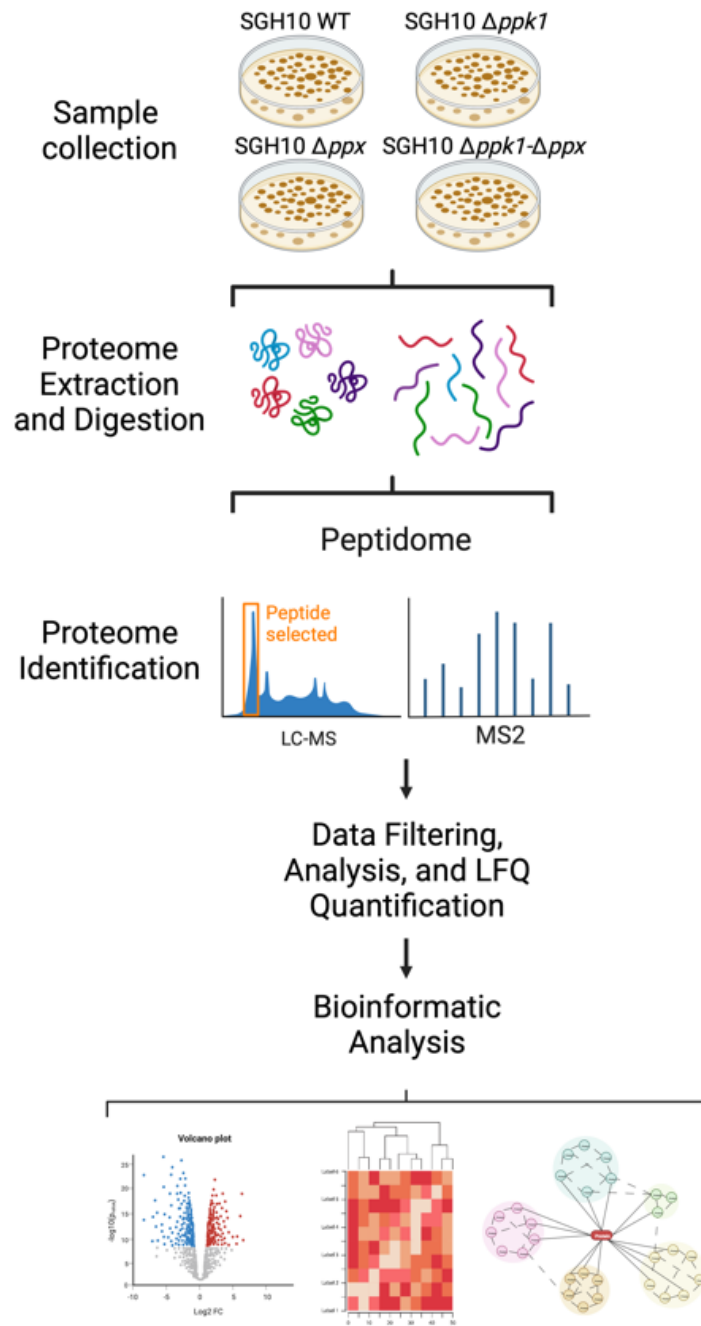


Figure 6. Diagram of the workflow used in protein identification.

2.5 Calculation of the z-score

The z-score was calculated based on the logFC of each protein belonging to the virulence categories derived from VFDB (Adherence, antiphagocytosis, toxin, siderophores, lipid A, serum resistance). It's important to note that this z-score doesn't refer to the standard score typically used in statistics but is a simple calculation aimed at indicating whether the biological process, molecular function, or cellular component is more likely to decrease (resulting in a negative value) or increase (resulting in a positive value). The calculation was performed using the following formula:

$$zscore = \frac{(up - down)}{\sqrt{count}}$$

The z-score was determined based on the number of proteins assigned as upregulated (logFC>0) or downregulated (logFC<0), denoted as "up" and "down," respectively, in the dataset. Subsequently, the average z-scores of each category were calculated for each mutant and plotted as "All virulence factors."

2.6 Growth curve

Mutant strains with alterations in polyP metabolism and the SGH10 WT strain were cultured overnight. A 1:1000 dilution in LB or MOPS medium was inoculated into a 96-well plate (the MOPS medium was supplemented with 0,4% glucose and 0.1 mM K₂HPO₄). The plate was then incubated for 24 hours in a TECAN infinite 200 pro plate reader at 37°C and 180 rpm. Readings were taken every 10 minutes (n= 6) to measure the optical density at 600 nm (OD₆₀₀).

2.7 Quantification of polyP under nutrient deprivation.

To investigate whether PPK1 deficiency affects bacterial polyP accumulation, a polyP quantification assay was performed (Lv et al., 2022a). Briefly, cultures of *K. pneumoniae* SGH10 and polyP mutants grown overnight were diluted into fresh LB broth and cultured at 180 rpm and 37°C for 2 hours. Then, 1 mL of bacterial cells was centrifuged twice in MOPS low-phosphate minimal medium (containing 0.4% glucose and 0.1 mM potassium phosphate) and incubated at 37°C for 2 hours to stimulate polyP accumulation. Next, 1 mL of bacterial cells was centrifuged at 10,000 rpm at 4°C for 5 minutes, and the bacterial pellet was suspended in 50 mM HEPES buffer (pH 7.5) and heated at 60°C for 10 minutes to increase bacterial membrane permeability. The pellet was then resuspended in DAPI assay buffer (containing 150 mM KCl, 20 mM HEPES-KOH, and 10 mM DAPI, pH 7.0) and incubated for 10 minutes at room temperature in the dark. The fluorescence intensity of the DAPI-polyP complex in *K. pneumoniae* was measured with excitation at 415 nm and emission at 550 nm (Smith and Morrissey, 2007). To visualize the localization and quantity of polyP in bacteria, the DAPI-polyP complex was also observed under a confocal microscope (Zeiss) by monitoring the accumulation of polyP before and after nutritional starvation.

2.8 Capsule production quantification

Capsule production was quantified by measuring the total amount of uronic acids, following the method previously described for *K. pneumoniae* (Walker et al., 2020). Briefly, uronic acids were extracted from 500 ml of culture using zwittergent, precipitated

with ethanol, and resuspended in a tetraborate/sulfuric acid solution. Then, 3-phenylphenol was added, and the uronic acid content was estimated by measuring the absorbance at 520 nm and comparing it to a standard curve generated with commercial glucuronic acid.

2.9 Low-speed centrifugation of bacteria

Four milliliters of a 10^9 CFU/ml growth-culture of the desired strain in LB were prepared in 15 ml Falcon tubes. The tubes were centrifuged at $2,000 \times g$ for 10 minutes and imaged against a black background. The supernatant's optical density at 600 nm (OD_{600}) was measured using a BioMate™ spectrophotometer (Thermo Scientific).

2.10 Quantification of Biofilm Biomass and EPS using Confocal Microscopy

To assess biofilm formation, we performed a published protocol with some modifications (Chen et al., 2020a). Briefly, we grew *K. pneumoniae* SGH10 wild-type and polyP mutant strains overnight in LB broth, then diluted them 1:100 in fresh LB broth. Next, we added 100 μ L of each dilution to a 96-well polystyrene microtiter plate and incubated it at 37°C for 24 hours. Wells containing only media were used as blanks. After removing planktonic cells, we washed the wells twice with sterile water and stained them with 150 μ L of 0.1% crystal violet for 30 minutes. Then, we rinsed the wells twice with sterile water and solubilized the stained biofilms with 95% ethanol. We quantified biofilm formation by measuring the OD_{595} using a TECAN infinite 200 pro plate reader. To quantify EPS components such as curli and cellulose, the Ebbabiolight 680 probe was

used, which bound to these components without influencing biofilm formation (Choong et al., 2016). EbbaBiolight 680 was diluted in a growth medium at a 1:1000 ratio for the biofilm assay. Then, the supplemented growth medium was inoculated with the bacterial culture. Next, the wells of a 96-well plate were filled with 100 μ l of the inoculated medium. The unused wells were filled with sterile water to prevent drying during incubation. The plate was covered with a lid or an adhesive seal. Fluorescence was measured at 540ex/680em in a TECAN infinite 200 pro plate reader. Each sample was measured in triplicate, and we calculated averages of the absorbance values for analysis. An overnight culture was diluted 1:100 in LB broth medium to investigate the accumulation of polyP in the biofilm and its influence on formation. Subsequently, a slide was submerged in 10 ml of the 1:100 culture inside a 50-ml falcon tube and incubated at 37°C for 24 hours. The slide was washed three times with nanopure water and incubated for 30 minutes with 5 μ g/ml DAPI to stain DNA and PolyP. The polyP accumulation was visualized using a CLSM Zeiss 757 confocal microscope, with a 358ex/461em laser to observe DNA and a 358ex/540em laser to observe polyP.

2.11 Scanning electron microscopy

To examine potential modifications at the superficial level, including the capsule and overall morphology, we conducted scanning electron microscopy (SEM) with some modifications (Tan et al., 2020). We prepared a lawn on LB agar from strains frozen at -80°C, then incubated for 24 hours at 37°C. Using a sterile swab, we collected enough bacteria and resuspended them in PBS 1X. We adjusted the OD₆₀₀ to 2.8 (1×10^9 CFU/ml)

and fixed 500 μ L of the suspension with 2.5% glutaraldehyde and 0.15% ruthenium red to improve capsule contrast. Samples were subjected to critical point drying and gold coating and subsequently observed in a high vacuum Zeiss EVO M15 scanning electron microscope. Overnight cultures of *K. pneumoniae* SGH10 and polyP mutants were diluted into fresh LB broth and cultured at 180 r.p.m. and 37°C for 2 hours to examine superficial morphology in the mutants and WT strains following nutrient deprivation. The bacterial cells were then centrifuged twice in MOPS low-phosphate minimal medium (containing 0.4% glucose and 0.1 mM potassium phosphate) and incubated at 37°C for 2 hours to stimulate polyP accumulation. The samples were treated in the same manner before observation using SEM.

2.12 Predation resistance assay

In this predation resistance assay, we semiquantitatively evaluated the possible attenuation of virulence in polyP metabolism mutants compared to the SGH10 WT strain. We modified a previously established protocol (Filion and Charette 2014). Bacterial colonies were taken from a -80°C stock to prepare overnight cultures, and 300 μ L were then seeded onto a plate using a Digralsky loop to generate a bacterial lawn. The plate was left to dry and incubated for 24 hours at 23°C. Meanwhile, *D. discoideum* was cultured in HL5 medium, and serial dilutions were prepared to obtain the following cell concentrations: 500,000 - 50,000 - 5,000 – 500 – 50 and 5 cells per 5 μ L. The bacterial lawns were then spotted with 5 μ L of the serial *D. discoideum* dilutions. The plates were allowed to dry and were incubated at 21°C for six days. Plaque formation was visually

examined on days 3 and 6. Isolates that did not enable amoebae growth were considered virulent for the amoeba. Bacterial strains that exhibited social development with 500 *D. discoideum* were considered sensitive to predation (Paquet and Charette 2016).

2.13 Social Development Assays

For social development assays, we followed a published protocol (Varas et al., 2018). Overnight cultures of each bacterial strain (30 μ L) were homogeneously included per well of a 24-well plate containing N agar (1 g peptone, 1 g glucose, 20 g agar in 1 L of 17 mM Soerensen phosphate buffer) and grown overnight at 23°C. A drop of a cellular suspension corresponding to 1×10^4 *D. discoideum* cells in HL5 was spotted in the middle of each well and the plates were further incubated at 23°C for six days. The social development of amoebae was monitored daily for six days, and the phase reached was scored, being classified as “aggregation,” “elevation,” and “culmination.” A score of “1” was assigned when amoebae aggregated, forming a phagocytosis plate, “2” when all the well surface elevated structures such as worms or fingers were observed, and “3” when fruiting bodies were formed across all the well surfaces. Transitions among these three phases were scored, with half of the value corresponding to the closest next stage. The number of fruiting bodies on a 1 cm² surface was also quantified for each strain under study and was compared with the commensal KpgE strain. Additionally, images of social development were obtained on days 1, 2, and 3 using an Olympus MVX10 stereomicroscope with a total magnification of 20X.

2.14 Phagocytosis assays

A lawn was prepared on LB agar from strains GFP frozen at -80°C and incubated for 24 hours at 37°C . Bacteria were collected using a sterile swab and resuspended in Sorensen 1X buffer. Cell density was adjusted to OD_{600} at 1×10^7 cells/mL. Axenic cultures of *D. discoideum* were changed to a concentration of 1×10^6 cells/mL and 1 mL of culture was deposited in 24-well plates. The plate was centrifuged at 600g for 10 minutes and incubated at 23°C for 24 hours. Each well was washed three times with Sorensen buffer and 1 mL of bacterial suspension was added to each well to obtain an MOI of 10. The plate was centrifuged at 600g for 30 minutes. The plate was then observed with the Lionheart FX automatic microscope, programmed to take photographs every 10 minutes for 24 to 48 hours in bright field (BF) and GFP and in 4 regions of interest per well at 23°C . The images were analyzed with Gen5 software version 3.08 (Lionheart FX) and ImageJ software version 1.52 (Fiji version).

3. Results

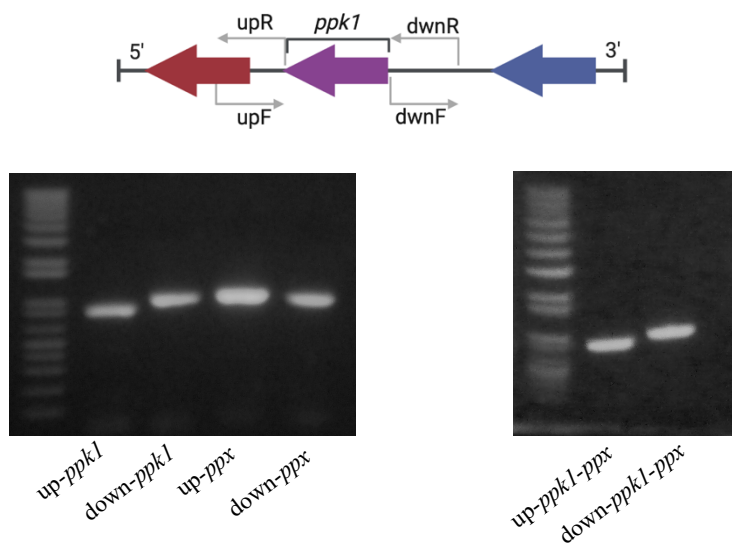
3.1 Generation of mutants in the polyphosphate (polyP) metabolism in the hypervirulent strain *Klebsiella pneumoniae* SGH10.

To understand the impact of inorganic polyphosphate metabolism on virulence factors in the HvKp strain, we generated three mutants in the *ppk1*, *ppx*, and *ppk1-ppx* genes, which form an operon. Fragments of approximately 1000 bp upstream and downstream were amplified for each target gene (Figure 7A). These fragments were purified and assembled into the pR6K-tet-sacB vector (Figure 7B), containing a tetracycline resistance cassette and *sacB* gene for counter-selection in sucrose. Subsequently, the vector was transformed into *E. coli* S17- λ pir strains, cultured on agar plates with tetracycline (75 μ g/ml). Colonies that grew underwent PCR to confirm the presence of the assembly (Figure 7C).

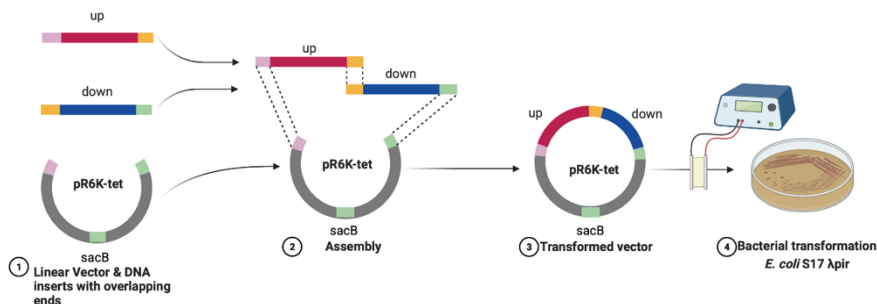
Overnight cultures were then grown for one colony of each construction (in LB medium supplemented with 75 μ g/ml tetracycline), along with the wild-type *K. pneumoniae* SGH10 strain. Conjugation was performed for 3 hours on a conjugation membrane, and the cells were plated on agar plates with tetracycline and ampicillin to select SGH10 colonies with the plasmid. PCR was employed to amplify the homology region (Figure 7D), confirming the presence of the first homologous recombination event. Two Δ *ppk1* colonies, two Δ *ppx* colonies, and eight Δ *ppk1-ppx* colonies were identified (Figure 7D). The colonies underwent three steps of sucrose cultivation to enrich the population of bacteria that experienced the second recombination event, resulting in clean deletions of the target genes without the resistance cassette and *sacB* gene. Figure 7E

showed fragments of approximately 600 bp, confirming the deletion of *ppk*, *ppx*, and *ppk1-ppx* genes in the SGH10 strain. Finally, we amplified and sequenced the homology fragments, resulting in a scar shown in Figure 7F after performing a blast with SGH10's complete genome.

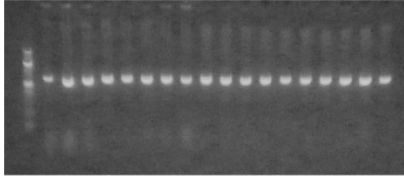
A



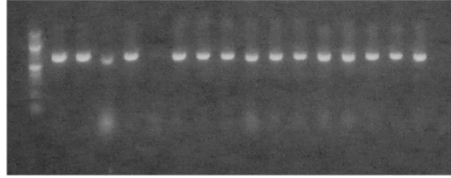
B



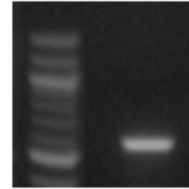
Transformants *E. coli* S17 λ pir-*ppk1*



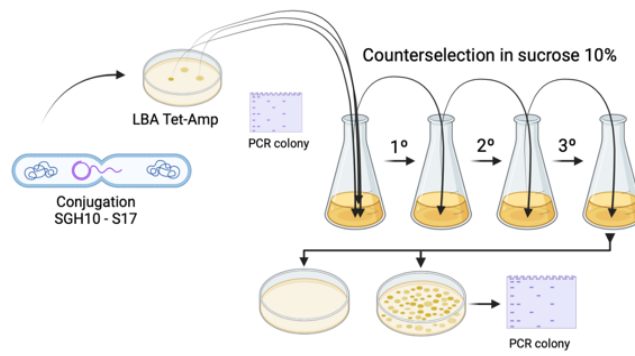
Transformants *E. coli* S17 λ pir *ppx*



Transformant
E. coli S17 λ pir *ppk1-ppx*



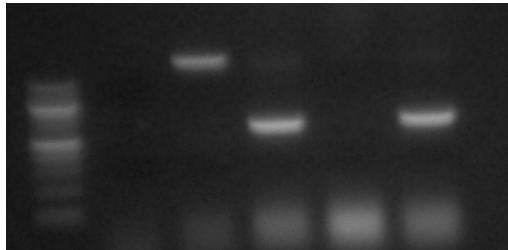
C



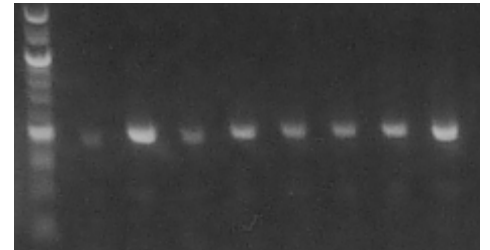
SGH10-*ppk1*



SGH10-*ppx*

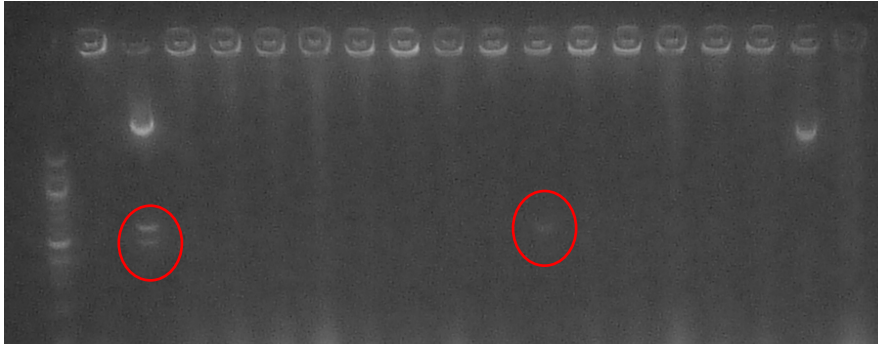


SGH10 *ppk1-ppx*

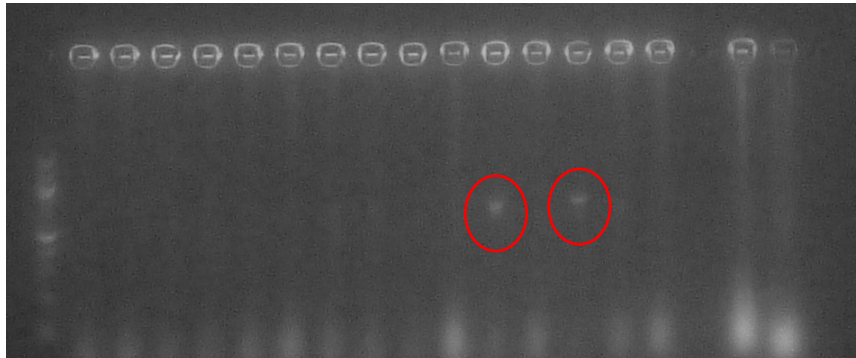


D

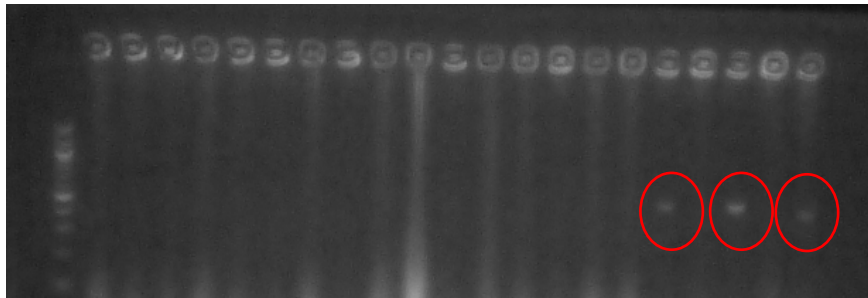
SGH10 *ppk1*



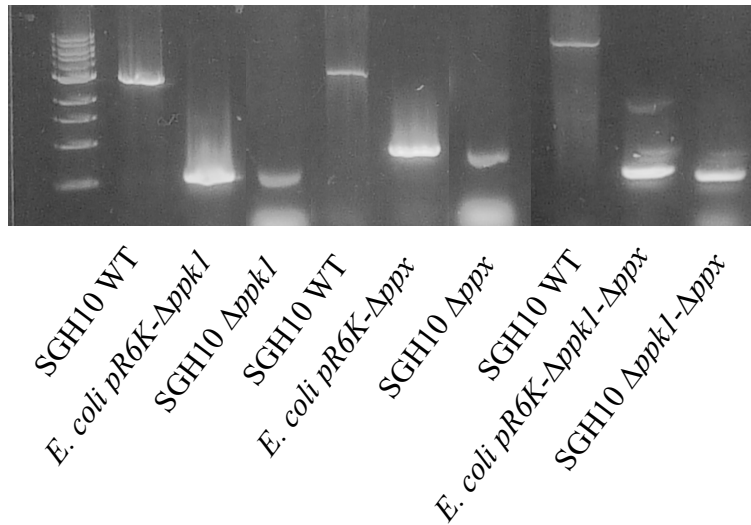
SGH10 *ppx*



SGH10 *ppk1-ppx*



E



F

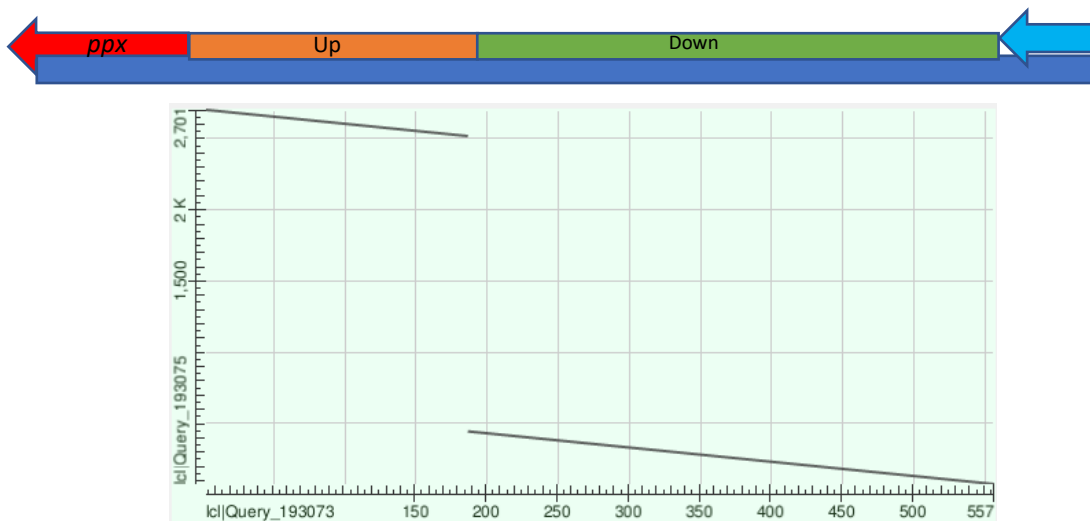


Figure 7. **Workflow for generating mutant strains in *ppk1*, *ppx*, and *ppk1-ppx* genes:** (A) Amplification of *ppk1*, *ppx*, and *ppk1-ppx* fragments from the gDNA of *K. pneumoniae* SGH10 strain. (B) Ligation of fragments into the pR6K-tet-sacB plasmid followed by bacterial transformation with *E. coli* S17 λ pir. (C) Conjugation between *K. pneumoniae* SGH10 and *E. coli* S17 λ pir-(polyp) with Tetracycline selection. (D) Countersélection in 10% sucrose. (E) Confirmation PCR for gene deletions. (F) Figure 7. Scar generated in the SGH10 genome for $\Delta ppk1$ is shown.

3.2 Mutants lacking genes involved in PolyP synthesis and degradation preserve the viability.

Given the urgent need to identify alternative targets that do not directly affect bacterial viability or fitness to mitigate the rapid development of resistance associated with the use of classical antimicrobials, we investigated the growth of mutants in polyphosphate metabolism under optimal conditions (LB broth, 37°C, 180 rpm) and in minimal medium (MOPS). The results revealed that the deletion of the $\Delta ppk1$, Δppx , and $\Delta ppk1$ - Δppx genes did not impact growth under normal conditions (Figure 8). However, under nutrient-deprived conditions (a condition that promotes polyP synthesis), a delay of approximately 2 hours in reaching exponential growth was observed in the $\Delta ppk1$ and $\Delta ppk1$ - Δppx mutants (Figure 9). This delay was not observed in the Δppx mutant, suggesting that the absence of PPK1 specifically affects average growth under nutrient-deficient conditions. Furthermore, the adding of different quantities of polyphosphate 140-mer restores growth under minimal nutrient conditions (Figure 9).

3.3 PPK1 is essential for polyP accumulation in the SGH10 strain.

PPK1 is the main enzyme responsible for polyphosphate synthesis in bacterial models such as *P. aeruginosa* and *Acinetobacter baumannii* (Varas et al., 2018; Lv et al., 2022b). However, its role in *K. pneumoniae* remains relatively unexplored. Therefore, our objective was to assess polyphosphate levels under favorable conditions for accumulation (minimal medium MOPS). To achieve this, bacteria were cultured in a rich medium (LB) until the mid-logarithmic phase and transferred to a nutrient-poor medium (MOPS) for

two hours. As expected, $\Delta ppk1$ and $\Delta ppk1-\Delta ppx$ mutants showed a significant decrease in polyphosphate levels compared to the SGH10 WT strain (Figure 10). In contrast, no notable change in polyphosphate levels was observed in the Δppx mutant compared to the wild type.

Furthermore, we utilized confocal microscopy with DAPI staining (Aschar-Sobbi et al., 2008) to visualize polyphosphate accumulation (Figure 11). When DAPI binds to DNA, its excitation/emission spectrum is 405/451; however, when DAPI binds to polyphosphate, its excitation/emission spectrum is 405/560, allowing us to visualize polyphosphate granules as a distinctive mark from DNA. After culturing bacteria in a rich medium and transferring them to a nutrient-poor medium (MOPS) for 2 hours, we observed a considerably lower number of bacteria in the $\Delta ppk1$ and $\Delta ppk1\Delta ppx$ mutants compared to the Δppx mutants and the SGH10 WT strain, consistent with the growth curve delay observed in minimal medium (Figure 9).

Additionally, the formation and accumulation of polyphosphate granules were reduced in the $\Delta ppk1$ and $\Delta ppk1\Delta ppx$ mutants, evidenced by the significant decline in DAPI-polyphosphate fluorescence intensity compared to the SGH10 WT and the Δppx mutant strain (Figure 11).

To confirm that the observed effects result from the deletion of PPK1, we used Mesalamine, a drug used in treating inflammatory bowel diseases, which has been shown to inhibit PPK1 activity in *E. coli* (Dahl et al., 2017). In Figure 11, we observed no polyphosphate accumulation, exhibiting a pattern similar to the $\Delta ppk1$ and $\Delta ppk1-\Delta ppx$ mutants. In conclusion, these findings suggest that PPK1 is the primary enzyme

controlling polyphosphate synthesis, and the absence of exopolyphosphatase (PPX) does not significantly increase polyphosphate synthesis or accumulation.

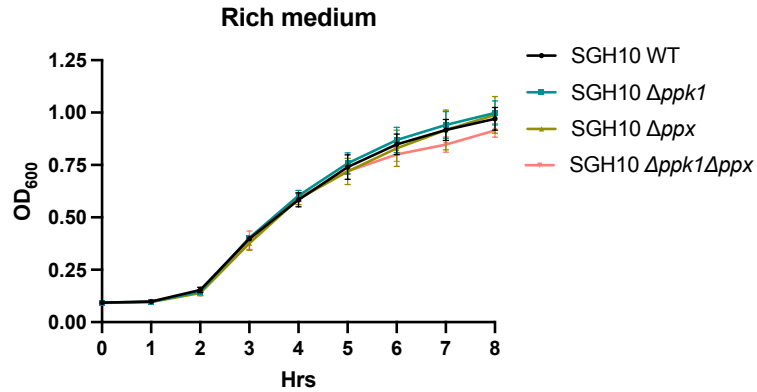


Figure 8. Growth curves in rich medium. Mutant strains in polyP metabolism and SGH10 WT were grown overnight. A 1:1000 dilution in LB was inoculated in a 96-well plate and was incubated for 24 h in a TECAN infinite 200 pro plate reader at 37°C and 180 rpm. Readings were taken every 10 minutes ($n = 6$) to DO_{600} .

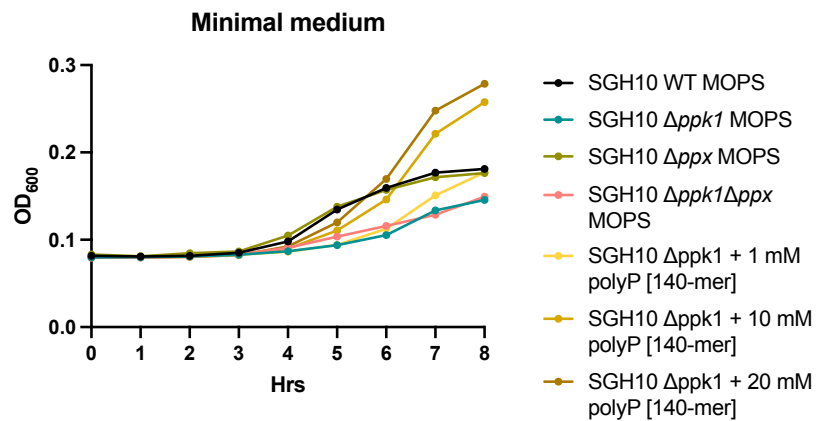


Figure 9. Growth curves in minimal medium. Mutant strains in polyP metabolism and SGH10 WT were grown overnight. A 1:1000 dilution in MOPS was inoculated in a 96-well plate (MOPS culture medium was inoculated with 4 g/l glucose and 0.1 mM H₂PO₄). 1, 10 and 20 mM of polyP [140-mer] were used for phenotype reconstitution. It was incubated for 24 h in a TECAN infinite 200 pro plate reader at 37°C and 180 rpm. Readings were taken every 10 minutes (n = 6) to DO₆₀₀

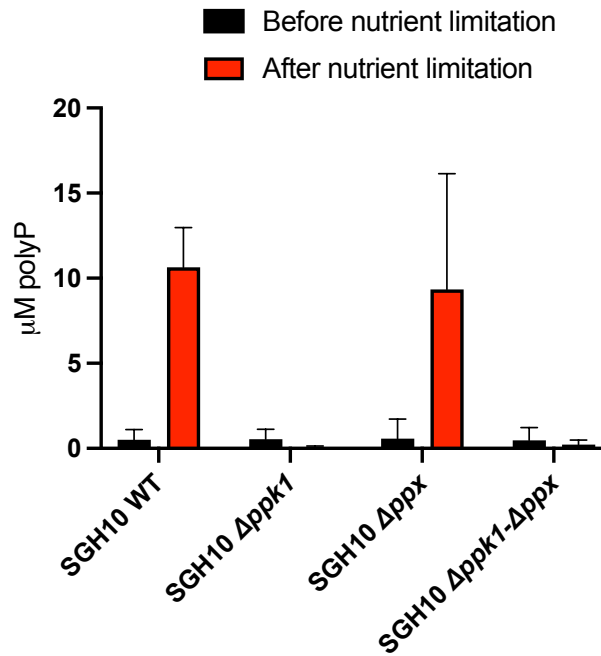


Figure 10. Nutritional downshift. An overnight culture was diluted 1:100 in 10 ml of LB broth and allowed to grow with agitation until the mid-logarithmic phase (approximately 2 h). One ml of culture was taken and washed three times with MOPS medium (0.4% glucose and 0.1 mM K_2HPO_4), then incubated with agitation for 2 h at 37°C. The level of polyP was quantified before and after the nutritional shift.

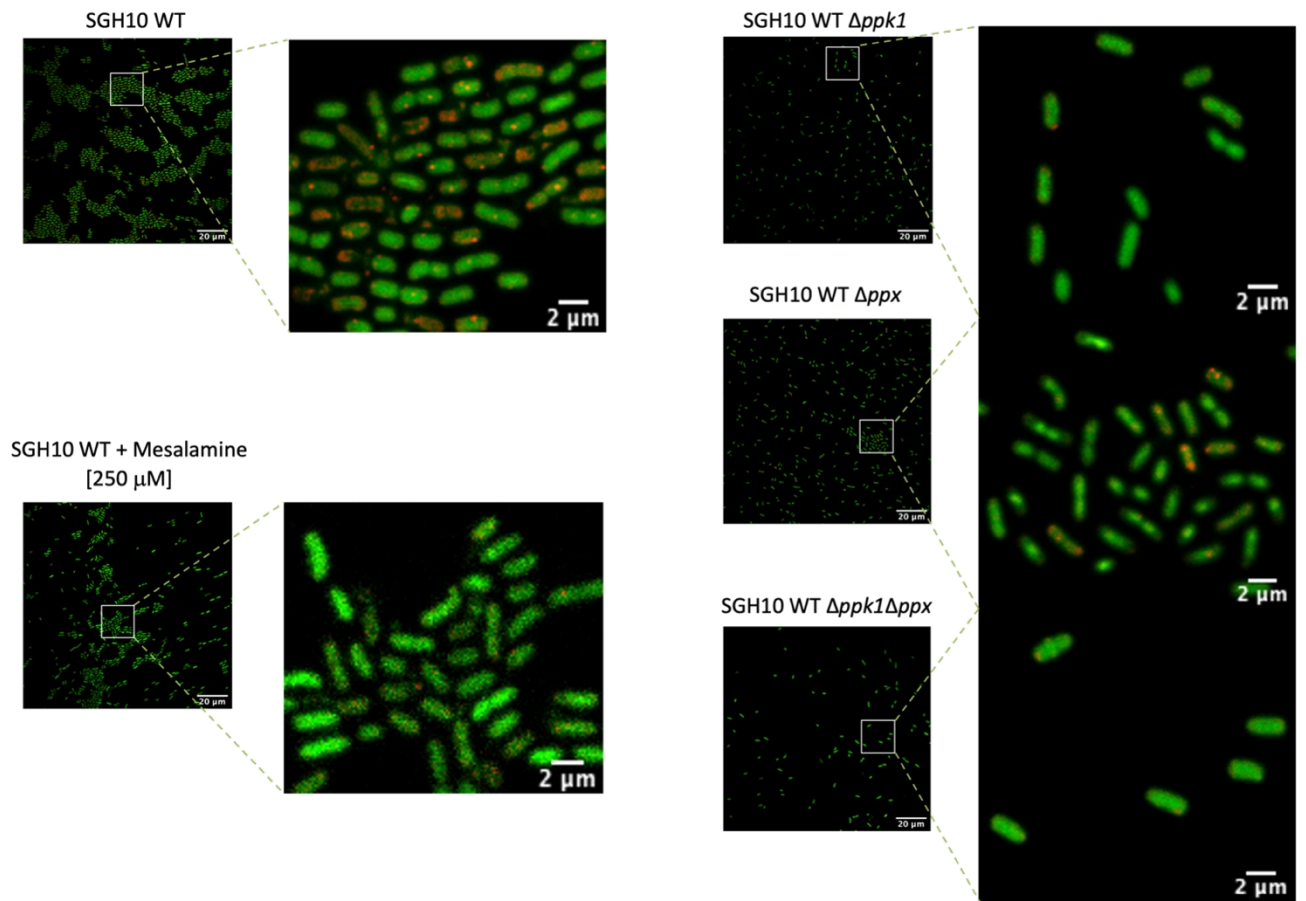


Figure 11. PolyP accumulation in nutrient deprivation. The culture was incubated in the dark with DAPI (5 $\mu\text{g}/\text{ml}$) for 30 minutes for confocal microscopy observation and observed using a 63x immersion objective. For visualization purposes, DAPI-DNA is shown in green, and DAPI-polyP is shown in red.

3.4 Altered mucus and amount of capsule in mutants in polyP metabolism

The capsule is one of the primary and most studied virulence factors in *Klebsiella pneumoniae*. While a wide range of capsular serotypes has been described, capsule types in HvKp are concentrated in a small group, K1 and K2, playing a significant role in the pathogenicity of various strains (Catalán-Nájera et al., 2017; Zhu et al., 2021). Most of these strains exhibit a HMV phenotype related to the length of the polysaccharide rather than its modification (Ovchinnikova et al., 2023). This HMV characteristic results in poor sedimentation during centrifugation, leading to a turbid supernatant, allowing turbidity measurements to serve as a quantitative indicator of HMV (Walker et al., 2020). In our study, we quantified mucoviscosity and observed that the $\Delta ppk1$ and $\Delta ppk1-\Delta ppx$ mutants, but not Δppx , showed significantly decreased HMV compared to the WT strain (Figure 12). As a non-mucoid control, we utilized *E. coli* and the strain *K. pneumoniae* SGH10 $\Delta wcaJ$, which lacks the synthesis of the initial glycosyltransferase WcaJ, resulting in non-mucoid colonies. We observed an absence of mucus in the supernatant, similar to the *E. coli* strain (Figure 12).

Additionally, we investigated the role of uronic acids (UA), essential components in numerous capsules, traditionally serving as indicators of capsule content and quantity (Walker et al., 2019). Interestingly, our results showed a slight but significant reduction in capsule production in the $\Delta ppk1$ and $\Delta ppk1-\Delta ppx$ mutants (Figure 13). Confirmation of the $\Delta wcaJ$ mutant's inability to form a capsule is demonstrated by this assay. These findings highlight the importance of PPK1 enzymatic activity and polyphosphate levels

in regulating capsule formation, further emphasizing their significant role in the virulence of hypervirulent strains.

To explore possible surface modifications contributing to the observed differences in mucoviscosity and capsule quantity in the mutants under study, we conducted scanning electron microscopy (SEM). Previous studies have indicated that the capsule of *K. pneumoniae* SGH10 is uniformly distributed over the cell surface and appears as filamentous projections that extend in multiple directions under SEM visualization (Tan et al., 2020). In line with this, we observed a similar situation in the SGH10 WT strain (Figure 14A). In contrast, the $\Delta ppk1$ mutant, and to a lesser extent, the $\Delta ppk1-\Delta ppx$ mutant, showed differences in capsule distribution in terms of length and surface coverage (Figure 14B and 14D). Since the length of the capsular polysaccharide is directly related to HMV, this result aligns with the significant reduction in mucoviscosity (Figure 12) and decreased capsule levels observed in $\Delta ppk1-\Delta ppx$ and $\Delta ppk1$ (Figure 13). We did not observe significant differences between Δppx and the SGH10 WT strain (Figure 14C). For the $\Delta wcaJ$ mutant, we observed a complete absence of the capsular polysaccharide, resulting in a smooth surface (Figure 14E).

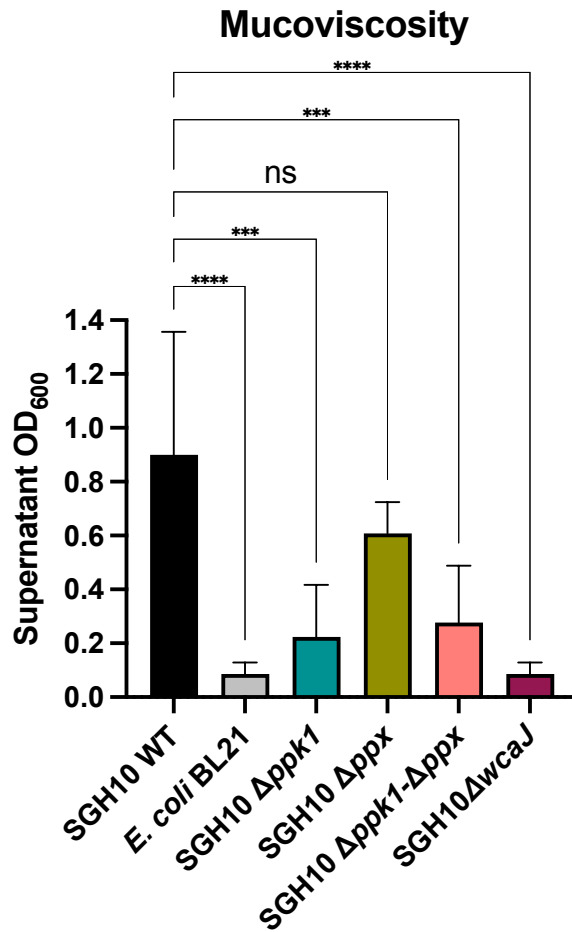


Figure 12. Mucus production in polyP metabolism mutants. (A) Strain mucoid was measured by low-speed centrifugation (3000 rpm for 10 min) in LB. The optical density at 600 nm (OD₆₀₀) of the supernatant above the pellet was measured and mean ± SD was plotted (n = 3). One-way ANOVA tests were performed for statistical analyses comparing the WT strain to the indicated mutants. *, P < 0,05. ***, P < 0,001.

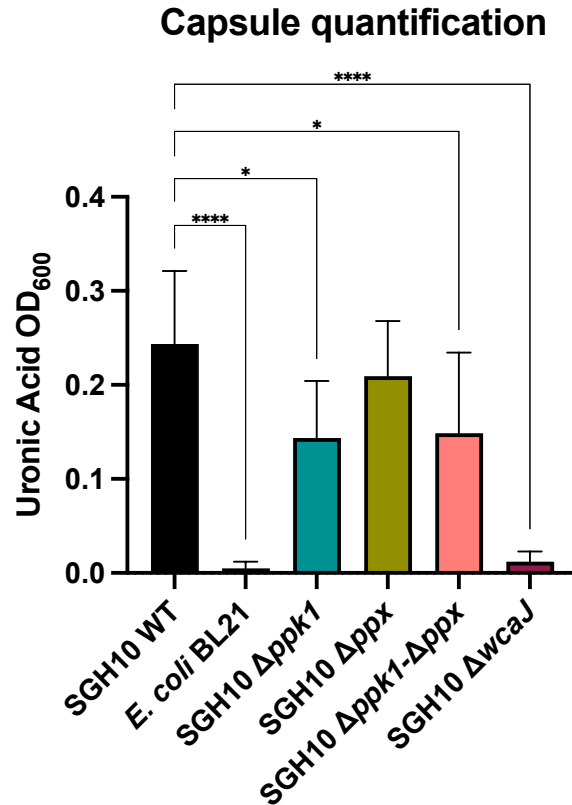


Figure 13. Capsule production. Capsule production of polyP metabolism mutants ($\Delta ppk1$, Δppx and $\Delta ppk1-\Delta ppx$) and $\Delta wcaJ$ strain (without capsule) compared to SGH10 WT strain. Uronic acid quantification analysis as described in Materials and Methods. One-way ANOVA tests were performed for statistical analyses comparing the WT strain to the indicated mutants. *, $P < 0,05$. ****, $P < 0,0001$.

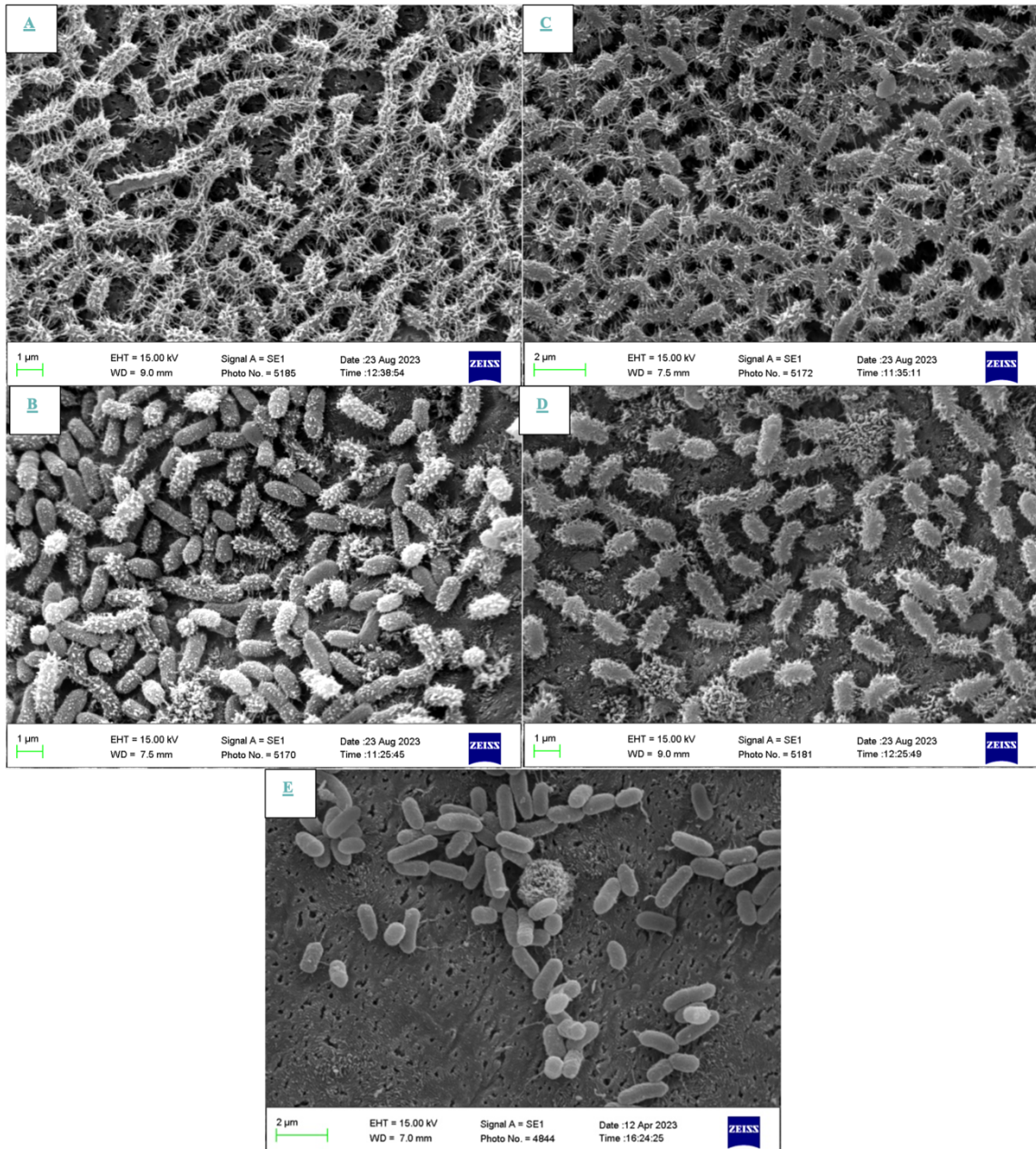


Figure 14. Cell imaging by Scanning electron microscopy. The images display log-phase cultures of (A) SGH10 WT, (B) SGH10 Δ *ppk1*, (C) SGH10 Δ *ppx*, (D) SGH10 Δ *ppk1* Δ *ppx*, and (E) SGH10 Δ *wcaJ* cells fixed in 2.5% glutaraldehyde and stained with 0.15% red ruthenium. The scale bar represents 1-2 μm .

3.5 PPK1 plays a crucial role in biofilm formation.

Biofilm represents the primary lifestyle of bacteria in the environment and within the host (Flemming et al., 2016). Due to how bacteria are structured, their metabolic state, and the protection they provide, biofilm is considered a crucial factor in bacterial virulence. Initial biofilm formation is facilitated by fimbrial adhesins encoded in the core genome (Wang et al., 2020b). These adhesins have significant clinical implications as they contribute to critical processes such as antimicrobial resistance and the chronic persistence of infectious diseases.

To investigate whether mutants involved in polyphosphate metabolism show alterations in biofilm formation, we conducted a biomass quantification assay using crystal violet staining (0.1%). The results revealed that $\Delta ppk1$ and $\Delta ppk1-\Delta ppx$ mutants exhibited a 66% and 56% decrease in biofilm formation compared to the SGH10 WT strain (Figure 15). This decrease was not observed in the Δppx mutant, suggesting that the absence of PPK1 directly affects biofilm formation. Furthermore, we used Mesalamine to validate this observation and observed a 76% reduction in biofilm biomass compared to the SGH10 WT strain.

As a complementary approach to evaluate biofilm formation, we quantified extracellular polymeric substances (EPS). For this purpose, we employed the Ebbabiolight 680 probe (Choong et al., 2016), an optotracer that binds to curli fibers and cellulose, increasing its fluorescence. A significant decrease in EPS levels was observed in $\Delta ppk1$ and $\Delta ppk1-\Delta ppx$ compared to the SGH10 WT strain. No differences were observed in the Δppx mutant (Figure 16). Additionally, the observation of a 24-hour biofilm grown on a

tilted 96-well microtiter plate under the confocal microscope further confirmed that $\Delta ppk1$ (Figure 17B) and $\Delta ppk1-\Delta ppx$ mutants (Figure 17D) exhibited reduced biofilm biomass compared to the WT and Δppx (Fig. 17A and 17C). In the case of the $\Delta wcaJ$ mutant, we observed a significant increase (57%) in the biofilm biomass (Figure 15). This correlates with the observed rise in EPS quantity (Figure 16) and a notable increase in adhered bacteria on the glass surface observed under confocal microscopy (Figure 17E).

To better understand the relationship between polyphosphate metabolism and biofilm formation, we conducted a macrocolony biofilm formation assay in a salt-free LB medium supplemented with Thioflavin S, which selectively binds to cellulose, evidencing possible differences in biofilm structure and organization (Figure 18). The SGH10 WT macrocolony biofilm showed a dense central mucoid region, stained green, possibly by EPS components, showing regular concentric rings. Conversely, the $\Delta ppk1$ mutant showed reduced mucosity in the colony's center, no concentric rings, and a smoother appearance with irregular edges. No evident differences were observed in the Δppx mutant compared to the wild-type strain. In $\Delta ppk1-\Delta ppx$, we observed a reduction in the mucoid ring in the center of the macrocolony biofilm, along with the absence of regular concentric rings. However, the edges were similar to the WT strain, presenting an intermediate phenotype between the wild-type strain and the $\Delta ppk1$ mutant. For the $\Delta wcaJ$ mutant, we observed a flat, dry macrobiofilm that lacked the central mucoid region characteristic of the SGH10 WT strain. However, it displayed similar concentric rings and regular edges, resembling those of the WT strain.

In conclusion, our findings demonstrate that PPK1 plays a crucial role in biofilm formation, affecting not only the proportion of cells that form biofilms (as observed in the microwell biofilm assays) but also EPS production and biofilm organization.

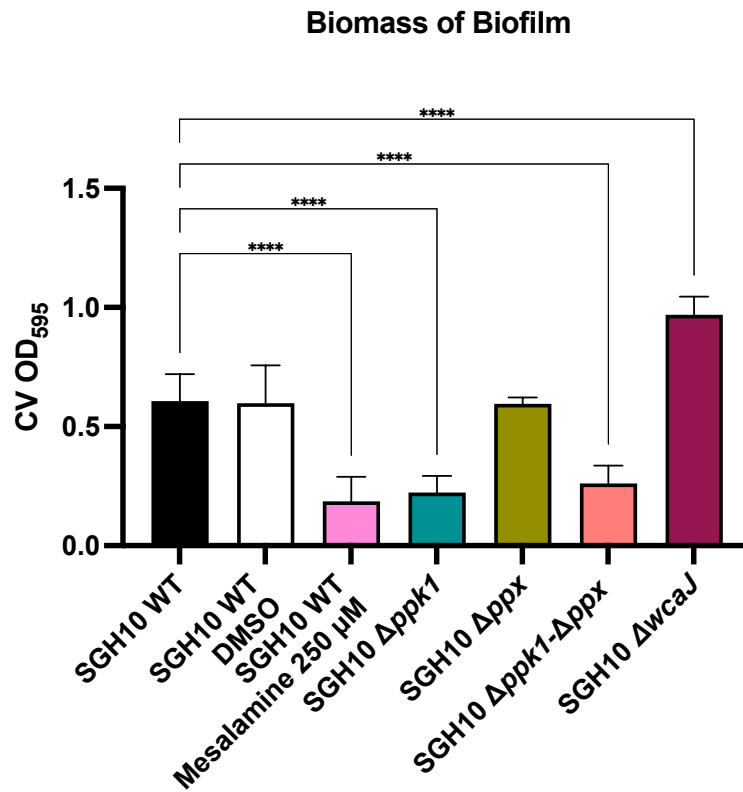


Figure 15. Quantification of biofilm biomass. Relative biofilm formation in mutants in polyP metabolism by crystal violet (CV) staining 0.1%. Overnight cultures were diluted to a OD 0,1 and plated in 96-well plates. The measurement was at 24 hrs at 595 nm.

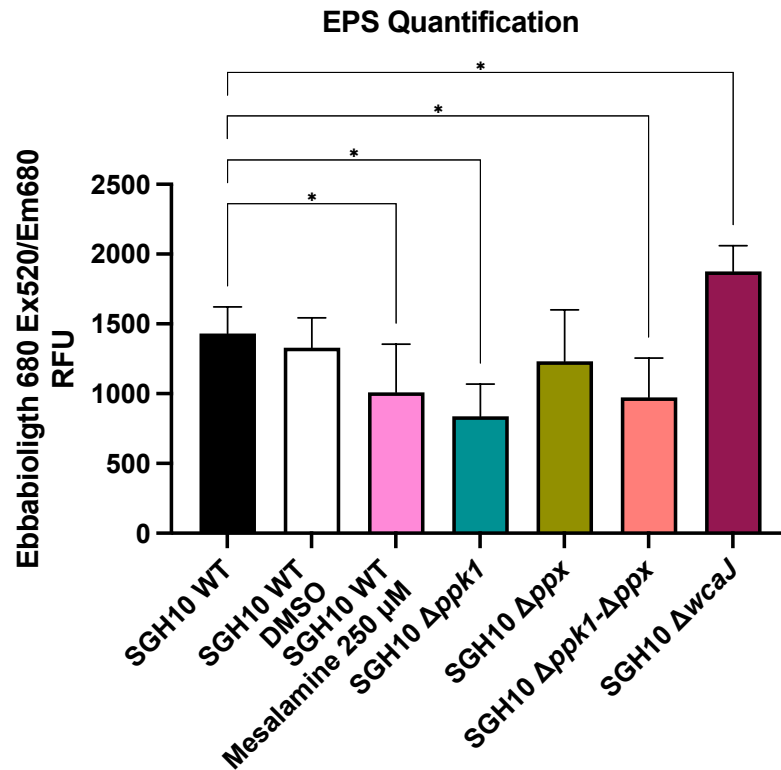


Figure 16. EbbaBiolight 680 is an optotracer for biofilm visualization and binds to cellulose and amyloid components in the biofilm. Colonies were grown on agar plates under biofilm-forming conditions. EbbaBiolight 680™ was diluted in PBS 1:1000 and added 100 µl into each well of a 96-well plate. Pick bacterial colonies from the agar plate and resuspend thoroughly into the pre-filled wells. Plates were placed in Plates in a spectrophotometer to quantify biofilm in the colony resuspensions.

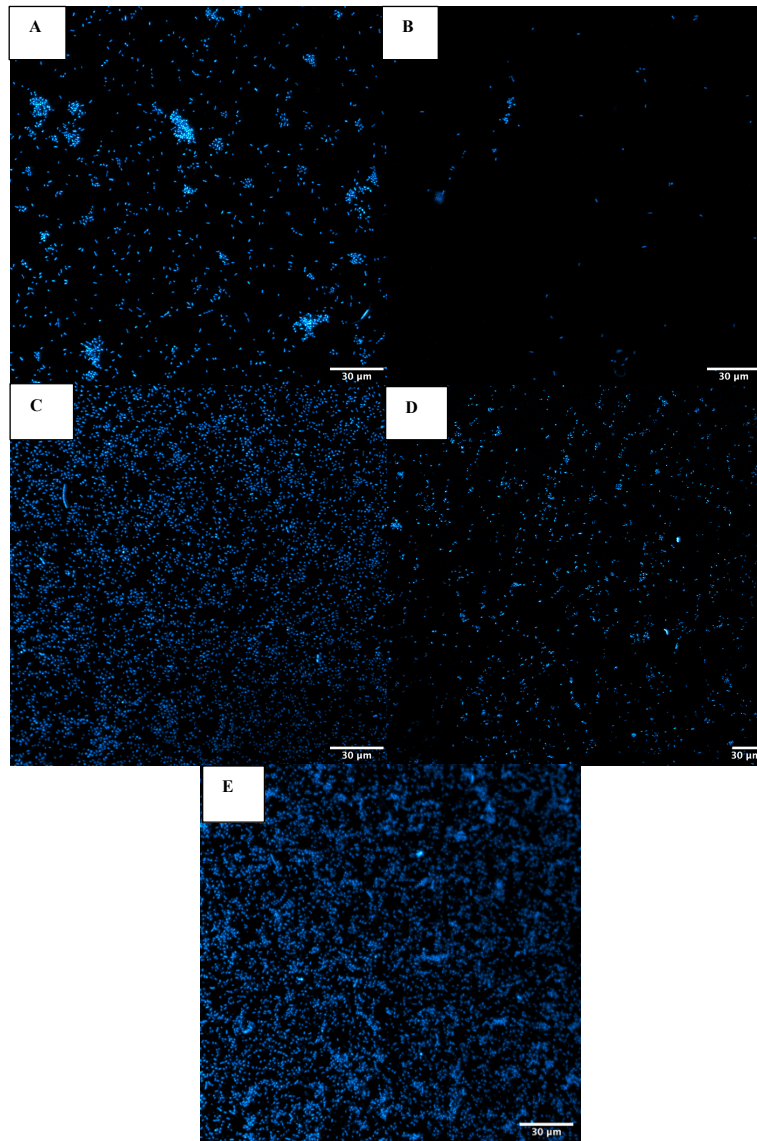


Figure 17. Confocal microscopy of biofilm. Overnight cultures were diluted 1:100 in LB and plated on a glass coverslip on a 6-well plate slanted at 80°. The plate was incubated for 24 hours. (A) SGH10 WT, (B) SGH10 $\Delta ppk1$, (C) SGH10 Δppx , (D) SGH10 $\Delta ppk1-\Delta ppx$, and (E) SGH10 $\Delta wcaJ$ cells. DAPI was used for staining for 30 min, labeling DNA ex/em 358/462. Image obtained in LSM 710 Zeiss microscope, 20X.

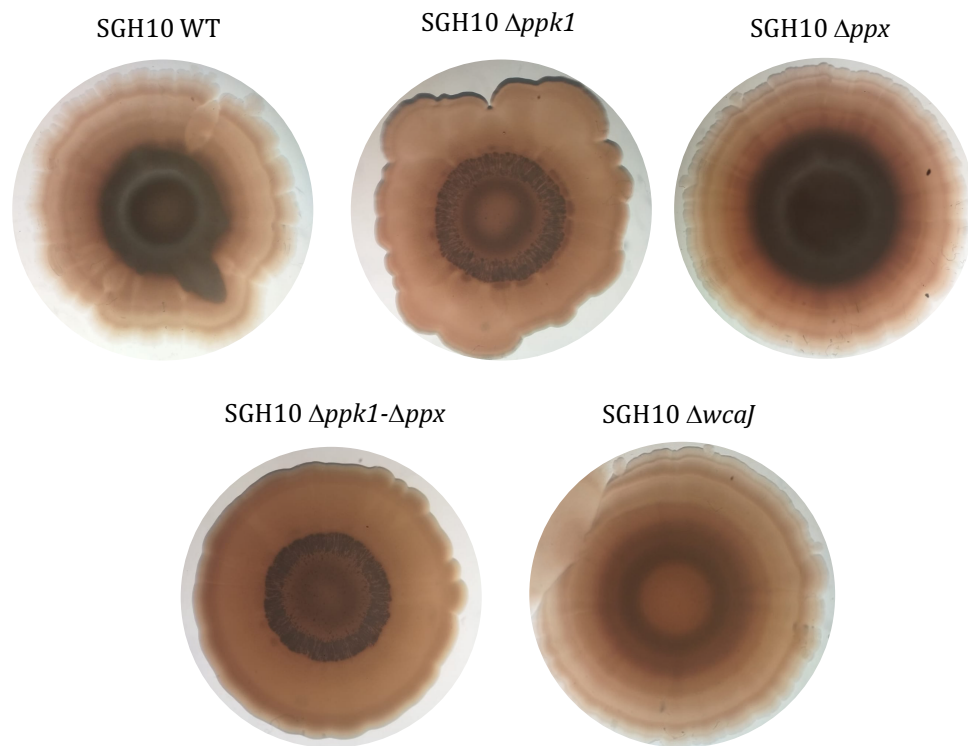


Figure 18. Macrocolony biofilm. It formed by inoculating an overnight culture in LB broth onto LB agar plates supplemented with 40 $\mu\text{g}/\text{mL}$ Thioflavin S. A 5 μL droplet of the culture was used for inoculation. The plates were subsequently incubated at 28 $^{\circ}\text{C}$ for ten days.

3.6 PPK1 is essential for HV *K. pneumoniae* virulence in *D. discoideum*

Our findings conclusively indicate that PPK1 is the primary enzyme responsible for polyP synthesis in the *K. pneumoniae* SGH10 strain and regulates capsule and biofilm formation, traits proposed as relevant for HvKp virulence.

To investigate the impact of polyP and PPK1 deficiency on virulence, we utilized the social amoeba *D. discoideum* as a model host, validated for other *K. pneumoniae* strains (Ortiz-Severín et al., 2015; Bravo-Toncio et al., 2016a; Marcoleta et al., 2018; Varas et al., 2018). When cultivated on lawns of avirulent bacterial strains, *D. discoideum* forms visible phagocytosis plaques. However, the amoeba fails to develop in the presence of virulent strains, and no phagocytosis plaques are observed.

Using this assay, we determined the minimum number of amoebas needed to generate a phagocytosis plaque. As shown before, if phagocytosis plaques are formed with 500 or fewer *D. discoideum* cells, bacteria exhibit susceptibility to predation, indicating attenuated virulence (Paquet and Charette, 2016b).

The resistance to predation of SGH10 WT and mutant derivatives was evaluated on the third and sixth days of the assay (Figure 19). The avirulent strain *K. pneumoniae* KpgE (commonly used as food for *D. discoideum*) was used as control, showing phagocytosis plaques from the third day with amoebas. For SGH10 WT, a phagocytosis plaque was observed only with 50,000 amoebas, indicating the strain's virulence towards *D. discoideum*.

In the case of mutants in polyP metabolism ($\Delta ppk1$; Δppx ; $\Delta ppk1-\Delta ppx$), we observed an attenuation in virulence, evidenced by the presence of phagocytosis plaques with 500 amoeba cells. Additionally, a differential impact on virulence was observed by comparing $\Delta ppk1$ and $\Delta ppk1-\Delta ppx$ with Δppx . On the sixth day, larger phagocytosis plaques were observed in the absence of the *ppk1* gene in both mutants, compared to the Δppx strain. This suggests that the lack of PPK1 has a more pronounced effect on attenuating virulence than the absence of PPX despite both mutations causing a decrease in virulence. Furthermore, to understand the impact of the capsule polysaccharide from the SGH10 strain on virulence, the $\Delta wcaJ$ mutant was also assayed. Phagocytosis plaques were observed by the third day across all concentrations of amoebae studied (Figure 19).

Previous studies have demonstrated that pathogenic bacteria with high virulence capabilities can impede the social development of *D. discoideum* (Bravo-Toncio et al., 2016a; Marcoleta et al., 2018; Varas et al., 2018). Conversely, attenuated or avirulent bacteria have a minimal impact on social development, which involves at least three stages: aggregation, including the formation of a phagocytosis plaque and subsequent cluster formation; elevation, concerning the formation of slugs and fingers; and culmination, comprising the formation and dispersal of fruiting bodies. Figure 20 shows the social development. The avirulent strain KpgE promoted normal social development, culminating between days 2 and 3 with an approximate count of 110 fruiting bodies/cm² on the third day (Figure 21 and 22). In contrast, the SGH10 WT strain inhibited social development within the 6-day study period (Figure 20). We were able to quantify an

average of 2.3 fruiting bodies/cm² on the third day (Figure 21). Mutants in polyP metabolism exhibited varying levels of virulence attenuation. *Δppk1* displayed the most marked effect, almost reaching the culmination of social development on the sixth day (Figure 20), with an average of 38 fruiting bodies/cm² on the third day (Figure 21). This was followed by *Δppk1-Δppx*, which exhibited 17.5 fruiting bodies/cm² on the third day, also reaching a stage before culmination (Figure 21 and 22). *Δppx* behaved as less attenuated, with a count of 2.5 fruiting bodies/cm² on the third day (Figure 21). The *ΔwcaJ* mutant exhibited complete attenuation of virulence, evidenced by the normal progression of social development culminating by day 2-3, with no observable differences compared to the KpgE strain. Additionally, a similar number of fruiting bodies were quantified by the third day, comparable to the KpgE strain.

To gather further evidence supporting our findings, we conducted epifluorescence microscopy to track *D. discoideum's* phagocytosis of bacteria expressing the green fluorescent protein sfGFP constitutively. Amoebas were infected with a MOI=10, and phagocytosis was monitored at 0-, 24-, and 48 h post-infection (Figure 23). For the avirulent KpgE strain, within the first 24 hours, we observed polarized groups of amoebas migrating towards aggregation centers to form multicellular clusters and a significant reduction in the number of bacteria present, as indicated by the decrease in green field fluorescence intensity (Figures 23-24). After 48 h, we observed abundant multicellular aggregation bodies visible at 4X magnification (Figure 23). In the case of the SGH10 WT strain, we did not detect the amoebae polarization characteristic of an aggregation process (Figure 23). Moreover, at 4X magnification, we did not observe well-defined multicellular

aggregation structures. Additionally, we observed substantial bacterial proliferation, as evidenced by a significant increase in green fluorescence intensity at 24 h (Figure 24). For the $\Delta ppk1$ mutant, we observed small amoeba clusters at 24 h and mounds visible at 4X magnification at 48 h (Figure 23). Regarding proliferation, it was significantly lower when compared to the SGH10 WT strain, both at 24 and 48 h (Figure 24). Similar results were obtained with the $\Delta ppk1-\Delta ppx$ mutant. Conversely, no significant differences were observed at 24-48 h between SGH10 WT and the Δppx mutant (Figure 23-24). Regarding the $\Delta wcaJ$ mutant, at 24 hours, we observed polarized groups of amoebas migrating towards aggregation centers to form multicellular clusters and a significant reduction in the number of bacteria present, as indicated by the decrease in fluorescence intensity in the green field (Figures 23-24). After 48 hours, we observed abundant multicellular aggregation bodies visible at 4X magnification (Figure 23), thus confirming the complete attenuation of virulence for this mutant in *D. discoideum*.

In conclusion, our study strongly supports the importance of PPK1 in hvKp virulence.

Predation resistance assay

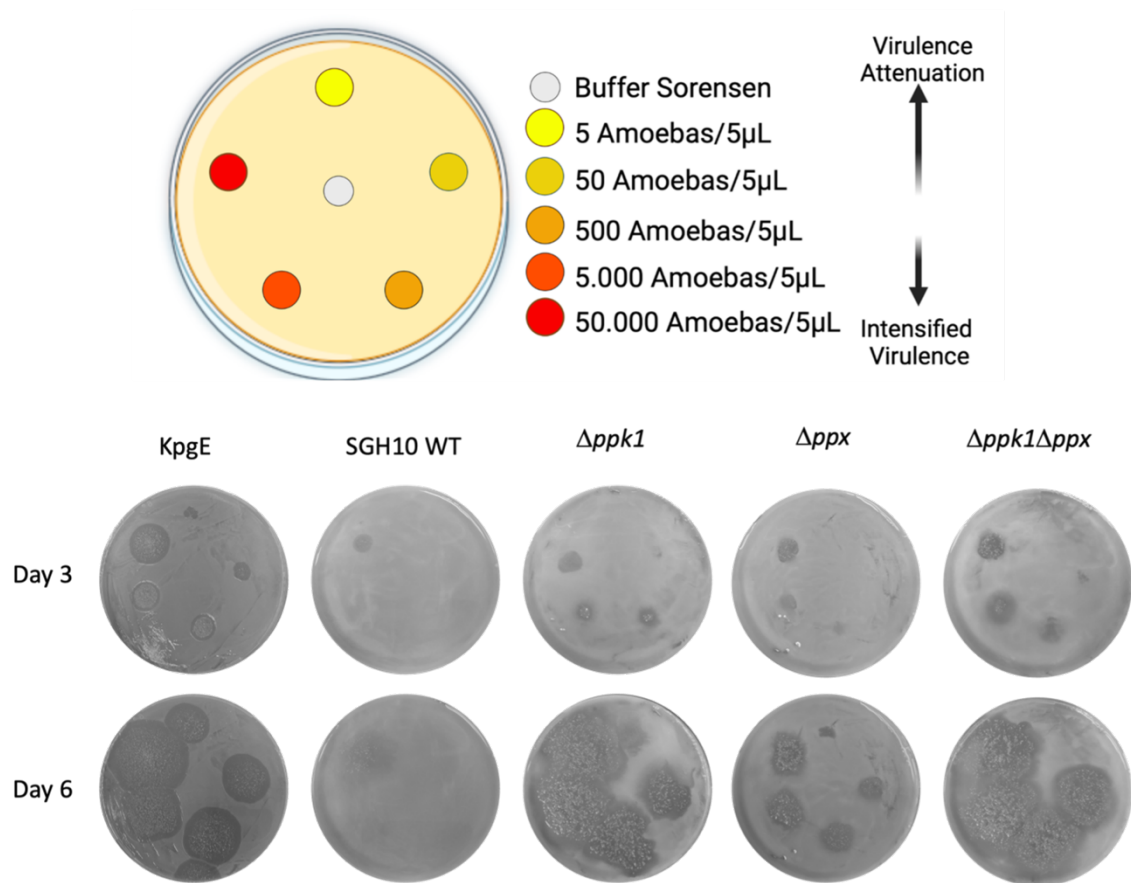


Figure 19. Predation resistance assay. Three hundred μL of overnight culture were seeded onto a plate using a Digralsky loop to generate a bacterial lawn. The plate was left to dry and incubated for 24 hours at 23°C . *D. discoideum* was cultured in HL5 medium, and serial dilutions were prepared to obtain the following cell concentrations: 5 – 50 – 500 – 50.000 cells per $5\ \mu\text{L}$ in Buffer Sorensen. Subsequently, $5\ \mu\text{L}$ of the serial dilutions of *D. discoideum* were applied to the bacterial agar plates. The plates were allowed to dry and were incubated at 21°C for six days. Plaque formation was visually examined on days 3 and 6. Isolates that did not enable amoebae growth were considered virulent for the amoeba. Bacterial strains that exhibited social development with 500 *D. discoideum* were

considered sensitive to predation. Bacterial strains that exhibited social development with 500 *D. discoideum* were considered sensitive to predation

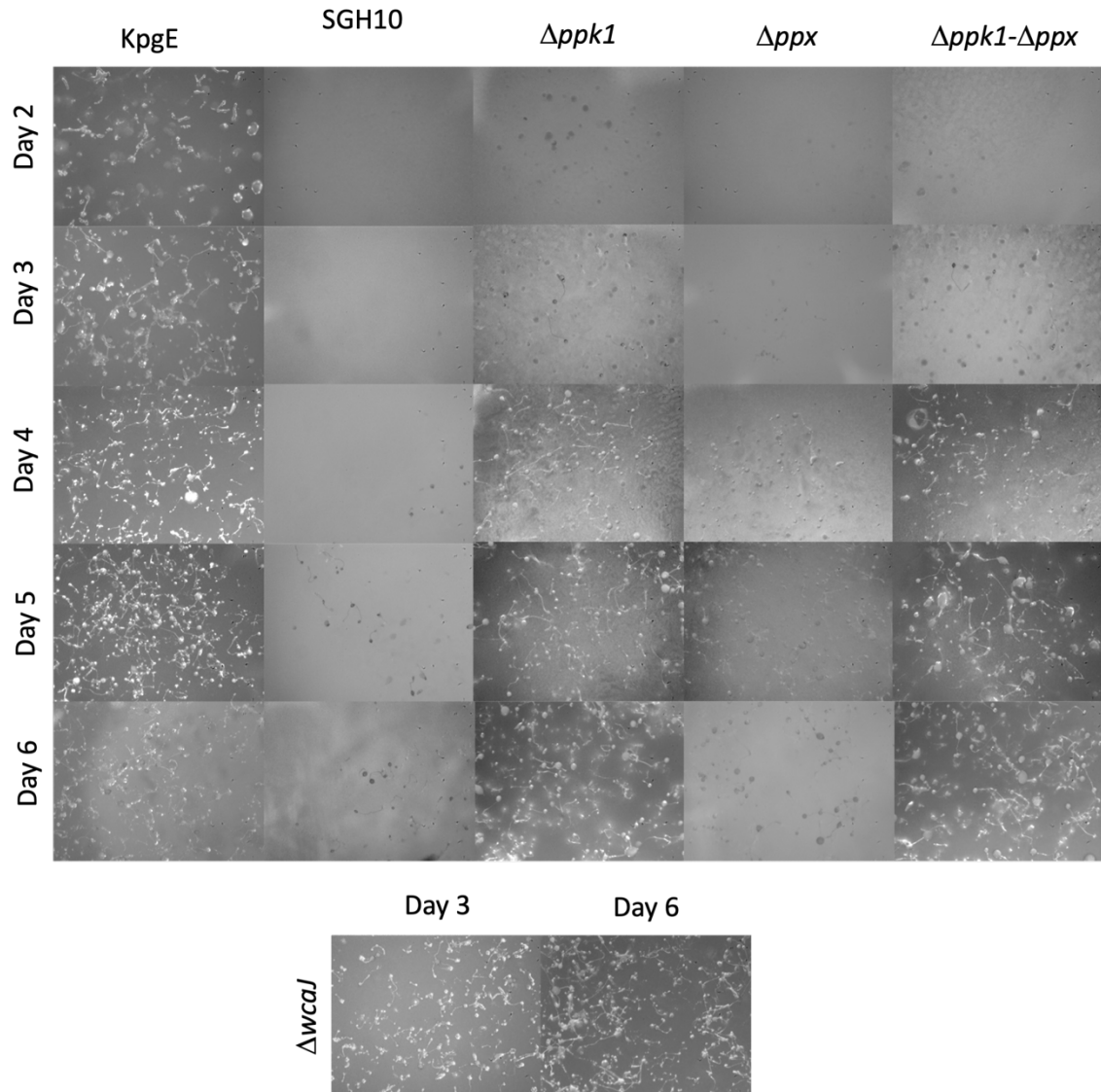


Figure 20. Social development assay. Thirty μL of overnight cultures of the strains under study were inoculated in a 24-well plate on N agar to generate a lawn. They were incubated for 24 hrs at 23 °C. *D. discoideum* was adjusted to $1 \times 10^6/\text{ml}$. A 10 μL drop of the dilution was inoculated on each lawn. The social development of the amoeba was followed for six days. The KpgE commensal strain was used as a control.

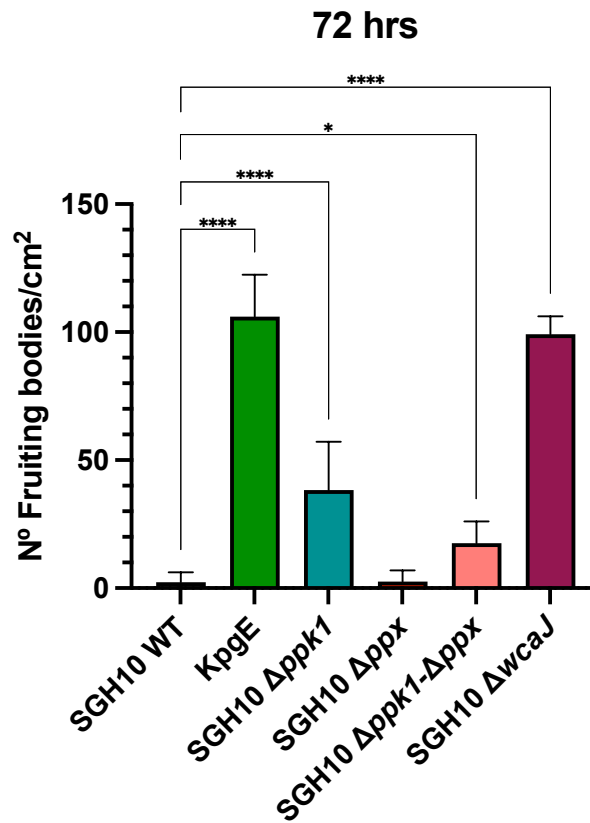


Figure 21 The number of fruiting bodies on the third day was counted and compared with the WT strain. One-way ANOVA tests were performed for statistical analysis, comparing the WT strain to the indicated mutants. **** $p < .00001$, * $p < 0,05$.

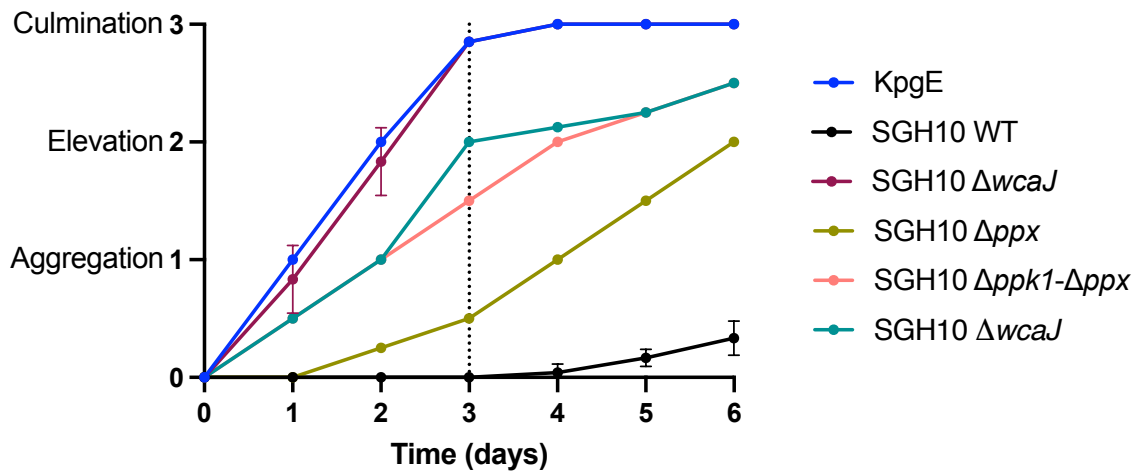


Figure 22. Development progress. It evaluated using a numerical scale defined according to the developmental phase reached at each time point.

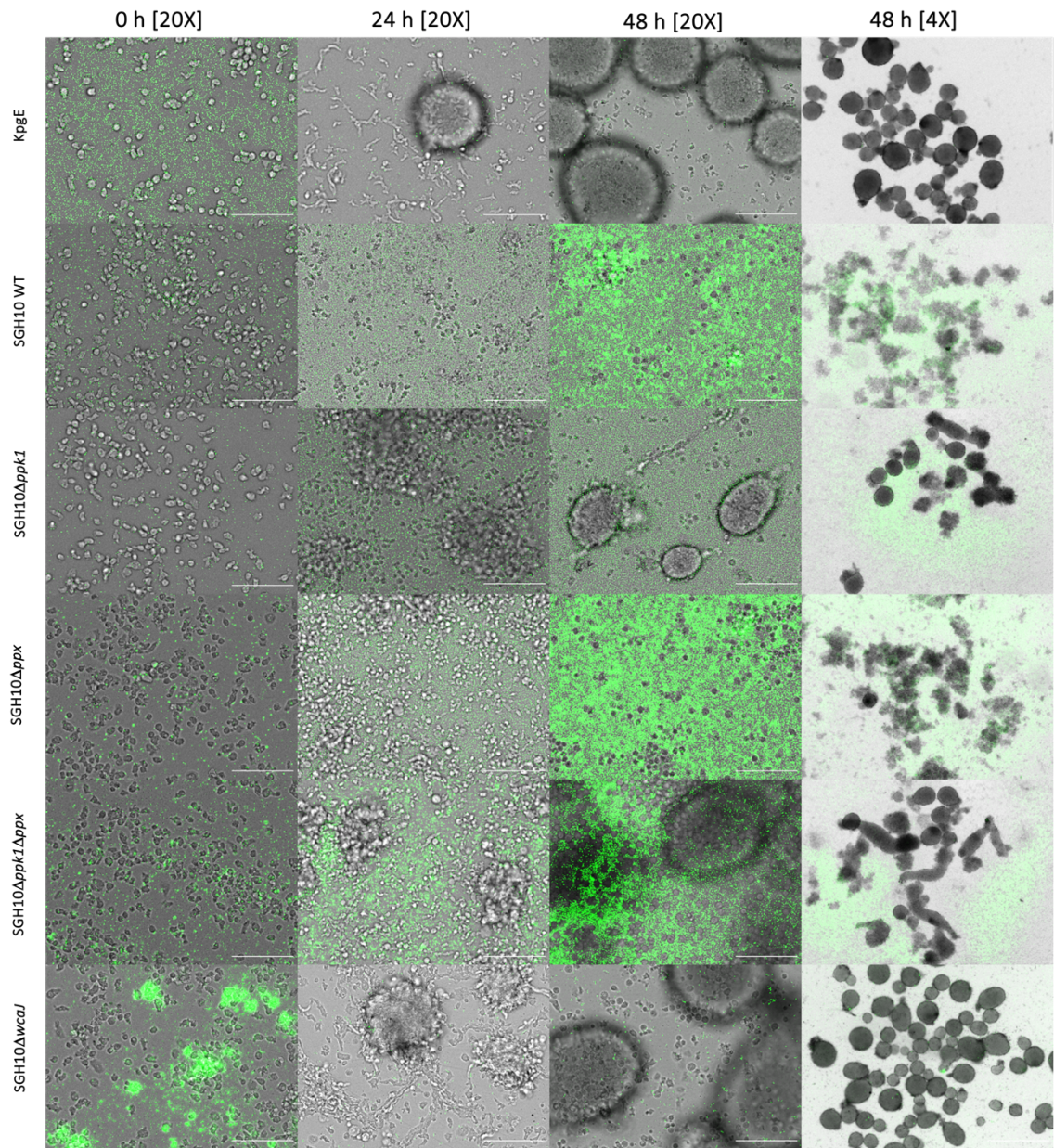


Figure 23. Timelapse of phagocytosis. Timelapse of a 48-hour phagocytosis assay in GFP channel (bacteria). The KpgE strain was used as a control. Scale 100 μ m. Images were acquired using an automated Lionheart FX microscope with a 20X objective. For multicellular development observation, a 4X objective was used.

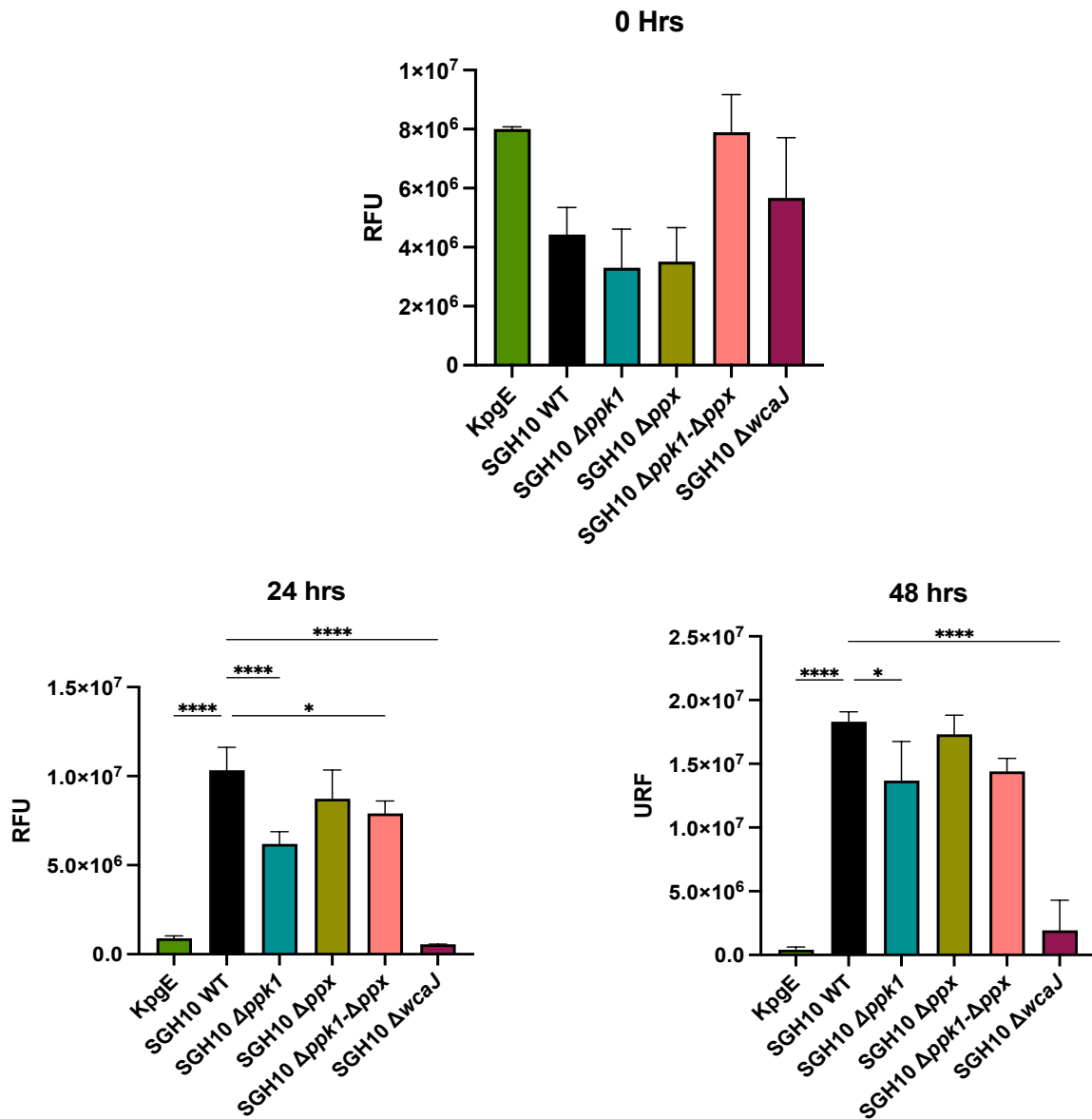


Figure 24. Fluorescence quantification was performed in ImageJ with three biological replicates. One-way ANOVA tests were performed for statistical analyses comparing the WT strain to the indicated mutants **** $p < .00001$, * $p < 0,05$.

3.7 Global Proteomic Profiling Reveals Key Proteins Involved in Virulence in *Klebsiella pneumoniae* SGH10

To investigate the underlying mechanisms responsible for the significant reduction in capsule production, biofilm formation, and virulence, we performed a shotgun proteomic analysis of the mutants with altered polyP metabolism. Samples were obtained from colonies grown on LB agar at 37°C and subjected to LC-MS/MS analysis using a Data Dependent Acquisition method and label-free quantification (LFQ). The WT strain was compared to each mutant strain. Principal component analysis (PCA) on the identified protein dataset, as shown in Figure 25, revealed the grouping of the samples into their corresponding clusters (SGH10 WT, $\Delta ppk1$, Δppx , and $\Delta ppk1-\Delta ppx$ groups). Later, among the 2,287 quantifiable proteins identified, 302, 728, and 673 were determined to be Differentially Expressed Proteins (DEPs) in the comparisons of WT / $\Delta ppk1$, WT / Δppx , and WT / $\Delta ppk1-\Delta ppx$, respectively (Table 3). The quantifiable proteins resulting from these comparisons were visualized as volcano plots (Figure 26), where significantly upregulated proteins were represented in blue and downregulated proteins in red.

To further investigate potential virulence factors associated with the observed results, DEPs were compared against the VFDB database, and those matching with a $\geq 50\%$ identity were selected for further analysis. The virulence factors were categorized into anti-phagocytosis, adherence, iron uptake, and toxins and visualized in a heatmap (Figure 27), a network of curated interactions (Figure 28) and a chordplot (Figure 29). Regarding the Adherence category, we observed a significant reduction in proteins from the *mrk* operon responsible for synthesizing type III fimbriae (MrkB, MrkC, MrkD, MrkH), particularly in the $\Delta ppk1$ mutant, and to a lesser extent in the $\Delta ppk1-\Delta ppx$ mutant.

Additionally, there was an increase in proteins that are part of the type I fimbriae synthesis pathway (FimA and FimC). In the case of Δppx , we observed a significant increase in proteins from type I (FimA, FimC) and type III fimbriae (MrkB, MrkC, MrkD, MrkH). Concerning anti-phagocytosis factors, we observed a significant reduction in essential proteins associated with capsule synthesis, transport, and regulation in *K. pneumoniae*, particularly in the double mutant $\Delta ppk1-\Delta ppx$. This mutant exhibited decreased expression of GalF, Wzi, Wza, WcsT, Wca, Ugd, and Gmd compared to the wild-type strain. Furthermore, in $\Delta ppk1$, Wzi and Ugd proteins showed negative regulation. This correlates with the decrease in the capsule produced by these mutants compared to the SGH10 WT strain. Δppx showed an overexpression of Wzi compared to the SGH10 WT strain.

Concerning iron uptake, proteins related to the synthesis of siderophores such as aerobactin, enterobactin, salmochelin, and yersiniabactin were found to be overexpressed in all polyP mutants, except for yersiniabactin in $\Delta ppk1$, where no significant differences were observed compared to the wild-type strain. Both Δppx and $\Delta ppk1-\Delta ppx$ exhibited upregulation of operons involved in the synthesis of aerobactin and enterobactin, as well as the protein YbtS, which is implicated in the final step of yersiniabactin union and modification, playing a crucial role in the overall siderophore biosynthesis process. In $\Delta ppk1$, several proteins involved in siderophore synthesis, including IucA (aerobactin), EntB, EntC, FepC (enterobactin), and IroD (salmochelin), were found to be overexpressed. Regarding the toxin category, in all polyP metabolism mutants, a significant downregulation was observed in most of the proteins from the colibactin genotoxin biosynthetic cluster. This downregulation was particularly evident in Δppx and

Δppk1-Δppx, affecting proteins such as ClbB, ClbD, ClbF, ClbG, ClbH, ClbI, ClbK, ClbL, ClbN, and ClbQ. In the case of *Δppk1*, the main protein involved in colibactin biosynthesis, ClbB, was downregulated along with ClbD.

In the Lipid A category, we observed a significant increase in proteins involved in the biosynthesis and modification of Lipid A, such as ArnA, ArnB, ArnC, PagP, and LpxO in *Δppx* and *Δppk1-Δppx*. *Δppk1* displayed similar differential expression levels in these proteins; however, no significant differences were observed for ArnA. Additionally, proteins PagP, LpxC, and FabR, related to Lipopolysaccharide (LPS) biosynthesis and modification, exhibited decreased expression levels compared to the WT strain. This prompted us to evaluate whether the differential expression of proteins involved in Lipid A modification would confer colistin resistance (Fig. 30). However, the mutants did not show increased colistin resistance, with a 4 μg/mL MIC. Finally, in Figure 31, we present a z-score plot that considers the abundances of 38 proteins related to each virulence category (adherence, anti-phagocytosis, toxin, siderophores, lipid A), highlighted in the heatmap. In this analysis, the *Δppk1* mutant exhibited a negative z-score compared to the WT for all virulence factors reported in the VFDB database. In conclusion, our global proteomic profiling of polyP metabolism mutants revealed significant alterations in protein expression related to biofilm formation, capsule regulation, iron uptake, and toxin production, corresponding to critical virulence-associated traits in hvKP.

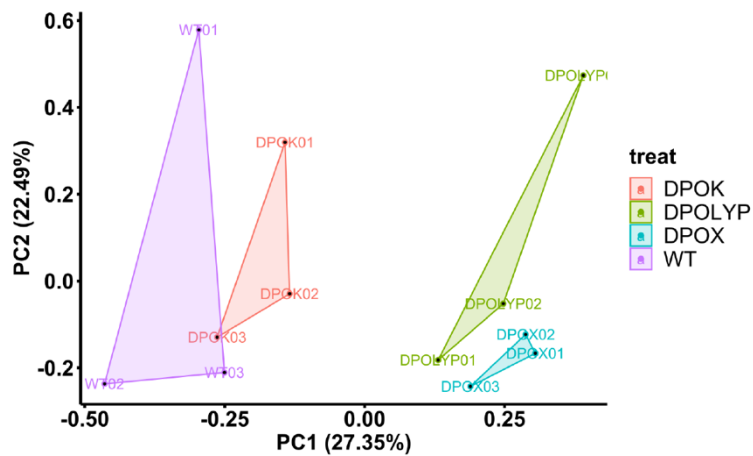
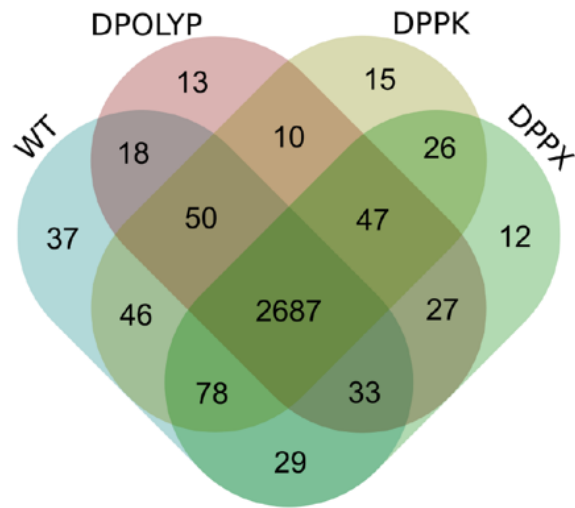


Figure 25. Principal Component Analysis (PCA) of the set of proteins identified per sample. Comparison of the protein group from the sum of all proteins per biological replicate depending on each treatment received.

Table 3. Number of quantifiable proteins and DEPs (Differential Expression Proteins) obtained for each comparison.

Comparison	Proteins	
	Quantifiable	DEPs (FDR < 0,05)
<i>Δppk1</i> vs WT		302
<i>Δppx</i> vs WT	2.287	728
<i>Δppk1-Δppx</i> vs WT		673

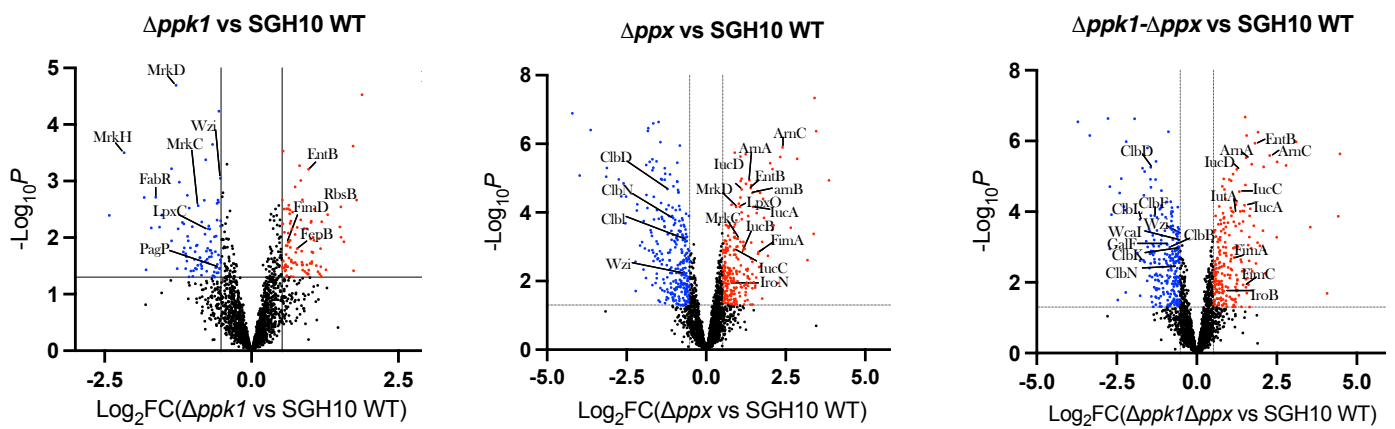


Figure 26. Global proteomic profiling of polyP metabolism mutant of hvKp. Volcano plot of the differentially expressed proteins from the comparison of each of the comparisons made. Red, highly expressed proteins. Blue, lower expressed proteins

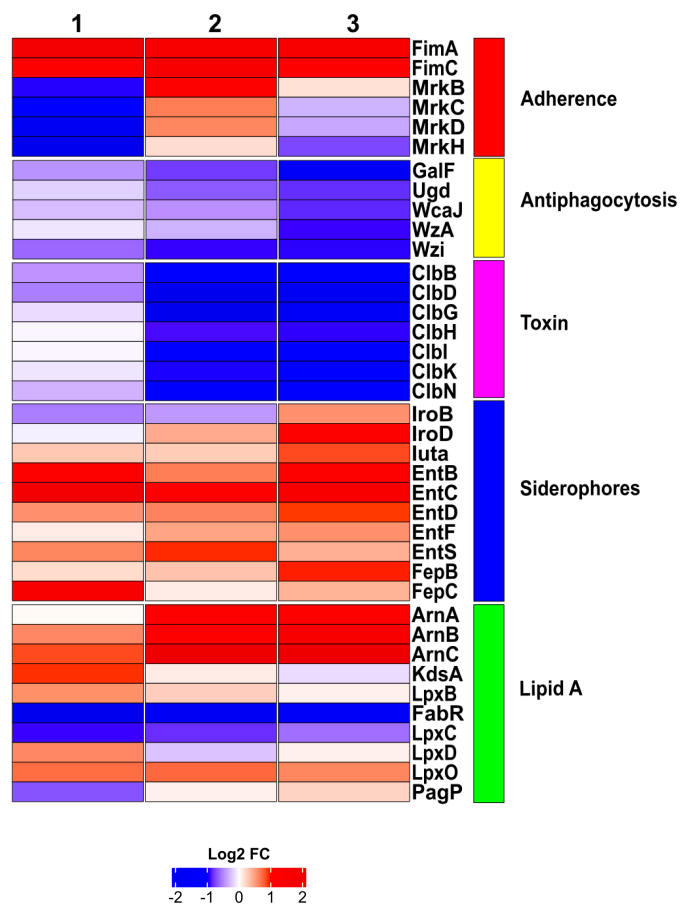


Figure 27. Heatmap shows differentially expressed virulence factors (VF). The proteome was compared with the VDFB database, and the VFs were classified according to the categories: Adherence, anti-phagocytosis, iron uptake, Toxin and Lipid A. (1) $\Delta ppk1$ vs SGH10; (2) Δppx vs SGH10 WT; (3) $\Delta ppk1$ - Δppx vs SGH10 WT.

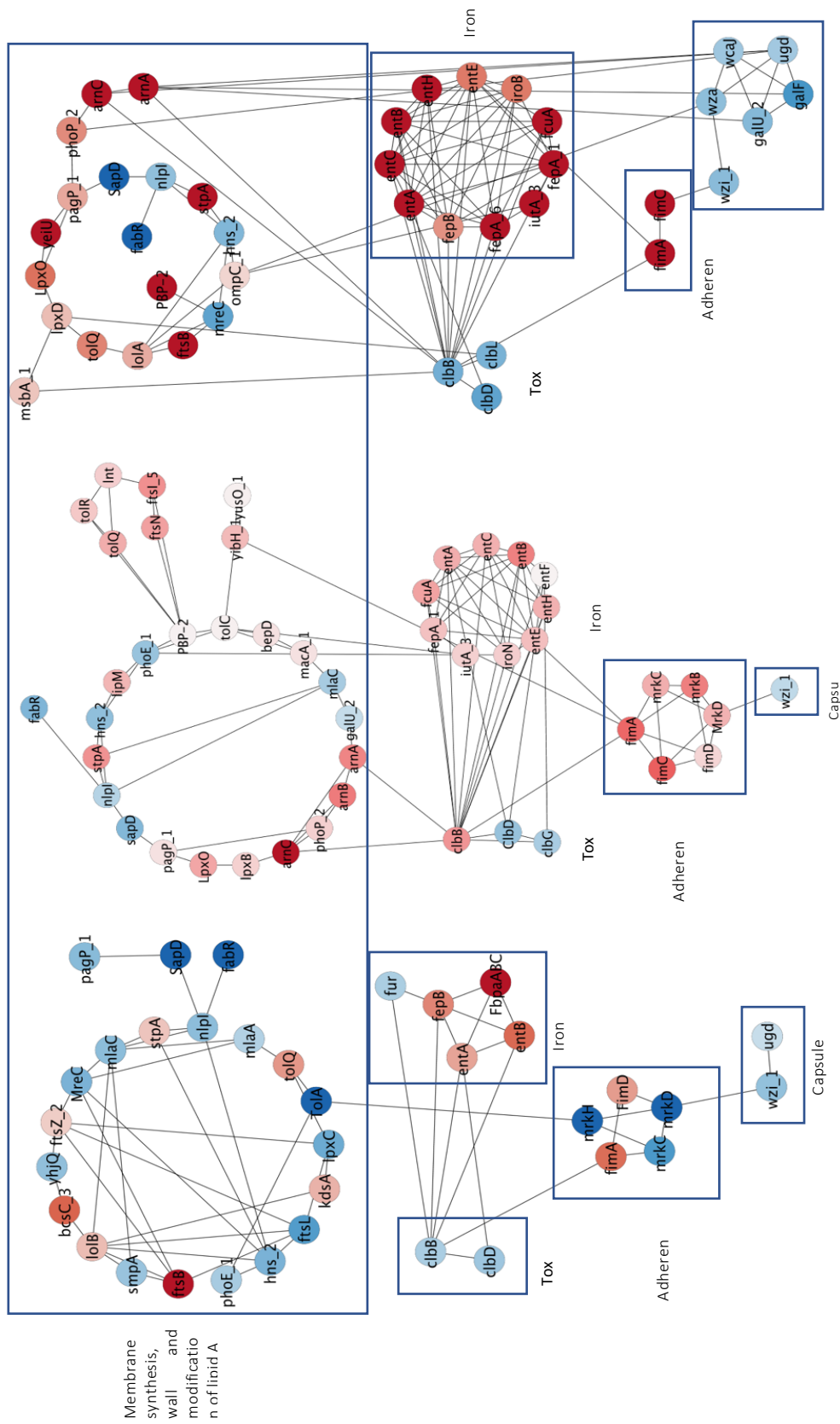


Figure 28. Network of curated interactions between proteins involved in the virulence of *Klebsiella pneumoniae*. Clusters of proteins related to capsule formation and biofilms are observed; siderophore synthesis; formation of membrane, wall and modification of lipid A; antibiotic resistance. The network was generated in Cytoscape.

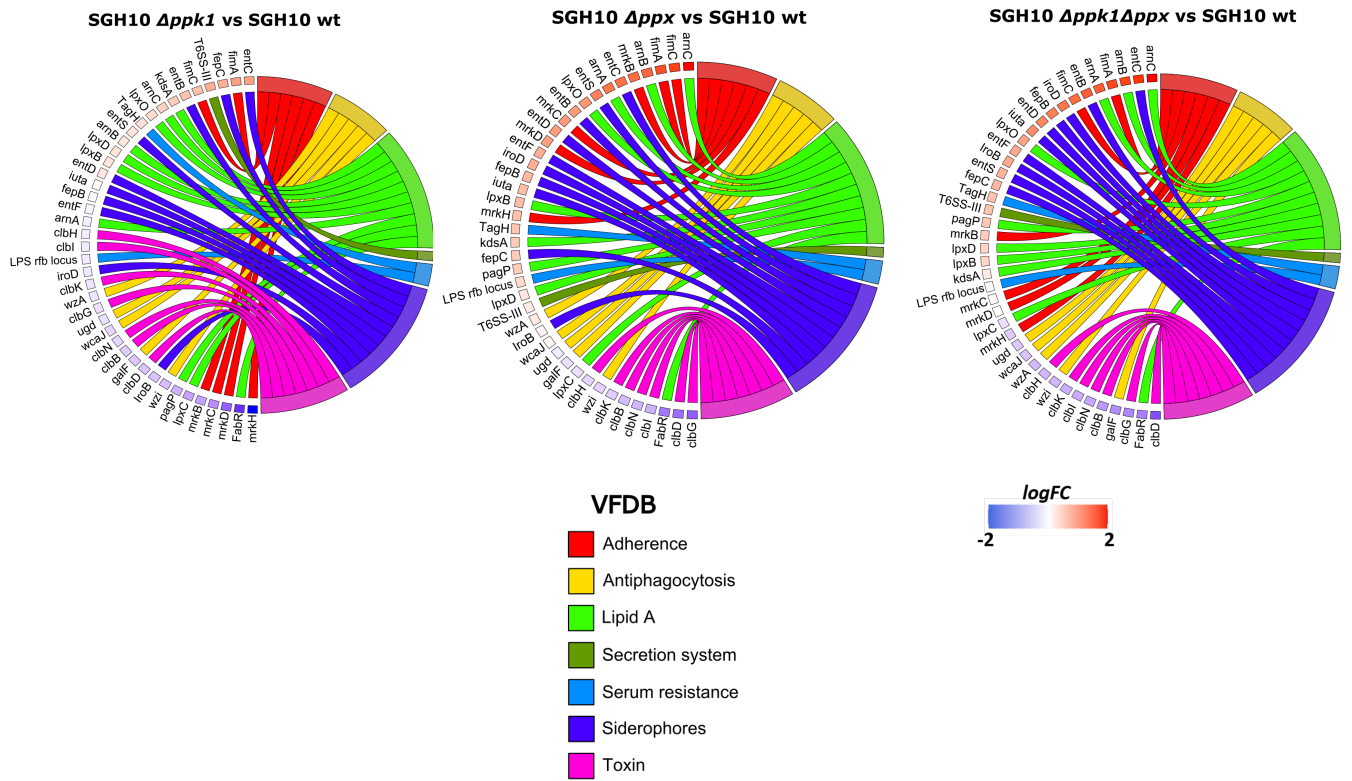


Figure 29. Interaction Chordplot. The chordplot graph illustrates protein-protein interactions categorized based on the VFDB database. Each arc corresponds to an interaction category, while the external nodes represent the identified proteins. The color of each node corresponds to the LogFC value from each analysis.

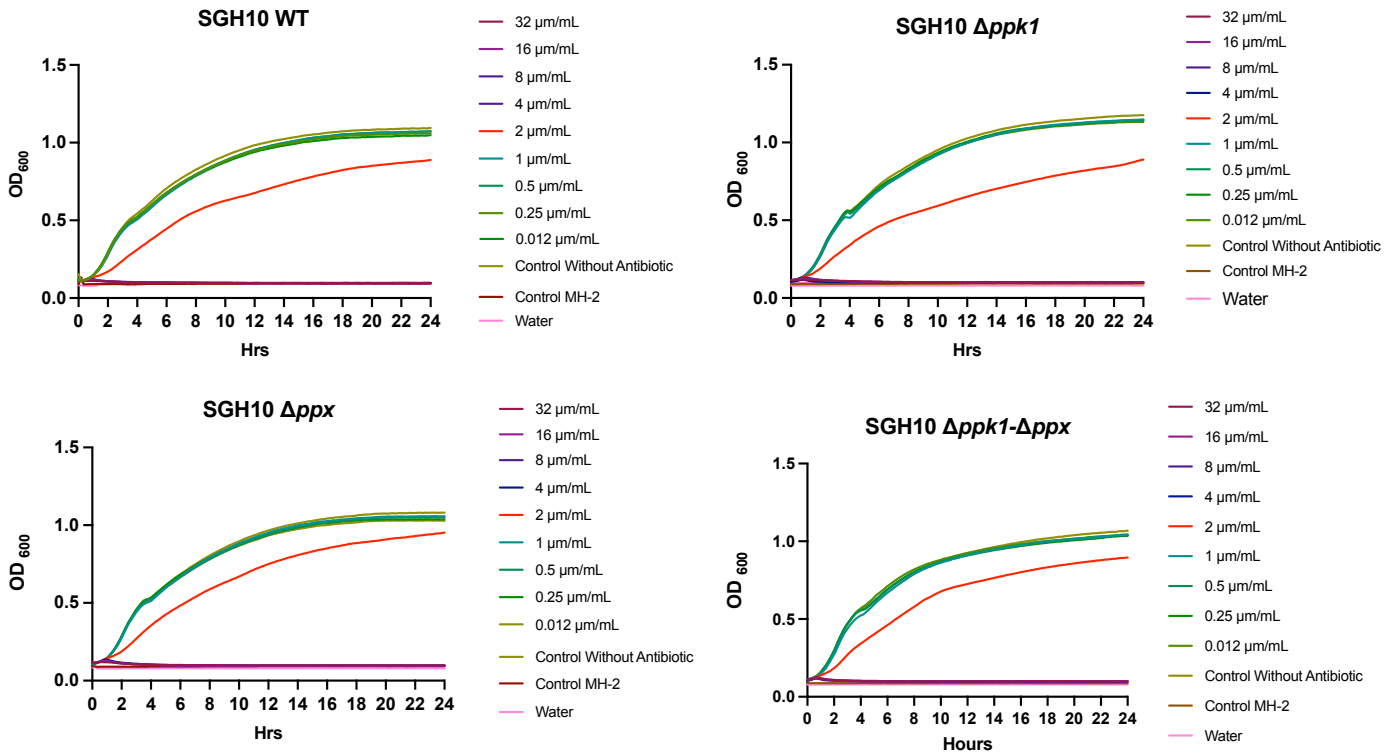


Figure 30. Colistin Resistance Assay. Concentrations ranging from 0.125 to 32 $\mu\text{g/mL}$ were evaluated using liquid cultures. The MIC (Minimum Inhibitory Concentration), the lowest antibiotic concentration that inhibits bacterial growth, was determined using *Pseudomonas aeruginosa* spp. PAO1 as a control.

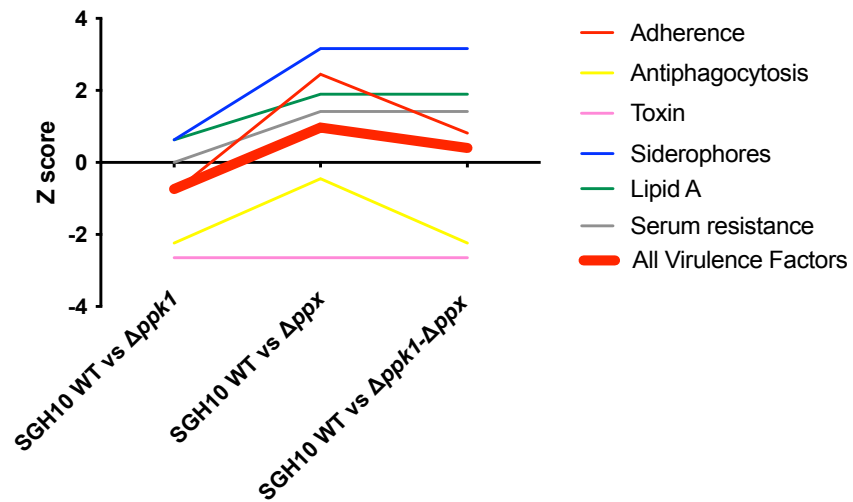


Figure 31. Z-score plot illustrating the global relative abundance of each protein associated with virulence factors. Positive z-scores indicate proteins with higher abundance, while negative z-scores indicate proteins with lower abundance than the overall mean. The red line represents the average of all z-scores for the virulence factors.

4. Discussion

Klebsiella pneumoniae is a growing health threat due to its antibiotic resistance and the emergence of highly virulent strains. These strains can infect healthy individuals and are adept at causing severe infections, posing risks to hospitalized patients and the general population (Wang et al., 2017b; Pal et al., 2019). Traditional approaches targeting bacterial viability through antibiotic use have led to the selection of multidrug-resistant strains, necessitating a shift in strategy. In line with the principle of “Disarm and not kill,” there is an increasing recognition that targeting virulence mechanisms rather than bacterial viability could provide a promising alternative to mitigate the risk of resistance development. In this study, we investigated the involvement of polyP metabolism in ST23 hvKp fitness and virulence, focusing on the PPK1 enzyme and its implications on capsule production, mucoviscosity, biofilm formation, and virulence over the *D. discoideum* host model.

In the hypervirulent strain SGH10, we observed that PPK1 is the primary enzyme responsible for synthesizing inorganic polyphosphates. As anticipated, the absence of PPK1 and a marked reduction in polyP did not substantially impact viability under favorable growth conditions (Lv et al., 2022b). However, when exposed to minimal conditions (stress response), a 2 h delay in reaching exponential growth was observed. This delay is expected, as nutrient scarcity is known to be one of the primary triggers for polyphosphate synthesis, and its absence leads to a noticeable growth delay that eventually recovers when increasing concentrations of polyP are added (Kornberg et al., 1999). In the PPX mutant, a drastic increase in polyP formation or accumulation in response to

nutritional downshift in the MOPS medium (0.4% glucose, 0.1 mM K₂HPO₄) was not observed. The classical model proposed by A. Kornberg's group for *E. coli* suggests that a stress response such as amino acid starvation leads to the accumulation of (p)ppGpp, which interacts with PPX and inhibits it, promoting polyP accumulation. However, based on recent evidences, other factors such as DksA and GreA proteins, significantly regulate polyP accumulation in response to amino acid starvation (Downey, 2019; Gray, 2019). This could explain our observations in the Δppx mutant. However, there is no pronounced effect on viability, suggesting that PPK1 could be an attractive target for antivirulence strategies in this hypervirulent strain. Similar results were reported for *P. aeruginosa* PAO1, where some PPK1 inhibitors affected its virulence, resembling the $\Delta ppk1$ knockout mutant phenotype (Bravo-Toncio et al., 2016b).

Several previous studies have demonstrated that the K1 capsule present in the SGH10 strain is a crucial virulence factor that enables evasion of immune recognition and resistance to phagocytosis (Tan et al., 2020). Recently, it has been shown that the length of the capsular polysaccharide is relevant to the characteristic HMV phenotype of hypervirulent strains, although not exclusive to them (Walker et al., 2020; Ovchinnikova et al., 2023). This length regulation is mediated by the RmpD protein, which interacts with Wzc to regulate polysaccharide length. Our results indicate that PPK1 promotes the HMV phenotype and capsule expression or synthesis. The $\Delta ppk1$ mutant displayed longer sedimentation times during low-speed centrifugation, a standard method to assess mucoviscosity (Palacios et al., 2018).

Additionally, the $\Delta ppk1$ and double mutant cells exhibited lower capsule levels, as indicated by a reduced uronic acid content and an altered distribution of capsule

polysaccharides, distinct from the SGH10 strain (Tan et al., 2020). In addition to the findings in *K. pneumoniae*, a $\Delta ppk1$ mutant of *P. aeruginosa* also shows altered surface structures (Fraley et al., 2007b). In *Neisseria meningitidis*, it has been demonstrated that polyP can interact with the membrane, forming a capsule-like structure (Tinsley et al., 1993a). This indicates that the role of PPK1 and polyP in capsule synthesis and structure may be conserved across different bacterial species.

The presence of polyP appears crucial for the proper assembly and organization of the capsule, and its absence or disruption can lead to abnormalities in the superficial structures. The defective membrane pattern observed in the $\Delta ppk1$ mutant of *P. aeruginosa* suggests that polyP regulates external biomolecule biosynthesis or assembly. Our proteomic analysis of the *K. pneumoniae* $\Delta ppk1$ and $\Delta ppk1-\Delta ppx$ mutants revealed decreased expression of proteins involved in capsular polysaccharide synthesis, such as Wzi-Ugd ($\Delta ppk1$), as well as GalF, GalU, Wza, WcaJ, Ugd ($\Delta ppk1-\Delta ppx$). This downregulation could explain the decrease in capsular polysaccharide production and mucoviscosity, as reported in the HV *K. pneumoniae* strain NTUH-K2044 (Wu et al., 2011). These findings suggest that polyP metabolism may be relevant in regulating capsule expression and the HMV phenotype.

Inorganic polyP may act as a signal molecule, triggering specific regulatory pathways controlling capsule biosynthesis. Similarly to *E. coli* and *P. aeruginosa*, where PPK1 is predominantly associated with the membrane (Fraley et al., 2007a), it is possible that in *K. pneumoniae*, this preferential localization has regulatory roles in biofilm formation and capsule and membrane processes. Furthermore, polyP may act as a phosphate donor to form sugar linkages in the capsule synthesis pathway (Müller et al., 2019). Phosphate is

crucial in numerous biological molecules and processes within bacteria, encompassing the synthesis of polysaccharides integral to the bacterial capsule. Mutants deficient in PPK1 and PPK1-PPX have previously exhibited a phenotype associated with phosphate-related effects in *E. coli* (Varas et al., 2017b). Phosphates are commonly present as phosphate groups in the structure of carbohydrates and other biomolecules. Polysaccharides, which constitute the capsule, can contain phosphate groups as part of their chemical structure or as a modification of their structure (Meredith and Woodard, 2006). These phosphate groups may correspond to side chains or substitutions on the sugar molecules forming the polysaccharide backbone (Perepelov et al., 1999). The presence of phosphate groups in the capsule can have functional implications, contributing to the overall charge and hydrophilicity of the capsule and then influencing its interactions with the environment, such as host tissues and immune cells. Phosphate groups can also be involved in the binding of cations and other molecules, further modulating the properties and functions of the capsule.

Biofilm formation is the primary lifestyle of bacteria in their natural state, serving as a successful strategy to thrive in niches subjected to various stressors and the most efficient way for the trafficking of mobile genetic elements (Element et al., 2023). There is a broad consensus in the literature regarding the ability of both classical and multidrug-resistant *K. pneumoniae* strains to form biofilms in various niches, particularly in immunocompromised individuals (Vuotto et al., 2014; Chhibber et al., 2017; Alcántar-Curiel et al., 2018; Wang et al., 2020b). The *fim* and *mrk* operons, responsible for encoding type I and type III fimbriae, respectively, play a crucial role in the initial adhesion to both biotic and abiotic surfaces (Schumachera and Zenga, 2016). Regarding hvKp strains, it

has been observed that their elongated capsular polysaccharides can cover the fimbriae, hindering their contact with surfaces and resulting in weaker biofilm formation (Dos Santos Goncalves et al., 2014; Wang et al., 2017a). However, conflicting reports suggest that the capsule may promote the formation of biofilm structures, particularly within infectious contexts (Wu et al., 2011; Zheng et al., 2018; Chen et al., 2020b). Our findings demonstrate the capability of the SGH10 strain to form biofilms on polystyrene plates and glass (Figures 15 and 17). The $\Delta ppk1$ and $\Delta ppk1-\Delta ppx$ mutants exhibited reduced biofilm formation compared to the WT strain. These results are consistent with previous reports in various models (Rashid et al., 2000b; Shi et al., 2004a; Drozd et al., 2014; Recalde et al., 2021; Lv et al., 2022b).

Interestingly, the adding of mesalamine, a drug used in the treatment of ulcerative colitis that also inhibits PPK1 (Dahl et al., 2017), induced similar levels of biomass reduction in the biofilm as those observed in $\Delta ppk1$ and $\Delta ppk1-\Delta ppx$ mutant cells, confirming the close association between biofilm formation and polyphosphates. While we observed biofilm formation in the SGH10 WT strain, it was significantly increased in the capsule-deficient $\Delta wcaJ$ mutant. This has been previously reported in an MDR *K. pneumoniae* strain (Pal et al., 2019). As mentioned earlier, several reports suggest that the capsule could prevent fimbriae from contacting surfaces to promote initial adhesion. However, although $\Delta ppk1$ and $\Delta ppk1-\Delta ppx$ mutants exhibited lower mucus and capsule production (indicating a higher biofilm formation), they significantly decreased the biofilm biomass and the total EPS produced. This suggests that PPK1 and polyP regulate both virulence factors through a pathway that has not yet been described.

The proteomic analysis further confirms the relevance of polyP metabolism in biofilm formation. In the case of the $\Delta ppk1$ mutant, we observed a decrease in the levels of MrkC, MrkD, and MrkH, accompanied by an increase in FimA and FimD *proteins*. Conversely, the Δppx mutant significantly increased Fim (FimA, FimC, FimD) and Mrk (MrkB, MrkC, MrkD) proteins. Similarly, the $\Delta ppk1$ - Δppx mutant exhibited elevated levels of FimA and FimC proteins. This dysregulation can be partially explained by a previous report pointing out that polyP degradation during the stationary phase promotes biofilm formation (Grillo-Puertas et al., 2012).

Consequently, the insufficient levels of polyphosphates in the $\Delta ppk1$ and $\Delta ppk1$ - Δppx mutants lead to the downregulation of proteins from the *mrk* operon. However, this explanation does not fully account for the increased proteins from the *fim* operon, indicating the involvement of broader regulatory mechanisms. A recent study has reported a direct correlation between biofilm formation and the colibactin operon in isolates of *E. coli* and *K. pneumoniae* (Ballén et al., 2022; Luo et al., 2023). Furthermore, it has been demonstrated that the inactivation of PPK by mutagenesis reduces the promoter activity of *clbB*, the gene that encodes for an essential enzyme for colistin biosynthesis, and decreases the production level of colibactin (Tang-Fichaux et al., 2020), it is possible that the absence of this enzyme also leads to a decrease in biofilm formation through this pathway. Recently, a phenotypic switch between type III fimbriae and the hypermucoviscous capsule in response to iron levels has been reported in the SGH10 strain (Chu et al., 2023a). The iron-regulated outer membrane protein IroP, encoded in the virulence plasmid, inhibits the expression of the *mrk* operon under low iron conditions, inhibiting biofilm formation. Since polyP is directly involved in intracellular iron

homeostasis as an iron chelator (Beaufay et al., 2020), the observed alterations in the capsule and biofilm might be related to this recently described phenomenon.

In addition, the role of polyP in forming functional amyloids in prokaryotes and its potential relationship with the appearance of these fibers in the context of biofilms should be considered (Erskine et al., 2018). Several amyloid-like proteins, such as curli in *E. coli*, have been described, highlighting the potential significance of amyloid formation in bacterial biofilms. Although *K. pneumoniae* lacks the curli operon, the GIE492 genomic island enabling the production of the antimicrobial peptide microcin E492 is highly prevalent among hvKp (Bieler et al., 2005). This microcin forms amyloid fibers in the culture supernatant of producing cells (Marcoleta et al., 2016). Although the biological role of this phenomenon is still unclear, it could be a structural part of biofilms.

Furthermore, it is worth considering the potential role of interbacterial communication and quorum sensing in biofilm formation. The coordinated behavior of bacteria within the biofilm community relies on intricate signaling networks that enable collective responses and establish structured microbial communities (Flemming et al., 2016). Further investigations regarding the interplay between polyphosphates, quorum sensing systems, and other signaling pathways will provide valuable insights into the complex dynamics of biofilm formation and the development of targeted interventions. Based on our findings, we propose that polyP could serve as potential extracellular signaling molecules within the biofilm matrix, acting as an energy source for dynamic biofilm processes and as a structural component due to their polyanionic nature, like eDNA (Müller et al., 2019). Further studies are warranted to ascertain the essential role of polyP as biofilm constituents rather than solely intracellular signaling molecules. Understanding the

intricate regulatory pathways involved, including interbacterial communication and quorum sensing, will provide valuable knowledge for developing strategies to control biofilm-associated infections and enhance the efficacy of antimicrobial therapies.

Unlike classical *K. pneumoniae* strains, which can be rapidly cleared during infection by the host defense system, hvKp strains can evade and resist macrophage- and neutrophil-mediated killing. However, *K. pneumoniae* is generally considered an extracellular pathogen (Paczosa and Meccas, 2016). However, reports show that hvKp strains can persist intracellularly for more than 24 hours by diverting the canonical endocytic pathway and surviving in a phagosome not associated with lysosomes (Cano et al., 2015). In this regard, *D. discoideum* has been successfully used as a host model to study virulence and phagocytosis resistance (Froquet et al., 2009; Bravo-Toncio et al., 2016a). Here, the predation resistance assay demonstrated the contribution of polyP metabolism to the virulence of the hypervirulent SGH10 strain (Figure. 5A). This reflects the involvement of PPK1 in mediating key aspects of virulence in hvKp.

The amoeba model also allowed us to evaluate alterations in social development, which, under standard laboratory conditions, takes two to three days to go through the stages of aggregation, elevation, and culmination (Varas et al., 2018). In the presence of a virulent strain, this process can be delayed or may not occur at all. $\Delta ppk1$ and $\Delta ppk1-\Delta ppx$ mutants showed reduced virulence with more fruiting bodies by the 3rd day. These results provide insight into the influence of polyP metabolism in this hypervirulent strain, as documented in other pathogens. The significant reduction in capsular polysaccharide production and the decrease in polysaccharide length would enhance the ability of *D. discoideum* to recognize molecular patterns such as fimbriae and LPS, promoting

phagocytosis. This idea is reinforced by using the $\Delta wcaJ$ mutant, which showed complete virulence attenuation due to the capsule's absence.

Additionally, the reduction in colibactin expression could potentially contribute to the attenuated virulence over this host model. Furthermore, long-chain bacterial polyphosphates (> 300 mer) have been shown to interfere with immune cell signaling pathways, preventing the arrival of macrophages and neutrophils at the site of infection (Bowlin and Gray, 2021) and inhibiting phagolysosome formation in *D. discoideum* (Rijal et al., 2020). The lack of polyP could make the bacteria more vulnerable to the immune response, as it cannot manipulate or prevent phagolysosome fusion.

We were particularly intrigued by the significant increase in the pool of siderophores in all mutants, especially in Δppx and $\Delta ppk1-\Delta ppx$ mutants. It has been recently reported that polyP can sequester free iron, acting as a reservoir under non-stress conditions and blocking the formation of reactive oxygen species (ROS) during stress by inhibiting the Fenton reaction (Beaufay et al., 2020). We believe that alterations in polyP metabolism might dysregulate the expression of siderophores under non-stress conditions, particularly in the Δppx mutant that accumulates slightly higher levels of polyP. The absence of PPX implies a reduced capacity for polyP degradation and, consequently, a reduced release of intracellular iron under these conditions. This could serve as a signal to induce the expression of siderophores to compensate for the lack of free iron necessary for metabolic activities.

It has been reported that aerobactin is essential for the pathogenicity in hvKp strains. Approximately 93% to 100% of hvKp strains synthesize aerobactin, with its genes

encoded on the virulence plasmid, accounting for about 90% of the siderophore activity (Russo and Marr, 2019). However, in our virulence assessment using *D. discoideum* under the studied conditions, we observed an attenuation in virulence, particularly in both $\Delta ppk1$ and $\Delta ppk1-\Delta ppx$ strains, which led to increased levels of siderophores. A recent report has suggested that the coexistence of *c-rmpA* with *p-rmpA* and *p-rmpA2* increases the lethality of K1 *K. pneumoniae* strains and the development of hepatic abscesses more than the coexistence of siderophores (Hu et al., 2023). Each virulence factor present in *K. pneumoniae* participates in the infectious process depending on external signals, as in the case of the recently described *iroP* switch (Chu et al., 2023b), where iron favors biofilm formation in iron-rich environments such as the intestine while reducing capsule production. Therefore, in our virulence model, the capsule becomes highly relevant as a mechanism hvKp strains use to evade phagocytosis. Further virulence assessments in other models are needed to determine if our observations regarding virulence attenuation are replicated.

Despite the extensive body of literature focusing on PPK1, the role of PPX in the physiology of either non-pathogenic or pathogenic bacteria remains largely unexplored. Particularly regarding the virulence traits manifested in Δppx mutants in bacteria, it has been reported that PPX is essential for the pathogenesis of *Mycobacterium tuberculosis* (Thayil et al., 2011), *Bacillus cereus* (Shi et al., 2004b) and *Neisseria meningitidis* (Tinsley et al., 1993b). Our findings in Δppx mutant demonstrated no significant alteration in its ability to evade phagocytosis and impact the development of amoeba's social life. In summary, our research highlights the role of polyP synthesis in modulating extracellular biomolecules and virulence factors in hypervirulent ST23 *K. pneumoniae*.

The study offers valuable insights into possible therapeutic targets for its treatment. However, more research is needed to fully understand the intricate relationship between polyP metabolism, siderophores, biofilm, capsule and the virulence of the ST23 *Klebsiella* hypervirulent strains.

5. Conclusions

This thesis aimed to study the impact of polyP metabolism on various virulence factors described for HvKp strains and how the disruption of this metabolism can attenuate virulence in the *D. discoideum* infection model. Given the limited number of articles related to polyP and *K. pneumoniae*, especially in HvKp strains, this thesis contributes to the research body in this area.

Based on the results, it was found that the enzyme PPK1 is essential for polyphosphate synthesis and plays a role in capsule formation, hypermucoviscosity, and biofilm formation. The absence of PPK1 affected growth under stress and the expression of genes related to capsules and biofilms. Furthermore, the mutants showed changes in siderophore production, suggesting an interaction with iron homeostasis. These findings highlight PPK1 as a potential target to mitigate virulence and enhance antimicrobial strategies in hypervirulent strains of *K. pneumoniae*.

6. Bibliographic references

- Alanis, A. J. (2005). Resistance to antibiotics: Are we in the post-antibiotic era? *Arch Med Res* 36, 697–705. doi: 10.1016/j.arcmed.2005.06.009.
- Alcántar-Curiel, M. D., Ledezma-Escalante, C. A., Jarillo-Quijada, M. D., Gayosso-Vázquez, C., Morfín-Otero, R., Rodríguez-Noriega, E., et al. (2018). Association of Antibiotic Resistance, Cell Adherence, and Biofilm Production with the Endemicity of Nosocomial *Klebsiella pneumoniae*. *Biomed Res Int* 2018. doi: 10.1155/2018/7012958.
- Arcari, G., Raponi, G., Sacco, F., Bibbolino, G., Di Lella, F. M., Alessandri, F., et al. (2021). *Klebsiella pneumoniae* infections in COVID-19 patients: a 2-month retrospective analysis in an Italian hospital. *Int J Antimicrob Agents* 57, 2020–2022. doi: 10.1016/j.ijantimicag.2020.106245.
- Archibald, L., Phillips, L., Monnet, D., McGowan, J. E., Tenover, F., and Gaynes, R. (1997). Antimicrobial resistance in isolates from inpatients and outpatients in the United States: Increasing importance of the intensive care unit. *Clinical Infectious Diseases* 24, 211–215. doi: 10.1093/clinids/24.2.211.
- Ares, M. A., Fernández-Vázquez, J. L., Pacheco, S., Martínez-Santos, V. I., Jarillo-Quijada, M. D., Torres, J., et al. (2017). Additional regulatory activities of MrkH for the transcriptional expression of the *Klebsiella pneumoniae* mrk genes: Antagonist of H-NS and repressor. *PLoS One* 12, 1–16. doi: 10.1371/journal.pone.0173285.
- Bachman, M. A., Oyler, J. E., Burns, S. H., Caza, M., Lépine, F., Dozois, C. M., et al. (2011). *Klebsiella pneumoniae* Yersiniabactin Promotes Respiratory Tract Infection through Evasion of Lipocalin 2. *Infect Immun* 79, 3309–3316. doi: 10.1128/IAI.05114-11.
- Baijal, K., and Downey, M. (2021). Targeting Polyphosphate Kinases in the Fight against *Pseudomonas aeruginosa*. *mBio* 12. doi: 10.1128/mBio.01477-21.
- Ballén, V., Gabasa, Y., Ratia, C., Sánchez, M., and Soto, S. (2022). Correlation Between Antimicrobial Resistance, Virulence Determinants and Biofilm Formation Ability Among Extraintestinal Pathogenic *Escherichia coli* Strains Isolated in Catalonia, Spain. *Front Microbiol* 12. doi: 10.3389/fmicb.2021.803862.
- Beaufay, F., Quarles, E., Franz, A., Katamanin, O., Wholey, W.-Y., and Jakob, U. (2020). Polyphosphate Functions *In Vivo* as an Iron Chelator and Fenton Reaction Inhibitor. *mBio* 11. doi: 10.1128/mBio.01017-20.
- Berbudi, A., Rahmadika, N., Tjahjadi, A. I., and Ruslami, R. (2020). Type 2 Diabetes and its Impact on the Immune System. *Curr Diabetes Rev* 16, 442–449. doi: 10.2174/1573399815666191024085838.
- Bertani, B., and Ruiz, N. (2018). Function and Biogenesis of Lipopolysaccharides. *EcoSal Plus* 8. doi: 10.1128/ecosalplus.ESP-0001-2018.
- Bieler, S., Estrada, L., Lagos, R., Baeza, M., Castilla, J., and Soto, C. (2005). Amyloid Formation Modulates the Biological Activity of a Bacterial Protein. *Journal of Biological Chemistry* 280, 26880–26885. doi: 10.1074/jbc.M502031200.

- Bowlin, M. Q., and Gray, M. J. (2021). Inorganic polyphosphate in host and microbe biology. *Trends Microbiol* 29, 1013–1023. doi: 10.1016/j.tim.2021.02.002.
- Bozzaro, S., and Eichinger, L. (2011). The Professional Phagocyte Dictyostelium discoideum as a Model Host for Bacterial Pathogens. Available at: <http://dictybase.org/>.
- Bravo-Toncio, C., Álvarez, J. A., Campos, F., Ortíz-Severín, J., Varas, M., Cabrera, R., et al. (2016a). Dictyostelium discoideum as a surrogate host–microbe model for antivirulence screening in Pseudomonas aeruginosa PAO1. *Int J Antimicrob Agents*, 1–7. doi: 10.1016/j.ijantimicag.2016.02.005.
- Bravo-Toncio, C., Álvarez, J. A., Campos, F., Ortíz-Severín, J., Varas, M., Cabrera, R., et al. (2016b). Dictyostelium discoideum as a surrogate host–microbe model for antivirulence screening in Pseudomonas aeruginosa PAO1. *Int J Antimicrob Agents*, 1–7. doi: 10.1016/j.ijantimicag.2016.02.005.
- Brown, M. R. W., and Kornberg, A. (2004). Inorganic polyphosphate in the origin and survival of species. *Proc Natl Acad Sci U S A* 101, 16085–16087.
- Calbo, E., and Garau, J. (2015). The changing epidemiology of hospital outbreaks due to ESBL-producing Klebsiella pneumoniae: The CTX-M-15 type consolidation. *Future Microbiol* 10, 1063–1075. doi: 10.2217/fmb.15.22.
- Cano, V., March, C., Insua, J. L., Aguiló, N., Llobet, E., Moranta, D., et al. (2015). Klebsiella pneumoniae survives within macrophages by avoiding delivery to lysosomes. *Cell Microbiol* 17, 1537–1560. doi: 10.1111/cmi.12466.
- Casadevall, A. (2017). The Pathogenic Potential of a Microbe. *mSphere* 2. doi: 10.1128/msphere.00015-17.
- Casadevall, A., and Pirofski, L.-A. (n.d.). Host-Pathogen Interactions: The Attributes of Virulence. Available at: <http://jid.oxfordjournals.org/>.
- Catalán-Nájera, J. C., Garza-Ramos, U., and Barrios-Camacho, H. (2017). Hypervirulence and hypermucoviscosity: Two different but complementary Klebsiella spp. phenotypes? *Virulence* 8, 1111–1123. doi: 10.1080/21505594.2017.1317412.
- Chávez, F. P., Lagos, C. F., Reyes-parada, M., Guiliani, N., and Jerez, C. A. (2011). Polyphosphate Synthesis as a Target for Novel Antibiotics. *Curr Enzym Inhib* 7, 163–168.
- Chen, F. J., Chan, C. H., Huang, Y. J., Liu, K. L., Peng, H. L., Chang, H. Y., et al. (2011). Structural and mechanical properties of Klebsiella pneumoniae type 3 fimbriae. *J Bacteriol* 193, 1718–1725. doi: 10.1128/JB.01395-10.
- Chen, J., Zhang, H., and Liao, X. (2023). Hypervirulent Klebsiella pneumoniae. *Infect Drug Resist* 16, 5243–5249. doi: 10.2147/IDR.S418523.
- Chen, T., Dong, G., Zhang, S., Zhang, X., Zhao, Y., Cao, J., et al. (2020a). Effects of iron on the growth, biofilm formation and virulence of Klebsiella pneumoniae causing liver abscess. *BMC Microbiol* 20, 1–7. doi: 10.1186/s12866-020-01727-5.
- Chen, T., Dong, G., Zhang, S., Zhang, X., Zhao, Y., Cao, J., et al. (2020b). Effects of iron on the growth, biofilm formation and virulence of Klebsiella pneumoniae causing liver abscess. *BMC Microbiol* 20. doi: 10.1186/s12866-020-01727-5.
- Chhibber, S., Gondil, V. S., Sharma, S., Kumar, M., Wangoo, N., and Sharma, R. K. (2017). A novel approach for combating Klebsiella pneumoniae biofilm using

- histidine functionalized silver nanoparticles. *Front Microbiol* 8, 1–10. doi: 10.3389/fmicb.2017.01104.
- Chisholm, R. L., and Firtel, R. A. (2004). Insights into morphogenesis from a simple developmental system. *Nat Rev Mol Cell Biol* 5, 531–541. doi: 10.1038/nrm1427.
- Choby, J. E., Howard-Anderson, J., and Weiss, D. S. (2020). Hypervirulent *Klebsiella pneumoniae* – clinical and molecular perspectives. *J Intern Med* 287, 283–300. doi: 10.1111/joim.13007.
- Choong, F. X., Bäck, M., Fahlén, S., Johansson, L. B. G., Melican, K., Rhen, M., et al. (2016). Real-Time optotracing of curli and cellulose in live Salmonella biofilms using luminescent oligothiophenes. *NPJ Biofilms Microbiomes* 2. doi: 10.1038/npjbiofilms.2016.24.
- Chu, W. H. W., Tan, Y. H., Tan, S. Y., Chen, Y., Yong, M., Lye, D. C., et al. (2023a). Acquisition of regulator on virulence plasmid of hypervirulent *Klebsiella* allows bacterial lifestyle switch in response to iron. *mBio*. doi: 10.1128/mbio.01297-23.
- Chu, W. H. W., Tan, Y. H., Tan, S. Y., Chen, Y., Yong, M., Lye, D. C., et al. (2023b). Acquisition of regulator on virulence plasmid of hypervirulent *Klebsiella* allows bacterial lifestyle switch in response to iron. *mBio*. doi: 10.1128/mbio.01297-23.
- Dahl, J. U., Gray, M. J., Bazopoulou, D., Beaufay, F., Lempart, J., Koenigsknecht, M. J., et al. (2017). The anti-inflammatory drug mesalamine targets bacterial polyphosphate accumulation. *Nat Microbiol* 2. doi: 10.1038/nmicrobiol.2016.267.
- De Oliveira, D. M. P., Forde, B. M., Kidd, T. J., Harris, P. N. A., Schembri, M. A., Beatson, S. A., et al. (2020). Antimicrobial resistance in ESKAPE pathogens. *Clin Microbiol Rev* 33, 1–49. doi: 10.1128/CMR.00181-19.
- Dos Santos Goncalves, M., Delattre, C., Balestrino, D., Charbonnel, N., Elboutachfai, R., Wadouachi, A., et al. (2014). Anti-biofilm activity: A function of *Klebsiella pneumoniae* capsular polysaccharide. *PLoS One* 9. doi: 10.1371/journal.pone.0099995.
- Downey, M. (2019). A stringent analysis of polyphosphate dynamics in escherichia coli. *J Bacteriol* 201, 1–6. doi: 10.1128/JB.00070-19.
- Drozd, M., Chandrashekar, K., and Rajashekar, G. (2014). Polyphosphate-mediated modulation of *Campylobacter jejuni* biofilm growth and stability. *Virulence* 5, 680–690. doi: 10.4161/viru.34348.
- Ernst, C. M., Braxton, J. R., Rodriguez-Osorio, C. A., Zagieboylo, A. P., Li, L., Pironti, A., et al. (2020). Adaptive evolution of virulence and persistence in carbapenem-resistant *Klebsiella pneumoniae*. *Nat Med* 26, 705–711. doi: 10.1038/s41591-020-0825-4.
- Erskine, E., MacPhee, C. E., and Stanley-Wall, N. R. (2018). Functional Amyloid and Other Protein Fibers in the Biofilm Matrix. *J Mol Biol* 430, 3642–3656. doi: 10.1016/j.jmb.2018.07.026.
- Faïs, T., Delmas, J., Barnich, N., Bonnet, R., and Dalmasso, G. (2018). Colibactin: More than a new bacterial toxin. *Toxins (Basel)* 10. doi: 10.3390/toxins10040151.
- Fey, P., Dodson, R. J., Basu, S., and Chisholm, R. L. (2013). “One Stop Shop for Everything Dictyostelium: dictyBase and the Dicty Stock Center in 2012,” in, 59–92. doi: 10.1007/978-1-62703-302-2_4.

- Filion, G., and Charette, S. J. (2014). Assessing *Pseudomonas aeruginosa* virulence using a nonmammalian host: *Dictyostelium discoideum*. *Methods in Molecular Biology* 1149, 671–680. doi: 10.1007/978-1-4939-0473-0_51.
- Flemming, H.-C., Wingender, J., Szewzyk, U., Steinberg, P., Rice, S. A., and Kjelleberg, S. (2016). Biofilms: an emergent form of bacterial life. *Nat Rev Microbiol* 14, 563–575. doi: 10.1038/nrmicro.2016.94.
- Follador, R., Heinz, E., Wyres, K. L., Ellington, M. J., Kowarik, M., Holt, K. E., et al. (2016). The diversity of *Klebsiella pneumoniae* surface polysaccharides. *Microb Genom* 2. doi: 10.1099/mgen.0.000073.
- Forcelledo, L., Rosete, Y., García-prieto, E., and García-meni, I. (2020). Since January 2020 Elsevier has created a COVID-19 resource centre with free information in English and Mandarin on the novel coronavirus COVID- 19 . The COVID-19 resource centre is hosted on Elsevier Connect , the company ’ s public news and information .
- Fraley, C. D., Rashid, M. H., Lee, S. S. K., Gottschalk, R., Harrison, J., Wood, P. J., et al. (2007a). A polyphosphate kinase 1 (*ppk1*) mutant of *Pseudomonas aeruginosa* exhibits multiple ultrastructural and functional defects. *Proceedings of the National Academy of Sciences* 104, 3526–3531. doi: 10.1073/pnas.0609733104.
- Fraley, C. D., Rashid, M. H., Lee, S. S. K., Gottschalk, R., Harrison, J., Wood, P. J., et al. (2007b). A polyphosphate kinase 1 (*ppk1*) mutant of *Pseudomonas aeruginosa* exhibits multiple ultrastructural and functional defects. *Proc Natl Acad Sci U S A* 104, 3526–3531.
- Friedlaender, C. (1882). Ueber die Schizomyceten bei der acuten fibr sen. *Archives of Pathological Anatomy and Physiology*, 319–324.
- Froquet, R., Lelong, E., Marchetti, A., and Cosson, P. (2009). *Dictyostelium discoideum*: a model host to measure bacterial virulence. *Nat Protoc* 4, 25–30. doi: 10.1038/nprot.2008.212.
- Fung, C.-P., Chang, F.-Y., Lin, J.-C., Ho, D. M.-T., Chen, C.-T., Chen, J.-H., et al. (2011). Immune response and pathophysiological features of *Klebsiella pneumoniae* liver abscesses in an animal model. *Laboratory Investigation* 91, 1029–1039. doi: 10.1038/labinvest.2011.52.
- Gonzalez-Ferrer, S., Peñaloza, H. F., Budnick, J. A., Bain, W. G., Nordstrom, H. R., Lee, J. S., et al. (2021). Finding Order in the Chaos: Outstanding Questions in *Klebsiella pneumoniae* Pathogenesis. *Infect Immun* 89. doi: 10.1128/IAI.00693-20.
- Gray, M. J. (2019). Inorganic polyphosphate accumulation in *Escherichia coli* is regulated by DksA but not by (p)ppGpp. *J Bacteriol* 201, 1–20. doi: 10.1128/JB.00664-18.
- Gray, M. J., and Jakob, U. (2015). Oxidative stress protection by polyphosphate-new roles for an old player. *Curr Opin Microbiol* 24, 1–6. doi: 10.1016/j.mib.2014.12.004.
- Gray, M. J., Wholey, W. Y., Wagner, N. O., Cremers, C. M., Mueller-Schickert, A., Hock, N. T., et al. (2014). Polyphosphate Is a Primordial Chaperone. *Mol Cell* 53, 689–699. doi: 10.1016/j.molcel.2014.01.012.
- Grillo-Puertas, M., Villegas, J. M., Rintoul, M. R., and Rapisarda, V. A. (2012). Polyphosphate Degradation in Stationary Phase Triggers Biofilm Formation via

- LuxS Quorum Sensing System in *Escherichia coli*. *PLoS One* 7, e50368. doi: 10.1371/journal.pone.0050368.
- Hider, R. C. (2007). Siderophore mediated absorption of iron. *Siderophores from Microorganisms and Plants*, 25–87. doi: 10.1007/bfb0111310.
- Holden, V. I., Wright, M. S., Houle, S., Collingwood, A., Dozois, C. M., Adams, M. D., et al. (2018). Iron Acquisition and Siderophore Release by Carbapenem-Resistant Sequence Type 258 *Klebsiella pneumoniae*. *mSphere* 3. doi: 10.1128/mSphere.00125-18.
- Hosoda, T., Harada, S., Okamoto, K., Ishino, S., Kaneko, M., Suzuki, M., et al. (2021). COVID-19 and fatal sepsis caused by hypervirulent *klebsiella pneumoniae*, Japan, 2020. *Emerg Infect Dis* 27, 556–559. doi: 10.3201/eid2702.204662.
- Hsu, C. R., Lin, T. L., Chen, Y. C., Chou, H. C., and Wang, J. T. (2011). The role of *Klebsiella pneumoniae* rmpA in capsular polysaccharide synthesis and virulence revisited. *Microbiology (N Y)* 157, 3446–3457. doi: 10.1099/mic.0.050336-0.
- Huang, C. R., Lu, C. H., Chang, H. W., Lee, P. Y., Lin, M. W., and Chang, W. N. (2002). Community-Acquired Spontaneous Bacterial Meningitis in Adult Diabetic Patients: An Analysis of Clinical Characteristics and Prognostic Factors. *Infection* 30, 346–350. doi: 10.1007/s15010-002-3010-4.
- Ifrid, E., Ouertatani-Sakouhi, H., Jauslin, T., Kicka, S., Chiriano, G., Harrison, C. F., et al. (2022). 5-ethyl-2'-deoxyuridine fragilizes *Klebsiella pneumoniae* outer wall and facilitates intracellular killing by phagocytic cells. *PLoS One* 17. doi: 10.1371/journal.pone.0269093.
- Ito, T., Yamamoto, S., Yamaguchi, K., Sato, M., Kaneko, Y., Goto, S., et al. (2020). Inorganic polyphosphate potentiates lipopolysaccharide-induced macrophage inflammatory response. *Journal of Biological Chemistry* 295, 4014–4023. doi: 10.1074/jbc.RA119.011763.
- Joseph, L., Merciecca, T., Forestier, C., Balestrino, D., and Miquel, S. (2021). From *Klebsiella pneumoniae* Colonization to Dissemination: An Overview of Studies Implementing Murine Models. *Microorganisms* 9, 1282. doi: 10.3390/microorganisms9061282.
- Karaiskos, I., and Giamarellou, H. (2020). Carbapenem-sparing strategies for ESBL producers: When and how. *Antibiotics* 9. doi: 10.3390/antibiotics9020061.
- Kim, K.-S., Rao, N. N., Fraley, C. D., and Kornberg, A. (2002a). Inorganic polyphosphate is essential for long-term survival and virulence factors in *Shigella* and *Salmonella* spp. *Proc Natl Acad Sci U S A* 99, 7675–7680.
- Kim, K.-S., Rao, N. N., Fraley, C. D., and Kornberg, A. (2002b). Inorganic polyphosphate is essential for long-term survival and virulence factors in *Shigella* and *Salmonella* spp. *Proceedings of the National Academy of Sciences* 99, 7675–7680. doi: 10.1073/pnas.112210499.
- Kliebe, C., Nies, B. A., Meyer, J. F., Tolxdorff-Neutzling, R. M., and Wiedemann, B. (1985). Evolution of plasmid-coded resistance to broad-spectrum cephalosporins. *Antimicrob Agents Chemother* 28, 302–307. doi: 10.1128/AAC.28.2.302.
- Knothe, H., Shah, P., Krcmery, V., Antal, M., and Mitsuhashi, S. (1983). Transferable resistance to cefotaxime, cefoxitin, cefamandole and cefuroxime in clinical isolates

- of *Klebsiella pneumoniae* and *Serratia marcescens*. *Infection* 11, 315–317. doi: 10.1007/BF01641355.
- Kornberg, A., Rao, N. N., and Ault-Riché, D. (1999). Inorganic polyphosphate: a molecule of many functions. *Annu Rev Biochem* 68, 89–125. doi: 10.1146/annurev.biochem.68.1.89.
- Kreppel, L. (2004). dictyBase: a new *Dictyostelium discoideum* genome database. *Nucleic Acids Res* 32, 332D – 333. doi: 10.1093/nar/gkh138.
- Kurz, C. L., and Ewbank, J. J. (2007). Infection in a dish: high-throughput analyses of bacterial pathogenesis. *Curr Opin Microbiol* 10, 10–16. doi: 10.1016/j.mib.2006.12.001.
- Lam, M. M. C., Wyres, K. L., Duchêne, S., Wick, R. R., Judd, L. M., Gan, Y.-H., et al. (2018). Population genomics of hypervirulent *Klebsiella pneumoniae* clonal-group 23 reveals early emergence and rapid global dissemination. *Nat Commun* 9, 2703. doi: 10.1038/s41467-018-05114-7.
- Lan, Y., Zhou, M., Jian, Z., Yan, Q., Wang, S., and Liu, W. (2019). Prevalence of *pks* gene cluster and characteristics of *Klebsiella pneumoniae*-induced bloodstream infections. *J Clin Lab Anal* 33. doi: 10.1002/jcla.22838.
- Lawlor, M. S., O'Connor, C., and Miller, V. L. (2007). Yersiniabactin Is a Virulence Factor for *Klebsiella pneumoniae* during Pulmonary Infection. *Infect Immun* 75, 1463–1472. doi: 10.1128/IAI.00372-06.
- Lee, C.-H., Chuah, S.-K., Tai, W.-C., Chang, C.-C., and Chen, F.-J. (2017). Delay in Human Neutrophil Constitutive Apoptosis after Infection with *Klebsiella pneumoniae* Serotype K1. *Front Cell Infect Microbiol* 7. doi: 10.3389/fcimb.2017.00087.
- Li, G., Sun, S., Zhao, Z. Y., and Sun, Y. (2019). The pathogenicity of *rmpA* or aerobactin-positive *Klebsiella pneumoniae* in infected mice. *Journal of International Medical Research* 47, 4344–4352. doi: 10.1177/0300060519863544.
- Liu, S., Huang, Z., Kong, J., Zhao, Y., Xu, M., Zhou, B., et al. (2022). Effects of aerobactin-encoding gene *iucB* and regulator of mucoid phenotype *rmpA* on the virulence of *Klebsiella pneumoniae* causing liver abscess. *Front Cell Infect Microbiol* 12. doi: 10.3389/fcimb.2022.968955.
- Liu, Y. C., Cheng, D. L., and Lin, C. L. (1986). *Klebsiella pneumoniae* Liver Abscess Associated With Septic Endophthalmitis. *Arch Intern Med* 146, 1913–1916. doi: 10.1001/archinte.1986.00360220057011.
- Lu, M. C., Chen, Y. T., Chiang, M. K., Wang, Y. C., Hsiao, P. Y., Huang, Y. J., et al. (2017). Colibactin contributes to the hypervirulence of *pks+* K1 CC23 *Klebsiella pneumoniae* in mouse meningitis infections. *Front Cell Infect Microbiol* 7. doi: 10.3389/fcimb.2017.00103.
- Luo, C., Chen, Y., Hu, X., Chen, S., Lin, Y., Liu, X., et al. (2023). Genetic and Functional Analysis of the *pks* Gene in Clinical *Klebsiella pneumoniae* Isolates. *Microbiol Spectr*. doi: 10.1128/spectrum.00174-23.
- Lv, H., Zhou, Y., Liu, B., Guan, J., Zhang, P., Deng, X., et al. (2022a). Polyphosphate Kinase Is Required for the Processes of Virulence and Persistence in *Acinetobacter baumannii*. *Microbiol Spectr* 10. doi: 10.1128/spectrum.01230-22.

- Lv, H., Zhou, Y., Liu, B., Guan, J., Zhang, P., Deng, X., et al. (2022b). Polyphosphate Kinase Is Required for the Processes of Virulence and Persistence in *Acinetobacter baumannii*. *Microbiol Spectr* 10. doi: 10.1128/spectrum.01230-22.
- Magiorakos, A. P., Srinivasan, A., Carey, R. B., Carmeli, Y., Falagas, M. E., Giske, C. G., et al. (2012). Multidrug-resistant, extensively drug-resistant and pandrug-resistant bacteria: An international expert proposal for interim standard definitions for acquired resistance. *Clinical Microbiology and Infection* 18, 268–281. doi: 10.1111/j.1469-0691.2011.03570.x.
- Marcoleta, A. E., Berríos-Pastén, C., Nuñez, G., Monasterio, O., and Lagos, R. (2016). *Klebsiella pneumoniae* Asparagine tDNAs Are Integration Hotspots for Different Genomic Islands Encoding Microcin E492 Production Determinants and Other Putative Virulence Factors Present in Hypervirulent Strains. *Front Microbiol* 7. doi: 10.3389/fmicb.2016.00849.
- Marcoleta, A. E., Varas, M. A., Ortiz-Severín, J., Vásquez, L., Berríos-Pastén, C., Sabag, A. V., et al. (2018). Evaluating different virulence traits of *Klebsiella pneumoniae* using *Dictyostelium discoideum* and zebrafish larvae as host models. *Front Cell Infect Microbiol* 8. doi: 10.3389/fcimb.2018.00030.
- Martin, R. M., and Bachman, M. A. (2018). Colonization, infection, and the accessory genome of *Klebsiella pneumoniae*. *Front Cell Infect Microbiol* 8, 1–15. doi: 10.3389/fcimb.2018.00004.
- Medina, J. M., Shreenidhi, P. M., Larsen, T. J., Queller, D. C., and Strassmann, J. E. (2019). Cooperation and conflict in the social amoeba *dictyostelium discoideum*. *International Journal of Developmental Biology* 63, 371–382. doi: 10.1387/ijdb.190158jm.
- Meredith, T. C., and Woodard, R. W. (2006). Characterization of *Escherichia coli* <scp>D</scp> -arabinose 5-phosphate isomerase encoded by *kpsF*: implications for group 2 capsule biosynthesis. *Biochemical Journal* 395, 427–432. doi: 10.1042/BJ20051828.
- Miethke, M., and Marahiel, M. A. (2007). Siderophore-Based Iron Acquisition and Pathogen Control. *Microbiology and Molecular Biology Reviews* 71, 413–451. doi: 10.1128/mmbr.00012-07.
- Mina, S. A., Zhu, G., Fanian, M., Chen, S., and Yang, G. (2024). Exploring reduced macrophage cell toxicity of hypervirulent *Klebsiella pneumoniae* compared to classical *Klebsiella pneumoniae*. *Microbiol Res* 278, 127515. doi: 10.1016/j.micres.2023.127515.
- Montrucchio, G., Corcione, S., Sales, G., Curtoni, A., Rosa, F. G. De, and Brazzi, L. (2020). Since January 2020 Elsevier has created a COVID-19 resource centre with free information in English and Mandarin on the novel coronavirus COVID- 19 . The COVID-19 resource centre is hosted on Elsevier Connect , the company ' s public news and information .
- Müller, W. E. G., Schröder, H. C., and Wang, X. (2019). Inorganic Polyphosphates As Storage for and Generator of Metabolic Energy in the Extracellular Matrix. *Chem Rev* 119, 12337–12374. doi: 10.1021/acs.chemrev.9b00460.

- Neville, N., Roberge, N., Ji, X., Stephen, P., Lu, J. L., and Jia, Z. (2021). A Dual-Specificity Inhibitor Targets Polyphosphate Kinase 1 and 2 Enzymes To Attenuate Virulence of *Pseudomonas aeruginosa*. *mBio* 12. doi: 10.1128/mBio.00592-21.
- Nocek, B., Kochinyan, S., Proudfoot, M., Brown, G., Evdokimova, E., Osipiuk, J., et al. (2008). Polyphosphate-dependent synthesis of ATP and ADP by the family-2 polyphosphate kinases in bacteria. *Proceedings of the National Academy of Sciences* 105, 17730–17735. doi: 10.1073/pnas.0807563105.
- Ortiz-Severín, J., Varas, M., Bravo-Toncio, C., Guiliani, N., and Chávez, F. P. (2015). Multiple antibiotic susceptibility of polyphosphate kinase mutants (ppk1 and ppk2) from *Pseudomonas aeruginosa* PAO1 as revealed by global phenotypic analysis. *Biol Res* 48, 1–6. doi: 10.1186/s40659-015-0012-0.
- Ovchinnikova, O. G., Treat, L. P., Teelucksingh, T., Clarke, B. R., Miner, T. A., Whitfield, C., et al. (2023). Hypermucoviscosity Regulator RmpD Interacts with Wzc and Controls Capsular Polysaccharide Chain Length. *mBio*. doi: 10.1128/mbio.00800-23.
- Paczosa, M. K., and Meccas, J. (2016). *Klebsiella pneumoniae*: Going on the Offense with a Strong Defense. *Microbiology and Molecular Biology Reviews* 80, 629–661. doi: 10.1128/mbr.00078-15.
- Pal, S., Verma, J., Mallick, S., Rastogi, S. K., Kumar, A., and Ghosh, A. S. (2019). Absence of the glycosyltransferase WcaJ in *Klebsiella pneumoniae* ATCC13883 affects biofilm formation, increases polymyxin resistance and reduces murine macrophage activation. *Microbiology (N Y)* 165, 891–904. doi: 10.1099/mic.0.000827.
- Palacios, M., Miner, T. A., Frederick, D. R., Sepulveda, V. E., Quinn, J. D., Walker, K. A., et al. (2018). Identification of two regulators of virulence that are conserved in *Klebsiella pneumoniae* classical and hypervirulent strains. *mBio* 9. doi: 10.1128/mBio.01443-18.
- Pan, M., Neilson, M. P., Grunfeld, A. M., Cruz, P., Wen, X., Insall, R. H., et al. (2018). A G-protein-coupled chemoattractant receptor recognizes lipopolysaccharide for bacterial phagocytosis. *PLoS Biol* 16. doi: 10.1371/journal.pbio.2005754.
- Paquet, V. E., and Charette, S. J. (2016a). Amoeba-resisting bacteria found in multilamellar bodies secreted by *Dictyostelium discoideum*: Social amoebae can also package bacteria. *FEMS Microbiol Ecol* 92. doi: 10.1093/femsec/fiw025.
- Paquet, V. E., and Charette, S. J. (2016b). Amoeba-resisting bacteria found in multilamellar bodies secreted by *Dictyostelium discoideum*: social amoebae can also package bacteria. *FEMS Microbiol Ecol* 92, fiw025. doi: 10.1093/femsec/fiw025.
- Patro, L. P. P., and Rathinavelan, T. (2019). Targeting the Sugary Armor of *Klebsiella* Species. *Front Cell Infect Microbiol* 9. doi: 10.3389/fcimb.2019.00367.
- Perepelov, A. V., Ujazda, E., Senchenkova, S. N., Shashkov, A. S., Kaca, W., and Knirel, Y. A. (1999). Structural and serological studies on the O-antigen of *Proteus mirabilis* O14, a new polysaccharide containing 2-[(R)-1-carboxyethylamino]ethyl phosphate. *Eur J Biochem* 261, 347–353. doi: 10.1046/j.1432-1327.1999.00251.x.

- Phd, S., Yeh, K.-M., Lin, J.-C., Chang, F.-Y., Chang, F.-Y., Siu, L. K., et al. (2012). *Klebsiella pneumoniae* liver abscess: a new invasive syndrome. Available at: www.thelancet.com/infection.
- Podschun, R., Pietsch, S., Höller, C., and Ullmann, U. (2001). Incidence of *Klebsiella* Species in Surface Waters and Their Expression of Virulence Factors. *Appl Environ Microbiol* 67, 3325–3327. doi: 10.1128/AEM.67.7.3325-3327.2001.
- Rashid, M. H., Rao, N. N., and Kornberg, A. (2000a). Inorganic polyphosphate is required for motility of bacterial pathogens. *J Bacteriol* 182, 225–227. doi: 10.1128/JB.182.1.225-227.2000.
- Rashid, M. H., Rumbaugh, K., Passador, L., Davies, D. G., Hamood, A. N., Iglewski, B. H., et al. (2000b). Polyphosphate kinase is essential for biofilm development, quorum sensing, and virulence of *Pseudomonas aeruginosa*. *Proc Natl Acad Sci U S A* 97, 9636–9641. doi: 10.1073/pnas.170283397.
- Recalde, A., van Wolferen, M., Sivabalasarma, S., Albers, S. V., Navarro, C. A., and Jerez, C. A. (2021). The role of polyphosphate in motility, adhesion, and biofilm formation in *sulfolobales*. *Microorganisms* 9, 1–13. doi: 10.3390/microorganisms9010193.
- Rice, L. B. (2008). Federal funding for the study of antimicrobial resistance in nosocomial pathogens: No ESKAPE. *Journal of Infectious Diseases* 197, 1079–1081. doi: 10.1086/533452.
- Rijal, R., Cadena, L. A., Smith, M. R., Carr, J. F., and Gomer, R. H. (2020). Polyphosphate is an extracellular signal that can facilitate bacterial survival in eukaryotic cells. *Proceedings of the National Academy of Sciences* 117, 31923–31934. doi: 10.1073/pnas.2012009117.
- Rijal, R., Kirolos, S. A., Rahman, R. J., and Gomer, R. H. (2022). Dictyostelium discoideum cells retain nutrients when the cells are about to outgrow their food source. *J Cell Sci* 135. doi: 10.1242/jcs.260107.
- Roberge, N., Neville, N., Douchant, K., Noordhof, C., Boev, N., Sjaarda, C., et al. (2021). Broad-Spectrum Inhibitor of Bacterial Polyphosphate Homeostasis Attenuates Virulence Factors and Helps Reveal Novel Physiology of *Klebsiella pneumoniae* and *Acinetobacter baumannii*. *Front Microbiol* 12. doi: 10.3389/fmicb.2021.764733.
- Russo, T. A., and Marr, C. M. (2019). Hypervirulent *Klebsiella pneumoniae*. *Clin Microbiol Rev* 32. doi: 10.1128/CMR.00001-19.
- Russo, T. A., Olson, R., MacDonald, U., Beanan, J., and Davidson, B. A. (2015). Aerobactin, but not yersiniabactin, salmochelin, or enterobactin, enables the growth/survival of hypervirulent (hypermucoviscous) *Klebsiella pneumoniae* ex vivo and in vivo. *Infect Immun* 83, 3325–3333. doi: 10.1128/IAI.00430-15.
- S, A., B, J., A, L., C, E., C, B., and JL, F. (2005). Polyphosphate kinase: a new colonization factor of *Helicobacter pylori*. *FEMS Microbiol Lett* 243, 45–50. doi: 10.1016/J.FEMSLE.2004.11.040.
- Sahly, H., Podschun, R., Oelschlaeger, T. A., Greiwe, M., Parolis, H., Hasty, D., et al. (2000). Capsule impedes adhesion to and invasion of epithelial cells by *Klebsiella pneumoniae*. *Infect Immun* 68, 6744–6749. doi: 10.1128/IAI.68.12.6744-6749.2000.

- Sapunar Z., J. (2016). EPIDEMIOLOGÍA DE LA DIABETES MELLITUS EN CHILE. *Revista Médica Clínica Las Condes* 27, 146–151. doi: 10.1016/j.rmclc.2016.04.003.
- Schembri, M. A., Blom, J., Krogfelt, K. A., and Klemm, P. (2005). Capsule and fimbria interaction in *Klebsiella pneumoniae*. *Infect Immun* 73, 4626–4633. doi: 10.1128/IAI.73.8.4626-4633.2005.
- Schumachera, M. A., and Zenga, W. (2016). Structures of the activator of k. pneumonia biofilm formation, mrkh, indicates pilz domains involved in c-di-gmp and DNA binding. *Proc Natl Acad Sci U S A* 113, 10067–10072. doi: 10.1073/pnas.1607503113.
- Shankar-Sinha, S., Valencia, G. A., Janes, B. K., Rosenberg, J. K., Whitfield, C., Bender, R. A., et al. (2004). The *Klebsiella pneumoniae* O Antigen Contributes to Bacteremia and Lethality during Murine Pneumonia. *Infect Immun* 72, 1423–1430. doi: 10.1128/IAI.72.3.1423-1430.2004.
- Shi, X., Rao, N. N., and Kornberg, A. (2004a). Inorganic polyphosphate in *Bacillus cereus*: Motility, biofilm formation, and sporulation. *Proc Natl Acad Sci U S A* 101, 17061–17065. doi: 10.1073/pnas.0407787101.
- Shi, X., Rao, N. N., and Kornberg, A. (2004b). Inorganic polyphosphate in *Bacillus cereus*: Motility, biofilm formation, and sporulation. *Proc Natl Acad Sci U S A* 101, 17061–17065. Available at: <http://www.pubmedcentral.nih.gov/articlerender.fcgi?artid=535361&tool=pmcentrez&rendertype=abstract>.
- Singh, R., Singh, M., Arora, G., Kumar, S., Tiwari, P., and Kidwai, S. (2013). Polyphosphate Deficiency in *Mycobacterium tuberculosis* Is Associated with Enhanced Drug Susceptibility and Impaired Growth in Guinea Pigs. *J Bacteriol* 195, 2839. doi: 10.1128/JB.00038-13.
- Smith, S. A., and Morrissey, J. H. (2007). Sensitive fluorescence detection of polyphosphate in polyacrylamide gels using 4',6-diamidino-2-phenylindol. *Electrophoresis* 28, 3461–3465. doi: 10.1002/elps.200700041.
- Song, H., Dharmasena, M. N., Wang, C., Shaw, G. X., Cherry, S., Tropea, J. E., et al. (2020). Structure and activity of PPX/GppA homologs from *Escherichia coli* and *Helicobacter pylori*. *FEBS J* 287, 1865–1885. doi: 10.1111/febs.15120.
- Struve, C., and Krogfelt, K. A. (2003). Role of capsule in *Klebsiella pneumoniae* virulence: Lack of correlation between in vitro and in vivo studies. *FEMS Microbiol Lett* 218, 149–154. doi: 10.1016/S0378-1097(02)01117-5.
- Suess, P. M., and Gomer, R. H. (2016). Extracellular polyphosphate inhibits proliferation in an autocrine negative feedback loop in *dictyostelium discoideum*. *Journal of Biological Chemistry* 291, 20260–20269. doi: 10.1074/jbc.M116.737825.
- Tacconelli, E., Carrara, E., Savoldi, A., Harbarth, S., Mendelson, M., Monnet, D. L., et al. (2018). Discovery, research, and development of new antibiotics: the WHO priority list of antibiotic-resistant bacteria and tuberculosis. *Lancet Infect Dis* 18, 318–327. doi: 10.1016/S1473-3099(17)30753-3.
- Tan, Y. H., Chen, Y., Chu, W. H. W., Sham, L. T., and Gan, Y. H. (2020). Cell envelope defects of different capsule-null mutants in K1 hypervirulent *Klebsiella*

- pneumoniae can affect bacterial pathogenesis. *Mol Microbiol* 113, 889–905. doi: 10.1111/mmi.14447.
- Tang-Fichaux, M., Chagneau, C. V., Bossuet-Greif, N., Nougayrède, J.-P., Oswald, É., and Branchu, P. (2020). The Polyphosphate Kinase of *Escherichia coli* Is Required for Full Production of the Genotoxin Colibactin. *mSphere* 5. doi: 10.1128/mSphere.01195-20.
- Terashima-Hasegawa, M., Ashino, T., Kawazoe, Y., Shiba, T., Manabe, A., and Numazawa, S. (2019). Inorganic polyphosphate protects against lipopolysaccharide-induced lethality and tissue injury through regulation of macrophage recruitment. *Biochem Pharmacol* 159, 96–105. doi: 10.1016/j.bcp.2018.11.017.
- Thayil, S. M., Morrison, N., Schechter, N., Rubin, H., and Karakousis, P. C. (2011). The role of the novel exopolyphosphatase MT0516 in *Mycobacterium tuberculosis* drug tolerance and persistence. *PLoS One* 6. doi: 10.1371/journal.pone.0028076.
- Tinsley, C. R., Manjula, B. N., and Gotschlich, E. C. (1993a). Purification and characterization of polyphosphate kinase from *Neisseria meningitidis*. *Infect Immun* 61, 3703–3710. doi: 10.1128/iai.61.9.3703-3710.1993.
- Tinsley, C. R., Manjula, B. N., and Gotschlich, E. C. (1993b). Purification and characterization of polyphosphate kinase from *Neisseria meningitidis*. *Infect Immun*. doi: 10.1128/iai.61.9.3703-3710.1993.
- Tiri, B., Sensi, E., Marsiliani, V., Cantarini, M., Priante, G., Vernelli, C., et al. (2020). Antimicrobial Stewardship Program, COVID-19, and Infection Control: Spread of Carbapenem-Resistant *Klebsiella pneumoniae* Colonization in ICU COVID-19 Patients. What Did Not Work? *J Clin Med* 9, 2744. doi: 10.3390/jcm9092744.
- Troxell, B. (2018). A type 6 secretion system (T6SS) encoded gene within *Salmonella enterica* serovar Enteritidis contributes to virulence. *Virulence* 9, 585–587. doi: 10.1080/21505594.2017.1421829.
- Tzeng, C. M., and Kornberg, A. (1998). Polyphosphate kinase is highly conserved in many bacterial pathogens. *Mol Microbiol* 29, 381–382. doi: 10.1046/j.1365-2958.1998.00887.x.
- Tzouveleki, L. S., Markogiannakis, A., Psychogiou, M., Tassios, P. T., and Daikos, G. L. (2012). Carbapenemases in *Klebsiella pneumoniae* and other Enterobacteriaceae: An evolving crisis of global dimensions. *Clin Microbiol Rev* 25, 682–707. doi: 10.1128/CMR.05035-11.
- Varas, M. A., Riquelme-Barrios, S., Valenzuela, C., Marcoleta, A. E., Berríos-Pastén, C., Santiviago, C. A., et al. (2018). Inorganic polyphosphate is essential for *Salmonella Typhimurium* Virulence and survival in *Dictyostelium discoideum*. *Front Cell Infect Microbiol* 8. doi: 10.3389/fcimb.2018.00008.
- Varas, M., Fariña, A., Díaz-Pascual, F., Ortiz-Severín, J., Marcoleta, A. E., Allende, M. L., et al. (2017a). Live-cell imaging of *Salmonella Typhimurium* interaction with zebrafish larvae after injection and immersion delivery methods. *J Microbiol Methods* 135, 20–25. doi: 10.1016/j.mimet.2017.01.020.
- Varas, M., Valdivieso, C., Mauriaca, C., Ortiz-Severín, J., Paradela, A., Poblete-Castro, I., et al. (2017b). Multi-level evaluation of *Escherichia coli* polyphosphate related mutants using global transcriptomic, proteomic and phenomic analyses. *Biochimica*

- et Biophysica Acta (BBA) - General Subjects* 1861, 871–883. doi: 10.1016/j.bbagen.2017.01.007.
- Varela, C., Mauriaca, C., Paradela, A., Albar, J. P., Jerez, C. A., and Chávez, F. P. (2010). New structural and functional defects in polyphosphate deficient bacteria: A cellular and proteomic study. *BMC Microbiol* 10, 7.
- Vuotto, C., Longo, F., Balice, M. P., Donelli, G., and Varaldo, P. E. (2014). Antibiotic resistance related to biofilm formation in *Klebsiella pneumoniae*. *Pathogens* 3, 743–758. doi: 10.3390/pathogens3030743.
- Wagner, C., and Hensel, M. (2011). “Adhesive Mechanisms of *Salmonella enterica*,” in, 17–34. doi: 10.1007/978-94-007-0940-9_2.
- Walker, K. A., Miner, T. A., Palacios, M., Trzilova, D., Frederick, D. R., Broberg, C. A., et al. (2019). A *klebsiella pneumoniae* regulatory mutant has reduced capsule expression but retains hypermucoviscosity. *mBio* 10, 1–16. doi: 10.1128/MBIO.00089-19.
- Walker, K. A., Treat, L. P., Sepúlveda, V. E., and Miller, V. L. (2020). The Small Protein RmpD Drives Hypermucoviscosity in *Klebsiella pneumoniae*. *mBio* 11. doi: 10.1128/mBio.01750-20.
- Wang, C.-H., Hsieh, Y.-H., Powers, Z. M., and Kao, C.-Y. (2020a). Defeating Antibiotic-Resistant Bacteria: Exploring Alternative Therapies for a Post-Antibiotic Era. *Int J Mol Sci* 21, 1061. doi: 10.3390/ijms21031061.
- Wang, G., Zhao, G., Chao, X., Xie, L., and Wang, H. (2020b). The characteristic of virulence, biofilm and antibiotic resistance of *klebsiella pneumoniae*. *Int J Environ Res Public Health* 17, 1–17. doi: 10.3390/ijerph17176278.
- Wang, H., Wilksch, J. J., Chen, L., Tan, J. W. H., Strugnell, R. A., and Gee, M. L. (2017a). Influence of Fimbriae on Bacterial Adhesion and Viscoelasticity and Correlations of the Two Properties with Biofilm Formation. *Langmuir* 33, 100–106. doi: 10.1021/acs.langmuir.6b03764.
- Wang, L., Shen, D., Wu, H., and Ma, Y. (2017b). Resistance of hypervirulent *Klebsiella pneumoniae* to both intracellular and extracellular killing of neutrophils. *PLoS One* 12, e0173638. doi: 10.1371/journal.pone.0173638.
- Wantuch, P. L., Knoop, C. J., Robinson, L. S., Vinogradov, E., Scott, N. E., Harding, C. M., et al. (2023). Capsular polysaccharide inhibits vaccine-induced O-antigen antibody binding and function across both classical and hypervirulent K2:O1 strains of *Klebsiella pneumoniae*. *PLoS Pathog* 19, e1011367. doi: 10.1371/journal.ppat.1011367.
- Wilksch, J. J., Yang, J., Clements, A., Gabbe, J. L., Short, K. R., Cao, H., et al. (2011). MrKH, a novel c-di-GMP-dependent transcriptional activator, controls *klebsiella pneumoniae* biofilm formation by regulating type 3 fimbriae expression. *PLoS Pathog* 7. doi: 10.1371/journal.ppat.1002204.
- Wu, J. H., Wu, A. M., Tsai, C. G., Chang, X.-Y., Tsai, S.-F., and Wu, T.-S. (2008). Contribution of Fucose-Containing Capsules in *Klebsiella pneumoniae* to Bacterial Virulence in Mice. *Exp Biol Med* 233, 64–70. doi: 10.3181/0706-RM-170.
- Wu, M.-C., Lin, T.-L., Hsieh, P.-F., Yang, H.-C., and Wang, J.-T. (2011). Isolation of Genes Involved in Biofilm Formation of a *Klebsiella pneumoniae* Strain Causing Pyogenic Liver Abscess. *PLoS One* 6, e23500. doi: 10.1371/journal.pone.0023500.

- Wyres, K. L., Lam, M. M. C., and Holt, K. E. (2020). Population genomics of *Klebsiella pneumoniae*. *Nat Rev Microbiol* 18, 344–359. doi: 10.1038/s41579-019-0315-1.
- Wyres, K. L., Wick, R. R., Gorrie, C., Jenney, A., Follador, R., Thomson, N. R., et al. (2016). Identification of *Klebsiella* capsule synthesis loci from whole genome data. *Microb Genom* 2, e000102. doi: 10.1099/mgen.0.000102.
- Xu, Q., Yang, X., Chan, E. W. C., and Chen, S. (2021). The hypermucoviscosity of hypervirulent *K. pneumoniae* confers the ability to evade neutrophil-mediated phagocytosis. *Virulence* 12, 2050–2059. doi: 10.1080/21505594.2021.1960101.
- Yigit, H., Queenan, A. M., Anderson, G. J., Domenech-Sanchez, A., Biddle, J. W., Steward, C. D., et al. (2001). Novel carbapenem-hydrolyzing β -lactamase, KPC-1, from a carbapenem-resistant strain of *Klebsiella pneumoniae*. *Antimicrob Agents Chemother* 45, 1151–1161. doi: 10.1128/AAC.45.4.1151-1161.2001.
- Zhang, H., Ishige, K., and Kornberg, A. (2002). A polyphosphate kinase (PPK2) widely conserved in bacteria. *Proc Natl Acad Sci U S A* 99, 16678–16683.
- Zheng, J., Lin, Z., Chen, C., Chen, Z., Lin, F., Wu, Y., et al. (2018). Biofilm Formation in *Klebsiella pneumoniae* Bacteremia Strains Was Found to be Associated with CC23 and the Presence of wcaG. *Front Cell Infect Microbiol* 8. doi: 10.3389/fcimb.2018.00021.
- Zhu, J., Wang, T., Chen, L., and Du, H. (2021). Virulence Factors in Hypervirulent *Klebsiella pneumoniae*. *Front Microbiol* 12, 1–14. doi: 10.3389/fmicb.2021.642484.

7. Annexes

Manuscripts directly related to the Thesis.

This document is confidential and is proprietary to the American Chemical Society and its authors. Do not copy or disclose without written permission. If you have received this item in error, notify the sender and delete all copies.

Inorganic polyphosphate affects biofilm assembly, capsule formation and virulence of hypervirulent ST23 *Klebsiella pneumoniae*

Journal:	ACS Infectious Diseases
Manuscript ID	id-2023-00509b.R2
Manuscript Type:	Article
Date Submitted by the Author:	14-Dec-2023
Complete List of Authors:	Rojas, Diego; University of Chile, Systems Microbiology Laboratory, Department of Biology, Faculty of Science Marcoleta, Andrés; Universidad de Chile, Departamento de Biología Gálvez-Silva, Matías; University of Chile, Systems Microbiology Laboratory, Department of Biology, Faculty of Science Varas, Macarena; University of Chile, Systems Microbiology Laboratory, Department of Biology, Faculty of Science Díaz, Mauricio; University of Chile, Systems Microbiology Laboratory, Department of Biology, Faculty of Science Hernández, Mauricio; Melisa Institute Vargas, Cristian; Melisa Institute Nourdin-Galindo, Guillermo; Melisa Institute Koch, Elard; Melisa Institute Saldivia, Pablo; Melisa Institute Vielma, Jorge; University of Chile, Systems Microbiology Laboratory, Department of Biology, Faculty of Science Gan, Yunn-Hwen; National University of Singapore, Department of Biochemistry Chen, Yahua; National University of Singapore, Department of Biochemistry Guiliani, Nicolás; Universidad de Chile, Laboratorio de Comunicación microbiana, Departamento de Biología, Facultad de Ciencias Chávez, Francisco; University of Chile, Systems Microbiology Laboratory, Department of Biology, Faculty of Science

SCHOLARONE™
Manuscripts

Inorganic polyphosphate affects biofilm assembly, capsule formation and virulence of hypervirulent ST23 *Klebsiella pneumoniae*

Diego Rojas¹, Andrés E. Marcoleta², Matías Gálvez-Silva^{1,2}, Macarena A. Varas^{1,2}, Mauricio Díaz³, Mauricio Hernández⁴, Cristian Vargas⁴, Guillermo Nourdin-Galindo⁴, Elard Koch⁴, Pablo Saldivia^{4,5}, Jorge Vielma^{1,2}, Yunn-Hwen Gan⁶, Yahua Chen⁶, Nicolás Guiliani³ and Francisco P. Chávez^{1*}

¹ Laboratorio de Microbiología de Sistemas, Departamento de Biología, Facultad de Ciencias, Universidad de Chile, CP 7800003, Santiago, Chile.

² Grupo de Microbiología Integrativa, Laboratorio de Biología Estructural y Molecular, Departamento de Biología, Facultad de Ciencias, Universidad de Chile, CP 7800003, Santiago, Chile

³ Laboratorio de Comunicación Microbiana, Departamento de Biología, Facultad de Ciencias, Universidad de Chile, CP 7800003, Santiago, Chile.

⁴ División Biotecnología, Instituto Melisa, CP 9660000, San Pedro de la Paz, Chile

⁵ Facultad de Ciencias Biológicas, Universidad de Concepción, CP 4070389, Concepción, Chile

⁶ Department of Biochemistry, Yong Loo Lin School of Medicine, National University of Singapore, CP 119077, Singapore.

Correspondence: fpchavez@uchile.cl; Tel.:+56229787185, Laboratorio de Microbiología de Sistemas, Las Palmeras 3425, Ñuñoa CP 7800003, Santiago, Chile

1
2
3 **ABSTRACT:** The emergence of hypervirulent *Klebsiella pneumoniae* (hvKP) strains poses a
4 significant threat to public health due to high mortality rates and propensity to cause
5 severe community-acquired infections in healthy individuals. The ability to form biofilms
6 and produce a protective capsule contributes to its enhanced virulence and is a significant
7 challenge to effective antibiotic treatment. Polyphosphate Kinase 1 (PPK1) is an enzyme
8 responsible for inorganic polyphosphate synthesis and plays a vital role in regulating
9 various physiological processes in bacteria. In this study, we investigated the impact of
10 polyP metabolism on the biofilm and capsule formation and virulence traits in hvKP using
11 *Dictyostelium discoideum* amoeba as a model host. We found that the PPK1 null-mutant was
12 impaired in biofilm and capsule formation and showed attenuated virulence in *D.*
13 *discoideum* compared to the wild-type strain. We performed a proteomic analysis to gain
14 further insight into the underlying molecular mechanism. The results revealed that the
15 PPK1 mutant had a differential expression of proteins involved in capsule synthesis (Wzi -
16 Ugd), biofilm formation (MrkC-D-H), synthesis of the colibactin genotoxin precursor (ClbB),
17 as well as proteins associated with the synthesis and modification of lipid A (ArnB -LpxC -
18 PagP). These proteomic findings corroborate the phenotypic observations and indicate that
19 the PPK1 mutation is associated with impaired biofilm and capsule formation and
20 attenuated virulence in hvKP. Overall, our study highlights the importance of polyP
21 synthesis in regulating extracellular biomolecules and virulence in *K. pneumoniae*, and
22 provides insights into potential therapeutic targets for treating *K. pneumoniae* infections.
23
24
25
26
27
28
29
30
31
32
33
34
35
36
37
38
39
40
41
42
43
44
45
46
47
48
49

50 **KEYWORDS:** Polyphosphate, Hypervirulent *Klebsiella*, Proteomics, *D. discoideum*,
51 Antivirulence.
52
53
54
55
56
57
58
59
60

1
2
3 Hypervirulent *Klebsiella pneumoniae* (hvKP) strains have emerged as a significant public
4 health threat due to their ability to cause severe and often fatal infections¹. Unlike
5 traditional *K. pneumoniae* strains which causing hospital-acquired infections in
6 immunocompromised patients, hvKP strains can cause community-acquired invasive
7 infections in healthy individuals without any underlying medical conditions ². These
8 infections can lead to various clinical manifestations, such as pyogenic liver abscesses
9 (PLA), meningitis, endophthalmitis, necrotizing fasciitis, and sepsis, with mortality rates as
10 high as 50% ³. Moreover, the dynamic nature of the *K. pneumoniae* genome and the
11 acquisition of virulence and resistance factors through horizontal gene transfer have
12 facilitated the rapid evolution of *K. pneumoniae* strains exhibiting both hypervirulence (hv)
13 and multidrug resistance (MDR), rendering them resistant to all conventional treatment
14 methods ⁴.

15
16
17
18
19
20
21
22
23
24
25
26
27
28
29
30
31
32 Frequently, hvKP strains show a thick and prominent capsule and a hypermucoviscous
33 phenotype ². These traits are associated with variants of the pLVKP virulence plasmid
34 (~200 kb)⁵ encoding the transcriptional regulators *rmpA1* and *rmpA2* that activate the
35 expression of the 20-gene *cps* operon/locus. Additionally, the *rmpD* gene encodes a small
36 protein required for hypermucoviscosity (HMV) ⁶, promoting increased capsular
37 polysaccharide chain length ⁷. Furthermore, this plasmid harbors the *iuc* genes involved in
38 aerobactin siderophore synthesis are linked to hvKP virulence ⁸.

39
40
41
42
43
44
45
46
47
48
49
50 Surface structures, such as lipopolysaccharide (LPS) and type I and III fimbriae, whose
51 determinants are frequently encoded in the chromosome, play a crucial role in the invasion
52 of epithelial cells and biofilm formation on biotic and abiotic surfaces⁹⁻¹². Genetic
53
54
55
56
57
58
59
60

1
2
3 experiments conducted in various models have revealed that biofilm and capsule
4
5 formation, particularly capsular serotypes K1 and K2, are the main mechanisms employed
6
7 by hvKP to evade the immune response ^{13,14}. Therefore, targeting biofilm and capsule
8
9 production could be a promising strategy to control *K. pneumoniae* infections. However,
10
11 further studies are necessary to elucidate the molecular mechanisms regulating these
12
13 processes in hvKP, especially in sequence type 23 (ST23), which encompasses most of the
14
15 hvKP strains associated with severe infections in humans, and emerging lineages exhibiting
16
17 the convergence of hypervirulence and resistance to carbapenems and other last-line
18
19 antibiotics ¹⁵. In this regard, the strain SGH10 was proposed as a as a model for studying
20
21 ST23 hvKP pathogenesis ¹⁶, and exploring novel approaches and targets to combat these
22
23 hypervirulent strains.
24
25
26
27
28
29

30 Inorganic polyphosphate (polyP) is ubiquitous in all living organisms, from bacteria to
31
32 humans, and plays a critical role in various cellular processes. In bacteria, polyP metabolism
33
34 has been shown to contribute to stress response, antibiotic resistance, persistence, and virulence
35
36 ¹⁷⁻¹⁹ For example, in *Pseudomonas aeruginosa*, polyP is involved in biofilm formation and
37
38 quorum sensing, contributing to its pathogenicity ²⁰⁻²². Similarly, *Salmonella enterica* utilizes
39
40 polyP for intracellular survival ^{23,24}, and recent studies have highlighted the significance of polyP
41
42 and the PPK1 enzyme catalyzing its synthesis, in intracellular survival within macrophages and
43
44 modulation of the immune response ^{25,26}. In *K. pneumoniae*, , the effect of gallein, an inhibitor of
45
46 polyP synthesis, has been studied, revealing a concentration-dependent decrease in biofilm
47
48 formation ²⁷. However, the precise mechanism by which polyP metabolism and PPK1 influence
49
50
51
52
53 *K. pneumoniae* virulence remains poorly understood. Here, we investigated the impact of PPK1
54
55
56
57
58
59
60

1
2
3 mutation on hvKP biofilm, capsule formation, and virulence traits of hypervirulent ST23 *K.*
4
5 *pneumoniae* using *Dictyostelium discoideum* amoeba as a model host.
6
7

8 **RESULTS**

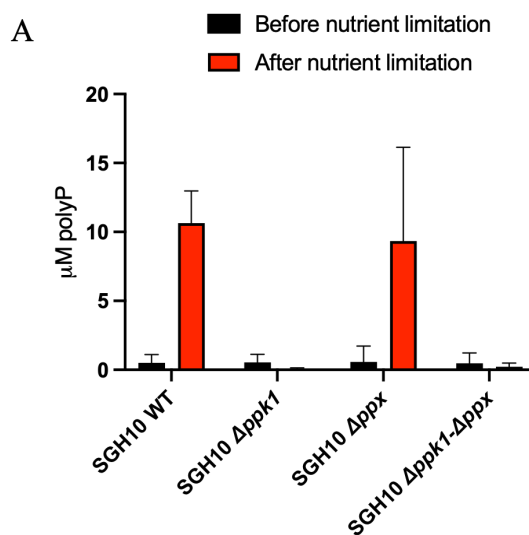
9 **Mutants lacking genes involved in PolyP synthesis and degradation preserve the** 10 11 **viability and show altered polyP accumulation/content** 12 13 14 15

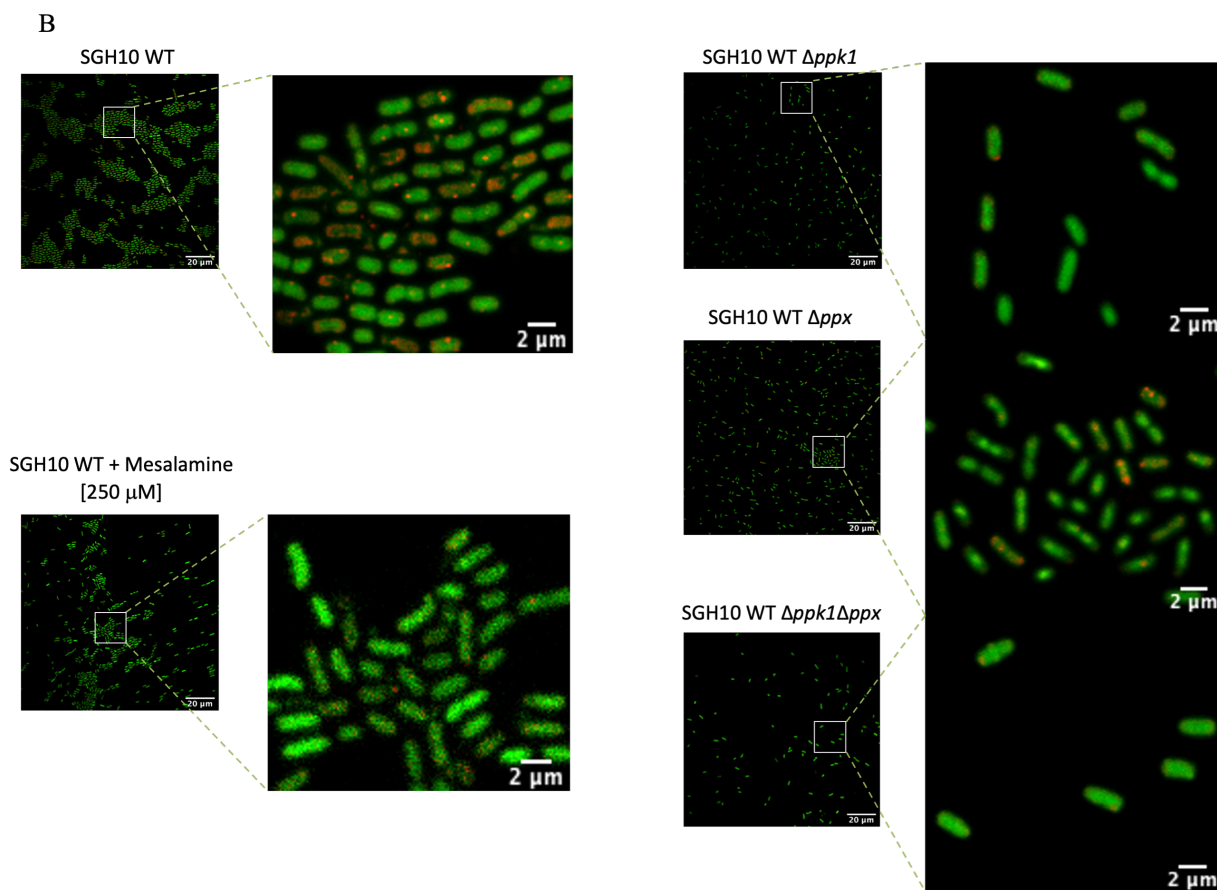
16
17 To investigate the influence of polyP metabolism on hvKp virulence, we generated deletion
18
19 mutants of the genes involved in the synthesis ($\Delta ppk1$) and degradation (Δppx) of polyP, as
20
21 well as the double mutant ($\Delta ppk1-\Delta ppx$), starting from the model ST23 hvKp strain SGH10
22
23 (Fig. 1S). The corresponding mutations were confirmed by Illumina genome sequencing.
24
25

26
27 We first evaluated the effect of the *ppk1* and *ppx* gene deletions on bacterial growth in rich
28
29 (LB broth) and minimal (MOPS) medium (Fig. S1). No significant differences were observed
30
31 between the wild type SGH10 and the mutants under nutrient-rich conditions (Fig. S2A).
32
33 However, under nutrient-deprived conditions, a delay of approximately 2 h in reaching
34
35 exponential growth was observed in the $\Delta ppk1$ and $\Delta ppk1-\Delta ppx$ mutants but not in Δppx
36
37 (Fig. S2B), suggesting that the absence of PPK1 specifically affects normal growth under
38
39 nutrient limitation. Furthermore, adding different concentrations of polyP 150-mer
40
41 restored growth of the mutants lacking *ppk1* in these conditions (Fig. S2B).
42
43
44
45

46
47 PPK1 is the main enzyme responsible for synthesizing polyP in bacterial models such as *P.*
48
49 *aeruginosa* and *Acinetobacter baumannii*^{24,28}. However, its role in *K. pneumoniae* has not
50
51 been extensively studied. Nutrient deprivation is a known condition that promotes the
52
53 accumulation of polyP in bacteria. To do this, the bacteria were cultured in rich medium
54
55
56
57
58
59
60

1
2
3 (LB) until mid-logarithmic phase and transferred to a nutrient-poor medium (MOPS) for
4
5 two hours. We observe a significant decrease in the $\Delta ppk1$ and $\Delta ppk1-\Delta ppx$ mutants
6
7 compared to the wild-type (WT) strain and the Δppx mutant (Fig. 1A). Furthermore, polyP
8
9 accumulation was visualized using confocal microscopy with DAPI staining ²⁹(Fig. 1B).
10
11 Compared to the Δppx and WT strains, a significantly lower number of bacteria in the
12
13 $\Delta ppk1$ and $\Delta ppk1-\Delta ppx$ mutants was observed, which correlated with the growth curve
14
15 delay observed in the minimal medium (Fig. S1B). Additionally, $\Delta ppk1$ and $\Delta ppk1-\Delta ppx$
16
17 strains showed less polyP granules, as evidenced by the reduction in the DAPI-polyP
18
19 fluorescence in compared to the WT and Δppx strains. Moreover, the addition of
20
21 Mesalamine, a PPK1 inhibitor ³⁰, caused a similar effect. Thus, our results suggest that
22
23 PPK1 is the primary enzyme responsible for polyP synthesis in *K. pneumoniae*, and the
24
25 absence of exopolyphosphatase (PPX) did not show noticeable effects on polyP synthesis or
26
27 accumulation.
28
29
30
31
32
33
34
35
36
37
38
39
40
41
42
43
44
45
46
47
48
49
50
51
52
53
54
55
56
57
58
59
60





32
33
34
35
36
37
38
39
40
41
42
43
44
45
46
47
48
49
50
51
52
53
54
55
56
57
58
59
60

Figure 1. PolyP accumulation under nutrient deprivation. (A) An overnight culture was diluted 1:100 in 10 mL of LB broth and allowed to grow with agitation until the mid-logarithmic phase (approximately 2 h). 1 mL of culture cells were pelleted and washed three times with MOPS medium (0.4% glucose and 0.1 mM K_2HPO_4), then incubated with agitation for 2 h at 37°C. The level of polyP was quantified before and after the nutritional shift. (B) The culture was set in the dark with DAPI (5 μg/mL) for 30 min and then mounted for observation by confocal microscopy using a 63X oil immersion objective. DNA was visualized using an excitation wavelength of 378 nm and an emission wavelength of 456 nm. PolyP was detected with excitation at 415 nm and emission at 550 nm. DAPI-DNA is represented in green, while DAPI-polyP is indicated in red for clarity in our visual representation.

PolyP metabolism mutants show altered capsule and mucoviscosity.

^{32,33,37}Given the relevance of the K1 capsule and HMV for hvKp virulence, we evaluated the role of polyP metabolism in these traits. HMV was quantified by low-speed centrifugation assays, where HMV strains tend to remain buoyant, resulting in a turbid supernatant⁶. The *Δppk1* and *Δppk1-Δppx* mutants but not *Δppx* showed significantly decreased HMV, compared to the WT strain (Fig. 2A). Furthermore, the quantification of uronic acids (UA) as essential *K. pneumoniae* capsule components³¹, showed a slight but significant reduction in capsule production in the *Δppk1* and *Δppk1-Δppx* mutants (Fig. 2B). These findings highlight the importance of PPK1 enzyme activity and polyP levels in regulating capsule formation and potentially virulence of hvKp.

To investigate whether the observed disparities in mucoviscosity and capsule production correlate with bacterial cell surface modifications, we visualized these strains via scanning electron microscopy (SEM). Previous studies have indicated that the SGH10 capsule is uniformly distributed over the cell surface and appears as filamentous projections that extend in multiple directions under SEM visualization³²⁻³⁴. In agreement, we observed a similar situation with the SGH10 strain (Figure 2C-A). In contrast, the *Δppk1*, and to a lesser extent, the *Δppk1-Δppx* mutant, showed differences in capsule morphology, both in terms of length and surface coverage. Since the length of the capsular polysaccharide is directly related to HMV, this result aligns with the significant reduction in mucoviscosity (Fig. 2A) and a decreased amount of capsule observed in *Δppk1-Δppx* and *Δppk1* (Fig. 2B). We did not observe significant differences between *Δppx* and the SGH10 WT strain.

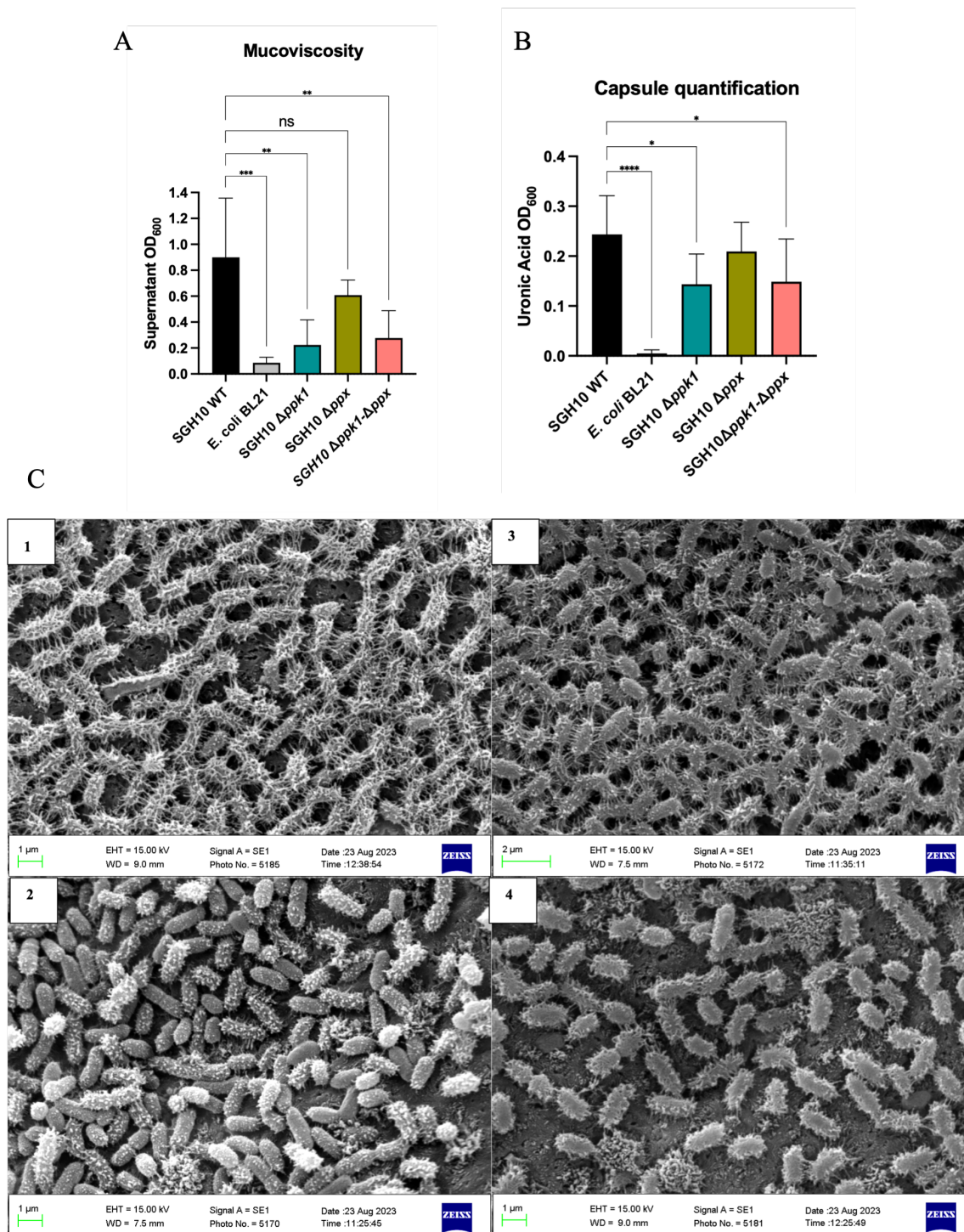


Figure 2. Capsule production and mucoviscosity in polyP-deficient *K. pneumoniae* mutants.

(A) Strain mucoid was measured by low-speed centrifugation (3000 rpm for 10 min) in LB.

The optical density at 600 nm (OD₆₀₀) of the supernatant above the pellet was measured

1
2
3 and mean \pm SD was plotted ($n = 3$). (B) Capsule production of polyP metabolism mutants
4 ($\Delta ppk1$, Δppx and $\Delta ppk1-\Delta ppx$). Uronic acid quantification analysis as described in
5
6 Materials and Methods. One-way ANOVA tests were performed for statistical analyses
7
8 comparing the WT strain to the indicated mutants. *, $P < 0.05$. ****, $P < 0.0001$. (C) Scanning
9
10 electron microscopy images of cells fixed in glutaraldehyde 2.5% and 0.15% ruthenium
11
12 red, obtained from log-phase cultures of SGH10 WT (1), SGH10 $\Delta ppk1$ (2), SGH10 Δppx (3)
13
14 and SGH10 $\Delta ppk1-\Delta ppx$ (4) cells. The scale bar is 1 μm .
15
16
17
18
19

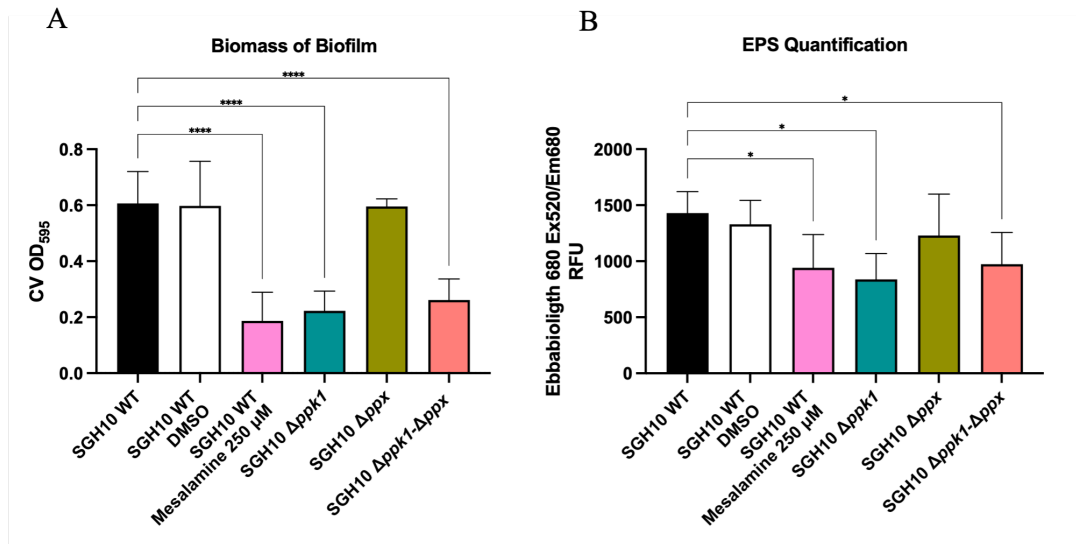
20 **PPK1 plays a crucial role in biofilm formation.**

21
22
23 Recently, it has been reported that mesalamine, a drug used to treat ulcerative colitis,
24
25 selectively inhibits PPK1 in gastrointestinal tract bacteria, decreasing biofilm formation
26
27 and virulence³⁰. To investigate whether mutants involved in polyP metabolism exhibit
28
29 alterations in biofilm formation, we conducted a biomass quantification assay using crystal
30
31 violet staining (0.1%). The $\Delta ppk1$ and $\Delta ppk1-\Delta ppx$ mutants showed a 66% and 56%
32
33 decrease in biofilm formation compared to the WT strain, respectively (Fig. 3A). This
34
35 decrease was not observed in the Δppx mutant, suggesting that the absence of PPK1
36
37 directly affects biofilm formation. Furthermore, we used mesalamine to validate this
38
39 observation and observed a 76% reduction in biofilm biomass compared to the WT strain
40
41 (Fig. 3A).
42
43
44
45
46
47

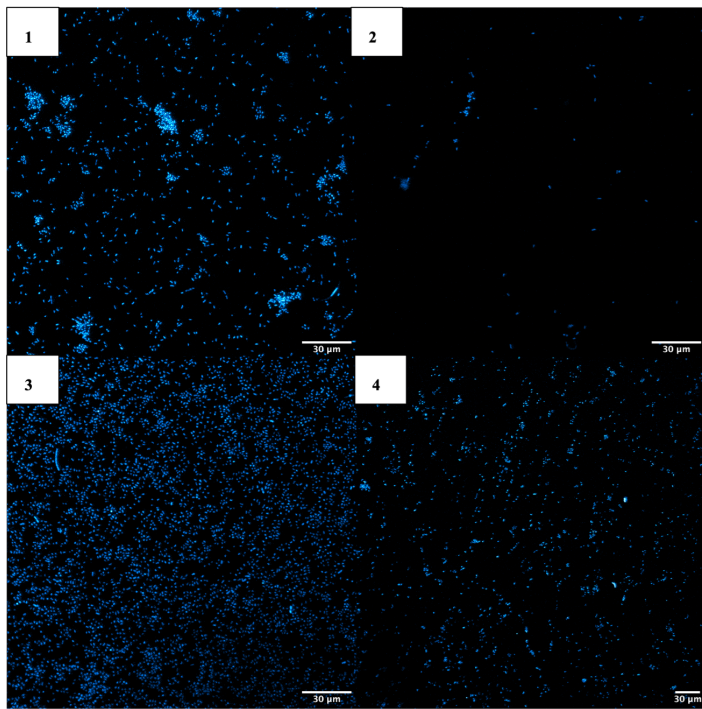
48 As a complementary approach to evaluate biofilm formation, we quantified the
49
50 extracellular polymeric substances (EPS) levels. For this purpose, we employed the
51
52 Ebbabiolight 680 probe³⁵ an optotracer that binds to curli and cellulose, increasing its
53
54 fluorescence. A significant decrease in EPS levels was observed in $\Delta ppk1$ and $\Delta ppk1-\Delta ppx$
55
56
57
58
59
60

1
2
3 compared to the SGH10 WT strain. No differences were observed in the Δppx mutant. (Fig.
4
5 3B). Furthermore, the observation of a 24 h biofilm grown on a tilted 96-well microtiter
6
7 plate under the confocal microscope further confirmed that the $\Delta ppk1$ and $\Delta ppk1-\Delta ppx$
8
9 mutants exhibited reduced biofilm biomass compared to the WT and Δppx (Fig 3C).
10
11

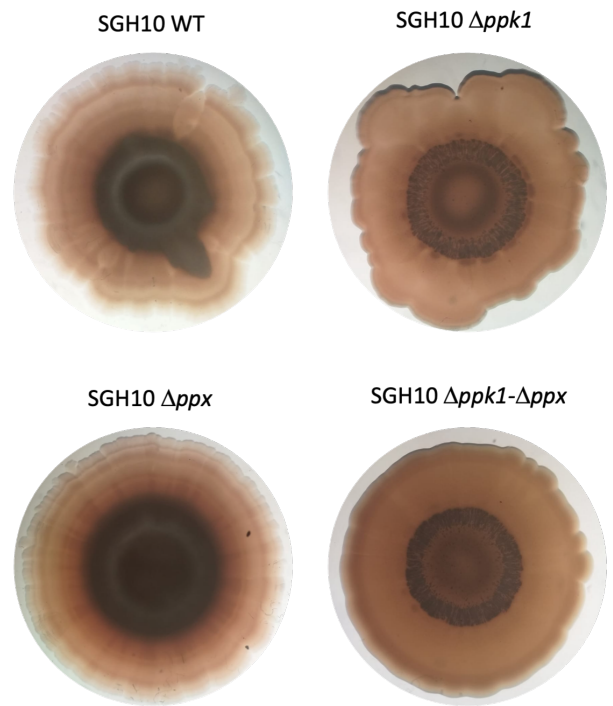
12
13 To better understand the relationship between polyP metabolism and biofilm formation,
14
15 we conducted a macrocolony biofilm formation assay in a salt-free LB medium
16
17 supplemented with Thioflavin S, which selectively binds to EPS, evidencing possible
18
19 differences in biofilm structure and organization. The SGH10 WT macrocolony biofilm
20
21 showed a dense central mucoid region, stained green, possibly by EPS components,
22
23 showing regular concentric rings. Conversely, the $\Delta ppk1$ mutant showed reduced mucosity
24
25 in the center of the colony, the absence of concentric rings, and a smoother appearance
26
27 with irregular edges. No evident differences were observed in the Δppx mutant compared
28
29 to the wild-type strain. In $\Delta ppk1-\Delta ppx$, we observed a reduction in the mucoid ring in the
30
31 center of the macrocolony biofilm, along with the absence of regular concentric rings.
32
33
34 However, the edges were like the WT strain, presenting an intermediate phenotype
35
36 between the wild-type strain and the $\Delta ppk1$ mutant. In conclusion, our findings
37
38 demonstrate that PPK1 plays a crucial role in biofilm formation, affecting not only the
39
40 proportion of cells that form biofilms (observed in the microwell biofilm assays) but also
41
42 EPS production and biofilm organization.
43
44
45
46
47
48
49
50
51
52
53
54
55
56
57
58
59
60



C



D



1
2
3 **Figure 3.** Biofilm formation is altered in polyP-deficient mutants. (A)

4
5 Measurement/Quantification of relative biofilm formation in polyP metabolism mutants by
6
7 0.1% crystal violet staining. Overnight cultures were diluted to an $OD_{600} = 0.1$ and plated in
8
9 96-well plates. The measurement was at 24 h at 595 nm. (B) EbbaBiolight 680 is an
10
11 optotracer for facilitating biofilm visualization, specifically targeting cellulose and amyloid
12
13 constituents within the biofilm matrix. Colonies were grown on agar plates under biofilm-
14
15 forming conditions. EbbaBiolight 680™ was diluted in PBS 1:1000 and 100 μ L were added
16
17 into each well of a 96-well plate. Pick bacterial colonies from the agar plate and resuspend
18
19 thoroughly into the pre-filled wells. Plates were placed in Plates in a spectrophotometer to
20
21 quantify biofilm in the colony resuspensions. One-way ANOVA tests were performed for
22
23 statistical analyses comparing the WT strain to the indicated mutants. *, $P < 0.05$ ****, $P <$
24
25 0.0001. (C) Confocal microscopy. SGH10 WT (1), SGH10 $\Delta ppk1$ (2), SGH10 Δppx (3), SGH10
26
27 $\Delta ppk1-\Delta ppx$ (4) Overnight cultures were diluted 1:100 in LB and plated on a glass coverslip
28
29 on a 6-well plate slanted at 80°. The plate was incubated for 24 hours. DAPI was used for
30
31 biomass staining for 30 min, labeling DNA ex/em 358/462. Image obtained in LSM 710
32
33 Zeiss microscope, 20X. (D) Macrocolony biofilm formed by inoculating an overnight culture
34
35 in LB broth onto LB agar plates supplemented with 40 μ g/mL Thioflavin S. A 5 μ L droplet
36
37 of the culture was used for inoculation. The plates were subsequently incubated at 28 °C
38
39
40
41
42
43
44
45
46
47
48
49
50
51
52
53
54
55
56
57
58
59
60 for 10 days.

1
2
3
4
5
6
7 **PPK1 is essential for HvKp virulence in *D. discoideum*.**

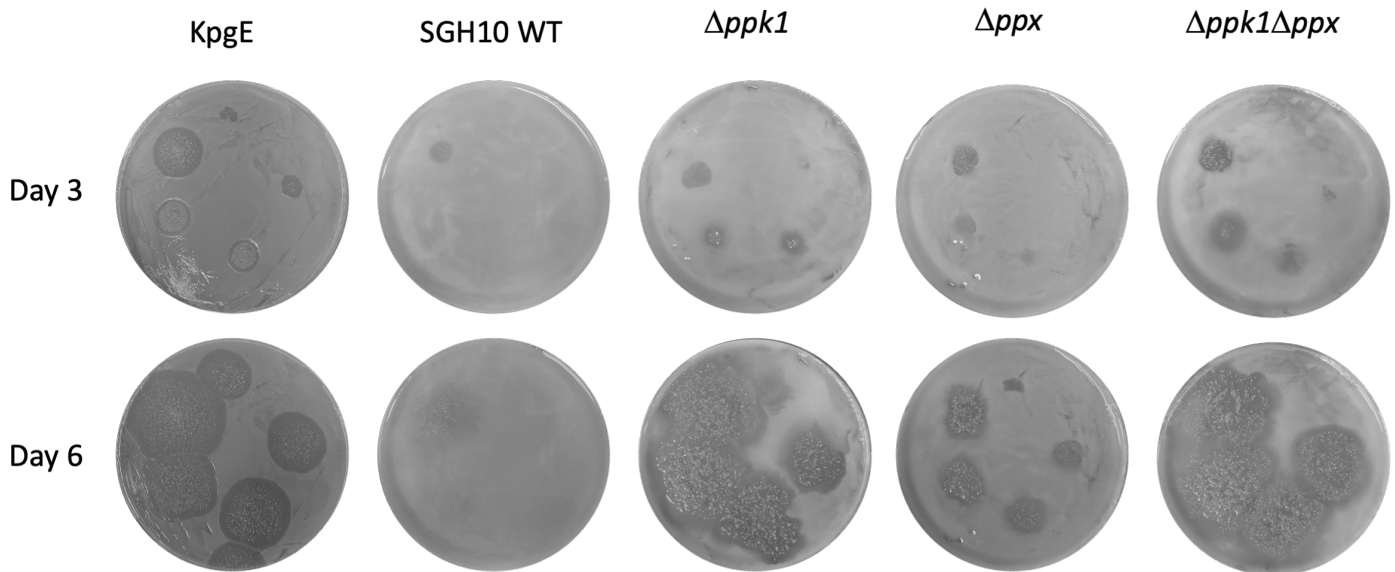
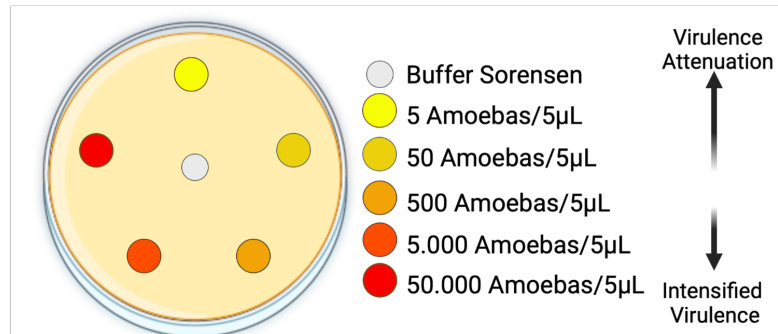
8
9
10 Our findings strongly indicate that PPK1 serves as the primary enzyme responsible for
11 polyP synthesis in the *K. pneumoniae* SGH10 strain and that it is involved in the regulation
12 of capsule and biofilm formation, traits that were proposed as relevant HvKp virulence
13 factors. To investigate the impact of polyP and PPK1 deficiency on virulence, we used the
14 social amoeba *D. discoideum* as a model host, previously validated for other *K. pneumoniae*
15 strains³⁷. When grown on lawns of avirulent bacterial strains, *D. discoideum* forms visible
16 phagocytosis plaques. However, the amoeba fails to develop in the presence of virulent
17 strains, and no phagocytosis plaques are observed³⁸. Using this assay, we determined the
18 minimum number of amoebas required to generate a phagocytosis plaque. As shown
19 previously, if phagocytosis plaques are formed with 500 or fewer *D. discoideum* cells, the
20 bacteria exhibit susceptibility to predation, indicating attenuated virulence³⁹.
21
22
23
24
25
26
27
28
29
30
31
32
33
34
35

36 Resistance to predation of SGH10 and the mutant derivatives was evaluated in the third
37 and sixth day of the assay (Fig. 4A). The avirulent strain *K. pneumoniae* KpgE (commonly
38 used as food for *D. discoideum*) was used as a control, showing phagocytosis plaques
39 starting from day 3 with amoebae. For SGH10, a phagocytosis plaque was observed only
40 with 50,000 amoebae, indicating the strain's virulence towards *D. discoideum*. In the case of
41 mutants in polyP metabolism ($\Delta ppk1$; Δppx ; $\Delta ppk1-\Delta ppx$), we observed an attenuation in
42 virulence, as evidenced by the presence of phagocytosis plaques with 500 amoebae cells.
43
44
45
46
47
48
49
50
51
52
53 Furthermore, a differential impact on virulence was observed when comparing $\Delta ppk1$ and
54 $\Delta ppk1-\Delta ppx$ with Δppx . On the sixth day, larger phagocytosis plaques were observed in the
55
56
57
58
59
60

1
2
3 absence of the *ppk1* gene in both mutants, compared to the Δppx strain. This suggests that
4
5 the lack of PPK1 has a more pronounced effect on attenuating virulence than the absence of
6
7 PPX, despite both mutations caused a decreased virulence.
8
9

A

Predation resistance assay

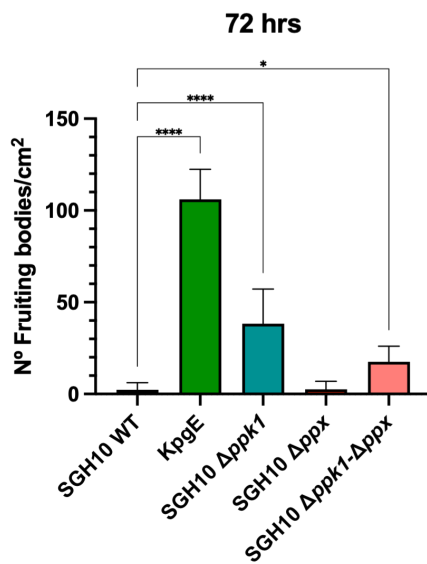
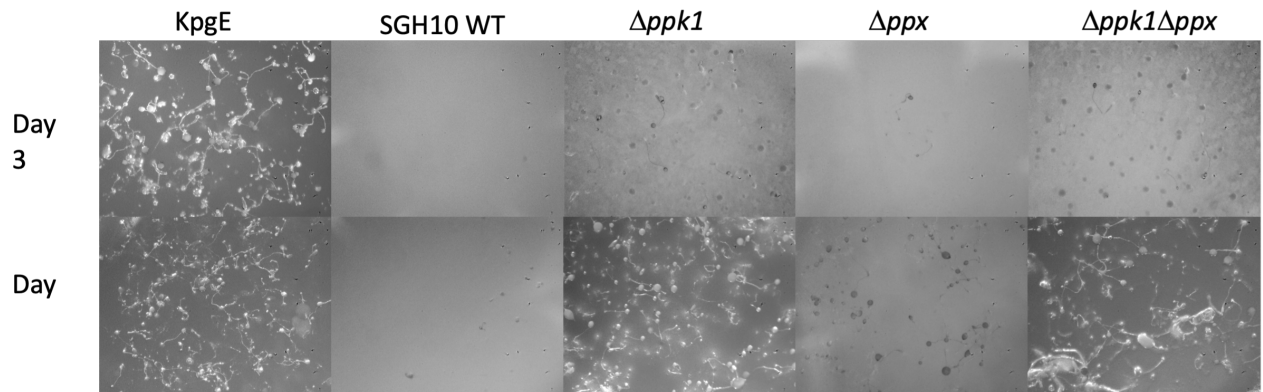
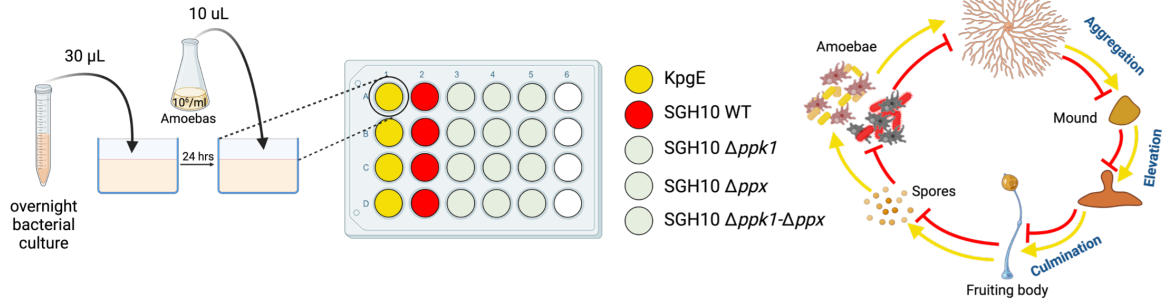


1
2
3 Previous studies have demonstrated that pathogenic bacteria with high virulence
4 capabilities can impede the social development of *D. discoideum*^{18,37,40}. Conversely,
5
6 attenuated or avirulent bacteria have a minimal impact on social development, which
7
8 involves at least three stages: aggregation, including the formation of a phagocytosis plaque
9
10 and subsequent cluster formation; elevation, involving the formation of slugs and fingers;
11
12 and culmination, comprising the formation and dispersal of fruiting bodies.
13
14
15
16
17

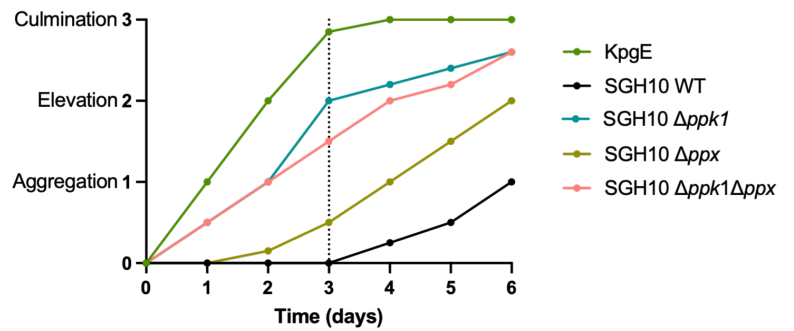
18 The avirulent strain KpgE promoted normal social development, culminating between days
19
20 2 and 3 with an approximate count of 110 fruiting bodies/cm² on the third day (Figure 4C-
21
22 D). In contrast, the SGH10 WT strain inhibited social development within the 6-day study
23
24 period (Figure 4C). We were able to quantify in isolation an average of 2.3 fruiting
25
26 bodies/cm² on the third day (Figure 4B-D). Mutants in polyP metabolism exhibited varying
27
28 levels of virulence attenuation. $\Delta ppk1$ displayed the most marked effect, almost reaching
29
30 the culmination of social development on the sixth day (Fig. 4D), with an average of 38
31
32 fruiting bodies/cm² on the third day (Fig. 4C). This was followed by $\Delta ppk1-\Delta ppx$, which
33
34 exhibited 17.5 fruiting bodies/cm² on the third day, also reaching a stage before
35
36 culmination (Fig. 4C). Δppx behaved as less attenuated, with a count of 2.5 fruiting
37
38 bodies/cm² on the third day (Fig. 4B-D).
39
40
41
42
43
44
45
46
47
48
49
50
51
52
53
54
55
56
57
58
59
60

B

Social development assay



D

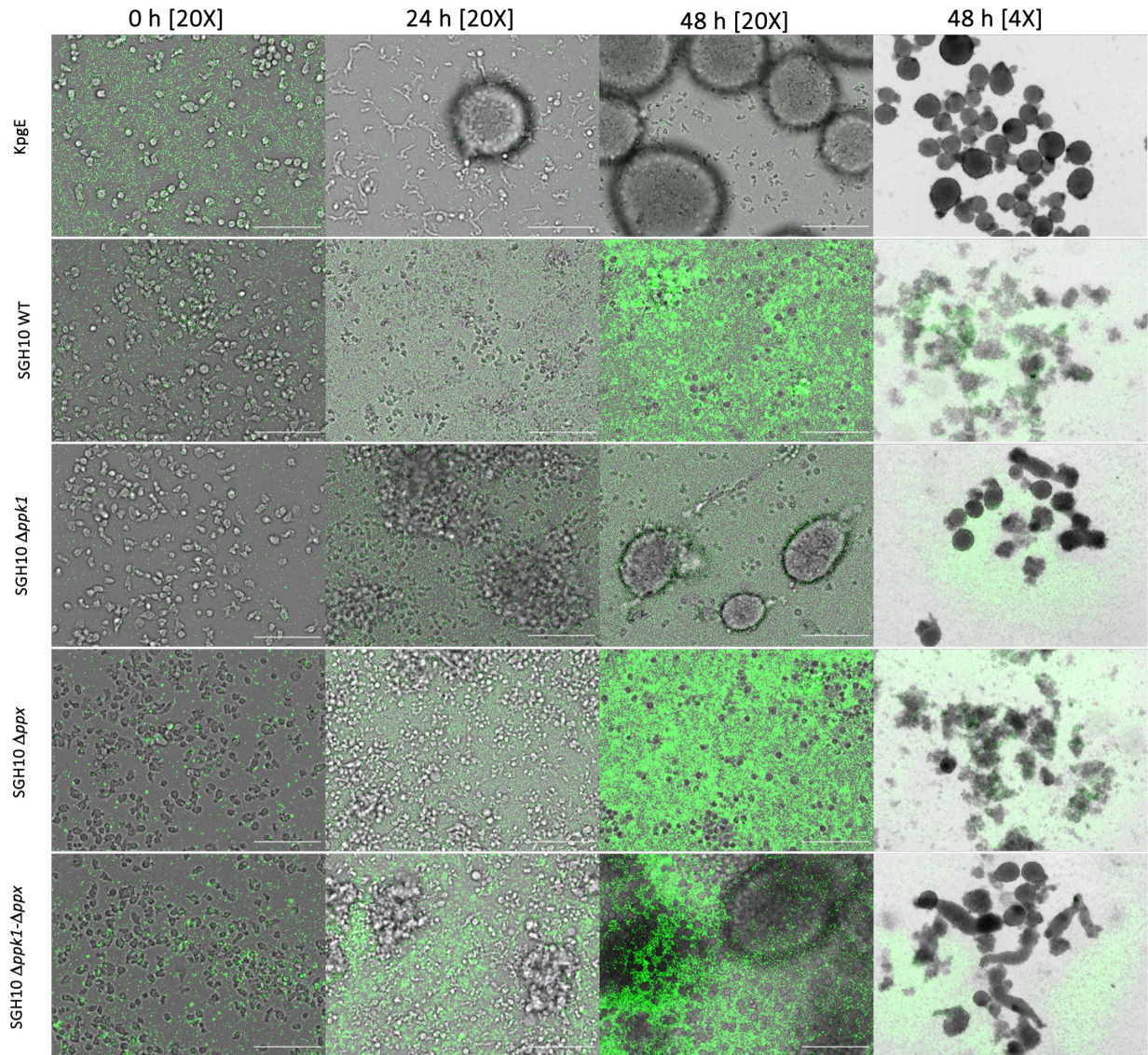


1
2
3 To get further evidence of our findings, we conducted epifluorescence microscopy to follow
4
5 *D. discoideum* phagocytosis of bacteria constitutively expressing the green fluorescent
6
7 protein sfGFP. Amoebae were infected with a MOI=10, and phagocytosis was monitored at
8
9 0-, 24-, and 48 h post-infection (Fig. 4E). For the avirulent KpgE strain, within the first 24
10
11 hours, we observed polarized groups of amoebae migrating towards aggregation centers to
12
13 form multicellular clusters and a significant reduction in the number of bacteria present, as
14
15 indicated by the decrease in green field fluorescence intensity (Fig. 4E and 4F). By 48 h, we
16
17 observed abundant multicellular aggregation bodies visible at a 4X magnification (Fig. 4E)..
18
19 In the case of the SGH10 WT strain, we did not observe the amoebae polarization
20
21 characteristic of an aggregation process (Fig. 4E). Moreover, at a 4X magnification, we did
22
23 not observe well-defined multicellular aggregation structures. Additionally, we observed a
24
25 substantial bacterial proliferation, as evidenced by a significant increase in the green
26
27 fluorescence intensity at 24 h (Fig. 4F).
28
29
30
31
32
33

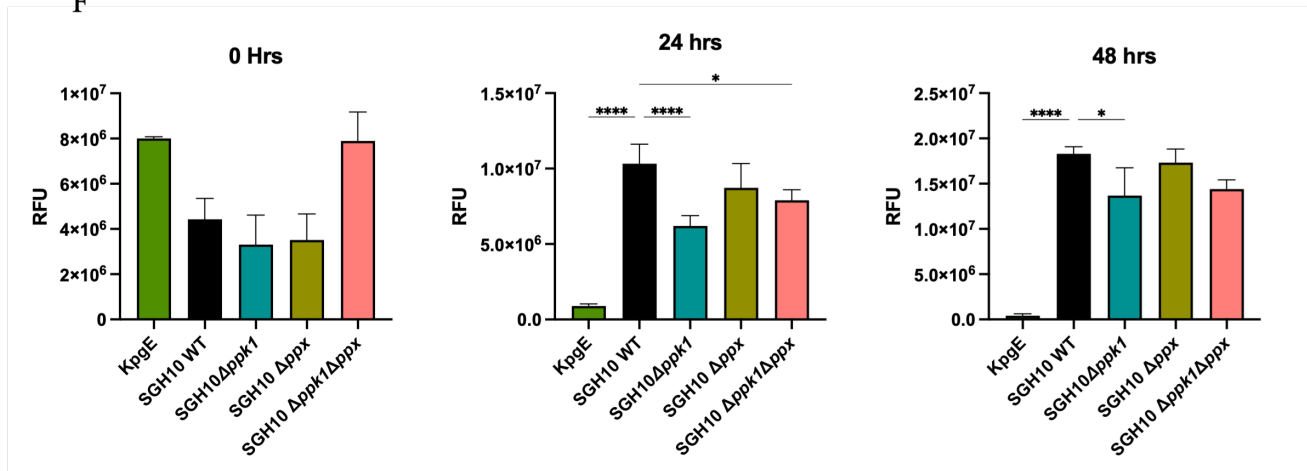
34 For the $\Delta ppk1$ mutant, we observed small amoebae clusters at 24 h and mounds visible at
35
36 4X magnification at 48 h (Fig. 4E).. Regarding proliferation, it was significantly lower when
37
38 compared to the SGH10 WT strain, both at 24 and 48 h (Fig. 4F). Similar results were
39
40 obtained with the $\Delta ppk1$ - Δppx mutant. Conversely, no significant differences were
41
42 observed at 24-48 h between SGH10 WT and the Δppx mutant (Fig. 4E-F). In conclusion,
43
44 our study strongly supports the importance of PPK1 in hvKp virulence.
45
46
47
48

49 In conclusion, our study strongly supports the involvement of PPK1 in the virulence of
50
51 hypervirulent *Klebsiella pneumoniae*.
52
53
54
55
56
57
58
59
60

E



F



1
2
3 **Figure 4.** (A) Predation resistance assay. 300 μ L of overnight culture were seeded onto a
4 plate using a Digralsky loop to generate a bacterial lawn. The plate was left to dry and
5
6 incubated for 24 hours at 23°C. *D. discoideum* was cultured in HL5 medium, and serial
7
8 dilutions were prepared to obtain the following cell concentrations: 5 – 50 – 500 – 50.000
9
10 cells per 5 μ L in Buffer Sorensen. Subsequently, 5 μ L of *D. discoideum* serial dilutions were
11
12 applied onto the bacterial agar plates, and the plates were allowed to dry and were
13
14 incubated at 21°C for 6 days. Plaque formation was visually examined on days 3 and 6.
15
16 Strains that did not enable amoebae growth were considered virulent for the amoeba.
17
18 Bacterial strains that exhibited social development with 500 *D. discoideum* were considered
19
20 sensitive to predation. (B) 30 mL of overnight cultures of the strains under study were
21
22 inoculated in a 24-well plate on N agar to generate a lawn. They were incubated for 24 h at
23
24 23 °C. *D. discoideum* was adjusted to 10^6 /ml. A 10 mL drop of the dilution was inoculated
25
26 on each law. Representative images of days 3 and 6 days are presented. The number of
27
28 fruiting bodies was counted on the 3rd day and compared with the WT strain (C) and the
29
30 social development of the amoeba was followed for six days (D). The KpgE commensal
31
32 strain was used as a control. (E) Timelapse of a 48-hour phagocytosis assay in GFP channel
33
34 (bacteria). KpgE was used as a control. Scale 100 μ m. Images were acquired using an
35
36 automated Lionheart FX microscope with a 20X objective. For multicellular development
37
38 observation, a 4X objective was used. (F) Fluorescence quantification was performed in
39
40 ImageJ with three biological replicates. One-way ANOVA tests were performed for
41
42 statistical analyses comparing the WT strain to the indicated mutants. **** $p < .00001$, * $p <$
43
44 0.05.
45
46
47
48
49
50
51
52
53
54
55
56
57
58
59
60

Global Proteomic Profiling of hvKp mutants in polyP metabolism genes.

To investigate the underlying mechanisms responsible for the significant reduction in capsule production, biofilm formation, and virulence, we performed a shotgun proteomic analysis of the mutants with altered polyP metabolism. Samples were obtained from colonies grown on LB agar at 37°C and subjected to LC-MS/MS analysis using a Data Dependent Acquisition method and label-free quantification (LFQ). The WT strain was compared to each mutant strain. Principal component analysis (PCA) on the identified protein dataset, as shown in Figure S4C, revealed the grouping of the samples into their corresponding clusters I(SGH10 WT, $\Delta ppk1$, Δppx , and $\Delta ppk1-\Delta ppx$ groups). Later, among the 2,287 quantifiable proteins identified, 302, 728, and 673 were determined to be Differentially Expressed Proteins (DEPs) in the comparisons of WT vs. $\Delta ppk1$, WT vs. Δppx , and WT vs. $\Delta ppk1-\Delta ppx$, respectively (Table S2). The quantifiable proteins resulting from these comparisons were visualized as volcano plots (Fig. 5A), where significantly upregulated proteins were represented in blue and downregulated proteins in red.

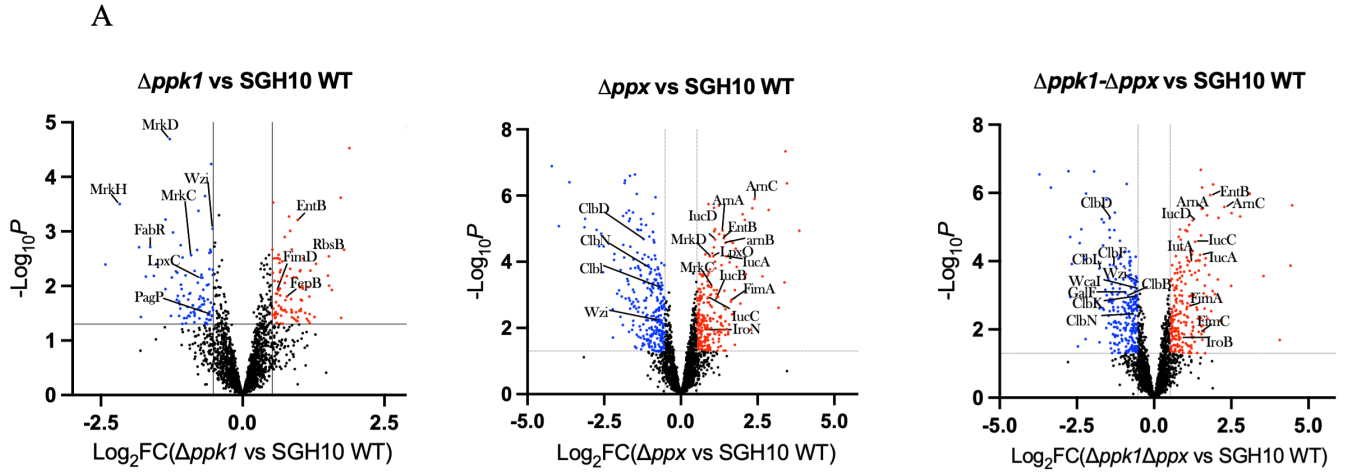
To further investigate potential virulence factors associated with the observed results, DEPs were compared against the VFDB database, and those matching with a $\geq 50\%$ identity were selected for further analysis. The virulence factors were categorized into anti-phagocytosis, adherence, iron uptake, and toxins and visualized in a heatmap (Fig. 5B), a network of curated interactions (Fig. S5) and a chordplot (Fig. S6). Regarding the Adherence category, we observed a significant reduction in proteins from the mrk operon responsible for synthesizing type III fimbriae (MrkB, MrkC, MrkD, MrkH), particularly in the $\Delta ppk1$ mutant, and to a lesser extent in the $\Delta ppk1-\Delta ppx$ mutant. Additionally, there was

1
2
3 an increase in proteins that are part of the type I fimbriae synthesis pathway (FimA and
4 FimC). In the case of Δppx , we observed a significant increase in proteins from both type I
5 (FimA, FimC) and type III fimbriae (MrkB, MrkC, MrkD, MrkH). Concerning anti-
6 phagocytosis factors, we observed a significant reduction in essential proteins associated
7 with capsule synthesis, transport, and regulation in *K. pneumoniae*, particularly in the
8 double mutant $\Delta ppk1-\Delta ppx$. This mutant exhibited decreased expression of GalF, Wzi, Wza,
9 WcsT, Wca, Ugd, and Gmd compared to the wild-type strain. Furthermore, in $\Delta ppk1$, Wzi
10 and Ugd proteins showed negative regulation. This correlates with the decrease in the
11 amount of capsule produced by these mutants compared to the SGH10 WT strain. Δppx
12 showed an overexpression of Wzi compared to the SGH10 WT strain.
13
14
15
16
17
18
19
20
21
22
23
24
25
26

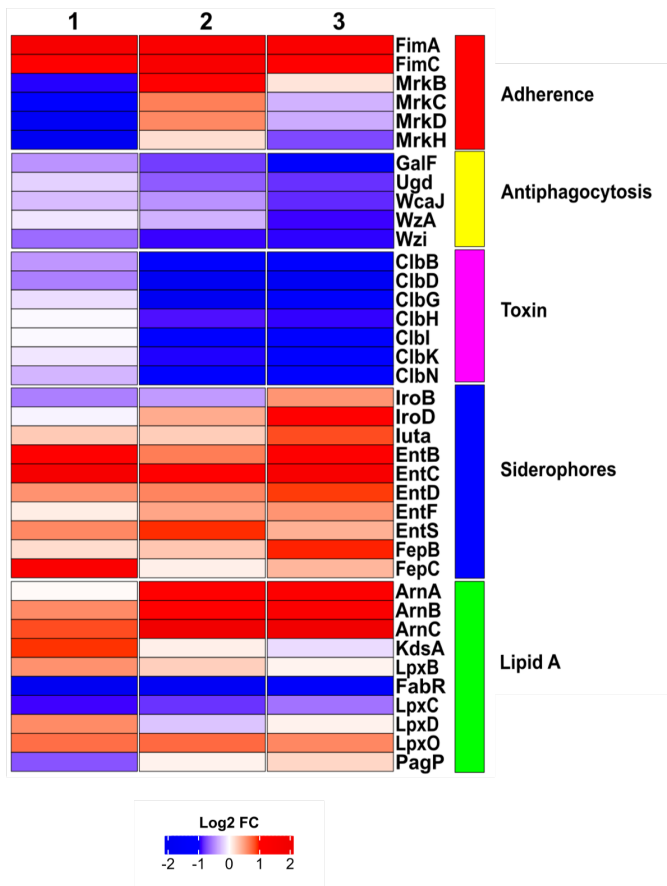
27 Concerning iron uptake, proteins related to the synthesis of siderophores such as
28 aerobactin, enterobactin, salmochelin, and yersiniabactin were found to be overexpressed
29 in all polyP mutants, except for yersiniabactin in $\Delta ppk1$, where no significant differences
30 were observed compared to the wild-type strain. Both Δppx and $\Delta ppk1-\Delta ppx$ exhibited
31 upregulation of operons involved in the synthesis of aerobactin and enterobactin, as well as
32 the protein YbtS, which is implicated in the final step of yersiniabactin union and
33 modification, playing a crucial role in the overall siderophore biosynthesis process. In
34 $\Delta ppk1$, several proteins involved in siderophore synthesis, including IucA (aerobactin),
35 EntB, EntC, FepC (enterobactin), and IroD (salmochelin), were found to be overexpressed.
36
37 Regarding the toxin category, in all polyP metabolism mutants, a significant
38 downregulation was observed in most of the proteins from the colibactin genotoxin
39 biosynthetic cluster. This downregulation was particularly evident in Δppx and $\Delta ppk1-$
40 Δppx , affecting proteins such as ClbB, ClbD, ClbF, ClbG, ClbH, ClbI, ClbK, ClbL, ClbN, and
41
42
43
44
45
46
47
48
49
50
51
52
53
54
55
56
57
58
59
60

1
2
3 ClbQ. In the case of $\Delta ppk1$, the main protein involved in colibactin biosynthesis, ClbB, was
4
5 downregulated along with ClbD.
6
7

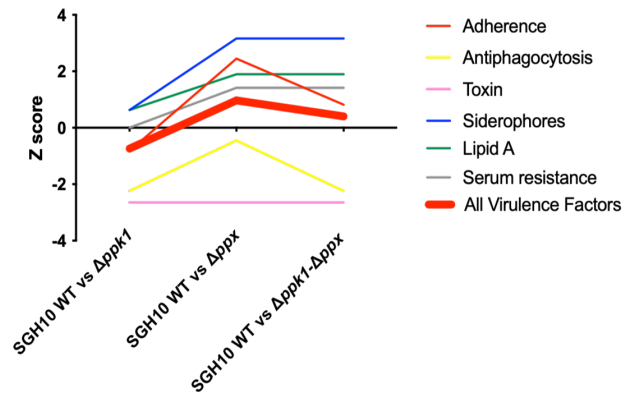
8
9 In the Lipid A category, we observed a significant increase in proteins involved in the
10
11 biosynthesis and modification of Lipid A, such as ArnA, ArnB, ArnC, PagP, and LpxO in $\Delta ppk1$
12
13 and $\Delta ppk1-\Delta ppk1$. $\Delta ppk1$ displayed similar differential expression levels in these proteins;
14
15 however, no significant differences were observed for ArnA. Additionally, proteins PagP,
16
17 LpxC, and FabR, related to Lipopolysaccharide (LPS) biosynthesis and modification,
18
19 exhibited decreased expression levels compared to the WT strain. This prompted us to
20
21 evaluate whether the differential expression of proteins involved in Lipid A modification
22
23 would confer colistin resistance (Fig. S7). However, the mutants did not show increased
24
25 colistin resistance, with a 4 $\mu\text{g}/\text{mL}$ MIC. Finally, in Figure 5C, we present a z-score plot that
26
27 considers the abundances of 38 proteins related to each virulence category (adherence,
28
29 anti-phagocytosis, toxin, siderophores, lipid A), highlighted in the heatmap. In this analysis,
30
31 the $\Delta ppk1$ mutant exhibited a negative z-score compared to the WT for all virulence factors
32
33 reported in the VFDB database. In conclusion, our global proteomic profiling of polyP
34
35 metabolism mutants revealed significant alterations in protein expression related to
36
37 biofilm formation, capsule regulation, iron uptake, and toxin production, corresponding to
38
39 key virulence-associated traits in hvKP.
40
41
42
43
44
45
46
47
48
49
50
51
52
53
54
55
56
57
58
59
60



B



C



1
2
3 **Figure 5.** Global proteomic profiling of polyP metabolism mutants in hvKP. (A) Volcano
4 plot of differentially expressed proteins from each polyP metabolism mutant strain. These
5 colored points indicate different proteins that display large magnitude fold-changes (x-
6 axis) and high statistical significance (-log₁₀ of p values, y-axis). The dashed horizontal line
7 shows the cut-off p-values, and the two vertical dashed lines indicate down (blue) /up
8 (red) differentially expressed proteins. Black points in the significant region mean these
9 proteins do not satisfy these conditions. (B) Heatmap shows differentially expressed
10 virulence factors (VF) of polyP metabolism mutants in hvKP (1) $\Delta ppk1$ VS SGH10 WT; (2)
11 Δppx VS SGH10 WT; (3) $\Delta ppk1$ - Δppx VS SGH10 WT. The proteome was compared with the
12 VDFB database, and the VFs were classified according to the categories: Adherence, anti-
13 phagocytosis, siderophores, toxin, lipid A, serum resistance, and secretion system. (C) Z-
14 score plot illustrating the global relative abundance of each of the proteins associated with
15 virulence factors. Positive z-scores indicate proteins with higher abundance, while negative
16 z-scores indicate proteins with lower abundance compared to the overall mean. The red
17 line represents the average of all z-scores for the virulence factors.

38 39 **DISCUSSION**

40
41
42 *K. pneumoniae* is a growing health threat due to its antibiotic resistance and the emergence
43 of highly virulent strains. These strains can infect healthy individuals and are adept at
44 causing severe infections, posing risks to hospitalized patients and the general
45 population⁴¹. Traditional approaches targeting bacterial viability through antibiotic use
46 have led to the selection of multidrug-resistant strains, necessitating a shift in strategy. In
47 line with the principle of "Disarm and not kill," there is an increasing recognition that
48
49
50
51
52
53
54
55
56
57
58
59
60

1
2
3 targeting virulence mechanisms rather than bacterial viability could provide a promising
4
5 alternative to mitigate the risk of resistance development. In this study, we investigated the
6
7 involvement of polyP metabolism in ST23 hvKp fitness and virulence, focusing on the PPK1
8
9 enzyme and its implications on capsule production, mucoviscosity, biofilm formation, and
10
11 virulence over the *D. discoideum* host model.
12
13
14

15
16 In the hypervirulent strain SGH10, we observed that PPK1 is the primary enzyme
17
18 responsible for synthesizing inorganic polyphosphates. As anticipated, the absence of PPK1
19
20 and a marked reduction in polyP did not substantially impact viability under favorable
21
22 growth conditions ²⁸. However, when exposed to minimal conditions (stress response), a 2-
23
24 h delay in reaching exponential growth was observed. This delay is expected, as nutrient
25
26 scarcity is known to be one of the main triggers for polyphosphate synthesis, and its
27
28 absence leads to a noticeable growth delay that eventually recovers when increasing
29
30 concentrations of polyP were added.¹⁷ In the PPX mutant, a drastic increase in polyP
31
32 formation or accumulation in response to nutritional downshift in the MOPS medium
33
34 (0.4% glucose, 0.1 mM K₂HPO₄) was not observed. The classical model proposed by A.
35
36 Kornberg's group for *E. coli* suggests that a stress response such as amino acid starvation
37
38 leads to the accumulation of (p)ppGpp, which interacts with PPX and inhibits it, promoting
39
40 polyP accumulation. However, based on recent evidence, other factors such as DksA and
41
42 GreA proteins significantly regulate polyP accumulation in response to amino acid
43
44 starvation ^{42,43}. This could explain our observations in the Δppx mutant. However, there is
45
46 no pronounced effect on viability, suggesting that PPK1 could be an attractive target for
47
48 antivirulence strategies in this hypervirulent strain. Similar results were reported for *P.*
49
50
51
52
53
54
55
56
57
58
59
60

1
2
3 *aeruginosa* PAO1, where some PPK1 inhibitors affected its virulence, resembling $\Delta ppk1$
4 knockout mutant phenotype⁴⁴.
5
6

7
8
9 Several previous studies have demonstrated that the K1 capsule present in the SGH10
10 strain is a crucial virulence factor that enables evasion of immune recognition and
11 resistance to phagocytosis³². Recently, it has been shown that the length of the capsular
12 polysaccharide is relevant to the characteristic HMV phenotype of hypervirulent strains,
13 although not exclusive to them^{6,7}. This length regulation is mediated by the RmpD protein,
14 which interacts with Wzc to regulate polysaccharide length. Our results indicate that PPK1
15 promotes the HMV phenotype and capsule expression or synthesis. The $\Delta ppk1$ mutant
16 displayed longer sedimentation times during low-speed centrifugation, a standard method
17 to assess mucoviscosity⁴⁵. Additionally, both the $\Delta ppk1$ and double mutant cells exhibited
18 lower capsule levels, indicated by reduced uronic acid content and an altered distribution
19 of capsule polysaccharides, which is distinct from the SGH10 strain.³² In addition to the
20 findings in *K. pneumoniae*, a $\Delta ppk1$ mutant of *P. aeruginosa* also shows altered surface
21 structures²¹. In *Neisseria meningitidis*, it has been demonstrated that polyP can interact
22 with the membrane, forming a capsule-like structure⁴⁶. This indicates that the role of PPK1
23 and polyP in capsule synthesis and structure may be conserved across different bacterial
24 species.
25
26
27
28
29
30
31
32
33
34
35
36
37
38
39
40
41
42
43
44
45

46
47 The presence of polyP appears crucial for the proper assembly and organization of the
48 capsule, and its absence or disruption can lead to abnormalities in the superficial
49 structures. The defective membrane pattern observed in the $\Delta ppk1$ mutant of *P. aeruginosa*
50 suggests that polyP regulates external biomolecule biosynthesis or assembly. Our
51
52
53
54
55
56
57
58
59
60

1
2
3 proteomic analysis of the *K. pneumoniae* $\Delta ppk1$ and $\Delta ppk1-\Delta ppx$ mutants revealed
4
5 decreased expression of proteins involved in capsular polysaccharide synthesis, such as
6
7 Wzi-Ugd ($\Delta ppk1$), as well as GalF, GalU, Wza, WcaJ, Ugd ($\Delta ppk1-\Delta ppx$). This downregulation
8
9 could explain the decrease in capsular polysaccharide production and mucoviscosity, as
10
11 reported in the HV *K. pneumoniae* strain NTUH-K2044 ¹¹. These findings suggest that polyP
12
13 metabolism may be relevant in regulating capsule expression and the HMV phenotype.
14
15

16
17
18 Inorganic polyP may act as a signal molecule, triggering specific regulatory pathways
19
20 controlling capsule biosynthesis. Similarly to *E. coli* and *P. aeruginosa*, where PPK1 is
21
22 predominantly associated with the membrane ⁴⁷, it is possible that in *K. pneumoniae*, this
23
24 preferential localization has regulatory roles in biofilm formation and capsule and
25
26 membrane processes. Furthermore, polyP may act as a phosphate donor to form sugar
27
28 linkages in the capsule synthesis pathway ⁴⁸. Phosphate is crucial in numerous biological
29
30 molecules and processes within bacteria, encompassing the synthesis of polysaccharides
31
32 integral to the bacterial capsule. Mutants deficient in PPK1 and PPK1-PPX have previously
33
34 exhibited a phenotype associated with phosphate-related effects in *E. coli* ⁴⁹. Phosphates
35
36 are commonly present as phosphate groups in the structure of carbohydrates and other
37
38 biomolecules. Polysaccharides, which constitute the capsule, can contain phosphate groups
39
40 as part of their chemical structure or as a modification of their structure ⁵⁰. These
41
42 phosphate groups may correspond to side chains or substitutions on the sugar molecules
43
44 forming the polysaccharide backbone ⁵¹. The presence of phosphate groups in the capsule
45
46 can have functional implications, contributing to the overall charge and hydrophilicity of
47
48 the capsule and then influencing its interactions with the environment, such as host tissues
49
50
51
52
53
54
55
56
57
58
59
60

1
2
3 and immune cells. Phosphate groups can also be involved in the binding of cations and
4
5 other molecules, further modulating the properties and functions of the capsule.
6
7

8
9 Biofilm formation is the primary lifestyle of bacteria in their natural state and serves as a
10
11 successful strategy to thrive in niches subjected to various stressors and the most efficient
12
13 way for the trafficking of mobile genetic elements ⁵². There is a broad consensus in the
14
15 literature regarding the ability of both classical and multidrug-resistant *Klebsiella*
16
17 *pneumoniae* strains to form biofilms in various niches, particularly in
18
19 immunocompromised individuals ⁵³⁻⁵⁶. The *fim* and *mrk* operons, responsible for encoding
20
21 type I and type III fimbriae, respectively, play a crucial role in the initial adhesion to both
22
23 biotic and abiotic surfaces ⁵⁷. Regarding hvKp strains, it has been observed that their
24
25 elongated capsular polysaccharides can cover the fimbriae, hindering their contact with
26
27 surfaces and resulting in weaker biofilm formation ^{10,58}. However, conflicting reports
28
29 suggest that the capsule may promote the formation of biofilm structures, particularly
30
31 within infectious contexts ^{11,12,59}. Our findings demonstrate the capability of the SGH10
32
33 strain to form biofilms on polystyrene plates, glass, and at the air-liquid interface. The
34
35 $\Delta ppk1$ and $\Delta ppk1-\Delta ppx$ mutants exhibited reduced biofilm formation compared to the WT
36
37 strain. These results are consistent with previous reports in various models ^{28,60-63}.
38
39 Interestingly, the use of mesalamine, a drug used in the treatment of ulcerative colitis that
40
41 also inhibits PPK1 ³⁰, showed similar levels of biomass reduction in the biofilm as observed
42
43 in $\Delta ppk1$ and $\Delta ppk1-\Delta ppx$ mutant cells, confirming the close association between biofilm
44
45 formation and polyphosphates.
46
47
48
49
50
51
52
53
54
55
56
57
58
59
60

1
2
3 The proteomic analysis further confirms the relevance of polyP metabolism in biofilm
4 formation. In the case of the $\Delta ppk1$ mutant, we observed a decrease in the transcription
5 levels of *mrkC*, *mrkD*, and *mrkH* genes, accompanied by an increase in *fimA* and *fimD*.
6
7
8
9
10 Conversely, the Δppx mutant significantly increased Fim (FimA, FimC, FimD) and Mrk
11 (MrkB, MrkC, MrkD) proteins. Similarly, the $\Delta ppk1$ - Δppx mutant exhibited elevated levels
12 of FimA and FimC proteins. This dysregulation can be partially explained by a previous
13 report pointing out that polyP degradation during the stationary phase promotes biofilm
14 formation⁶⁴. Consequently, the insufficient levels of polyphosphates in the $\Delta ppk1$ and
15 $\Delta ppk1$ - Δppx mutants lead to the downregulation of proteins from the *mrk* operon.
16
17
18
19
20
21
22
23
24 However, this explanation does not fully account for the increased proteins from the *fim*
25 operon, indicating the involvement of broader regulatory mechanisms. A recent study has
26 reported a direct correlation between biofilm formation and the colibactin operon in
27 isolates of *E. coli* and *K. pneumoniae*^{65,66}. Furthermore, since it has been demonstrated that
28 the inactivation of PPK by mutagenesis reduces the promoter activity of *clbB* (the gene that
29 encodes for an essential enzyme for colistin biosynthesis) and decreases the production
30 level of colibactin⁶⁷, it is possible that the absence of this enzyme also leads to a decrease
31 in biofilm formation through this pathway. Recently, a phenotypic switch between type III
32 fimbriae and the hypermucoviscous capsule in response to iron levels has been reported in
33 the SGH10 strain.^{70,27} The iron-regulated outer membrane protein IroP, encoded in the
34 virulence plasmid, inhibits the expression of the *mrk* operon under low iron conditions,
35 inhibiting biofilm formation. Since polyP are directly involved in intracellular iron
36 homeostasis as an iron chelator⁶⁸, the observed alterations in the capsule and biofilm
37 might be related to this recently described phenomenon.
38
39
40
41
42
43
44
45
46
47
48
49
50
51
52
53
54
55
56
57
58
59
60

1
2
3 In addition, the role of polyP in forming functional amyloids in prokaryotes and its
4 potential relationship with the appearance of these fibers in the context of biofilms should
5 be considered ⁶⁹. Several amyloid-like proteins, such as curli in *E. coli*, have been described,
6 highlighting the potential significance of amyloid formation in bacterial biofilms. Although
7
8 *K. pneumoniae* lacks the curli operon, the GIE492 genomic island enabling the production of
9 the antimicrobial peptide microcin E492 is highly prevalent among hvKP ⁷⁰. This microcin
10 forms amyloid fibers in the culture supernatant of producing cells⁷¹, although the
11 biological role of this phenomenon is still unclear. Possibly, it could be a structural part of
12 biofilms. Furthermore, it is worth considering the potential role of interbacterial
13 communication and quorum sensing in biofilm formation. The coordinated behavior of
14 bacteria within the biofilm community relies on intricate signaling networks that enable
15 collective responses and establish structured microbial communities ⁷². Further
16 investigations regarding the interplay between polyphosphates, quorum sensing systems,
17 and other signaling pathways will provide valuable insights into the complex dynamics of
18 biofilm formation and the development of targeted interventions. Based on our findings,
19 we propose that polyP could serve as potential extracellular signaling molecules within the
20 biofilm matrix, acting as an energy source for dynamic biofilm processes and as a structural
21 component due to their polyanionic nature, like eDNA ⁴⁸. Further studies are warranted to
22 ascertain the essential role of polyP as biofilm constituents rather than solely intracellular
23 signaling molecules. Understanding the intricate regulatory pathways involved, including
24 interbacterial communication and quorum sensing, will provide valuable knowledge for
25 developing strategies to control biofilm-associated infections and enhance the efficacy of
26 antimicrobial therapies.

1
2
3 Unlike classical *K. pneumoniae* strains, which can be rapidly cleared during infection by the
4 host defense system, hvKP strains can evade and resist macrophage- and neutrophil-
5 mediated killing, although *K. pneumoniae* is generally considered an extracellular pathogen
6
7
8
9
10
11 ². However, reports show that hvKP strains can persist intracellularly for more than 24
12 hours by diverting the canonical endocytic pathway and surviving in a phagosome not
13 associated with lysosomes ⁷³. In this regard, *D. discoideum* has been successfully used as a
14 host model to study virulence and phagocytosis resistance ^{40,74}. Here, the predation
15 resistance assay demonstrated the contribution of polyP metabolism to the virulence of the
16 hypervirulent SGH10 strain (Fig. 5A). This reflects the involvement of PPK1 in mediating
17 key aspects of virulence in hvKp.
18
19
20
21
22
23
24
25
26

27 The amoeba model also allowed us to evaluate alterations in social development, which,
28 under standard laboratory conditions, takes two to three days to go through the stages of
29 aggregation, elevation, and culmination ¹⁸. In the presence of a virulent strain, this process
30 can be delayed or may not occur at all. $\Delta ppk1$ and $\Delta ppk1\text{-}\Delta ppx$ mutants showed reduced
31 virulence with more fruiting bodies by the 3rd day. These results provide insight into the
32 influence of polyP metabolism in this hypervirulent strain, as documented in other
33 pathogens. The significant reduction in capsular polysaccharide production, along with the
34 decrease in polysaccharide length, would enhance the ability of *D. discoideum* to recognize
35 molecular patterns such as fimbriae and LPS, promoting phagocytosis. Additionally, the
36 reduction in colibactin expression could be a potential factor contributing to the attenuated
37 virulence over this host model. Furthermore, long-chain bacterial polyphosphates (> 300
38 mer) have been shown to interfere with immune cell signaling pathways, preventing the
39 arrival of macrophages and neutrophils at the site of infection ²⁶ and inhibiting
40
41
42
43
44
45
46
47
48
49
50
51
52
53
54
55
56
57
58
59
60

1
2
3 phagolysosome formation in *D. discoideum*²⁵. The lack of polyP could make the bacteria
4
5 more vulnerable to the immune response, as it cannot manipulate or prevent
6
7 phagolysosome fusion.
8
9

10
11 We were particularly intrigued by the significant increase in the pool of siderophores in all
12
13 mutants, especially in Δppx and $\Delta ppk1-\Delta ppx$ mutants. It has been recently reported that
14
15 polyP can sequester free iron, acting as a reservoir under non-stress conditions and
16
17 blocking the formation of reactive oxygen species (ROS) during stress by inhibiting the
18
19 Fenton reaction⁶⁸. We believe that alterations in polyP metabolism might dysregulate the
20
21 expression of siderophores under non-stress conditions, particularly in the Δppx mutant
22
23 that accumulates slightly higher levels of polyP. The absence of PPX implies a reduced
24
25 capacity for polyP degradation and consequently, a diminished release of intracellular iron
26
27 under these conditions. This could serve as a signal to induce the expression of
28
29 siderophores to compensate for the lack of free iron necessary for metabolic activities.
30
31
32
33

34
35 It has been reported that aerobactin is particularly essential for the pathogenicity in hvKP
36
37 strains. Approximately 93% to 100% of hvKP strains synthesize aerobactin, with its genes
38
39 encoded on the virulence plasmid, accounting for about 90% of the siderophore activity¹³.
40
41 However, in our virulence assessment using *D. discoideum* under the studied conditions, we
42
43 observed an attenuation in virulence, particularly in the $\Delta ppk1$ and $\Delta ppk1-\Delta ppx$ strains,
44
45 which led to increased levels of siderophores. A recent report has suggested that the
46
47 coexistence of c-rmpA with p-rmpA and p-rmpA2 increases the lethality of K1 *K.*
48
49 *pneumoniae* strains and the development of hepatic abscesses more than the coexistence
50
51 of siderophores.⁷⁵ Each virulence factor present in *K. pneumoniae* participates in the
52
53
54
55
56
57
58
59
60

1
2
3 infectious process depending on external signals, as in the case of the recently described
4 iroP switch⁷⁶, where iron favors biofilm formation in iron-rich environments such as the
5 intestine while reducing capsule production. Therefore, in our virulence model, the capsule
6 becomes highly relevant as a mechanism used by hvKP strains to evade phagocytosis.
7
8 Further virulence assessments in other models are needed to determine if our observations
9 regarding virulence attenuation are reproduced.
10
11

12
13
14
15
16
17
18 Despite the extensive body of literature focusing on PPK1, the role of PPX in the physiology
19 of either non-pathogenic or pathogenic bacteria remains largely unexplored. Particularly
20 regarding the virulence traits manifested in Δppx mutants in bacteria, it has been reported
21 that PPX is essential for the pathogenesis of *Mycobacterium tuberculosis*⁷⁹, *Bacillus cereus*
22⁸⁰ and *Neisseria meningitidis*⁸¹. Our findings in Δppx mutant demonstrated no significant
23 alteration in its ability to evade phagocytosis and impact the amoeba's social development.
24
25
26
27
28
29
30
31

32
33 In summary, our research highlights the role of polyP synthesis in modulating extracellular
34 biomolecules and virulence factors in hypervirulent ST23 *K. pneumoniae*. The study offers
35 valuable insights into possible therapeutic targets for its treatment. However, more
36 research is needed to fully understand the intricate relationship between polyP
37 metabolism, siderophores, and the virulence of the ST23 *Klebsiella* hypervirulent strains.
38
39
40
41
42
43
44

45 **CONCLUSION**

46
47
48 This study investigated the impact of polyphosphate metabolism in the hypervirulent
49 strain *K. pneumoniae* SGH10. It was found that the enzyme PPK1 is essential for
50 polyphosphate synthesis and plays a role in capsule formation, hypermucoviscosity, and
51 biofilm formation. The absence of PPK1 affected growth under stress and the expression of
52
53
54
55
56
57
58
59
60

genes related to capsules and biofilms. Furthermore, the mutants showed changes in siderophore production, suggesting an interaction with iron homeostasis. These findings highlight PPK1 as a potential target to mitigate virulence and enhance antimicrobial strategies in hypervirulent strains of *K. pneumoniae*.

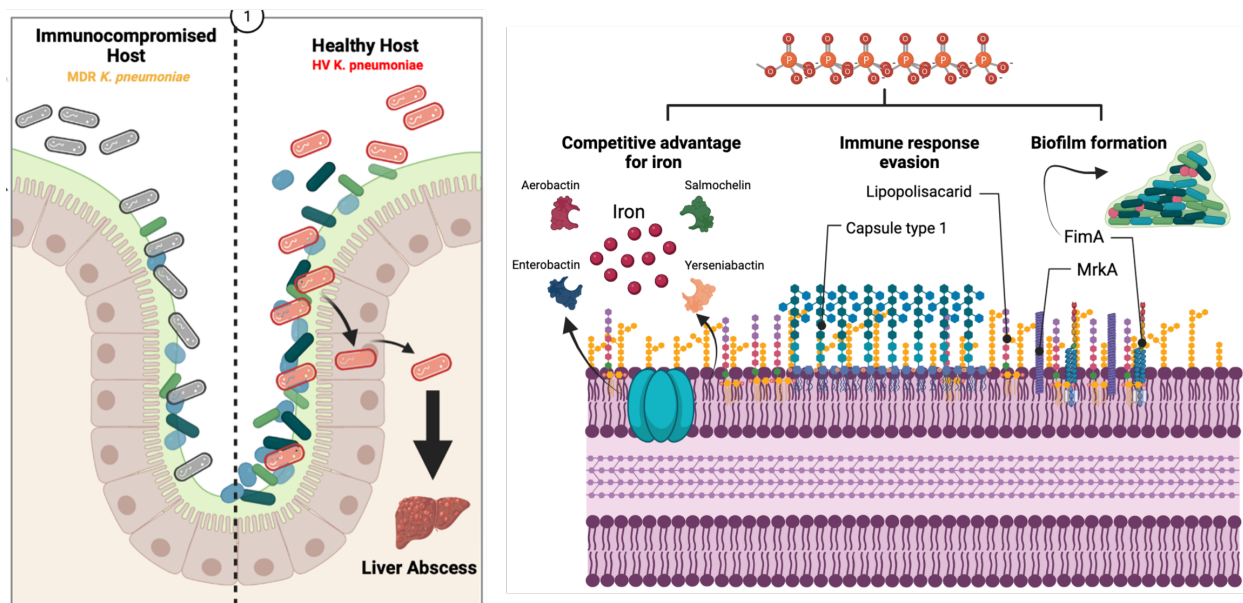


Figure 6. Model. In classic *Klebsiella pneumoniae* strains causing nosocomial infections, colonization of the intestines typically requires prior dysbiosis induced by factors like antibiotics or immunocompromised patients. In contrast, hypervirulent *Klebsiella pneumoniae* strains could colonize the intestines and invade organs such as the liver, leading to abscesses throughout the body, regardless of the patient's prior condition. To achieve this, they possess various virulence factors that facilitate colonization, invasion, and dissemination from the site of infection. In our study, we established a connection between polyP metabolism and critical aspects of the expression and regulation of key virulence factors. This included alterations in capsule formation, the hypermucoviscous phenotype, decreased biofilm formation, and changes in virulence.

METHODS

1. Strains, plasmids, and growth conditions

The details of the used strains and plasmids can be found in Table S2. *E. coli* and *K. pneumoniae* strains were grown routinely at 37°C in LB broth (10 g/L Tryptone, 5 g/L Yeast Extract, 5 g/L NaCl). For solid medium, 1.5% w/v agar was added. MOPS medium supplemented with 0.4% glucose and 0.1% K₂HPO₄ was used for the nutrient deprivation assay. For the macrobiofilm assays, LB agar without NaCl supplemented with Thioflavin S (40 µg/mL) or Congo Red (40 µg/mL) was used, and 100 µg/mL Ampicillin or Carbenicillin, 50 µg/mL Kanamycin, or 10 µg/mL Tetracycline was used for antibiotic selection.

2. Growth conditions of *D. discoideum*

We obtained the *D. discoideum* strain AX4 (DBS0302402) from the Dicty Stock Center⁸²⁻⁸⁴ and cultured it using standard protocols⁸⁵. Briefly, the *D. discoideum* vegetative cells were maintained at 23°C in SM medium containing 10 g/L glucose, 10 g/L peptone, 1 g/L yeast extract, 1 g/L MgSO₄ × 7H₂O, 1.9 g/L KH₂PO₄, 0.6 g/L K₂HPO₄, and 20 g/L agar. They were grown on a confluent lawn of *Klebsiella aerogenes* DBS0305928 (KpGE, also from the Dicty Stock Center). Before the assays, amoebae were grown at 23°C with agitation (180 rpm) in liquid HL5 medium, which contained 14 g/L tryptone, 7 g/L yeast extract, 0.35 g/L Na₂HPO₄, 1.2 g/L KH₂PO₄, and 14 g/L glucose at pH 6.3. These cultures were axenic, meaning they were free of bacteria. We harvested amoebae in the early exponential phase (1-2 × 10⁶ cells/mL) and centrifuged them at 2000 rpm for 5 min. Before the infection assays, we discarded the supernatant. We washed the pellet three times using Soerensen buffer (2 g/L KH₂PO₄, 0.36 g/L Na₂HPO₄ × 2 H₂O, pH 6.0) or adjusted it to 10⁶ cells/mL in

1
2
3 HL5 medium for social development assays. We determined the number of viable amoeba
4 cells by performing Trypan blue exclusion and counting in a Neubauer chamber. For the
5 social development assay involving *D. discoideum*, Agar N (1 g peptone, 1 g glucose, 20 g
6 agar in 1 L of 17 mM Soerensen phosphate buffer) was employed as the substrate.
7
8
9
10
11
12
13 Meanwhile, Agar SM served as the substrate in the predation resistance assay.

14 15 3. Construction of *K. pneumoniae* SGH10 mutants

16
17 For *K. pneumoniae* scarless site-directed mutagenesis, we followed the protocol
18 described previously³². Briefly, we first amplified ~1000 bp fragments upstream and
19 downstream of the target gene using *K. pneumoniae* SGH10 genomic DNAs template and
20 the Q5 high-fidelity DNA polymerase (New England Biolabs). Then, these fragments were
21 assembled along with the previously PCR-amplified vector pR6KTet-SacB using the
22 NEBuilder® HiFi DNA Assembly Master Mix (New England Biolabs). The assembled
23 constructs were then transformed by electroporation into *E. coli* S17-1 λ pir (donor strain),
24 and then conjugated into *K. pneumoniae* SGH10 (recipient strain), selecting for
25 transconjugants by plating in LB agar plates supplemented with tetracycline (50 μ g/mL)
26 and ampicillin (100 μ g/mL). Afterward, several rounds of sucrose counterselection were
27 done to select for the second recombination event, leading to the loss of the plasmid
28 backbone comprising the *sacB* gene. For this, single tetracycline-resistant clones were
29 passaged in an LB medium without sodium chloride but supplemented with 20% sucrose.
30
31 Successful deletion of the gene of interest was evaluated by PCR amplification of the
32 respective region from tetracycline-sensitive double recombinant clones and confirmed by
33 Sanger sequencing. Moreover, to rule out possible off-target mutations, we performed
34
35
36
37
38
39
40
41
42
43
44
45
46
47
48
49
50
51
52
53
54
55
56
57
58
59
60
Illumina whole-genome sequencing of the mutant strains, and the reads were mapped to

1
2
3 the *K. pneumoniae* SGH10 complete genome using BWA-MEM⁸⁶. The Sanger and Illumina
4
5
6 sequence data from the mutant strains were deposited in the NCBI database under the
7
8 GenBank accessions OR753271-73, and the SRA accessions linked to the BioProject
9
10 PRJNA1031676, respectively.
11
12
13
14
15
16

17 4. Quantitative proteomics profiling

18
19 The samples were obtained by selecting colonies grown under ideal conditions
20
21 directly from an LB-Agar culture plate at 37°C. These were then frozen for processing.
22
23

24 a. Protein Extraction

25
26 Protease/phosphatase inhibitor (#1861284, Thermo Scientific) was added to each
27
28 sample at a 1X final concentration. Then, the samples were lyophilized and resuspended in
29
30 8M urea with 25 mM ammonium bicarbonate pH 8 and later, they were homogenized using
31
32 ultrasound for 1 min with 10 s pulses (on/off) at an amplitude of 50% using a cold bath.
33
34 Then, they were incubated on ice for 5 min and later centrifuged to remove debris at
35
36 19,000 x g for 10 min at 4°C. Samples were immediately quantified using the Qubit Protein
37
38 Assay reagent (#Q33212, Invitrogen).
39
40
41
42

43 b. MS Preparation

44
45 The resulting proteins were subjected to chloroform/methanol extraction. Then, they
46
47 were equilibrated at room temperature for 10 min, centrifuged at 15,000 x g for 5 min at
48
49 4°C, and discarded into the supernatant. The resulting pellet was washed 3 times with cold
50
51 80% acetone. Subsequently, the protein pellet was dried in a rotary concentrator. Samples
52
53 were resuspended in 30 µL 8M Urea and 25 mM ammonium bicarbonate. Then, they were
54
55
56
57
58
59
60

1
2
3 reduced with DTT to a final concentration of 20 mM in 25 mM ammonium bicarbonate and
4
5 incubated for 1 hour at room temperature. They were then alkylated by adding
6
7 iodoacetamide to a final concentration of 20 mM in 25 mM ammonium bicarbonate and
8
9 incubated for 1 hour in the dark at room temperature. Subsequently, the samples are
10
11 diluted 8 times with 25 mM ammonium bicarbonate.
12
13
14

15
16 Digestion was performed with sequencing grade Trypsin (#V5071, Promega) in a 1:50
17
18 ratio of protease: protein (mass/mass) and incubated for 16 h at 37°C. Digestion was
19
20 stopped by pH adding 10% formic acid. Then, the samples were subjected to Clean Up Sep-
21
22 Pak C18 Spin Columns (Waters), according to the supplier's instructions. Subsequently, the
23
24 clean peptides were dried in a rotary concentrator at 2000 rpm overnight at 40°C.
25
26
27

28 c. LC-MS/MS (Liquid Chromatography – Tandem Mass Spectrometry)

29
30 200 ng of the tryptic peptides obtained in the previous step were injected into a
31
32 nanoELUTE nanoUHPLC (Bruker Daltonics) coupled to a timsTOF Pro mass spectrometer
33
34 (“Trapped Ion Mobility Spectrometry – Quadrupole Time Of Flight Mass Spectrometer”,
35
36 Bruker Daltonics) using an Aurora Ultimate column. UHPLC (25 cm x 75 µm ID, 1.6 µm C18,
37
38 CSI, IonOpticks, Australia). Liquid chromatography used a 90-min gradient of 2% to 35%
39
40 buffer B (0.1% Formic Ac. - Acetonitrile). The collection of results was performed using the
41
42 TimsControl 2.0 software (Bruker Daltonics) under 10 PASEF cycles, with a mass range of
43
44 100-1,700 m/z, capillary ionization of 1,500 V, and a temperature of 180°C, TOF frequency
45
46 of 10 KHz at a resolution of 40,000 FWHM.
47
48
49
50
51

52 d. Protein Identification

53
54
55 The data obtained were analyzed with the MSFragger 3.5 software through the
56
57
58
59
60

1
2
3 Fragpipe v18.0 platform (<https://fragpipe.nesvilab.org/>) using the “default” workflow in a
4 data analysis server consisting of 48 cores and 512 Gb of RAM. Mass tolerance parameters
5 of 50 ppm were used, using monoisotopic masses and 0.05 Da fragment ions. Among the
6 digestion options, trypsin was used as the enzyme-specific digestion mode and a maximum
7 of 2 missed cleavages per peptide. The following were used as post-translational
8 modifications (PTM): Cysteine carbamidomethylation, as fixed PTM: Methionine oxidation
9 (M), N-terminal acetylation, Asparagine and Glutamine (NQ) deamination, as variable
10 PTMs. The database used for identification was the proteome of *Klebsiella pneumoniae*
11 strain SGH10 (5,405 total entries). The FDR estimate was included using a decoy database.
12 As a filter, an FDR $\geq 1\%$ and 1 minimum unique peptide per protein were used for
13 identification.
14
15
16
17
18
19
20
21
22
23
24
25
26
27
28
29

30 g. Protein Quantification LFQ (Free Label Quantification)

31
32
33 The columns corresponding to the Uniprot access codes and intensity values were
34 selected using the protein identification results. Data were concatenated, and missing
35 values in the intensity columns were imputed. The resulting matrix was subjected to
36 normalization by medians. Differential expression proteins were determined by applying a
37 T-Test with a Benjamini-Horschberg multiple correction test (adjusted p-value < 0.05).
38 DEPs (Differentially Expressed Proteins) were identified between the comparisons:
39 $\Delta ppk1$ vs. WT, Δppx vs. WT and $\Delta ppk1-\Delta ppx$ vs. WT. The mass spectrometry proteomics
40 data have been deposited to the ProteomeXchange Consortium via the PRIDE ⁸⁷ partner
41 repository with the dataset identifier PXD046644.
42
43
44
45
46
47
48
49
50
51
52
53
54

55 5. Calculation of the z-score

1
2
3 The z-score was calculated based on the logFC of each protein belonging to the virulence
4 categories derived from VFDB (Adherence, antiphagocytosis, toxin, siderophores, lipid A,
5 serum resistance). It's important to note that this z-score doesn't refer to the standard
6 score typically used in statistics but is a simple calculation aimed at indicating whether the
7 biological process, molecular function, or cellular component is more likely to decrease
8 (resulting in a negative value) or increase (resulting in a positive value). The calculation
9 was performed using the following formula:

$$zscore = \frac{(up - down)}{\sqrt{count}}$$

10
11
12
13
14
15
16
17
18
19
20
21
22
23 The z-score was determined based on the number of proteins assigned as upregulated
24 (logFC>0) or downregulated (logFC<0), denoted as "up" and "down," respectively, in the
25 dataset. Subsequently, the average z-scores of each category were calculated for each
26 mutant and plotted as "All virulence factors."
27
28
29
30
31
32
33
34

35 6. Growth and polyP production under nutrient deprivation

36
37 Mutant strains with alterations in polyP metabolism and the SGH10 WT strain were
38 cultured overnight. A 1:1000 dilution in LB or MOPS medium was inoculated into a 96-well
39 plate (the MOPS medium was supplemented with 0,4% glucose and 0.1 mM K₂HPO₄). The
40 plate was then incubated for 24 h in a TECAN infinite 200 pro plate reader at 37°C and 180
41 rpm. Readings were taken every 10 min (n = 6) to measure the optical density at 600 nm
42 (OD₆₀₀).
43
44
45
46
47
48
49
50

51
52 To investigate whether PPK1 deficiency affects bacterial polyP accumulation, a polyP
53 quantification assay was performed⁸⁸. Briefly, cultures of *K. pneumoniae* SGH10 and polyP
54
55
56
57
58
59
60

1
2
3 mutants grown overnight were diluted into fresh LB broth and cultured at 180 rpm and
4
5 37°C for 2 h. Then, 1 mL of bacterial cells was centrifuged twice in MOPS low-phosphate
6
7 minimal medium (containing 0.4% glucose and 0.1 mM potassium phosphate) and
8
9 incubated at 37°C for 2 h to stimulate polyP accumulation. Then, cells were harvested by
10
11 centrifugation in a 1,5 mL. The supernatant was entirely removed from the cell pellets.
12
13 Subsequently, the cell pellets were resuspended in 250 µL of GITC lysis buffer (consisting
14
15 of 4 M guanidine isothiocyanate, 50 mM Tris-HCl, pH 7) and subjected to lysis through
16
17 incubation at 95 °C for 10 minutes. The lysates were then stored at -80 °C. For the
18
19 polyphosphate extraction, 250 µL of 95% ethanol was added to each GITC-lysed sample,
20
21 followed by vigorous mixing. This mixture was applied to a silica membrane spin column
22
23 and centrifuged for 30 s at 16,100 x g. The flow-through was discarded, and 750 µL of a
24
25 solution containing 5 mM Tris-HCl (pH 7.5), 50 mM NaCl, 5 mM EDTA, and 50% ethanol
26
27 was added before centrifuging for 30 seconds at 16,100 x g. Once again, the flow-through
28
29 was discarded, and a 2-minute centrifugation at 16,100 x g was carried out. The column
30
31 was placed in a clean 1.5 mL microfuge tube, and 150 µL of 50 mM Tris-HCl (pH 8) was
32
33 added. Following a 5-min incubation at room temperature, polyP was eluted by
34
35 centrifuging for 2 minutes at 8,000 x g. PolyP was quantified using the Phosfinity-Quant kit
36
37 from Aminoverse, employing the scPPX enzyme.
38
39
40
41
42
43
44
45
46
47
48

- 49 7. Determination of the minimal inhibitory concentration (MIC) for colistin by broth
50
51 microdilution assays.
52
53
54
55
56
57
58
59
60

1
2
3 The colistin resistance of SGH10 WT, $\Delta ppk1$, Δppx , $\Delta ppk1-\Delta ppx$ was tested at
4 concentrations ranging from 0.125 to 32 $\mu\text{g}/\text{mL}$. To do this, liquid cultures were grown in
5 cation-adjusted Müller-Hinton broth (MH-2) from isolated colonies and incubated
6 overnight at 37°C until reaching the stationary phase. Subsequently, 96-well plates were
7 filled with 200 μL of MH-2 broth, supplemented with various concentrations of this
8 antibiotic through serial dilutions in a 2-fold manner. Bacteria were then inoculated into
9 the wells. Finally, the cultures were incubated for 32 hours with agitation at 37°C. During
10 this period, bacterial growth was determined by measuring optical density at 600 nm using
11 a Tecan M200 Infinite Pro microplate reader. MIC was defined as the lowest antibiotic
12 concentration with no bacterial growth. *Pseudomonas aeruginosa* spp. PAO1 strain was
13 used as a control for MIC determination.
14
15
16
17
18
19
20
21
22
23
24
25
26
27
28
29

30 8. Capsule production quantification

31
32 Capsule production was quantified by measuring the total amount of uronic acids,
33 following the method previously described for *K. pneumoniae* ⁶. Briefly, uronic acids were
34 extracted from 500 mL of culture using zwittergent, precipitated with ethanol, and
35 resuspended in a tetraborate/sulfuric acid solution. Then, 3-phenyl phenol was added, and
36 the uronic acid content was estimated by measuring the absorbance at 520 nm and
37 comparing it to a standard curve generated with commercial glucuronic acid.
38
39
40
41
42
43
44
45
46
47
48
49
50
51
52

53 9. Low-speed centrifugation assay

54
55
56
57
58
59
60

1
2
3 Four milliliters of a 10^9 CFU/mL solution of the desired strain in LB were prepared in
4 15 mL Falcon tubes. The tubes were centrifuged at $2,000 \times g$ for 10 min and imaged against
5 a black background. The supernatant's OD_{600nm} was measured using a BioMate™
6 spectrophotometer (Thermo Scientific).
7
8
9
10
11

12 13 10. Quantification of Biofilm Biomass and EPS and Visualization Using Confocal

14 15 Microscopy

16
17 Biofilm formation was assessed using a previously described protocol ⁸⁹, with some
18 modifications. Briefly, *K. pneumoniae* SGH10 wild-type and polyP mutant strains were
19 grown overnight in LB broth, then diluted 1:100 in fresh LB broth. Next, 100 μ L of each
20 dilution was added to a 96-well polystyrene microtiter plate and incubated at 37°C for 24
21 h. Wells containing only media were used as blanks. After removing planktonic cells, wells
22 were washed twice with sterile water and stained with 150 μ L of 0.1% crystal violet for 30
23 min. Then, wells were rinsed twice with sterile water, and the stained biofilms were
24 solubilized with 95% ethanol. Biofilm formation was quantified by measuring the OD_{595nm}
25 using a TECAN infinite 200 pro plate reader. To quantify EPS components such as curli and
26 cellulose, the Ebbabiolight 680 probe was used because it bounds to these components
27 without influencing biofilm formation. EbbaBiolight 680 was diluted in a growth medium at
28 a 1:1000 ratio for the biofilm assay. Then, the supplemented growth medium was
29 inoculated with the bacterial culture. Next, the wells of a 96-well plate were filled with 100
30 μ L of the inoculated medium. The unused wells were filled with sterile water to prevent
31 drying during incubation. The plate was covered with a lid or an adhesive seal.
32
33 Fluorescence was measured at 540ex/680em in a TECAN infinite 200 pro plate reader.
34
35 Each sample was measured in triplicate, and we calculated averages of the absorbance
36
37
38
39
40
41
42
43
44
45
46
47
48
49
50
51
52
53
54
55
56
57
58
59
60

1
2
3 values for analysis. To investigate the accumulation of polyP in the biofilm and its influence
4
5 on formation, an overnight culture was diluted 1:100 in the LB broth medium.
6

7
8 Subsequently, a slide was submerged in 10 mL of the 1:100 culture inside a 50-mL falcon
9
10 tube and incubated at 37°C for 24 h. The slide was washed three times with nanopure
11
12 water and incubated for 30 minutes with 5 µg/mL DAPI to stain DNA and PolyP. The polyP
13
14 accumulation was visualized using a CLSM Zeiss 757 confocal microscope, with a
15
16 358ex/461em laser to observe DNA and a 358ex/540em laser to observe polyP.
17
18
19

20 11. Scanning electron microscopy

21
22 To examine potential modifications at the superficial level, including the capsule and
23
24 overall morphology, we conducted scanning electron microscopy (SEM)³² with some
25
26 changes. We prepared a lawn on LB agar from strains frozen at -80°C, then incubated for
27
28 24 h at 37°C. Using a sterile swab, we collected enough bacteria and resuspended them in
29
30 PBS 1X. We adjusted the OD_{600nm} to 2.8 (10⁹ CFU/ml) and fixed 500 µL of the suspension
31
32 with 2.5% glutaraldehyde and 0.15% ruthenium red to improve the capsule visualization
33
34 contrast. Samples were subjected to critical point drying and gold coating and subsequently
35
36 observed in a high vacuum Zeiss EVO M15 scanning electron microscope. To examine
37
38 superficial morphology in the mutants and WT strains following nutrient deprivation,
39
40 overnight cultures of *K. pneumoniae* SGH10 and polyP mutants were diluted into fresh LB
41
42 broth and cultured at 180 rpm and 37°C for 2 h. The bacterial cells were centrifuged twice
43
44 in MOPS low-phosphate minimal medium (containing 0.4% glucose and 0.1 mM potassium
45
46 phosphate) and incubated at 37°C for 2 h to stimulate polyP accumulation. The samples
47
48 were treated in the same manner before observation using SEM.
49
50
51
52
53
54
55
56
57
58
59
60

12. *D. discoideum* predation resistance assay

In this predation resistance assay, we semiquantitatively evaluated the possible attenuation of virulence in polyP metabolism mutants compared to the SGH10 WT strain. We modified a previously established protocol³⁸. Bacterial colonies were taken from a -80°C stock to prepare overnight cultures, and 300 µL were then seeded onto a plate using a Digrafsky loop to generate a bacterial lawn. The plate was left to dry and incubated for 24 h at 23°C. Meanwhile, *D. discoideum* was cultured in HL5 medium, and serial dilutions were prepared to obtain the following cell concentrations: 500,000 - 50,000 - 5,000 - 500 - 50 and 5 cells per 5 µL. The bacterial lawns were then spotted with 5 µL of the serial *D. discoideum* dilutions. The plates were allowed to dry and were incubated at 21°C for 6 days. Plaque formation was visually examined on days 3 and 6. Isolates that did not enable amoebae growth were considered virulent for the amoeba. Bacterial strains that exhibited social development with 500 *D. discoideum* cells or less were considered sensitive to predation³⁹.

13. *D. discoideum* social development Assays

For social development assays, we followed a published protocol¹⁸. Overnight cultures of each bacterial strain (30 µL) were homogeneously included per well of a 24-well plate containing N agar (1 g peptone, 1 g glucose, 20 g agar in 1 L of 17 mM Soerensen phosphate buffer) and grown overnight at 23°C. A drop of a cellular suspension corresponding to 10⁴ *D. discoideum* cells in HL5 was spotted in the middle of each well and the plates were further incubated at 23°C for 6 days. The social development of amoebae was monitored daily for 6 days, and the phase reached was scored, being classified as “aggregation,”

1
2
3 “elevation,” and “culmination.” A score of “1” was assigned when amoebae aggregated,
4 forming a phagocytosis plate, “2” when all the well surface elevated structures such as
5 worms or fingers were observed, and “3” when fruiting bodies were formed across all the
6 well surfaces. Transitions among these three phases were scored, with half of the value
7 corresponding to the closest next stage. The number of fruiting bodies on a 1 cm² surface
8 was also quantified for each strain under study and was compared with the commensal
9 KpgE strain. Additionally, images of social development were captured on days 1, 2, and 3
10 using a Zeiss Stemi 305 stereomicroscope with a total magnification of 10X, coupled to a 5
11 MP OPTIKA camera.
12
13
14
15
16
17
18
19
20
21
22
23
24

25 14. Phagocytosis assays

26 A lawn was prepared on LB agar from strains GFP frozen at -80°C and incubated for 24 h at
27 37°C. Bacteria were collected using a sterile swab and resuspended in Sorensen 1X buffer.
28 Cell density was adjusted to OD_{600nm} at 10⁷ cells/mL. Axenic cultures of *D. discoideum* were
29 set to a concentration of 10⁶ cells/mL and 1 mL of culture was deposited in 24-well plates.
30 The plate was centrifuged at 600 x g for 10 minutes and incubated at 23°C for 24 h. Each
31 well was washed three times with Sorensen buffer and 1 mL of bacterial suspension was
32 added to each well to obtain an MOI of 10. The plate was centrifuged at 600 x g for 30 min.
33 The plate was then observed with the Lionheart FX automatic microscope, programmed to
34 take photographs every 10 minutes for 24 to 48 h in bright field (BF) and GFP and in 4
35 regions of interest per well at 23°C. The images were analyzed with Gen5 software version
36 3.08 (Lionheart FX) and ImageJ software version 2.14.0 (Fiji version).
37
38
39
40
41
42
43
44
45
46
47
48
49
50
51
52
53
54
55
56
57
58
59
60

AUTHOR INFORMATION

Corresponding Author

* E-mail: fpchavez@uchile.cl, Tel.:+56229787185, Laboratorio de Microbiología de Sistemas, Las Palmeras 3425, Ñuñoa CP 7800003, Santiago, Chile.

Author Contributions

FC and AM conceived the study. DR, FC, AM, MV, MG, JV, and MD designed the experiments. DR and FC analyzed the data and interpreted the results. YG and YC developed the methodology for mutant generation. DR and MD carried out the mutant generation. DR, MD, and JV conducted the experiments. MH, CV, GN, EK, and PS performed proteomic processing and analysis. DR and FC wrote the manuscript. FC, AM, NG, and MH critically reviewed the manuscript. All the authors approved the final version of the manuscript.

Founding Sources

This work was funded by the FONDECYT projects F. Chavez 1211852, and A. Marcoleta 1221193. Additionally, it received contributions from the FONDEQUIP project Lionheart EQM180216, and support from the María Ghilardi Foundation to D. Rojas.

Supporting Information

Available free of charge

Includes a list of primers used for mutant generation; growth curves; social development assay and proteomic analysis

ACKNOWLEDGMENT

We express our gratitude to Nicole Molina for her support in preparing the required materials, and to Dr. T. Shiba for generously providing us with polyP of various sizes: short, medium, and large.

Notes

The authors declare no competing financial interest.

REFERENCES

1. Choby JE, Howard-Anderson J, Weiss DS. Hypervirulent *Klebsiella pneumoniae* – clinical and molecular perspectives. *J Intern Med.* 2020;287(3):283-300. doi:10.1111/joim.13007
2. Paczosa MK, Mecsas J. *Klebsiella pneumoniae*: Going on the Offense with a Strong Defense. *Microbiology and Molecular Biology Reviews.* 2016;80(3):629-661. doi:10.1128/membr.00078-15
3. Gonzalez-Ferrer S, Peñaloza H, Budnick J, Bain W, Nordstrom H, Lee J, Van Tyne D. Finding Order in the Chaos: Outstanding Questions in *Klebsiella pneumoniae* Pathogenesis. *Infect Immun.* 2021;89(4). doi:10.1128/IAI.00693-20
4. Wyres KL, Holt KE. *Klebsiella pneumoniae* as a key trafficker of drug resistance genes from environmental to clinically important bacteria. *Curr Opin Microbiol.* 2018;45:131-139. doi:10.1016/j.mib.2018.04.004
5. Chen YT, Chang HY, Lai YC, Pan CC, Tsai SF, Peng HL. Sequencing and analysis of the large virulence plasmid pLVPK of *Klebsiella pneumoniae* CG43. *Gene.* 2004;337:189-198. doi:10.1016/j.gene.2004.05.008
6. Walker KA, Treat LP, Sepúlveda VE, Miller VL. The Small Protein RmpD Drives Hypermucoviscosity in *Klebsiella pneumoniae*. Heran Darwin K, ed. *mBio.* 2020;11(5). doi:10.1128/mBio.01750-20
7. Ovchinnikova OG, Treat LP, Teelucksingh T, Clarke, Bradley R, Miner, Taryn A, Whitfield, Chri, Walker, Kimberly A, Miller, Virginia L. Hypermucoviscosity Regulator RmpD Interacts with Wzc and Controls Capsular Polysaccharide Chain Length. *mBio.* Published online May 4, 2023. doi:10.1128/mbio.00800-23
8. Russo TA, Olson R, MacDonald U, Beanan J, Davidson BA. Aerobactin, but not yersiniabactin, salmochelin, or enterobactin, enables the growth/survival of hypervirulent (hypermucoviscous) *Klebsiella pneumoniae* ex vivo and in vivo. *Infect Immun.* 2015;83(8):3325-3333. doi:10.1128/IAI.00430-15
9. Struve C, Bojer M, Krogfelt KA. Characterization of *Klebsiella pneumoniae* type 1 fimbriae by detection of phase variation during colonization and infection and impact on virulence. *Infect Immun.* 2008;76(9):4055-4065. doi:10.1128/IAI.00494-08
10. Wang H, Wilksch JJ, Chen L, Tan JWH, Strugnell RA, Gee ML. Influence of Fimbriae on Bacterial Adhesion and Viscoelasticity and Correlations of the Two Properties with Biofilm Formation. *Langmuir.* 2017;33(1):100-106. doi:10.1021/acs.langmuir.6b03764
11. Wu MC, Lin TL, Hsieh PF, Yang HC, Wang JT. Isolation of Genes Involved in Biofilm Formation of a *Klebsiella pneumoniae* Strain Causing Pyogenic Liver Abscess. *PLoS One.* 2011;6(8):e23500. doi:10.1371/journal.pone.0023500
12. Zheng J xin, Lin Z wei, Chen C, Chen Z, Lin Fo-jun, Wu Y, Yang Si-yu, Sun X, Yao Wei-ming, Li Duo-yun, Yu Zhi-jian, Jin Jia-lin, Qu D, Deng Qi-wen. Biofilm Formation in

- 1
2
3 *Klebsiella pneumoniae* Bacteremia Strains Was Found to be Associated with CC23 and the
4 Presence of wcaG. *Front Cell Infect Microbiol.* 2018;8. doi:10.3389/fcimb.2018.00021
5
- 6 13. Russo TA, Marr CM. Hypervirulent *Klebsiella pneumoniae*. *Clin Microbiol Rev.*
7 2019;32(3). doi:10.1128/CMR.00001-19
8
- 9 14. Xu Q, Yang X, Chan EWC, Chen S. The hypermucoviscosity of hypervirulent *K.*
10 *pneumoniae* confers the ability to evade neutrophil-mediated phagocytosis. *Virulence.*
11 2021;12(1):2050-2059. doi:10.1080/21505594.2021.1960101
12
- 13 15. Wyres KL, Lam MMC, Holt KE. Population genomics of *Klebsiella pneumoniae*. *Nat Rev*
14 *Microbiol.* 2020;18(6):344-359. doi:10.1038/s41579-019-0315-1
15
- 16 16. Lam MMC, Wyres KL, Duchêne S, Wick, Ryan R, Judd, Louise M, Gan Yunn-Hwe, Hoh
17 Chu-Ha, Archuleta Sophi, Molton James S, Kalimuddin Shiri. Population genomics of
18 hypervirulent *Klebsiella pneumoniae* clonal-group 23 reveals early emergence and rapid
19 global dissemination. *Nat Commun.* 2018;9(1):2703. doi:10.1038/s41467-018-05114-7
20
- 21 17. Kornberg A, Rao NN, Ault-Riché D. Inorganic polyphosphate: a molecule of many
22 functions. *Annu Rev Biochem.* 1999;68(1):89-125. doi:10.1146/annurev.biochem.68.1.89
23
- 24 18. Varas MA, Riquelme-Barrios S, Valenzuela C, Marcoleta A, Berríos-Pastén C, Santiviago
25 C. Chávez, F. Inorganic polyphosphate is essential for *Salmonella Typhimurium* Virulence
26 and survival in *Dictyostelium discoideum*. *Front Cell Infect Microbiol.* 2018;8(JAN).
27 doi:10.3389/fcimb.2018.00008
28
- 29 19. Xie L, Jakob U. Inorganic polyphosphate, a multifunctional polyanionic protein scaffold.
30 *Journal of Biological Chemistry.* 2019;294(6):2180-2190. doi:10.1074/jbc.REV118.002808
31
- 32 20. Rashid MH, Kornberg A. Inorganic polyphosphate is needed for swimming, swarming, and
33 twitching motilities of *Pseudomonas aeruginosa*. *Proc Natl Acad Sci U S A.*
34 2000;97(9):4885-4890.
35
- 36 21. Fraley CD, Rashid MH, Lee SSK, Gottschalk, Rebecca, Harrison J, Wood Pauline J, Brown
37 M, Kornberg, A. A polyphosphate kinase 1 (ppk1) mutant of *Pseudomonas aeruginosa*
38 exhibits multiple ultrastructural and functional defects. *Proc Natl Acad Sci U S A.*
39 2007;104(9):3526-3531.
40
- 41 22. Ortiz-Severín J, Varas M, Bravo-Toncio C, Guiliani N, Chávez FP. Multiple antibiotic
42 susceptibility of polyphosphate kinase mutants (ppk1 and ppk2) from *Pseudomonas*
43 *aeruginosa* PAO1 as revealed by global phenotypic analysis. *Biol Res.* 2015;48:1-6.
44 doi:10.1186/s40659-015-0012-0
45
- 46 23. Kim KS, Rao NN, Fraley CD, Kornberg A. Inorganic polyphosphate is essential for long-
47 term survival and virulence factors in *Shigella* and *Salmonella* spp. *Proceedings of the*
48 *National Academy of Sciences.* 2002;99(11):7675-7680. doi:10.1073/pnas.112210499
49
- 50 24. Varas MA, Riquelme-Barrios S, Valenzuela C, Marcoleta A, Berríos-Pastén C, Santiviago
51 C. Chávez, F. Inorganic polyphosphate is essential for *Salmonella Typhimurium* Virulence
52
53
54
55
56
57
58
59
60

- 1
2
3 and survival in *Dictyostelium discoideum*. *Front Cell Infect Microbiol*. 2018;8(JAN).
4 doi:10.3389/fcimb.2018.00008.
5
- 6
7 25. Rijal R, Cadena LA, Smith MR, Carr JF, Gomer RH. Polyphosphate is an extracellular signal
8 that can facilitate bacterial survival in eukaryotic cells. *Proceedings of the National Academy*
9 *of Sciences*. 2020;117(50):31923-31934. doi:10.1073/pnas.2012009117
- 10
11 26. Bowlin MQ, Gray MJ. Inorganic polyphosphate in host and microbe biology. *Trends*
12 *Microbiol*. 2021;29(11):1013-1023. doi:10.1016/j.tim.2021.02.002
- 13
14 27. Roberge N, Neville N, Douchant K, Noordhof C, Boev N, Sjaarda C, Sheth P, Jia Z. Broad-
15 Spectrum Inhibitor of Bacterial Polyphosphate Homeostasis Attenuates Virulence Factors
16 and Helps Reveal Novel Physiology of *Klebsiella pneumoniae* and *Acinetobacter*
17 *baumannii*. *Front Microbiol*. 2021;12. doi:10.3389/fmicb.2021.764733
- 18
19 28. Lv H, Zhou Y, Liu B, Guan J, Zhang P, Deng X, Li D, W Jianfeng. Polyphosphate Kinase
20 Is Required for the Processes of Virulence and Persistence in *Acinetobacter baumannii*.
21 *Microbiol Spectr*. 2022;10(4). doi:10.1128/spectrum.01230-22
- 22
23 29. Aschar-Sobbi R, Abramov AY, Diao C, Kargacin GJ, French RJ, Pavlov E. High sensitivity,
24 quantitative measurements of polyphosphate using a new DAPI-based approach. *J Fluoresc*.
25 2008;18(5):859-866. doi:10.1007/s10895-008-0315-4
- 26
27 30. Dahl JU, Gray MJ, Bazopoulou D, Beaufay, Lempart F, Koenigsnecht J, Wang Y, Jason
28 R, William L, Vincent B, Duxin S, Ursula J. The anti-inflammatory drug mesalamine targets
29 bacterial polyphosphate accumulation. *Nat Microbiol*. 2017;2(January).
30 doi:10.1038/nmicrobiol.2016.267
- 31
32 31. Walker KA, Miner TA, Palacios M, Dominika T, Daniel F, Christopher B, Sepúlveda V,
33 Joshua D, Miller V. A *klebsiella pneumoniae* regulatory mutant has reduced capsule
34 expression but retains hypermucoviscosity. *mBio*. 2019;10(2):1-16.
35 doi:10.1128/MBIO.00089-19
- 36
37 32. Tan YH, Chen Y, Chu WHW, Sham LT, Gan YH. Cell envelope defects of different capsule-
38 null mutants in K1 hypervirulent *Klebsiella pneumoniae* can affect bacterial pathogenesis.
39 *Mol Microbiol*. 2020;113(5):889-905. doi:10.1111/mmi.14447
- 40
41 33. Phanphak S, Georgiades P, Li R, King J, Roberts IS, Waigh TA. Super-Resolution
42 Fluorescence Microscopy Study of the Production of K1 Capsules by *Escherichia coli* :
43 Evidence for the Differential Distribution of the Capsule at the Poles and the Equator of the
44 Cell. *Langmuir*. 2019;35(16):5635-5646. doi:10.1021/acs.langmuir.8b04122
- 45
46 34. Rendueles O. Deciphering the role of the capsule of *Klebsiella pneumoniae* during
47 pathogenesis: A cautionary tale. *Mol Microbiol*. 2020;113(5):883-888.
48 doi:10.1111/mmi.14474
- 49
50 35. Choong FX, Huzell S, Rosenberg M, Johannes E, Madhu N, Tianqi Z, Keira M, Daniel O,
51 Agneta A. A semi high-throughput method for real-time monitoring of curli producing
52
53
54
55
56
57
58
59
60

- 1
2
3 *Salmonella* biofilms on air-solid interfaces. *Biofilm*. 2021;3:100060.
4 doi:10.1016/j.bioflm.2021.100060
5
- 6
7 36. Marcoleta AE, Varas MA, Ortiz-Severín J, Vásquez L, Berríos-Pastén C, Sabag A.V,
8 Chávez F.P, Allende M.L, Santiviago C.A, Monasterio O. Evaluating different virulence
9 traits of *Klebsiella pneumoniae* using *Dictyostelium discoideum* and zebrafish larvae as host
10 models. *Front Cell Infect Microbiol*. 2018;8(FEB). doi:10.3389/fcimb.2018.00030
11
- 12 37. Filion G, Charette SJ. Assessing *Pseudomonas aeruginosa* virulence using a nonmammalian
13 host: *Dictyostelium discoideum*. *Methods in Molecular Biology*. 2014;1149:671-680.
14 doi:10.1007/978-1-4939-0473-0_51
15
- 16 38. Paquet VE, Charette SJ. Amoeba-resisting bacteria found in multilamellar bodies secreted
17 by *Dictyostelium discoideum*: social amoebae can also package bacteria. *FEMS Microbiol*
18 *Ecol*. 2016;92(3):fiw025. doi:10.1093/femsec/fiw025
19
- 20 39. Bravo-Toncio C, Álvarez JA, Campos F, Ortiz-Severín J, Varas M, Cabrera R, Lagos C,
21 Chávez FP. *Dictyostelium discoideum* as a surrogate host–microbe model for antivirulence
22 screening in *Pseudomonas aeruginosa* PAO1. *Int J Antimicrob Agents*. Published online
23 2016:1-7. doi:10.1016/j.ijantimicag.2016.02.005
24
- 25 40. Wang L, Shen D, Wu H, Ma Y. Resistance of hypervirulent *Klebsiella pneumoniae* to both
26 intracellular and extracellular killing of neutrophils. *PLoS One*. 2017;12(3):e0173638.
27 doi:10.1371/journal.pone.0173638
28
- 29 41. Downey M. A stringent analysis of polyphosphate dynamics in *Escherichia coli*. *J Bacteriol*.
30 2019;201(9):1-6. doi:10.1128/JB.00070-19
31
- 32 42. Gray MJ. Inorganic polyphosphate accumulation in *Escherichia coli* is regulated by DksA
33 but not by (p)ppGpp. *J Bacteriol*. 2019;201(9):1-20. doi:10.1128/JB.00664-18
34
- 35 43. Bravo-Toncio C, Álvarez JA, Campos F, Ortiz-Severín J, Varas M, Cabrera R, Lagos C,
36 Chávez FP. *Dictyostelium discoideum* as a surrogate host–microbe model for antivirulence
37 screening in *Pseudomonas aeruginosa* PAO1. *Int J Antimicrob Agents*. Published online
38 2016:1-7. doi:10.1016/j.ijantimicag.2016.02.005
39
- 40 44. Palacios M, Miner TA, Frederick DR, Sepulveda V, Quinn J, Walker K, Miller V.
41 Identification of two regulators of virulence that are conserved in *Klebsiella pneumoniae*
42 classical and hypervirulent strains. *mBio*. 2018;9(4). doi:10.1128/mBio.01443-18
43
- 44 45. Tinsley CR, Manjula BN, Gotschlich EC. Purification and characterization of polyphosphate
45 kinase from *Neisseria meningitidis*. *Infect Immun*. 1993;61(9):3703-3710.
46 doi:10.1128/iai.61.9.3703-3710.1993
47
- 48 46. Fraley CD, Rashid MH, Lee SSK, Gottschalk R, Harrison J, Wood P, Brown M, Kornberg
49 A. A polyphosphate kinase 1 (*ppk1*) mutant of *Pseudomonas aeruginosa* exhibits multiple
50 ultrastructural and functional defects. *Proceedings of the National Academy of Sciences*.
51 2007;104(9):3526-3531. doi:10.1073/pnas.0609733104
52
53
54
55
56
57
58
59
60

- 1
2
3 47. Müller WEG, Schröder HC, Wang X. Inorganic Polyphosphates As Storage for and
4 Generator of Metabolic Energy in the Extracellular Matrix. *Chem Rev.* 2019;119(24):12337-
5 12374. doi:10.1021/acs.chemrev.9b00460
6
7 48. Varas M, Valdivieso C, Mauriaca C, Ortíz-Severín J, Parabela A, Poblete-Castro I, Cabrera
8 R, Chávez FP. Multi-level evaluation of *Escherichia coli* polyphosphate related mutants
9 using global transcriptomic, proteomic and phenomic analyses. *Biochimica et Biophysica*
10 *Acta (BBA) - General Subjects.* 2017;1861(4):871-883. doi:10.1016/j.bbagen.2017.01.007
11
12 49. Meredith TC, Woodard RW. Characterization of *Escherichia coli* D-arabinose 5-phosphate
13 isomerase encoded by *kpsF*: implications for group 2 capsule biosynthesis. *Biochemical*
14 *Journal.* 2006;395(2):427-432. doi:10.1042/BJ20051828
15
16 50. Perepelov A V., Ujazda E, Senchenkova SN, Shashkov AS, Kaca W, Knirel YA. Structural
17 and serological studies on the O-antigen of *Proteus mirabilis* O14, a new polysaccharide
18 containing 2-[(R)-1-carboxyethylamino]ethyl phosphate. *Eur J Biochem.* 1999;261(2):347-
19 353. doi:10.1046/j.1432-1327.1999.00251.x
20
21 51. Element SJ, Moran RA, Beattie E, Hall RJ, van Schaik W, Buckner MMC. Growth in a
22 biofilm promotes conjugation of a *bla*_{NDM-1} -bearing plasmid between *Klebsiella*
23 *pneumoniae* strains. *mSphere.* Published online July 7, 2023. doi:10.1128/msphere.00170-
24 23
25
26 52. Vuotto C, Longo F, Balice MP, Donelli G, Varaldo PE. Antibiotic resistance related to
27 biofilm formation in *Klebsiella pneumoniae*. *Pathogens.* 2014;3(3):743-758.
28 doi:10.3390/pathogens3030743
29
30 53. Wang G, Zhao G, Chao X, Xie L, Wang H. The characteristic of virulence, biofilm and
31 antibiotic resistance of *Klebsiella pneumoniae*. *Int J Environ Res Public Health.*
32 2020;17(17):1-17. doi:10.3390/ijerph17176278
33
34 54. Chhibber S, Gondil VS, Sharma S, Kumar M, Wangoo N, Sharma RK. A novel approach
35 for combating *Klebsiella pneumoniae* biofilm using histidine functionalized silver
36 nanoparticles. *Front Microbiol.* 2017;8(JUN):1-10. doi:10.3389/fmicb.2017.01104
37
38 55. Alcántar-Curiel MD, Ledezma-Escalante CA, Jarillo-Quijada MD, Gayosso-Vázquez C,
39 Morfín-Otero R, Rodríguez-Noriega E, Cedillo-Ramírez ML, Santos-Preciado JI, Girón, J.
40 Association of Antibiotic Resistance, Cell Adherence, and Biofilm Production with the
41 Endemicity of Nosocomial *Klebsiella pneumoniae*. *Biomed Res Int.* 2018;2018.
42 doi:10.1155/2018/7012958
43
44 56. Schumachera MA, Zenga W. Structures of the activator of *K. pneumoniae* biofilm formation,
45 mrkh, indicates pilz domains involved in c-di-gmp and DNA binding. *Proc Natl Acad Sci U*
46 *S A.* 2016;113(36):10067-10072. doi:10.1073/pnas.1607503113
47
48 57. Dos Santos Goncalves M, Delattre C, Balestrino D, Charbonnel, N, Elboutachfai R,
49 Wadouachi A, Badel S, Bernardi T, Michaud P, Forestier C. Anti-biofilm activity: A
50 function of *Klebsiella pneumoniae* capsular polysaccharide. *PLoS One.* 2014;9(6).
51 doi:10.1371/journal.pone.0099995
52
53
54
55
56
57
58
59
60

- 1
2
3 58. Chen T, Dong G, Zhang S, Zhang, Xw, Zhao Y, Cao J, Wu, Q. Effects of iron on the growth,
4 biofilm formation and virulence of *Klebsiella pneumoniae* causing liver abscess. *BMC*
5 *Microbiol.* 2020;20(1). doi:10.1186/s12866-020-01727-5
6
7 59. Shi X, Rao NN, Kornberg A. Inorganic polyphosphate in *Bacillus cereus*: Motility, biofilm
8 formation, and sporulation. *Proc Natl Acad Sci U S A.* 2004;101(49):17061-17065.
9 doi:10.1073/pnas.0407787101
10
11 60. Drozd M, Chandrashekar K, Rajashekara G. Polyphosphate-mediated modulation of
12 *Campylobacter jejuni* biofilm growth and stability. *Virulence.* 2014;5(6):680-690.
13 doi:10.4161/viru.34348
14
15 61. Recalde A, van Wolferen M, Sivabalasarma S, Albers SV, Navarro CA, Jerez CA. The role
16 of polyphosphate in motility, adhesion, and biofilm formation in sulfolobales.
17 *Microorganisms.* 2021;9(1):1-13. doi:10.3390/microorganisms9010193
18
19 62. Rashid MH, Rumbaugh K, Passador L, Davies D, Hamoo A, Iglewski B, Iglewski B,
20 Kornberg A. Polyphosphate kinase is essential for biofilm development, quorum sensing,
21 and virulence of *Pseudomonas aeruginosa*. *Proc Natl Acad Sci U S A.* 2000;97(17):9636-
22 9641. doi:10.1073/pnas.170283397
23
24 63. Grillo-Puertas M, Villegas JM, Rintoul MR, Rapisarda VA. Polyphosphate Degradation in
25 Stationary Phase Triggers Biofilm Formation via LuxS Quorum Sensing System in
26 *Escherichia coli*. *PLoS One.* 2012;7(11):e50368. doi:10.1371/journal.pone.0050368
27
28 64. Ballén V, Gabasa Y, Ratia C, Sánchez M, Soto S. Correlation Between Antimicrobial
29 Resistance, Virulence Determinants and Biofilm Formation Ability Among Extraintestinal
30 Pathogenic *Escherichia coli* Strains Isolated in Catalonia, Spain. *Front Microbiol.* 2022;12.
31 doi:10.3389/fmicb.2021.803862
32
33 65. Luo C, Chen Y, Hu X, Chen S, Lin Y, Liu X, Yang B. Genetic and Functional Analysis of
34 the *pks* Gene in Clinical *Klebsiella pneumoniae* Isolates. *Microbiol Spectr.* Published online
35 June 21, 2023. doi:10.1128/spectrum.00174-23
36
37 66. Tang-Fichaux M, Chagneau C V., Bossuet-Greif N, Nougayrède JP, Oswald É, Branchu P.
38 The Polyphosphate Kinase of *Escherichia coli* Is Required for Full Production of the
39 Genotoxin Colibactin. *mSphere.* 2020;5(6). doi:10.1128/mSphere.01195-20
40
41 67. Beaufay F, Quarles E, Franz A, Katamanin O, Wholey WY, Jakob U. Polyphosphate
42 Functions *In Vivo* as an Iron Chelator and Fenton Reaction Inhibitor. *mBio.* 2020;11(4).
43 doi:10.1128/mBio.01017-20
44
45 68. Erskine E, MacPhee CE, Stanley-Wall NR. Functional Amyloid and Other Protein Fibers in
46 the Biofilm Matrix. *J Mol Biol.* 2018;430(20):3642-3656. doi:10.1016/j.jmb.2018.07.026
47
48 69. Bieler S, Estrada L, Lagos R, Baeza M, Castilla J, Soto C. Amyloid Formation Modulates
49 the Biological Activity of a Bacterial Protein. *Journal of Biological Chemistry.*
50 2005;280(29):26880-26885. doi:10.1074/jbc.M502031200
51
52
53
54
55
56
57
58
59

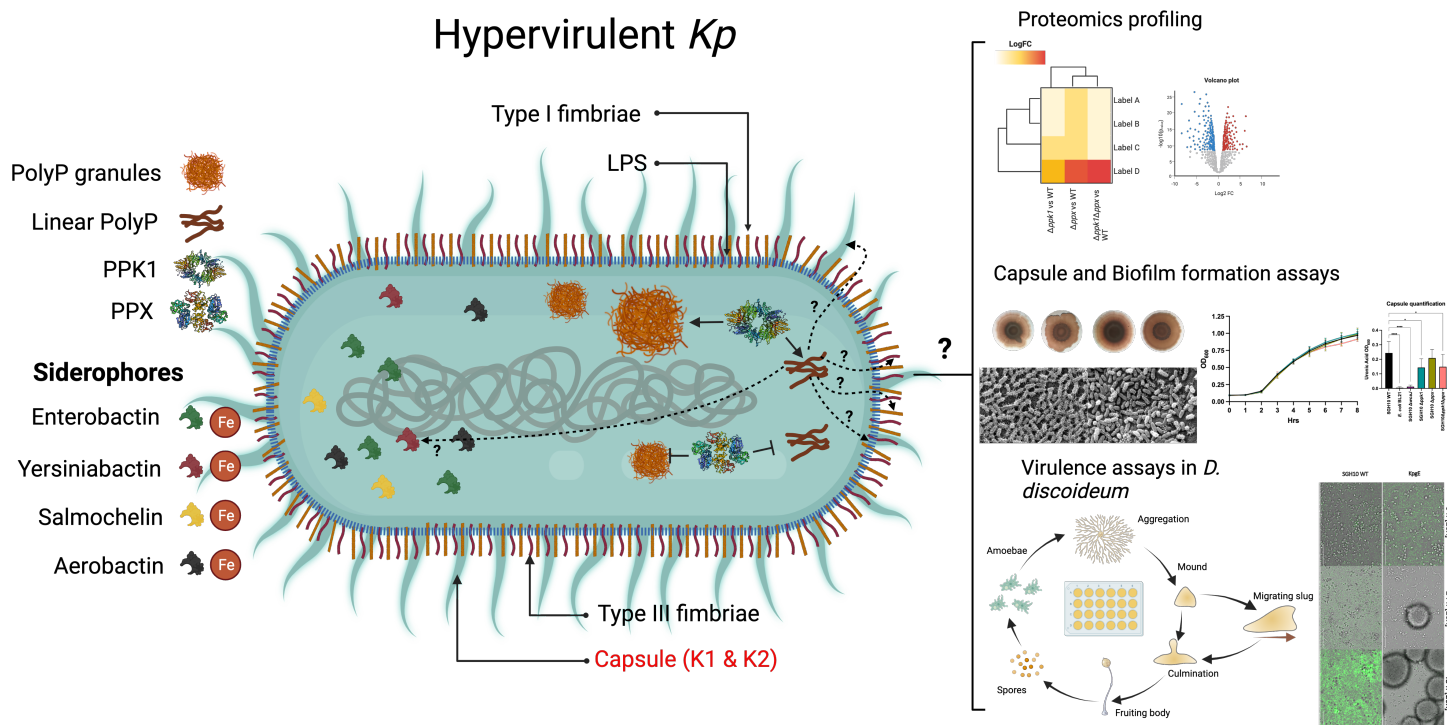
- 1
2
3 70. Marcoleta AE, Berríos-Pastén C, Nuñez G, Monasterio O, Lagos R. *Klebsiella pneumoniae*
4 Asparagine tDNAs Are Integration Hotspots for Different Genomic Islands Encoding
5 Microcin E492 Production Determinants and Other Putative Virulence Factors Present in
6 Hypervirulent Strains. *Front Microbiol.* 2016;7. doi:10.3389/fmicb.2016.00849
7
8
9 71. Flemming HC, Wingender J, Szewzyk U, Steinberg P, Rice SA, Kjelleberg S. Biofilms: an
10 emergent form of bacterial life. *Nat Rev Microbiol.* 2016;14(9):563-575.
11 doi:10.1038/nrmicro.2016.94
12
13 72. Cano V, March C, Insua JL, Aguiló N, Llobet E, Moranta D, Regueiro V, Brennan GP,
14 Millán-Lou MI, Martín C. *Klebsiella pneumoniae* survives within macrophages by avoiding
15 delivery to lysosomes. *Cell Microbiol.* 2015;17(11):1537-1560. doi:10.1111/cmi.12466
16
17 73. Froquet R, Lelong E, Marchetti A, Cosson P. *Dictyostelium discoideum*: a model host to
18 measure bacterial virulence. *Nat Protoc.* 2009;4(1):25-30. doi:10.1038/nprot.2008.212
19
20 74. Hu D, Chen W, Wu J, Luo X, Yu L, Qu Y, Zhang X, Zhang J, Ma B. Coexistence of c-rmpA
21 with p-rmpA and p-rmpA2 rather than excessive siderophores confers higher virulence in
22 K1 *Klebsiella pneumoniae*. *Pathology.* Published online September 2023.
23 doi:10.1016/j.pathol.2023.07.007
24
25 75. Chu WHW, Tan YH, Tan SY, Chen Y, Yong M, Lye DC, Kalimuddin S, Archuleta S, Gan
26 YH. Acquisition of regulator on virulence plasmid of hypervirulent *Klebsiella* allows
27 bacterial lifestyle switch in response to iron. *mBio.* Published online August 2, 2023.
28 doi:10.1128/mbio.01297-23
29
30
31 76. Thayil SM, Morrison N, Schechter N, Rubin H, Karakousis PC. The role of the novel
32 exopolyphosphatase MT0516 in *Mycobacterium tuberculosis* drug tolerance and
33 persistence. *PLoS One.* 2011;6(11). doi:10.1371/journal.pone.0028076
34
35 77. Shi X, Rao NN, Kornberg A. Inorganic polyphosphate in *Bacillus cereus*: Motility, biofilm
36 formation, and sporulation. *Proc Natl Acad Sci U S A.* 2004;101(49):17061-17065.
37 [http://www.pubmedcentral.nih.gov/articlerender.fcgi?artid=535361&tool=pmcentrez&rend](http://www.pubmedcentral.nih.gov/articlerender.fcgi?artid=535361&tool=pmcentrez&rendertype=abstract)
38 [ertype=abstract](http://www.pubmedcentral.nih.gov/articlerender.fcgi?artid=535361&tool=pmcentrez&rendertype=abstract)
39
40
41 78. Tinsley CR, Manjula BN, Gotschlich EC. Purification and characterization of polyphosphate
42 kinase from *Neisseria meningitidis*. *Infect Immun.* Published online 1993.
43 doi:10.1128/iai.61.9.3703-3710.1993
44
45 79. Kreppel L. dictyBase: a new *Dictyostelium discoideum* genome database. *Nucleic Acids Res.*
46 2004;32(90001):332D - 333. doi:10.1093/nar/gkh138
47
48 80. Basu S, Fey P, Pandit Y, Dodson R, Kibbe WA, Chisholm RL. dictyBase 2013: integrating
49 multiple Dictyostelid species. *Nucleic Acids Res.* 2012;41(D1):D676-D683.
50 doi:10.1093/nar/gks1064
51
52 81. Fey P, Dodson RJ, Basu S, Chisholm RL. One Stop Shop for Everything *Dictyostelium*:
53 dictyBase and the Dicty Stock Center in 2012. In: ; 2013:59-92. doi:10.1007/978-1-62703-
54 302-2_4
55
56
57
58
59
60

- 1
2
3
4
5
6
7
8
9
10
11
12
13
14
15
16
17
18
19
20
21
22
23
24
25
26
27
28
29
30
31
32
33
34
35
36
37
38
39
40
41
42
43
44
45
46
47
48
49
50
51
52
53
54
55
56
57
58
59
60
82. Fey P, Kowal AS, Gaudet P, Pilcher KE, Chisholm RL. Protocols for growth and development of *Dictyostelium discoideum*. *Nat Protoc.* 2007;2(6):1307-1316. doi:10.1038/nprot.2007.178
 83. Li H, Durbin R. Fast and accurate short read alignment with Burrows–Wheeler transform. *Bioinformatics.* 2009;25(14):1754-1760. doi:10.1093/bioinformatics/btp324
 84. Perez-Riverol Y, Bai J, Bandla C, García-Seisdedos D, Hewapathirana S, Kamatchinathan S, Kundu DJ, Prakash A, Frericks-Zipper A, Eisenacher M. The PRIDE database resources in 2022: a hub for mass spectrometry-based proteomics evidences. *Nucleic Acids Res.* 2022;50(D1):D543-D552. doi:10.1093/nar/gkab1038
 85. Pokhrel A, Lingo JC, Wolschendorf F, Gray MJ. Assaying for Inorganic Polyphosphate in Bacteria. *Journal of Visualized Experiments.* 2019;(143). doi:10.3791/58818
 86. Chen T, Dong G, Zhang S, Zhang X, Zhao Y, Cao J, Zhou T, Wu Q. Effects of iron on the growth, biofilm formation and virulence of *Klebsiella pneumoniae* causing liver abscess. *BMC Microbiol.* 2020;20(1):1-7. doi:10.1186/s12866-020-01727-5

For Table of Contents Use Only

Inorganic polyphosphate affects biofilm assembly, capsule formation and virulence of hypervirulent ST23 *Klebsiella pneumoniae*

Diego Rojas¹, Andrés E. Marcoleta², Matías Gálvez-Silva^{1,2}, Macarena A. Varas^{1,2}, Mauricio Díaz³, Mauricio Hernández⁴, Cristian Vargas⁴, Guillermo Nourdin-Galindo⁴, Elard Koch⁴, Pablo Saldivia^{4,5}, Jorge Vielma^{1,2}, Yunn-Hwen Gan⁶, Yahua Chen⁶, Nicolás Guiliani³ and Francisco P. Chávez^{1*}



1
2
3 Bacterial stress response often involves polyphosphate (polyP) accumulation, critical for
4 various functions, including virulence. Yet, its role in hypervirulent *Klebsiella pneumoniae*
5 strains remains unexplored. Our study manipulated polyP levels through gene mutations
6 affecting its synthesis (ppk1) and degradation (ppx) and established a link between polyP
7 and virulence expression/regulation, notably in capsule and biofilm formation. Using
8 *Dictyostelium discoideum* as a model, we observed a corresponding decrease in virulence.
9
10 Proteomic analysis further identified proteins associated with these virulence mechanisms,
11 underscoring polyP's importance and potential as a target for new anti-virulence drugs.
12
13
14
15
16
17
18
19
20
21
22
23
24
25
26
27
28
29
30
31
32
33
34
35
36
37
38
39
40
41
42
43
44
45
46
47
48
49
50
51
52
53
54
55
56
57
58
59
60

1
2
3
4
5
6
7
8
9
10
11
12
13
14
15
16
17
18
19
20
21
22
23
24
25
26
27
28
29
30
31
32
33
34
35
36
37
38
39
40
41
42
43
44
45
46
47
48
49
50
51
52
53
54
55
56
57
58
59
60

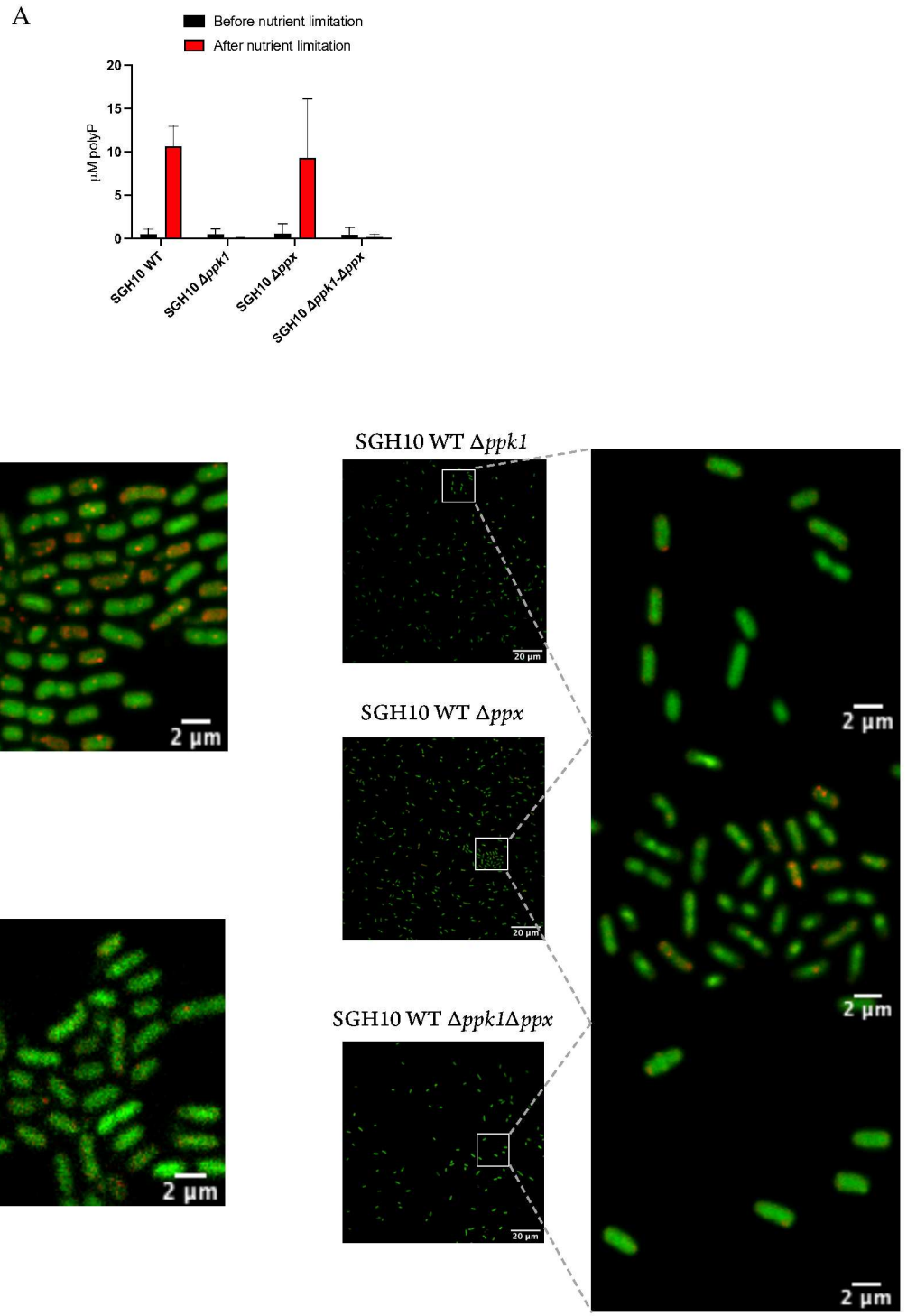
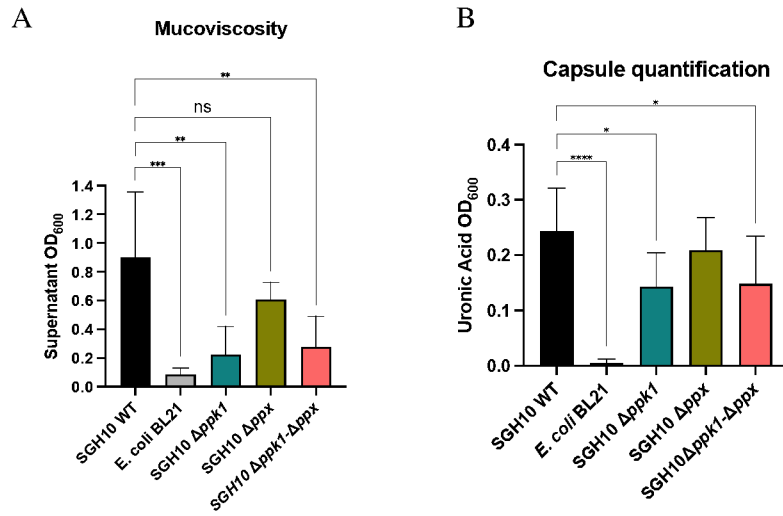


Figure 1



C

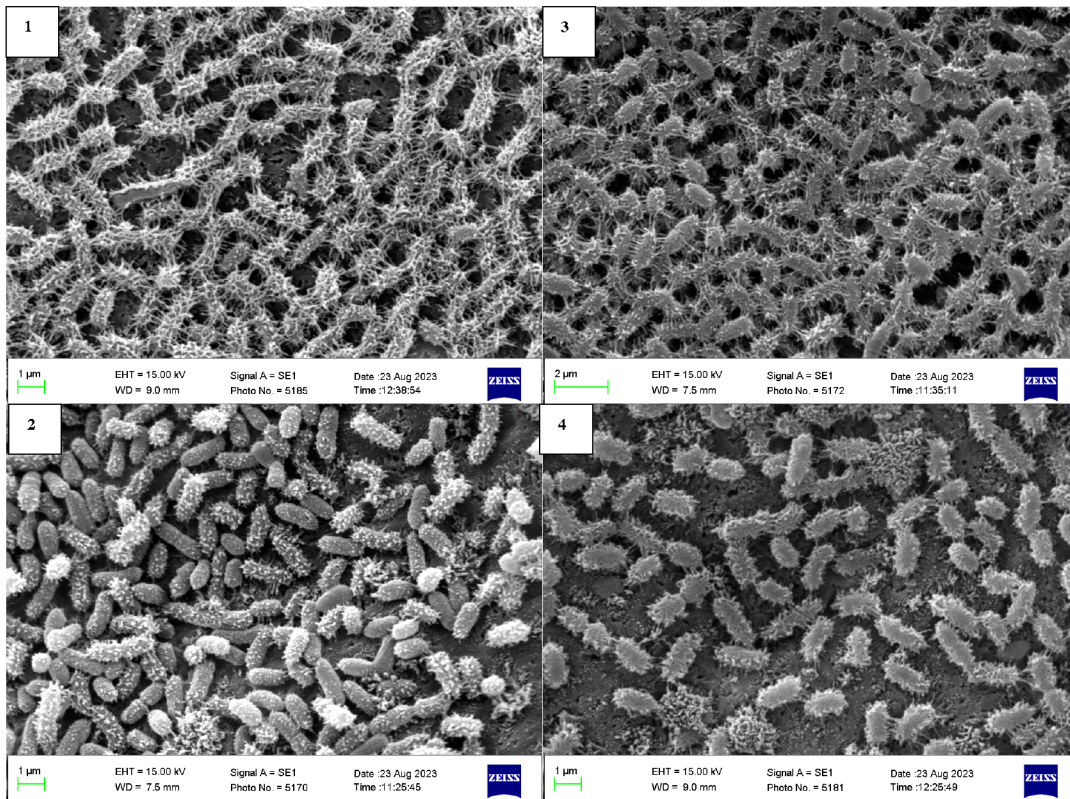


Figure 2

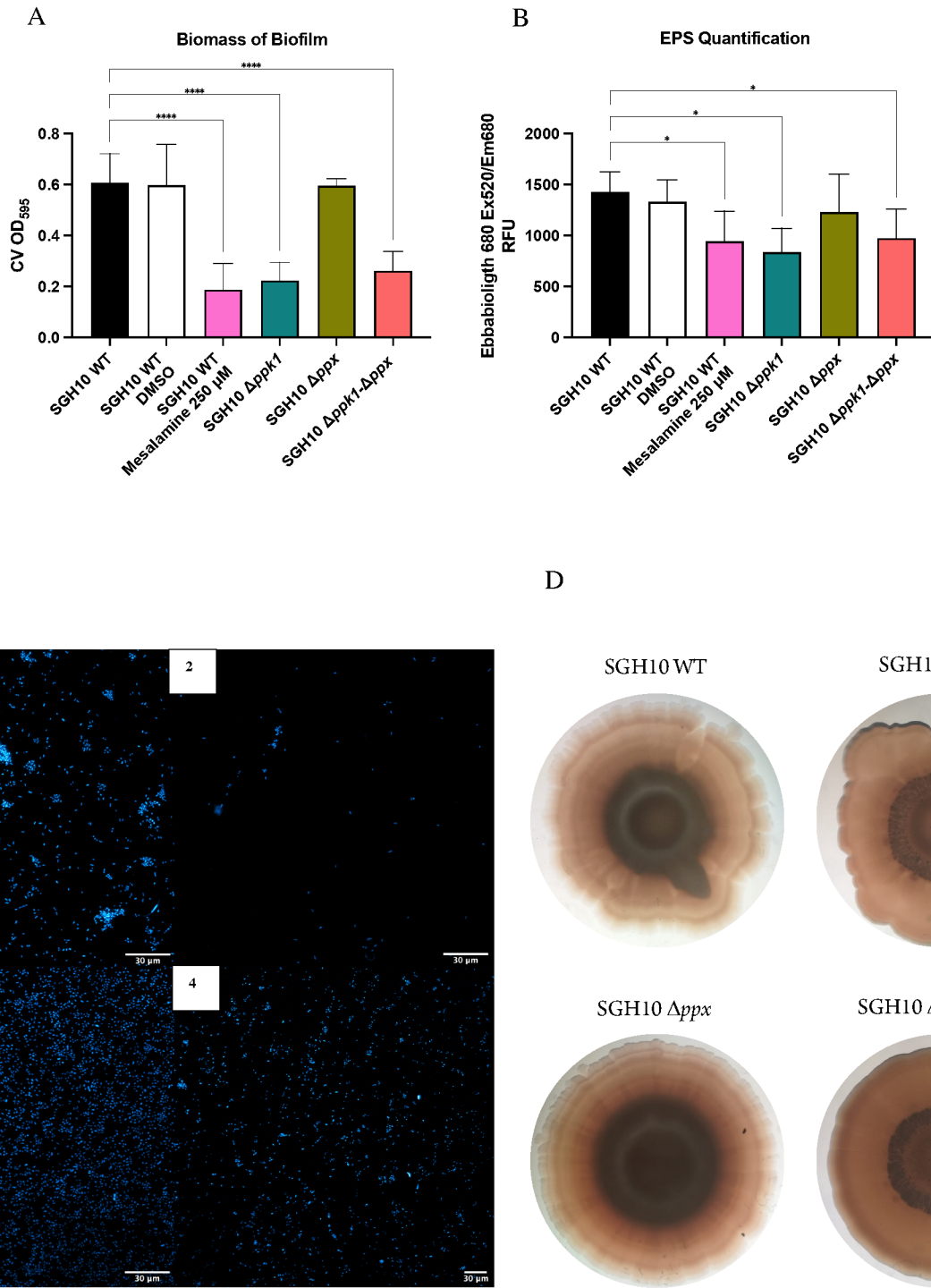
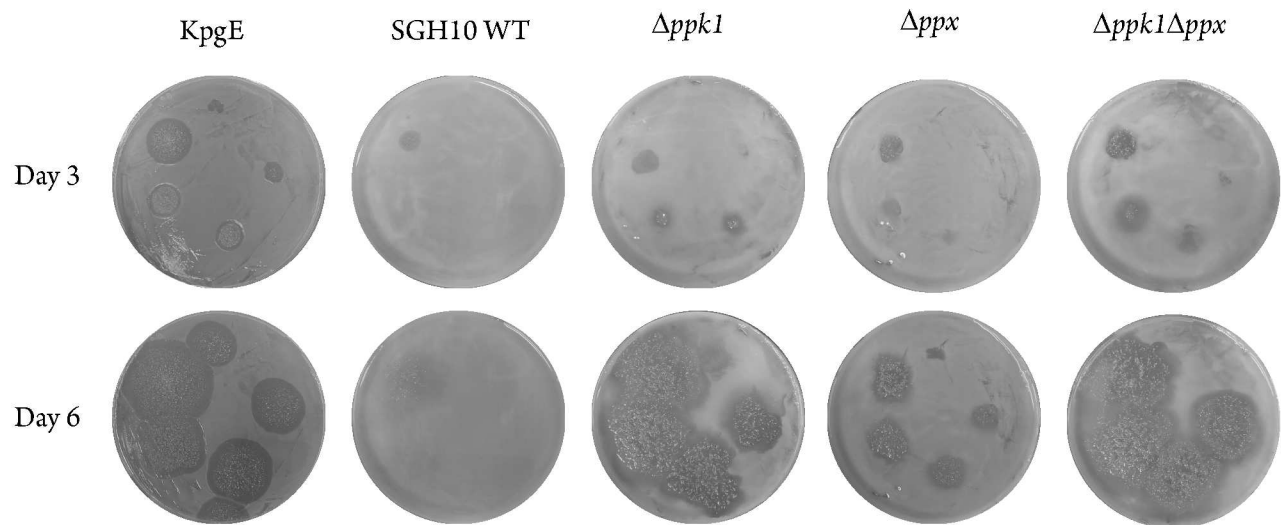
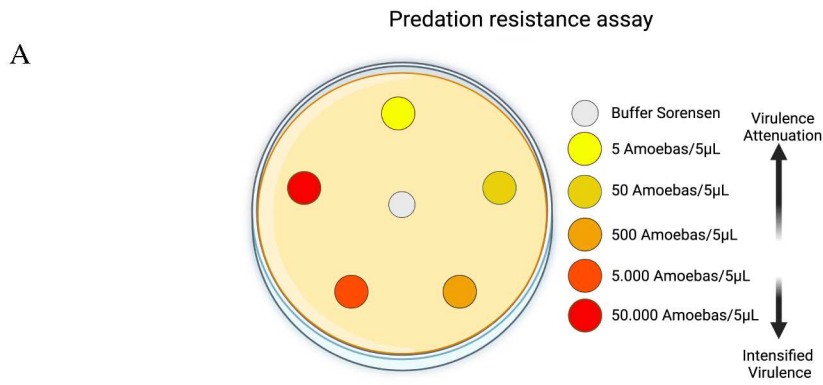
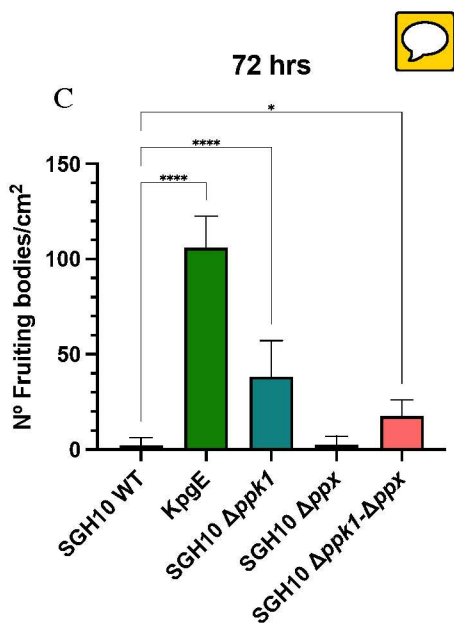
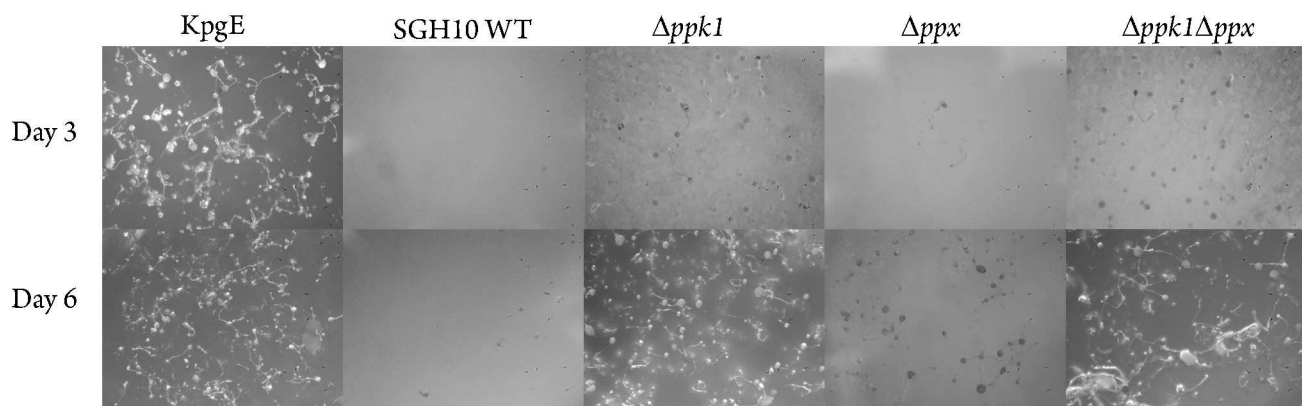
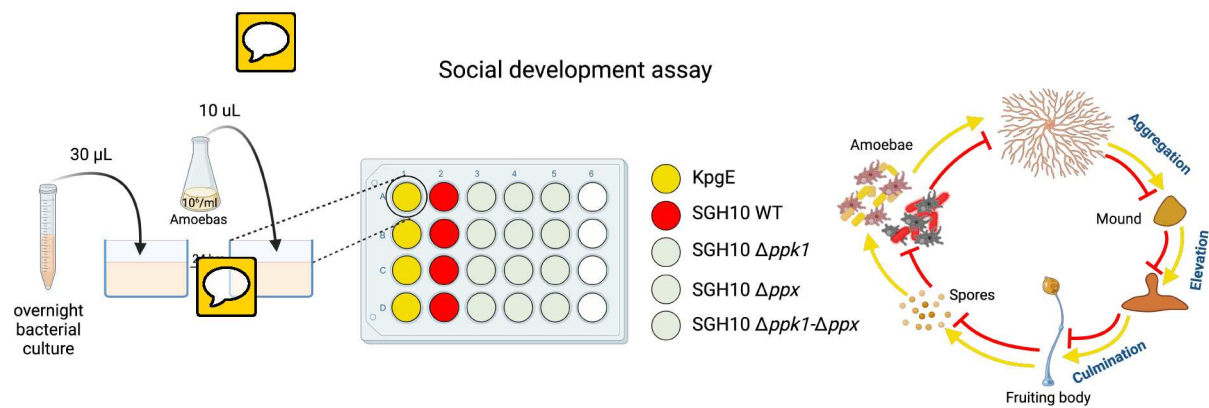


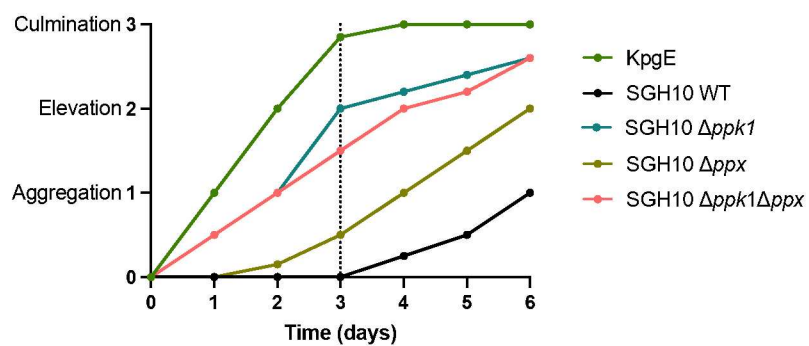
Figure 3

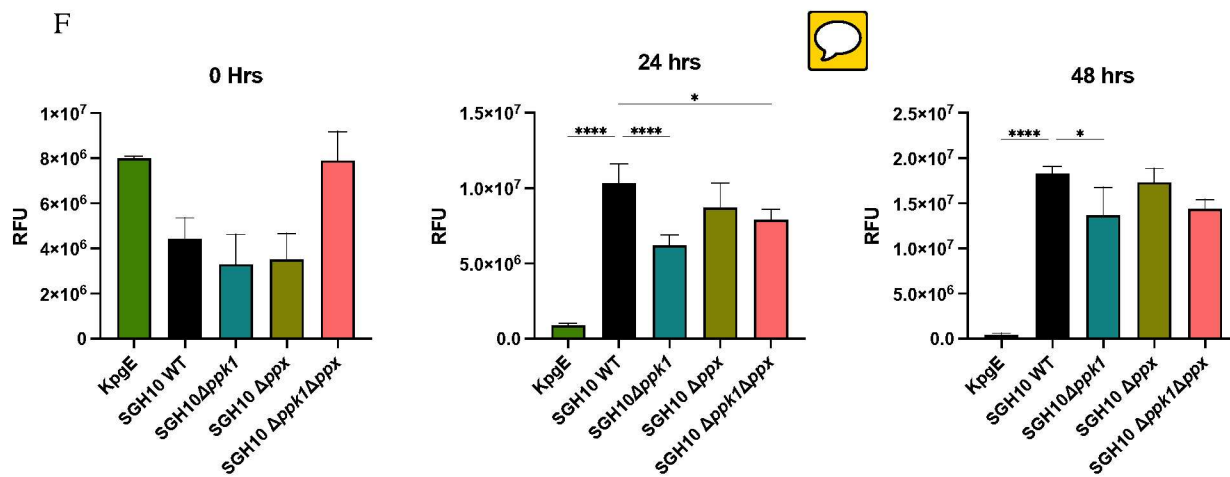
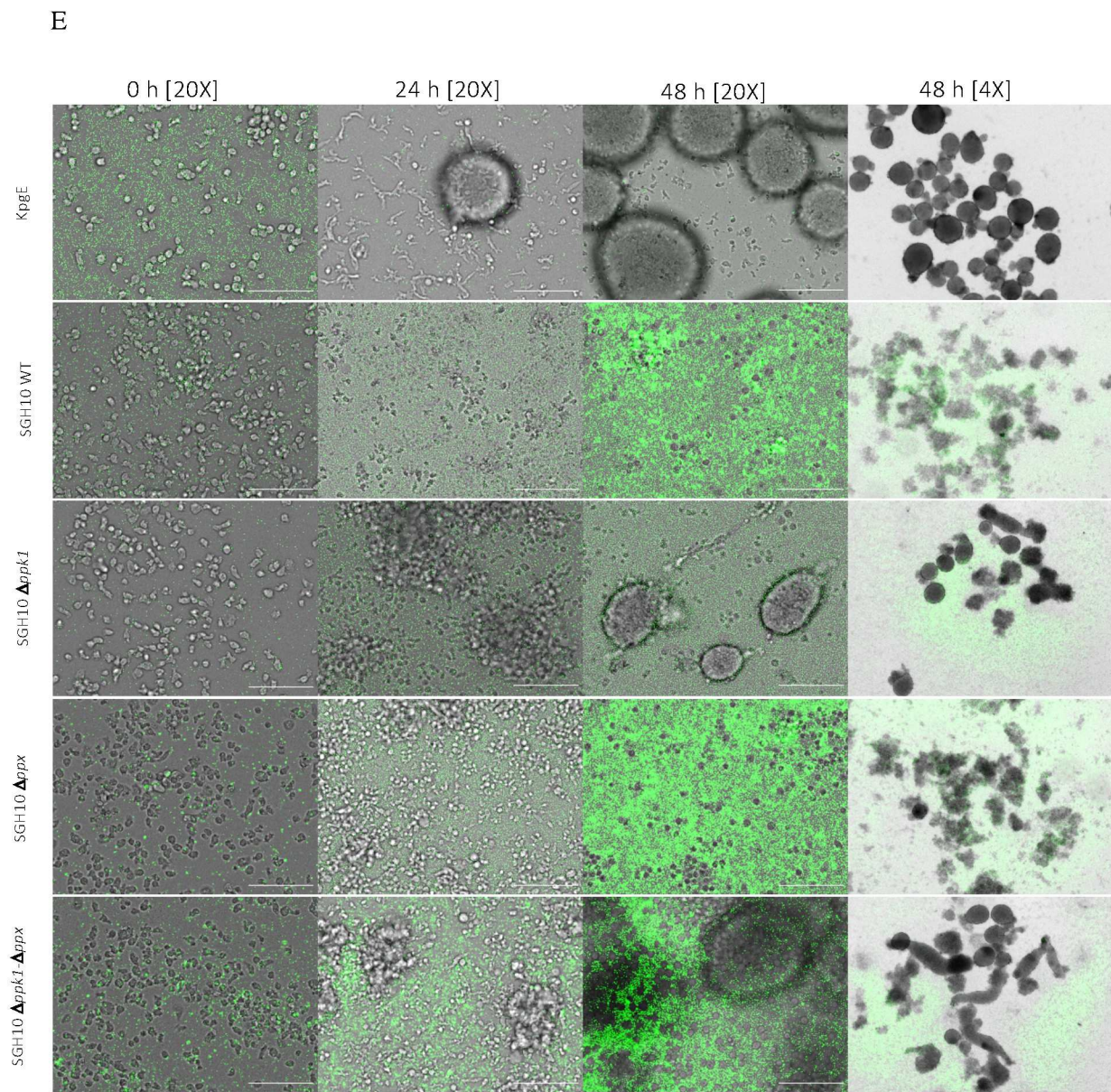


B



D





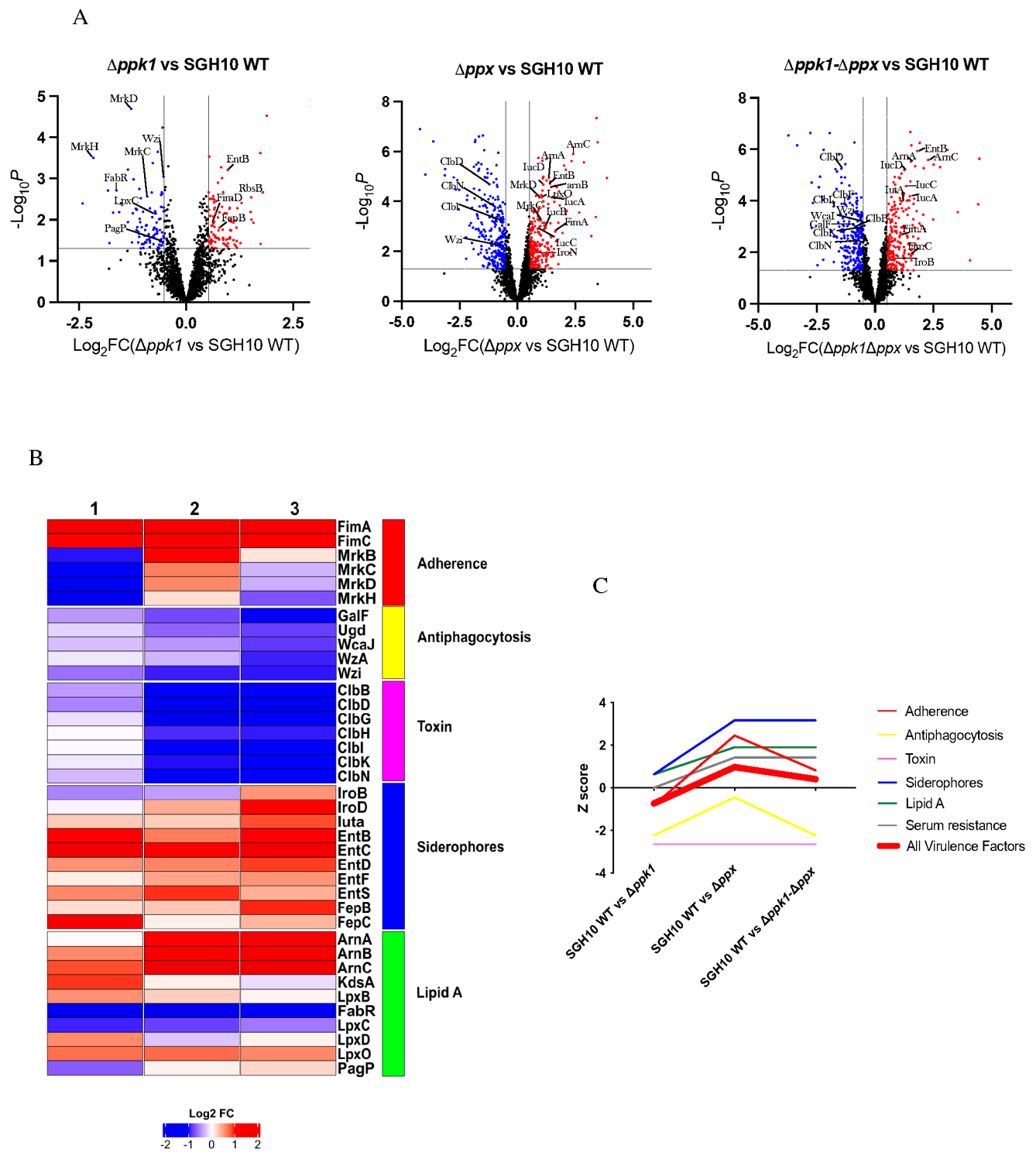


Figure 5

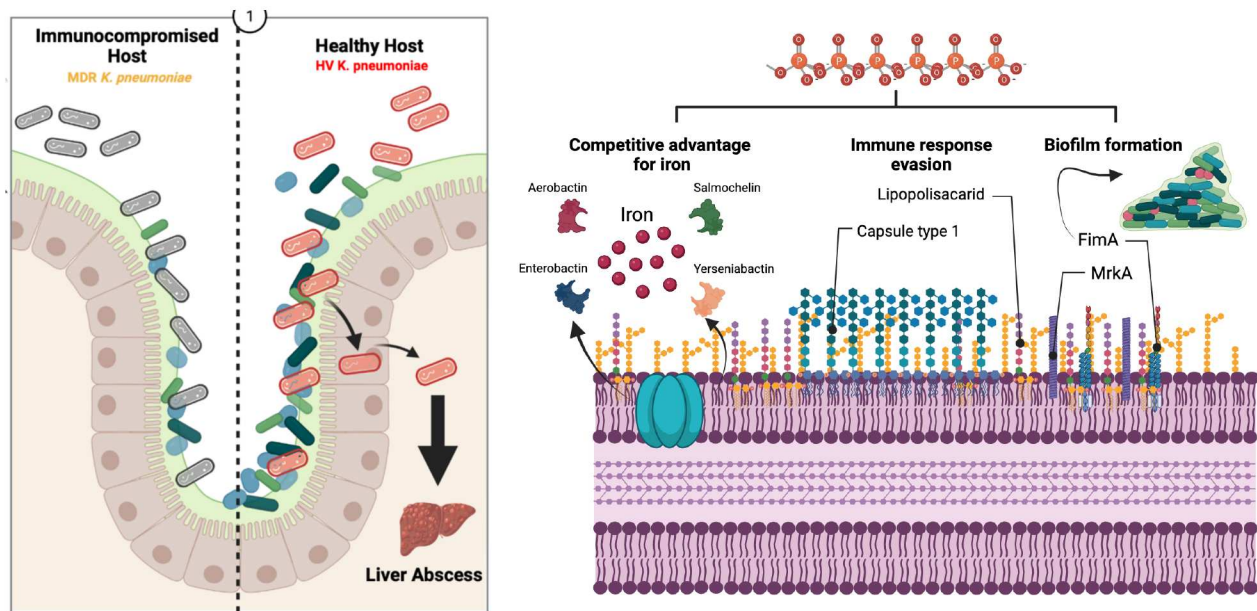


Figure 6

Flow Cytometry and Automated Microscopy Integration for Phagocytic Analysis of hypervirulent *Klebsiella pneumoniae* in *Dictyostelium discoideum*

Diego Rojas, Antonia Ramos, Matías Gálvez, Andrés E. Marcoleta, Francisco P. Chávez

Abstract

1 Introduction

Dictyostelium discoideum is a microorganism commonly found in forest soils, known for its ability to feed on bacteria and yeast through phagocytosis. Consequently, it has been extensively utilized as a model organism for phagocytic cells and as a host for opportunistic pathogens, primarily to investigate mechanisms of resistance to phagocytosis, as well as intracellular replication and survival of these pathogens. As a professional phagocyte, *D. discoideum* shares several specific functions with innate immune phagocytic cells in mammals, rendering it an appropriate organism for studying various aspects of phagocytosis and assessing the influence of virulence factors present in environmentally isolated pathogenic bacteria, as well as those encountered in clinical settings. The ease of cultivation, low maintenance and propagation costs, lack of genetic redundancy, and high susceptibility to genome manipulation due to its haploid condition, coupled with a comprehensive organism database (<http://dictybase.org/>) containing protocols, genetic tools, mutant strains, and more, collectively establish *D. discoideum* as a pivotal model organism for the study of diverse bacterial phenotypes of interest. In the protocols outlined in this chapter, virulence can be assessed through a variety of readily adaptable and scalable methodologies suitable for any laboratory equipped with basic cell culture facilities.

2 Materials

2.1 Reagents

1. Stock solution of 100 mg/mL Carbenicillin and Kanamycin: Dissolve 1 g of each antibiotic in 10 mL of distilled water. Sterilize by filtration and aliquot into 1 mL portions. Store at -20°C.
2. Stock solution of 300 mg/mL Streptomycin sulfate: Dissolve 3 grams of streptomycin sulfate in 10 mL of distilled water. Sterilize by filtration and aliquot into 1 mL portions. Store at -20°C.
3. Stock solution of 250 mg/mL of ciprofloxacin: Dissolve 2.5 g of ciprofloxacin in 10 mL of 0.1 M NaOH. Sterilize by filtration and divide it into 1 mL aliquots. Store at -20°C.

4. Stock solution of propidium iodide

2.2 Media

1. LB broth: Use as described by the manufacturer. Store at room temperature.

2. Liquid HL5 Medium: Dissolve 14 g of tryptone, 7 g of yeast extract, 0.66 g of Na₂PO₄, 1.2 g of KH₂PO₄, and 14 g of glucose. Adjust the volume to 900 mL. Set the pH to 6.5. Bring the volume up to 1000 mL with distilled water. Autoclave for 15 minutes. Store at room temperature (see **Note 1**).

3. SM Agar: Dissolve 10 g of glucose, 1 g of yeast extract, 10 g of granulated peptone (Merck), 1.08 g of MgSO₄·7H₂O, 1.9 g of KH₂PO₄, and 0.6 g of K₂HPO₄. Adjust the volume to 900 mL and add 20 g of agar. Set the pH to 6.5. Bring the volume up to 1000 mL with distilled water. Autoclave for 15 minutes (see **Note 2**). Store at room temperature.

4. Sørensen Buffer: Dissolve 2 g of KH₂PO₄ and 0.55 g of Na₂HPO₄·7H₂O. Adjust the volume to 1000 mL. Autoclave for 20 min. Store at room temperature.

5. N agar: Dissolve 1 g of peptone, 1 g glucose and 1 g of agar in 1000 mL of Sørensen Buffer. Autoclave for 15 min. Store at room temperature.

2.3 Microorganisms

1. *D. discoideum*: For storing stock cultures, place them in a freezer at -80°C. Pellet 2x10⁷ *D. discoideum* cells from an exponentially growing culture (2-4x10⁶ cells/mL) by centrifuging at 500g for 4-5 minutes or at 1500 rpm for 5 minutes. Resuspend the pellet in 1800 µL of HL5. Divide this volume into 2 cryotubes and add 100 µL of DMSO to each (10% DMSO). Store at -80°C (see **Note 3**).

2. *K. aerogenes*, *K. pneumoniae* and *K. pneumoniae* transfected with GFP: Store stock cultures in a freezer at -80°C. To ensure the reproducibility of virulence assays, always use cultures from the -80°C freezer and streak them directly onto LB agar plates supplemented with carbenicillin (100 µg/mL). Supplemented LB agar plates with 100 µg/mL carbenicillin and 50 µg/mL Kanamycin for the GFP+ strain. Incubate at 37°C.

2.4 Other materials

Stereoscopic microscope

Automated microscope Lionheart FX (Agilent)

Flow Cytometer

24-well plates with lids

96-well plates with lids
Plate centrifuge
Sterile pipette tips
Spectrophotometer
Vortex
L-shaped inoculation loop
Round inoculation loop
Cell scraper
10 mL serological pipette.
Hemocytometer (Neubauer improved, 0.100 mm depth).
Tube rotator
5mL Eppendorf tubes
Hemocytometer (Neubauer improved, 0.100 mm depth).

3 Methods

3.1 Maintenance and propagation of *D. discoideum*

The usual method for cultivating and maintaining *D. discoideum* cells is on a lawn of *Klebsiella aerogenes* on SM agar. The doubling time of the amoeba is approximately 8-12 hours for axenic strains. The incubation period from seeding is 3-4 days until the formation of phagocytosis plaques. These are observed as "clear" zones where the bacteria have been phagocytized by *D. discoideum*.

1. Prepare a pre-culture in 4 mL of LB medium containing *Klebsiella aerogenes* (carbenicillin 100 µg/mL) at 37°C, 180 rpm, for 18 hours.
2. Prepare 90 mm Petri dishes with 25 mL of SM agar.
3. Inoculate 180 µL of the bacterial culture onto the SM agar and spread it evenly using an L-shaped inoculation loop to create a bacterial lawn.
4. Quickly retrieve the cryotube with frozen amoebas from the -80°C freezer and keep them on ice. Scrape the cryotube gently with a sterile round inoculation loop and streak it gently onto the agar plate previously spread with bacteria (*see Note 4*).
5. Wrap the plates in aluminum foil and incubate them upside down at 22-23°C for 3-4 days (*see Note 5 and 6*).

6. Using a sterile inoculation loop or sticks, take a sample from the slanted edge of a phagocytosis plate.

7. Inoculate into a 250 mL cell culture bottle containing 15 mL of HL5 liquid medium (see **Note 7**) supplemented with 15 μ L of Carbenicillin (100mg/mL) and 15 μ L of Streptomycin (300mg/mL) (see **Note 8**). **This is passage S0**. Incubate for 3 to 4 days at 23°C.

8. Gently wash the S0 culture with 10 mL of Sørensen buffer to avoid amoeba detachment (see **Note 9**).

9. Add 10 mL of HL-5 medium to dislodge *D. discoideum* using a cell scraper. Harvest the amoebas in a 50 mL Falcon tube and add an additional 10 μ L of HL-5 to the Falcon tube. Take an aliquot for cell counting and adjust the amoebas to a minimum density of 5×10^4 cells/mL (see **Note 10**).

10. Inoculate the *D. discoideum* concentration and adjust the volume with HL-5 to 15 mL, adding Carbenicillin (100mg/mL). **This is passage S1**. Incubate for 3 days at 23°C. (see Figure 1)

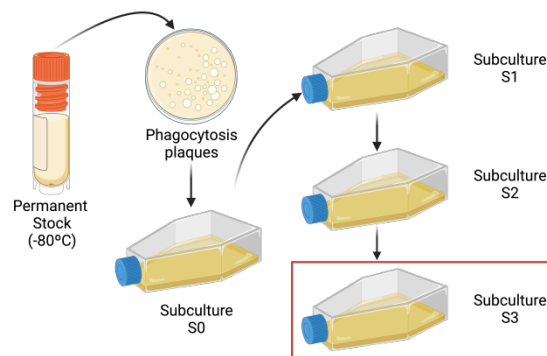


Figure 1. Scheme of the sub-culturing steps for *D. discoideum*.

3.2 Predation resistance assay

Predation refers to the act of one organism (*D. discoideum*) feeding on another (Bacteria) as a source of food. When a small initial number of amoebas grow on a lawn of commensal or avirulent bacteria, visible phagocytosis plaques form by the 2nd or 3rd day of cultivation. In contrast, when amoebas are cultured on a lawn of virulent bacteria, no visible phagocytosis plaques are formed when a low concentration of amoebas is inoculated at the beginning of the assay. This sometimes requires higher concentrations of amoebas to achieve the formation of visible phagocytosis plaques. The predation resistance assay can be used to study the virulent capabilities of bacteria isolated from the environment, as well as clinical settings. It also allows for the investigation of the influence of genes on the virulence of a strain under study.

3.2.1 *K. pneumoniae* Manipulation

1. Starting from a -80°C stock, streak *K. pneumoniae* strains onto LB agar plates (50 µg/mL carbenicillin) and incubate them overnight at 37°C.
2. Pick a single colony with a sterile loop and resuspend it in 4 mL of LB broth (50 µg/mL carbenicillin). Incubate this culture overnight at 37°C with shaking at 180 rpm.
3. Take 200 or 300 µL of the overnight culture and evenly distribute it on an SM agar plate using an L-shaped inoculation loop. Allow the bacterial lawns to dry by incubating the plate in a laminar flow hood or under a Bunsen burner (*see Note 11*).
4. Incubate the plate at 23°C.

3.2.2 *D. discoideum* Manipulation

1. When amoebas reach passage S3 (*see Note 12*), count *D. discoideum* using a Neubauer chamber and adjust it to a concentration of 1×10^6 cells/mL in a final volume of 50 mL, then transfer them to a 250 mL flask. Incubate the flask at 23°C with agitation at 50 rpm overnight.
2. Use the Neubauer chamber to count *D. discoideum* and adjust it to the required density for the assay. To do this, pour the 50 mL amoeba suspension into a 50 mL tube and centrifuge it at 2000 rpm for 5 minutes. Resuspend the pellet in 50 mL of Sørensen buffer and transfer it to a 250 mL flask. Take a 10 µL aliquot in an Eppendorf tube. Add 10 µL of trypan blue (*see Note 13*) and resuspend to mix.
3. Take 10 µL and fill the Neubauer chamber by capillarity, then count the number of amoebas in each grid square.
4. Adjust the amount of amoebas so that for every 5 µL of volume, you have a concentration of 5, 50, 500, 50,000, and 500,000/5 µL of amoebas.
5. Add 5 µL of each *D. discoideum* concentration onto the *K. pneumoniae* lawn previously grown at 23°C and distribute them at equidistant points on the lawn. In the center, place 5 µL of Sørensen buffer as a negative control. Let it dry under the laminar flow hood.
6. Cover the Petri dish with aluminum foil and incubate the inverted plate at 23°C. Record the results (*see Note 14*). (Fig. 2)

The assay can be adjusted according to the strain under study. If you are working with a mucoid or hypermucoid strain, such as *K. pneumoniae* SGH10, it is recommended not to invert the plate to prevent mucosity from adhering to the Petri dish lid. Additionally, you can perform competition studies by co-cultivating bacteria with unknown virulence in different proportions with commensal or avirulent strains to establish the presence of released virulence factors that may affect the normal development of the amoeba, even in the presence of commensal or avirulent bacteria in the lawn.

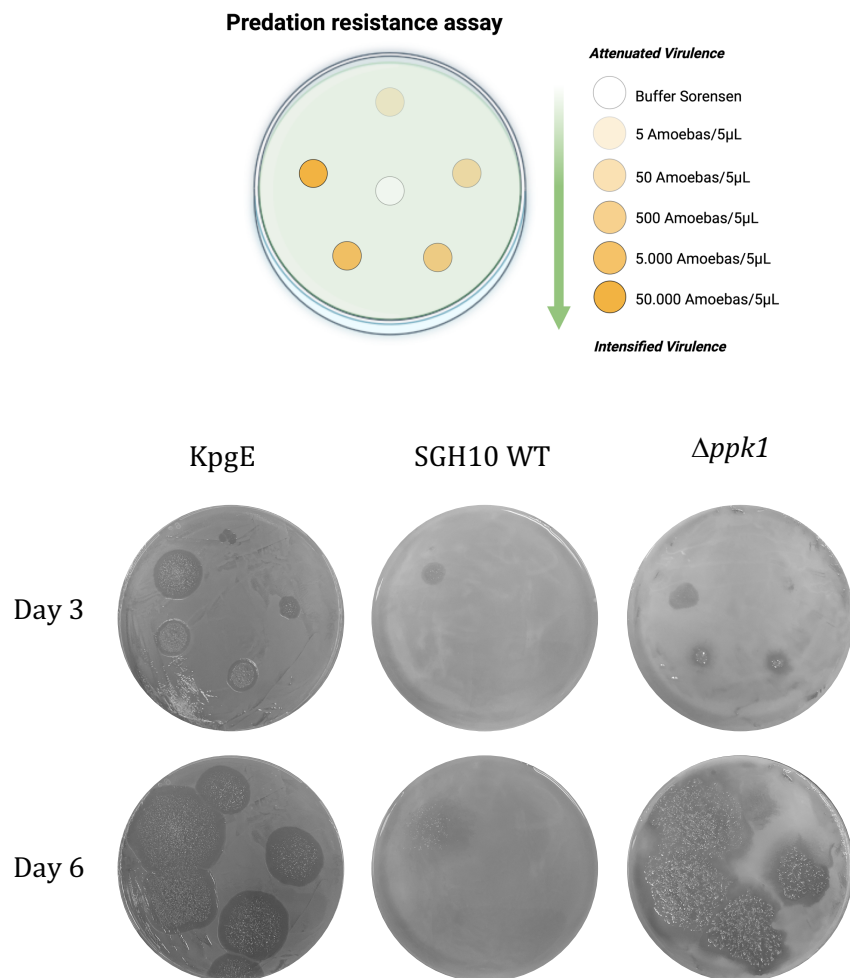


Figure 2. Expected Results: In this assay, the effect of a mutation in the gene responsible for inorganic polyphosphate synthesis (*ppk1*) in the hyper-virulent strain *K. pneumoniae* SGH10 on virulence in *D. discoideum* was evaluated. When *D. discoideum* grows on a lawn of avirulent bacteria such as KpgE (*K. aerogenes*), phagocytosis plaques are observed at all concentrations on the third and sixth day. In contrast, phagocytosis plaques are not observed on a lawn of the hyper-virulent strain at low concentrations, except for the highest concentration used in the

assay. Furthermore, the effect of the *ppk1* gene mutation on virulence attenuation can be evidenced by observing phagocytosis plaques at low concentrations on the third and sixth day of result recording.

3.3 Social Development Assay

When *D. discoideum* grows on a lawn of commensal bacteria, it undergoes a multicellular development process resulting in the formation of fruiting bodies within 2-3 days on the plate. This process includes phagocytosis plaque formation, amoeba aggregation, polarization, and cell movement, leading to the formation of cell streams that converge at aggregation centers. It progresses through mound formation, slug and finger stages, ultimately culminating in fruiting body development. Any disruption in this process due to the growth of *D. discoideum* on a lawn of bacteria of interest can provide a measure of the virulence of these bacteria. The methodology presented here assigns a score to each event in the social development cycle and provides a quantitative measure of fruiting bodies formed on a lawn of bacteria under study compared to commensal bacteria.

3.3.1 *K. pneumoniae* Manipulation

1. Prepare a 24-well plate with 2 mL of Agar N using a 10 mL serological pipette (see **Note 15**). Allow the agar to cool under the laminar flow hood or Bunsen burner. Wrap them in aluminum foil and store at room temperature until use.
2. Starting from a -80°C stock, streak *K. pneumoniae* strains onto LB agar plates (50 µg/mL carbenicillin) and incubate them overnight at 37°C.
3. Pick a single colony with a sterile loop and resuspend it in 4 mL of LB broth (50 µg/mL carbenicillin). Incubate this culture overnight at 37°C with shaking at 180 rpm.
4. Dispense 30 µL of the bacterial suspension into each well, considering one well for the control with *D. discoideum* only (see **Note 16**). Tilt the plate in different directions to ensure the bacterial suspension contacts the Agar N surface (see **Note 17**). Allow it to dry under the laminar flow hood. Incubate overnight at 23°C.

3.3.2 *D. discoideum* Manipulation

1. Repeat steps 3.2.2.1, 3.2.2.2, and 3.2.2.3.
2. Adjust the amount of amoebas to 1x10⁶cells/mL. To inoculate 10,000 amoebas, add 10 µL of the suspension onto the lawn and let it dry under the laminar flow hood. Wrap in Alusa Foil and incubate at 23°C for 6 days.

- Record the results over 6 days, capturing images with a stereomicroscope equipped with a digital camera to monitor the phases of social development. Each achieved phase is classified as "aggregation," "elevation," and "culmination." A score of '1' will be assigned when amoebas aggregate to form a phagocytosis plaque, '2' when elevated structures like worms or fingers are observed across the surface, and '3' when fruiting bodies form across the surface of the well. Transitions between any of these three phases will be scored with half the value of the closest next stage.
- On the third day, count the fruiting bodies formed on the plate. Use image analysis software such as ImageJ, and outline a 1 cm² grid centered in the well, counting the number of fruiting bodies.

The social development assay can be adjusted according to the research question. You can study the effect of a chemical compound, a drug, or the interaction of a consortium of bacteria and assess their impact on the progress of social development (Fig. 3).

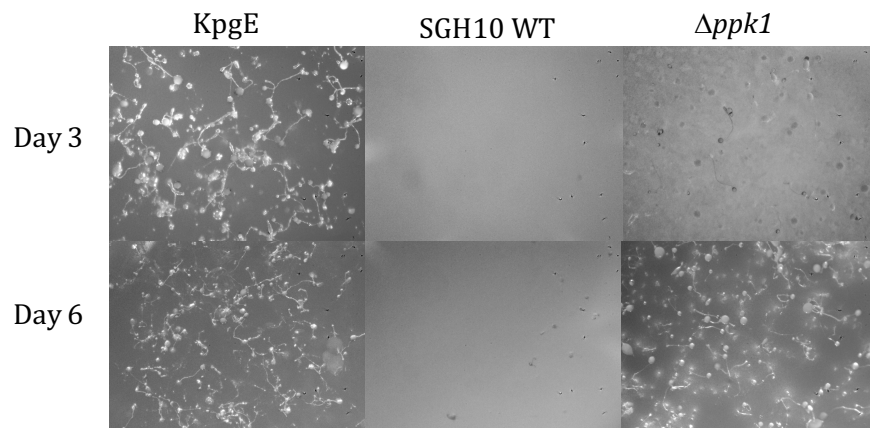
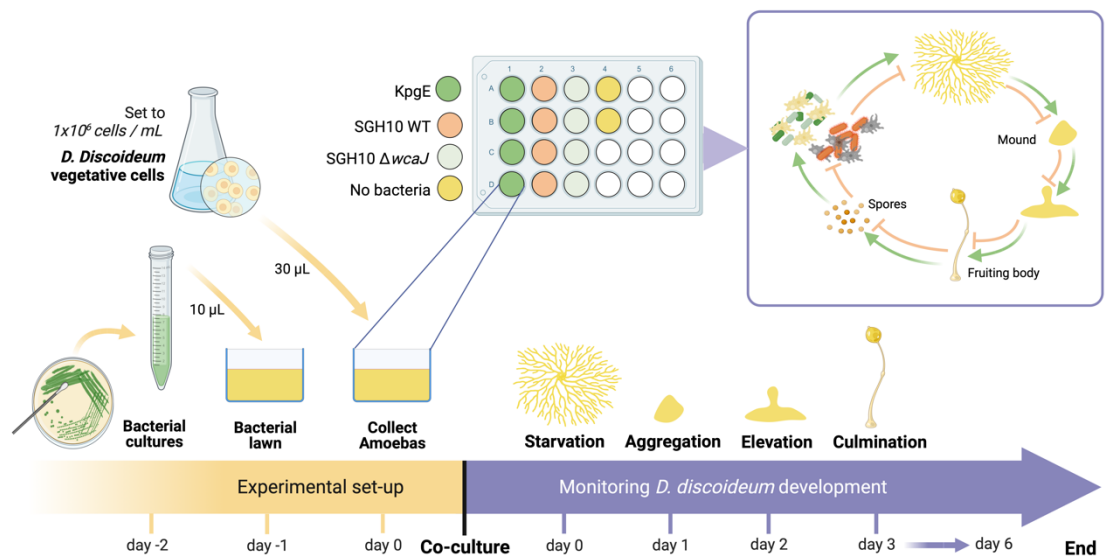


Figure 3. Expected Results: In this essay, a daily record (over 6 days) was maintained to track the key milestones in the social development of *D. discoideum*, using the avirulent strain KpgE and the pathogen model strain *K. pneumoniae* SGH10. Attenuation of virulence is observed in the *K.p.* SGH10 Δ *ppk1* mutant. This is a straightforward and scalable methodology that provides pertinent insights for studying virulence factors in both environmental and clinical bacteria, highlighting the utility of mutants and pharmaceuticals in the process.

3.4 Phagocytosis Resistance Assay

The use of *D. discoideum* has significantly facilitated the study of the process of bacterial phagocytosis, as it exhibits a high similarity to phagocytes in the innate immune system of higher mammals with very similar phagocytosis mechanisms. When *D. Dictyostelium* is co-incubated with commensal or avirulent bacteria, a strong fluorescent signal is expected within the cells early on, indicating a high bacterial load. Over time, this signal decreases as *D. Dictyostelium* cells consume the bacteria in the media. In contrast, co-incubation with virulent bacteria results in only a weak fluorescent signal, which remains relatively constant over time. The phagocytosis resistance assay can assess the virulence of bacteria isolated from various environments, including clinical settings. It also allows for the investigation of the influence of genes on the virulence of the studied strain. In this section, we present a detailed protocol for assessing phagocytosis resistance using live-cell imaging, time-lapse techniques and flow cytometry for observation and analysis in the pathogen-host interaction.

3.4.1 Live-cell imaging

3.4.2 *D. discoideum* Manipulation

1. Repeat steps 3.2.2.1, 3.2.2.2 (Use HL-5 medium to resuspend the pellet), and 3.2.2.3.
2. Adjust the amoeba concentration to 1×10^6 cells/mL in HL5 medium. Dispense 1 mL of the suspension per well into a 24-well plate.
3. Centrifuge the plate at 600 g for 5 minutes at room temperature. Incubate for 24 hours at 23°C (see **Note 18**).

3.4.3 *K. pneumoniae* Manipulation

1. Starting from a -80°C stock, prepare a lawn of *K. pneumoniae* GFP strains on LB agar plates (50 µg/mL carbenicillin, 50 µg/mL Kanamycin) and incubate them overnight at 37°C.

2. Use a sterile loop to collect bacteria. Resuspend the bacteria in 1 mL of Sørensen buffer. Vortex vigorously to fully disperse the bacteria (see **Note 19**).

3. Adjust the cell density to an OD₆₀₀ of 1x10⁷cells/mL.

3.4.4 Co-incubation

1. Wash each well of *D. discoideum* with Sørensen buffer, taking care not to disrupt the amoeba monolayer. Add 1 mL of Sørensen buffer to the inner surface of the well. Perform three washes.

2. Inoculate each well with 1 mL of the bacterial suspension (1x10⁷cells/mL) to achieve an MOI of 10.

3. Centrifuge the plate at 600g for 30 minutes at room temperature.

3.4.5 Live Cell Imaging: Lionheart programming and data acquisition.

1. Set the equipment temperature to 23°C and configure it to capture images every 10 minutes for 24 hours in both brightfield and GFP channels.

2. Mount the plate on the Lionheart FX microscope and select two regions of interest (ROI) per well at a 20X magnification (see **Note 20**). Adjust the objective height to obtain a sharp image and set different focal planes.

3. Analyze the acquired images using Gen5 software and generate a video of the recordings. Evaluate the total fluorescence intensity. Any differences observed in the RFU (Relative Fluorescence Units) of the samples can be analyzed using GraphPad Prism software. (Fig. 4).

3.4.6 Time-Lapse

If your laboratory lacks an automated microscope for Live-cell imaging, you can still observe using a confocal or epifluorescence microscope to perform a Time-lapse. Follow these steps:

1. After centrifuging the plate, perform observations under the confocal or epifluorescence microscope, using brightfield to visualize amoebas and the GFP channel to observe bacteria at 20X magnification. This is Time 0 h.

2. Incubate the plate at 23°C at specific time intervals, which can be 2, 6, 12, 24, and 48 hours. At each hour of incubation, repeat step 1. Also, observe at 4X magnification to identify aggregation streams, clusters, slugs, fingers, and fruiting bodies.

3. Capture representative images at each time interval and analyze them using image analysis software like ImageJ. Identify relative fluorescence units to determine whether the strain under study is phagocytosis-resistant by comparing it to the avirulent strain (see **Note 21**).

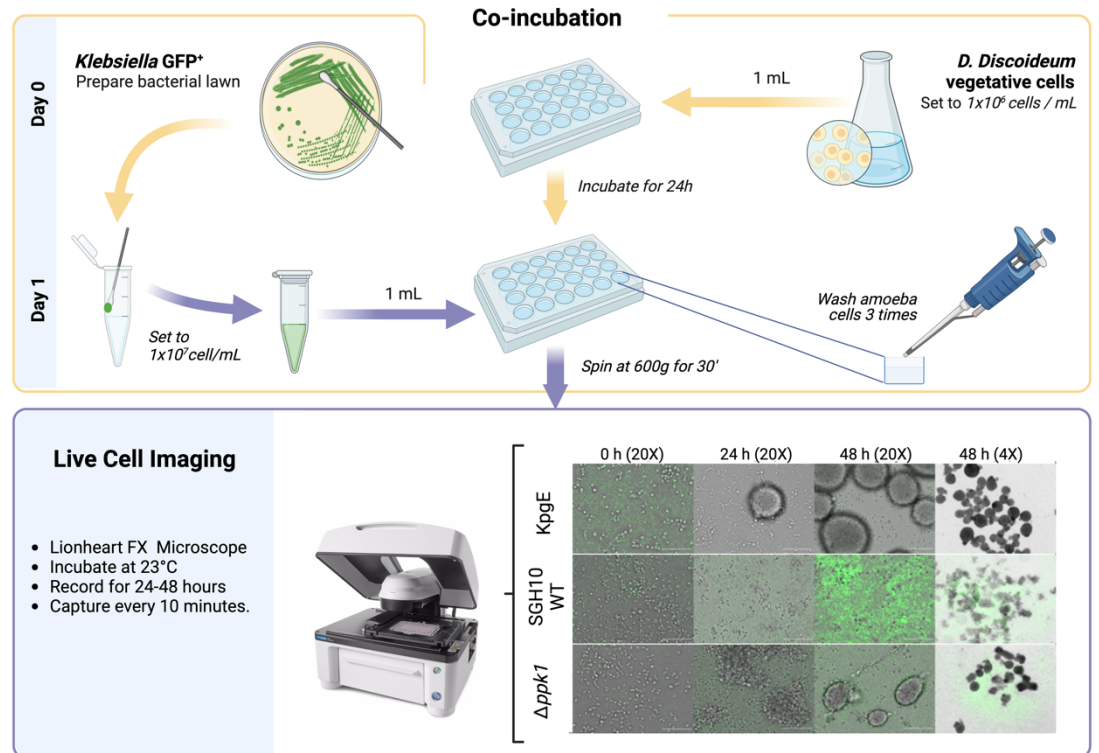


Figure 4. Expected Results: In this assay, we investigate the dynamic interaction between *D. discoideum* and *K. pneumoniae* using real-time microscopy. A significant decrease in fluorescence is observed in the avirulent strain KpgE at 24 hours. For the hypervirulent strain *K.p.* SGH10 WT, fluorescence increases from 24 to 48 hours, with no discernible finger or fruiting body formation. The $\Delta ppk1$ mutant displays virulence attenuation, as evidenced by the organization of amoebas into multicellular forms at 48 hours. It is possible to employ alternative fluorophores for labeling phagolysosomes and studying intracellular dynamics in the phagocytosis process.

3.4.7 Flow cytometry

The rate of phagocytosis can be quantified by measuring the number of bacteria inside *D. Dictyostelium* cells over time. When using transfected bacteria that express a fluorescent molecule such as Green fluorescent protein (GFP), this can be detected by flow cytometry after different co-incubation times.

3.4.8 *K. pneumoniae* Manipulation

1. Starting from a -80°C stock, streak *K. pneumoniae* strains onto LB agar plates (supplemented with the respective selection antibiotic for the transfected strain) and incubate overnight at 37°C.
2. Pick a single colony with a sterile loop and create a bacterial lawn on LB agar plates. Incubate overnight at 37°C.
3. Collect sufficient bacteria from the plate using a sterile loop and transfer them into the internal walls of a 5 mL Eppendorf tube. Add 1 mL of Sorensen buffer and vortex vigorously until homogeneous. Measure the concentration using a spectrophotometer and adjust it to a concentration of 1×10^8 cells/mL.

3.3.9 *D. discoideum* Manipulation

1. When amoebas reach passage S3, collect enough cells and remove the media by centrifuging at 2000 rpm for 5 minutes. Discard the supernatant and wash three times with Sorensen buffer.
2. Use the Neubauer chamber to count *D. discoideum* cells and adjust the concentration to 1×10^6 cells/mL.

3.4.10 Coincubation

1. For each co-incubation time point (see **Note 22**), combine 2 mL of *D. discoideum* culture (1×10^6 cells/mL) with 200 μ L of bacterial culture (1×10^6 cells/mL) (MOI 10). Co-incubate them at 23°C in 5 mL Eppendorf tubes on a tube rotator (see **Note 23**).
2. After the required time, take 200 μ L of the co-incubation mixture to determine the extracellular titer as an external control of the experiment. Perform serial dilutions (up to 10^{-7}) in a 96-well plate and plate dilutions from 10^{-3} to 10^{-7} on LB agar plates using a micro-drop (5 μ L) with triplicates. Incubate at 37°C for 24 hours and then count the colonies.
3. The remaining co-incubation mixture (1.8 mL) is used for flow cytometry analysis. Treat it with ciprofloxacin (250 μ g/mL) for 10 minutes, vortexing every 2-3 minutes to ensure the clearance of

extracellular bacteria and those possibly attached to *D. discoideum* cells. After treatment, spin the tubes at 2000 rpm for 5 minutes to eliminate bacteria and their debris. Resuspend the pellet in 500 μL of Sorensen buffer and add 1 μL of a 1 $\mu\text{g}/\mu\text{L}$ propidium iodide solution to evaluate cell viability.

3.4.11 Flow Cytometry Analysis

The acquisition and analysis of flow cytometry data (see **Note 24**) were performed using Flowing Software, with 10,000 events recorded for each condition. The gating strategy was as follows:

1. The population was first separated by Forward Scatter to identify single cells.
2. The single-cell population was then further separated by Side Scatter to distinguish it from cellular debris.
3. The sub-population was subsequently separated based on propidium iodide fluorescence. Any cells positive for this signal were excluded from the analysis as they were considered dead (see **Note 25**).
4. Once the live single-cell population was determined, amoebas exhibiting a positive GFP signal were selected, indicating the presence of bacteria. (Fig. 5)

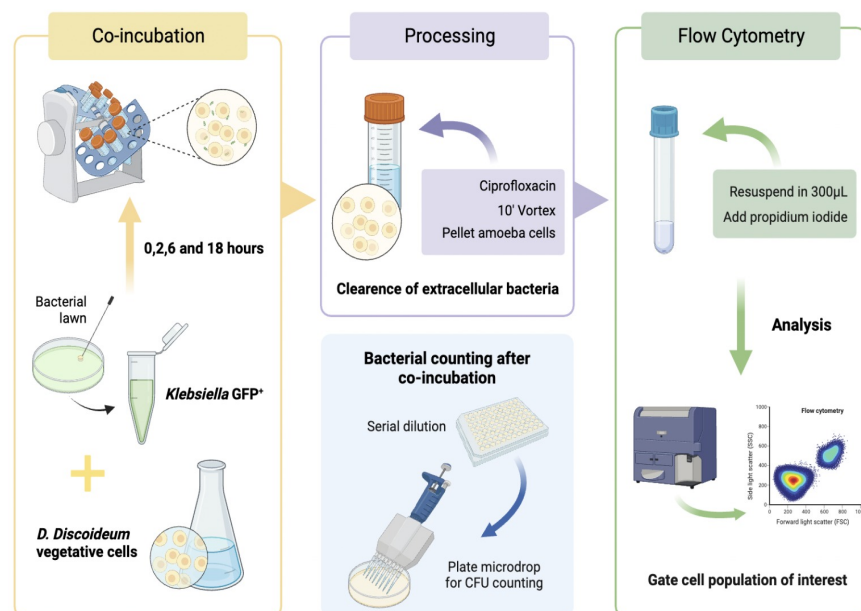


Figure 5. Protocol of the phagocytosis resistance assay by flow

4 Notes

1. This medium is used for initiating and maintaining axenic cultures of *D. discoideum*. It is crucial to avoid medium caramelization (caused by excessive autoclaving time) as it can affect the nutrient content of the medium and, consequently, the optimal growth of the amoeba. The optimal time is 15 min.
2. This solid medium is employed for the growth and maintenance of *D. discoideum* in conjunction with bacteria (*K. aerogenes* or *E. coli B/r*). The recommended volume per 90mm plate is 25 mL.
3. When the -80°C freezer is situated at a considerable distance from the laboratory, it is advisable to store amoebas in smaller aliquots to prevent sample loss in case of thawing.
4. This process should be carried out quickly to prevent the contents of the cryotube from thawing, and gently to avoid damaging the agar with the loop.
5. Phagocytosis plaques should start to appear within 3-4 days of incubation. Once this happens, it is possible to initiate an axenic culture and store the plate covered with Parafilm at 4°C for maintenance and renewal.
6. During the formation of phagocytosis plaques, it's important that the amoebas are evenly distributed on the agar surface and efficiently phagocytize the bacteria. If they are too active due to light exposure, they may concentrate in specific areas of the plate and not distribute uniformly. This could result in the formation of irregular plaques or a lack of phagocytic activity in some areas.
7. Ensure that the volume of HL5 medium does not exceed 1/5 of the total flask volume to allow proper oxygenation of the culture.
8. It is crucial to initiate the axenic culture with both antibiotics (when inoculating from a phagocytosis plate). Failure to do so may result in bacterial overgrowth in the culture. For subsequent subcultures, use only Carbenicillin (15 µL from a stock solution at 100mg/mL for 15 mL of HL5 medium).
9. Carefully pour the Sørensen buffer into the bottle neck to prevent the buffer from detaching the amoeba film.
10. Liquid cultures of *D. discoideum* should remain in the exponential growth phase ($1-4 \times 10^6$ cells/mL); therefore, they should be subcultured periodically. The minimum density to which the amoeba should be subcultured is 5×10^4 cells/mL to avoid entering a lag phase for an indeterminate period at lower densities. If you plan to use or refresh the culture in 2 more days,

it's advisable to subculture at a density of 1 or 2×10^5 cells/mL. If you need cells in exponential phase quickly, you can subculture at higher densities (e.g., 3 , 4 , and 5×10^5). The densities for subculturing are determined based on the growth kinetics of the culture. It's good practice to visually monitor and count the growth (over time, you gain experience correlating turbidity with the approximate cell density of the culture). What you should do is establish a schedule specifying the days for subculturing, the densities, the days for revival from the frozen -80°C stock and the days for refreshing maintenance plates, to maintain healthy axenic cultures of *D. discoideum*. If the density of a culture exceeds 4×10^6 cells/mL, it is recommended not to use it, as the cells will have initiated development, thus altering the physiology of the culture.

11. It is important to evenly distribute the bacteria on the agar to form a uniform bacterial lawn across the entire plate without any gaps. To achieve this, once you notice dry areas on the plate when held up to the light, use the L-shaped inoculation loop to redistribute the bacteria across the entire plate until it dries completely under the laminar flow hood.

12. The reason for using *D. discoideum* cells at passage S3 (third generation) instead of S1 (first generation) or S2 (second generation) is that in the initial generations of culture, cells may be in a less stable or less adapted state to the culture environment. By performing successive passages, cells can better adapt to the culture conditions and reach a more stable and homogeneous state. In the case of *D. discoideum*, it is important to note that these cells are particularly sensitive to stress and can change their behavior based on the culture conditions. Therefore, to conduct more reproducible and consistent experiments, it is common to use cells in later passages (S3 or later)

13. This staining allows the distinction between live and dead cells. Live cells appear white under the microscope as they actively expel the dye, while dead cells appear blue.

14. You can generate records for each of the 6 days of the assay or at the 3rd and 6th day. It's important to establish the days on which you will record data to ensure reproducible results.

15. The use of hot medium can affect the calibration of micropipettes, so use serological pipettes or a syringe to fill the wells.

16. If you are testing the effect of a drug or molecule, it's important to add a well to observe whether the compound itself is affecting the social development of *D. discoideum*.

17. Tilt the plate in all directions to ensure proper distribution of the suspension, preventing any Agar N surface from being devoid of bacteria.

18. You may eventually skip centrifugation since, after 24 hours of incubation, amoebas settle at the bottom of the plate, forming a monolayer.

19. If working with a mucoid or hypermucoviscous strain, we recommend depositing the bacteria on the inner surface of a 5 mL tube without touching the Sørensen buffer, then vigorously vortexing for approximately 5 minutes. This promotes gradual bacterial detachment.

20. Select regions that are not oversaturated with bacteria in the GFP channel and amoebas in the brightfield.

21. When using the *K. aerogenes* (KpgE) strain as a control, you will observe a rapid reduction in GFP-labeled bacteria within the first 2-6 hours. This is due to amoebic phagocytosis.

22. This assay requires measuring different time points to study the phagocytosis dynamics. Adjust the time points depending on the strain and experimental logistics. In this case, five time points were used: 0 hours, 2 hours, 6 hours, 18 hours, and 24 hours of co-incubation.

23. Since both cultures are prepared in advance, maintain them at 23°C with constant rotation to ensure that cells are in a similar state regardless of the co-incubation start time.

24. During flow cytometry analysis, it is crucial to have a control sample of *D. discoideum* cells without bacteria to normalize the fluorescence values based on their intrinsic fluorescence.

25. It is important to note that not all bacterial strains exhibit the same GFP fluorescence. Therefore, normalization is essential to accurately correlate the fluorescence signal with the quantity of bacteria inside when working with different strains.

Manuscripts that are not directly related to the thesis.



***Dictyostelium discoideum*-assisted pharmacognosy of plant resources for discovering antivirulence molecules targeting *Klebsiella pneumoniae*.**

Journal:	<i>Phytotherapy Research</i>
Manuscript ID	PTR-23-3190
Wiley - Manuscript type:	Research Article
Date Submitted by the Author:	23-Nov-2023
Complete List of Authors:	Hernandez, Marcos; University of Chile Faculty of Sciences, University of Chile Areche, Carlos; University of Chile Faculty of Sciences, University of Chile Castañeta, Grover; University of Chile Faculty of Sciences, University of Chile Rojas, Diego; University of Chile Faculty of Sciences, University of Chile Varas, Macarena; University of Chile Faculty of Sciences, University of Chile Marcoleta, Andres; University of Chile Faculty of Sciences, University of Chile Chavez, Francisco; University of Chile Faculty of Sciences, University of Chile
Keyword:	Multi-Drug resistant pathogen, Pharmacognosy, Antimicrobials, Antibiotic resistance, Cytotoxicity

SCHOLARONE™
Manuscripts

1
2
3
4
5
6
7 *Dictyostelium discoideum*-assisted pharmacognosy
8 of plant resources for discovering antivirulence
9 molecules targeting *Klebsiella pneumoniae*.
10
11
12
13

14 *Marcos Hernández*^{1,2}, *Carlos Areche*², *Grover Castañeta*², *Diego Rojas*¹, *Macarena A. Varas*¹,

16
17 *Andrés E. Marcoleta*³ and *Francisco P. Chávez*^{1*}
18
19
20
21
22
23
24
25

26
27 ¹ Laboratorio de Microbiología de Sistemas, Departamento de Biología, Facultad de Ciencias,
28
29 Universidad de Chile, Santiago, Chile. fpchavez@uchile.cl
30
31
32
33

34 ² Departamento de Química, Facultad de Ciencias, Universidad de Chile, Santiago, Chile;
35
36
37 areche@uchile.cl
38
39
40
41

42 ³ Grupo de Microbiología Integrativa, Laboratorio de Biología Estructural y Molecular,
43
44
45 Departamento de Biología, Facultad de Ciencias, Universidad de Chile, Santiago, Chile
46
47
48

49 * Correspondence: fpchavez@uchile.cl; Tel.: +56229787185, Laboratorio de Microbiología de
50
51
52
53 Sistemas, Las Palmeras 3425, Ñuñoa CP 7800003, Santiago, Chile
54
55
56
57
58
59
60

1
2
3
4 KEYWORDS. Antimicrobials, multidrug-resistant pathogens, antivirulence, plant extracts,
5
6
7 pharmacognosy.
8
9
10
11
12
13
14
15
16
17
18
19
20
21
22
23
24
25
26
27
28
29
30
31
32
33
34
35
36
37
38
39
40
41
42
43
44
45
46
47
48
49
50
51
52
53
54
55
56
57
58
59
60

For Peer Review

ABSTRACT

The rise of antibiotic-resistant bacterial strains represents an important challenge for global health, underscoring the critical need for innovative strategies to confront this threat. Natural products and their derivatives have emerged as a promising reservoir for drug discovery. The social amoeba *Dictyostelium discoideum* is a potent model organism in this effort. Employing this invertebrate model, we introduce a novel perspective to investigate natural plant extracts in search of molecules with potential antivirulence activity. Our work established a easy-scalable developmental assay targeting a virulent strain of *Klebsiella pneumoniae*, with *Helenium aromaticum* as the representative plant. The main objective was to identify tentative compounds from the *Helenium aromaticum* extract that attenuate the virulence of *K. pneumoniae* virulence without inducing cytotoxic effects on amoeba cells. Notably, the methanolic root extract of *H. aromaticum* fulfilled these prerequisites compared to the dichloromethane extract. Using UHPLC-ESI-MS/MS, 63 compounds were tentatively identified in both extracts, 47 in the methanolic and 29 in the dichloromethane, with 13 compounds in common. This research underscores the potential of employing *D. discoideum*-assisted pharmacognosy to discover new antivirulence agents against multidrug-resistant pathogens.

1
2
3
4
5
6
7
8
9
10
11
12
13
14
15
16
17
18
19
20
21
22
23
24
25
26
27
28
29
30
31
32
33
34
35
36
37
38
39
40
41
42
43
44
45
46
47
48
49
50
51
52
53
54
55
56
57
58
59
60

For Peer Review

INTRODUCTION

Antibiotic resistance is a serious global threat to public health. The overuse and misuse of antibiotics have led to the emergence of multidrug-resistant (MDR) bacterial strains that are difficult to treat ¹. *Klebsiella pneumoniae* is a bacterium responsible for pneumonia, urinary tract infections, and sepsis, which has become increasingly resistant to antibiotics, including carbapenems, the last line of defense against MDR *K. pneumoniae* infections. The emergence of carbapenem-resistant *K. pneumoniae* strains has been a major challenge in clinical settings, as few effective treatment options are available. Antivirulence therapy is an emerging strategy for combating antibiotic resistance ².

Contrary to traditional antibiotics that target essential cellular functions, antimicrobial agents focus on bacterial virulence factors critical for infection but not for bacterial growth and development. Antivirulence agents provide multiple benefits compared to conventional antibiotics; these include reducing the selection pressure leading to resistance and minimizing side effects often linked with broad-spectrum antibiotics². This perspective on novel antimicrobial agents makes exploring natural resources even more pertinent.

1
2
3
4 In pharmacognosy, identifying and characterizing bioactive compounds from natural sources
5
6
7 such as plants, fungi, and marine organisms are vital for drug discovery and therapeutic
8
9
10 applications. Plant resources have been explored as a potential source of antimicrobial agents due
11
12
13 to their rich chemical diversity and long history of use in traditional medicine ^{3,4}. Given the
14
15
16 complex mixtures of compounds often found in these natural products, reliable assays for
17
18
19 evaluating biological activity, toxicity, and specificity are crucial. Therefore, combining rigorous
20
21
22 analytical methods such as high-performance liquid chromatography (HPLC) coupled with mass
23
24
25 spectrometry with bioassays for isolating and identifying molecules with potential
26
27
28 pharmacological efficacy is highly desirable. Phenotypic bioassays help to ensure the quality,
29
30
31 safety, and effectiveness of herbal medicines, supplements, and pharmaceuticals derived from
32
33
34 natural extracts. Accordingly, implementing accurate and sensitive assays is indispensable in
35
36
37 pharmacognosy, bridging the gap between traditional ethnomedicine and modern pharmaceutical
38
39
40 research. However, the lack of virulence-based scalable assays for plant pharmacognosy is a
41
42
43 bottleneck for discovering novel antivirulence molecules.
44
45
46
47
48
49
50

51 *Dictyostelium discoideum*, a soil-dwelling social amoeba, has emerged as a valuable model for
52
53
54 host-pathogen interactions and drug discovery ⁵. *D. discoideum* is amenable to high-throughput
55
56
57
58
59
60

1
2
3
4 screening of natural product extracts and has been used as a host model system for several human
5
6
7 pathogens, including *Mycobacterium tuberculosis* ⁶, *Legionella pneumophila* ⁷, *Pseudomonas*
8
9
10 *aeruginosa* ⁸⁻¹⁰ and *Klebsiella pneumoniae* ¹¹. Some reports have used this invertebrate model
11
12
13 system to screen the cytotoxicity of natural extracts¹²⁻¹⁴; however, few have simultaneously used
14
15
16 the social amoeba to screen potential anti-virulence drugs without cytotoxic side effects ¹⁰.
17
18
19 Continuing with this effort, in this study, we established an easily scalable social developmental
20
21
22 assay in *D. discoideum* to evaluate the antivirulence activity and cytotoxicity of extracts from the
23
24
25 plant *Helenium aromaticum* against a virulent *K. pneumoniae* strain. The genus *Helenium* is part
26
27
28 of the *Asteraceae* family, one of the largest botanical families with numerous species with
29
30
31 traditional medicinal uses. It is distributed in the North and part of South America^{15,16} and
32
33
34 particularly, *Helenium aromaticum* has shown promising therapeutic potential, particularly its
35
36
37 sesquiterpene lactones ^{15,17}.
38
39
40
41
42
43
44
45
46
47
48
49

50 RESULTS AND DISCUSSIONS. 51 52 53 54 55 56 57 58 59 60

1
2
3
4 **Preparation of plant extracts.** The first objective required the preparation of extracts from various
5
6
7 parts of the *H. aromaticum* plant for the targeted screening of bioactive molecules capable of
8
9
10 attenuating the virulence of *K. pneumoniae* RYC 492, a strain shown to be virulent over *D.*
11
12
13 *discoideum*¹¹. A total of six extracts were obtained, corresponding to the dichloromethane or
14
15
16 methanol extracts from flowers, foliage, or roots.
17

18
19
20
21 ***D. discoideum* cytotoxicity and virulence assays of plant extracts.** Second, using the social
22
23
24 amoeba *D. discoideum* as a model organism, we assessed the cytotoxicity of all the extracts based
25
26
27 on a previously described methodology¹¹. The assay operates on the principle that secondary
28
29
30 metabolites from various plant extracts if cytotoxic, will impede the social development of *D.*
31
32
33 *discoideum* by delaying its social cycle. Conversely, non-cytotoxic compounds will facilitate
34
35
36 social development's normal progression and culmination. According to this criterion, the six *H.*
37
38
39 *aromaticum* extracts were evaluated. The course of social development was considered within six
40
41
42 days under our experimental conditions, and three concentrations (25 µg/mL, 50 µg/mL, and 100
43
44
45 µg/mL) of the different extracts were evaluated. Usually, the amoeba completes the social cycle in
46
47
48 48 hours under these conditions. As shown in Figure 1, amoebae development was affected by all
49
50
51 the dichloromethane plant extracts (flowers, foliage, and roots). By day 3, the culmination of the
52
53
54
55
56
57
58
59
60

amoeba's cycle was reached in the controls; however, in all dichloromethane extracts, even the initial phases of the social cycle were not observed. Based on these observations, the dichloromethane extracts probably include cytotoxic compounds, indicating that further purification would be necessary to use them as a therapeutic molecule source. On the contrary, the methanolic extracts displayed no inhibitory effects on the amoeba's social development, indicating a reduced presence of cytotoxic compounds (Figure 2A for roots). This conclusion is also sustained for flowers and foliage extracts, as shown in Figures 1SA and 2SA, where all the tested extracts allowed a normal social development of the amoeba.

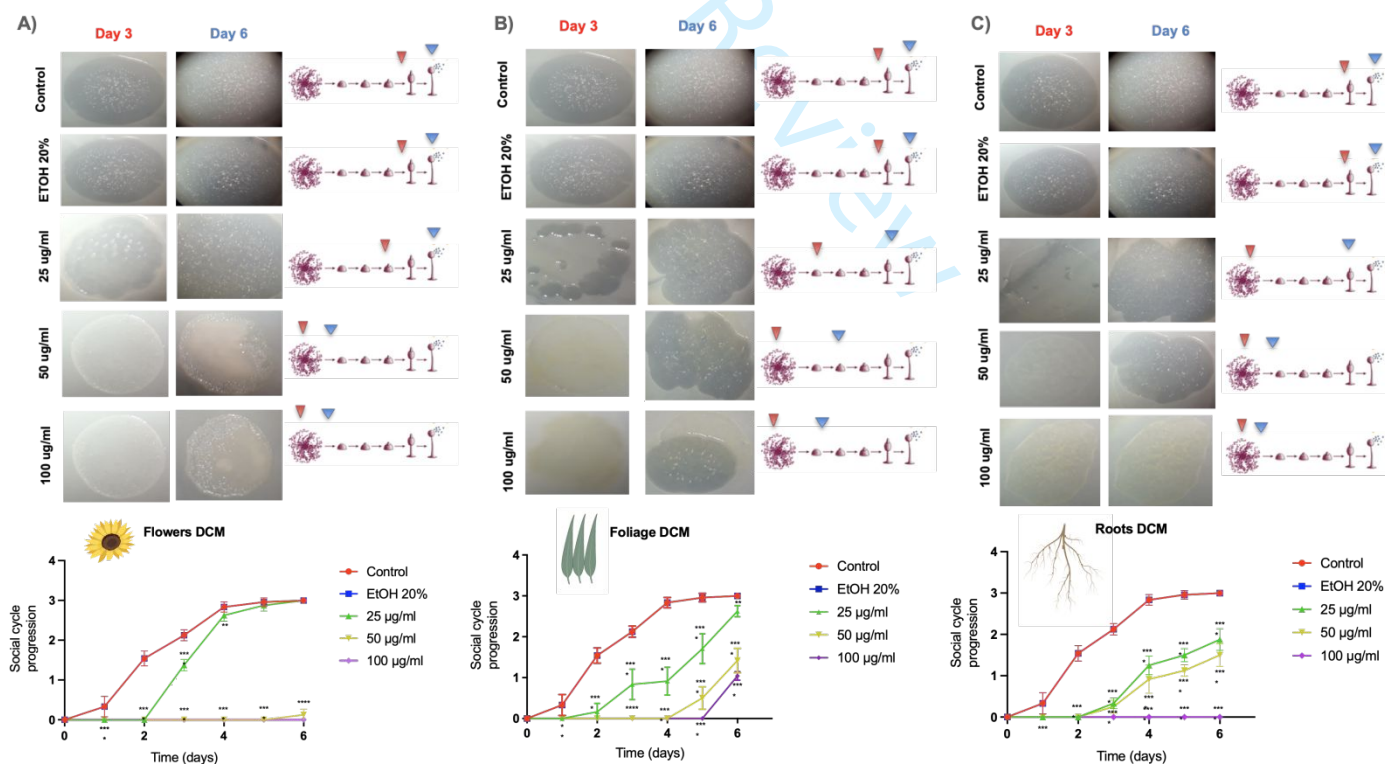


Figure 1. Cytotoxic evaluation of dichloromethane extracts of *H. aromaticum*. A) Flowers, B) Foliage and C) Roots. Statistical analysis was performed using a two-way ANOVA test with multiple comparisons and Dunnett's post-test (n=9) (* = $p < 0.05$, ** = $p < 0.005$, *** = $p < 0.001$, ** ** = $p < 0.0001$). The red and blue arrowheads indicate the progression reached on day 3 and day 6, respectively.

All methanolic extracts that showed no cytotoxic effects on the amoeba were evaluated for their antibiotic and antivirulence assets. As shown in Figure 2 and Table 1, the methanolic root extract attenuated the virulence of *K. pneumoniae* RYC492 relative to the control without compromising bacterial viability in the antibiosis assays. However, the methanolic extracts of foliage and flowers (as shown in Figures 1S and 2S and Table 1) revealed neither antibiotic nor antivirulence activity against *K. pneumoniae* RYC492. Finally, we assessed the antimicrobial activity of the dichloromethane extracts from foliage and roots, with no antibiotic activity observed (Table 1). In summary, only methanolic root extract mitigated *K. pneumoniae* RYC492 virulence.

Table 1. Antibiosis evaluation of *H. aromaticum* extracts against the virulent *K. pneumoniae* RYC492 strain.

Extracts	Bacterial species	Concentrations			Controls		
		25 $\mu\text{g/ml}$	50 $\mu\text{g/ml}$	100 $\mu\text{g/ml}$	C + (KAN) resistance	C + (GEN)	C - (ETHANOL 20%)

Flower dichloromethane		Nd	Nd	Nd	Nd	Nd	Nd	Diameter of the inhibition zone in (mm) *
Stem-leaf dichloromethane		-	-	+/-	+/-	+++	-	
Root dichloromethane		-	-	+/-	+/-	+++	-	
Flower methanolic	<i>Klebsiella pneumoniae</i> RYC 492	-	-	+/-	+/-	+++	-	
Stem-leaf methanolic		-	-	+/-	+/-	+++	-	
Root methanolic		-	-	+/-	+/-	+++	-	

* Inhibition zone, including disc diameter (6 mm) average value of repetitions n=9.

(+++) \leq 1,8 cm, (++) \leq 1,3 cm, (+) \leq 0,9 cm, (+/-) \leq 0,5 cm, (-) 0 cm, C – (negative control), C + (Kan) resistance control, C + (GEN) positive control.

Chemical composition of plant extracts. Determining the chemical composition of compounds is fundamental to the pharmacognosy process, as it guides and increases the likelihood of selecting the most suitable extract for therapeutic applications. Thus, we employed high-resolution tandem mass spectrometry to identify the predominant compounds present in the extracts. A total of 63 compounds were tentatively identified (Figure 3 and Table S1), where 47 compounds were identified in the methanolic extract and 29 in the dichloromethane extract, with 13 compounds common to both extracts. All these compounds were identified by UHPLC-

Q/Orbitrap/ESI/MS/MS, which is a specific technique that identifies the compounds by their molecular weight and their characteristic fragmentations.

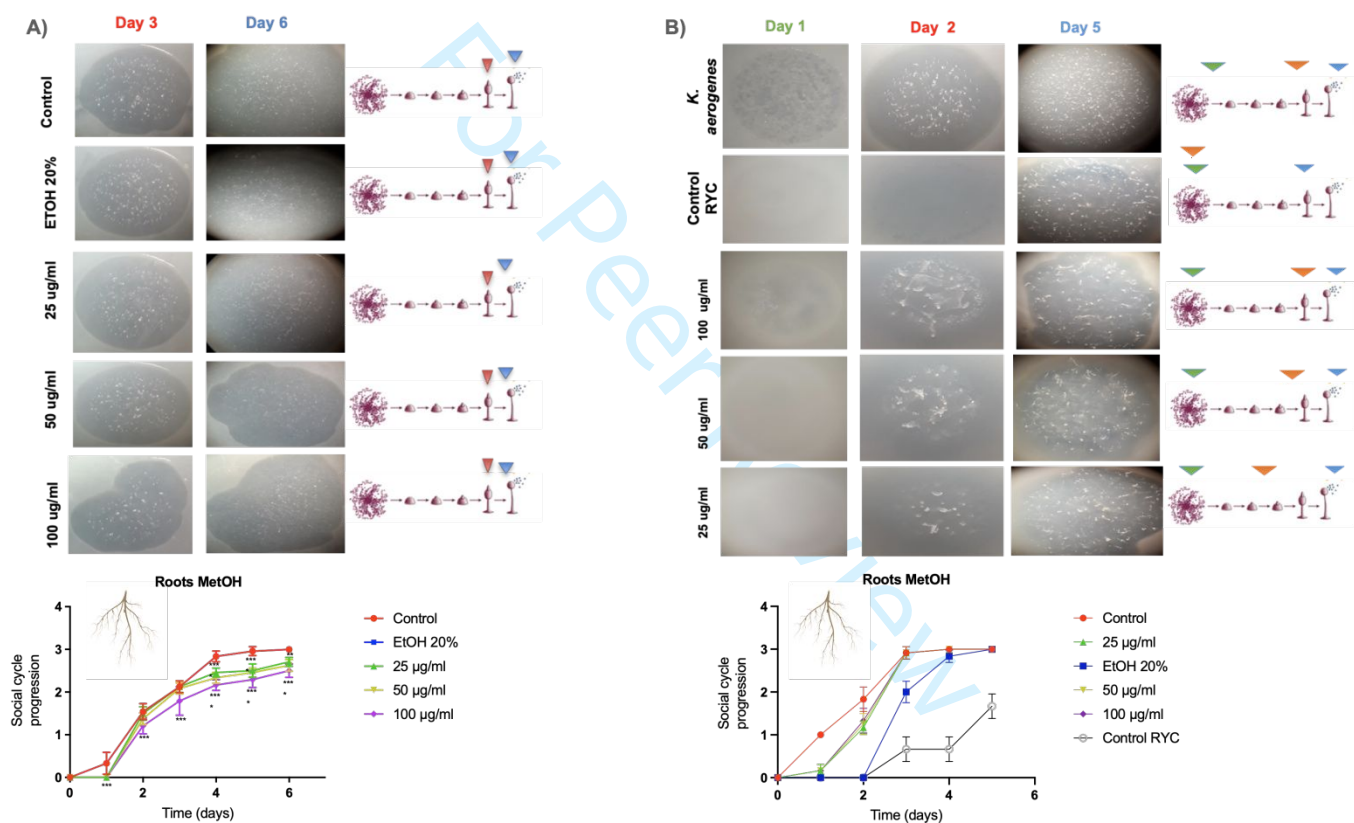


Figure 2. Evaluation of the cytotoxic (A) and antivirulence (B) activities of the roots methanolic extracts of *H. aromaticum*. Statistical analysis was performed using a two-way ANOVA test with multiple comparisons and Dunnett's post-test (n=9) (* = $p < 0.05$, ** = $p < 0.005$, *** = $p < 0.001$, ** ** = $p < 0.0001$).

1
2
3
4 Regarding phenolic compounds, 9 were identified in the methanolic extract and one in the
5
6
7 dichloromethane extract. These compounds include dihydroxybenzoic pentoside and caffeic acid,
8
9
10 chlorogenic acid. Fourteen flavonoids were identified, encompassing glycosylated derivatives of
11
12
13 kaempferol, among others. Eleven terpenes were identified, primarily sesquiterpenic lactones,
14
15
16 including various helenalin derivatives. Peaks corresponding to glycosylated terpenes, such as 10-
17
18
19 hydroxyloganin and loganin, were also found. Other compounds, such as organic acids (succinic
20
21
22 acid) and carbohydrates (aldopentose), include six lipids, such as azelaic acid and pinellic acid.
23
24
25
26
27 Sixteen compounds remained unidentified.
28

29
30
31 In summary, of the 63 compounds identified, the predominant groups were phenolic compounds,
32
33
34 including terpenoids and flavonoids, likely associated with observed biological activity. For
35
36
37 instance, sesquiterpene lactones, such as helenalin and its derivatives, might be responsible for the
38
39
40 observed cytotoxicity, as previously reported^{18,19}. On the other hand, some flavonoids and
41
42
43
44 terpenes can be accountable for attenuated virulence, as previously reported for *Klebsiella*
45
46
47
48 *pneumoniae*²⁰.
49

50
51
52 Combining the phenotypic assays, which included antibiotic, cytotoxic, and antivirulence
53
54
55 evaluations, with chemical analysis can be crucial to discern both the antivirulence and cytotoxic
56
57
58

components within the plant extracts. However, further experiments with purified chemical candidates should be performed to conclusively ascertain the identity of the molecules responsible for these observed activities.

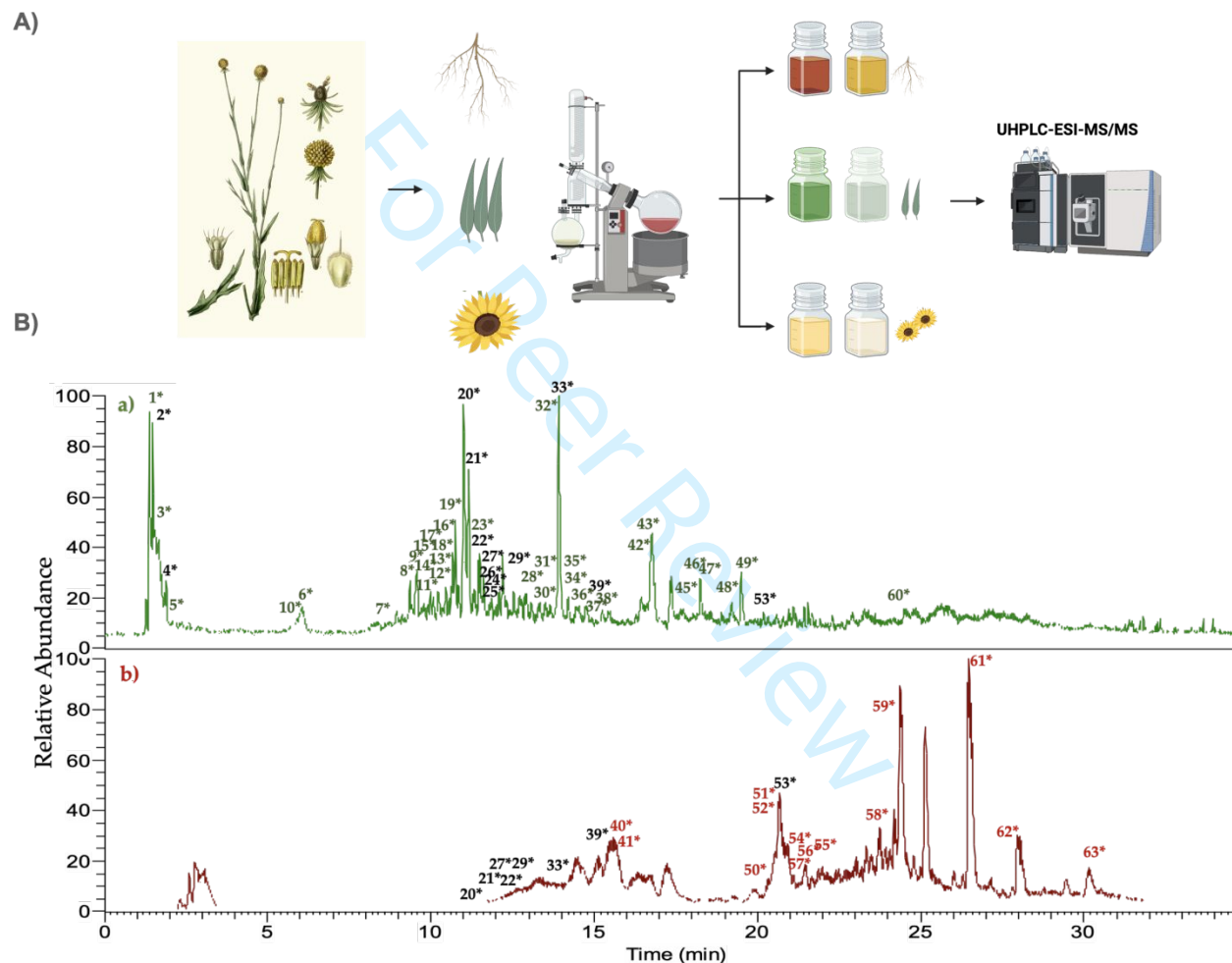


Figure 3. A) Overview of the extraction and identification process of *H. aromaticum* plant extracts. B) UHPLC-Q/Orbitrap/ESI/MS/MS chromatograms of the methanolic (green) and dichloromethane (red) extracts from the root of *H. aromaticum*.

CONCLUSIONS

1
2
3
4 Our study developed a platform to identify secondary metabolites or natural plant extracts from *H.*
5
6
7 *aromaticum* that attenuated *K. pneumoniae* virulence without affecting *D. discoideum* viability.
8

9
10 The amoeba-assisted pharmacognosy of plant resources valuation revealed that only methanolic
11
12
13 extract from *H. aromaticum* roots fulfilled these criteria. Our approach offers a sustainable method
14
15
16
17 to discover novel antivirulence agents, potentially leading to more targeted therapies with reduced
18
19
20 resistance risks compared to traditional antibiotics.
21
22

23 24 25 EXPERIMENTAL SECTION

26
27
28
29 **Microbial strains and growth conditions.** Various bacterial and amoebae strains were used in this
30
31
32 work. The *Klebsiella pneumoniae* RYC492 strain, recognized for producing the antibacterial
33
34
35 peptide microcin E492 and salmochelin siderophores and exhibiting resistance to both kanamycin
36
37
38 and ampicillin, was used for virulence assays. This strain was shown to be virulent over *D.*
39
40
41 *discoideum*²¹. Routinely, *Klebsiella aerogenes* DBS0305928 strain was used to support the growth
42
43
44 of *D. discoideum*²². For our amoebae experiments, we used the *D. discoideum* axenic strain AX4
45
46
47 (DBS0302402), which emerged as a spontaneous mutation from its parental strain AX3 and was
48
49
50
51
52 obtained from DictyBase Stock Center²³.
53
54
55
56
57
58
59
60

1
2
3 **Social development assays for cytotoxicity and *K. pneumoniae* virulence evaluations in *D.***

4
5
6
7 ***discoideum*.** For the social development assays, SM agar plates embedded with a lawn of *K.*
8
9
10 *aerogenes* (pre-incubated at 37°C for 18 h) were employed ¹¹. Cytotoxic evaluations of the six
11
12
13 plant extracts were conducted at 25, 50 and 100 µg/mL concentrations in 20% ethanol. Finally, the
14
15
16 same 20% ethanol solution was used as a control growth. Briefly, 5 µL of an axenic *D. discoideum*
17
18
19 cell suspension from selected subcultures (S3 to S5), at an exponential phase density of 2x10⁶
20
21
22 cells/mL, was used, totaling an inoculation of 10,000 amoebae cells. Plates were incubated at 23°
23
24
25 C, and social development was monitored for 6 days, tracking aggregation, elevation, and
26
27
28 culmination phases ²⁴. Scoring ranged from "1" for aggregated amoebae forming a phagocytosis
29
30
31 plaque to "3" for fully formed fruiting bodies, with transitions scored as half-values. Observations
32
33
34 were made every 24 hours over 6 days, and the data were plotted and analyzed using GraphPad
35
36
37 Prism.
38
39
40
41
42
43
44

45 ***H. aromaticum* collection, extracts preparation and compound identification.** The plant species
46
47
48 were collected from San Carlos de Apoquindo, Las Condes, Metropolitan Region, Chile, from
49
50
51 January to February 2018 at latitude (S): -33.40693, longitude (W): -70.50047. The species was
52
53
54 identified by Gloria Rojas Villegas, the Head of the Botanical Area and Herbarium at the National
55
56
57
58
59
60

1
2
3
4 Museum of Natural History of Chile. The specimens were processed, deposited at the museum,
5
6
7 and identified as *H. aromaticum* (Hook.) L.H. Bailey with a voucher number 169131.
8
9

10
11 The plant samples were oven-dried at 37°C, ground, and macerated with dichloromethane and
12
13
14 methanol at room temperature for 72 h, repeating the process thrice with direct sonication for 1
15
16
17 minute and centrifugation at 10,000 xg. The extracted product was filtered and concentrated using
18
19
20 a rotary evaporator at 40°C, then stored at -20°C. For compound identification in *H. aromaticum*
21
22
23
24 extracts with either potential antivirulence or cytotoxic activity, an Ultra-High Pressure Liquid
25
26
27 Chromatograph coupled with a diode array detector and high-resolution mass spectrometer
28
29
30 (UHPLC-ESI-MS/MS) was employed. Sample preparation involved macerating ~3 g of the
31
32
33
34 species with methanol (three times, 30 ml each, for 3 days/extraction) to yield 10 mg of the extract.
35
36
37
38

39 ASSOCIATED CONTENT

40 41 42 43 **Supporting Information.**

44
45
46 The following files are available free of charge.

47
48
49
50 Supplementary figures S1 and S2 (PDF)

51
52
53
54 Supplementary Table 1 (PDF)

AUTHOR INFORMATION

Corresponding Author

* Francisco P. Chávez (fpchavez@uchile.cl), Phone: +56229787185

Author Contributions

The manuscript was written through the contributions of all authors. FC and AM conceived the study. FC, AM, MH, MV and CA designed the experiments. MH, GC, DR, MV and FC analyzed and interpreted the data. MH conducted the experiments. MH and FC wrote the manuscript. FC, MH, AM, and CA critically reviewed the manuscript. All the authors approved the final version of the manuscript.

DECLARATIONS

Funding Sources

Fondecyt Grant 1211852 from the Chilean Government

Conflicts of Interests/Competing interests

The authors declare that there is no competing interests or personal relationships that could affect the work reported in this article.

1
2
3
4 ACKNOWLEDGMENT
5
6

7 This work was funded by Fondecyt Grants 1211852 (FCH), 1221193 (AM) and 1220075 (CA).
8
9

10 MH received the scholarship “Presidente de la República” from the Peruvian Government. We
11
12
13 thank Nicole Molina for her excellent technician skills in preparing *D. discoideum* cultures.
14
15
16
17
18
19

20 ABBREVIATIONS
21
22

23 DCM, dichloromethane; UHPLC, Ultra-High Pressure Liquid Chromatograph; ESI-MS/MS,
24
25
26 Electrospray Ionization Mass Spectrometry; MDR, Multi-Drug resistant; EtOH, Ethanol.
27
28
29
30
31
32
33
34
35
36
37
38
39
40
41
42
43
44
45
46
47
48
49
50
51
52
53
54
55
56
57
58
59
60

REFERENCES

- (1) Clegg, S.; Murphy, C. N. Epidemiology and Virulence of *Klebsiella pneumoniae*. *Microbiol Spectr* **2016**, *4* (1). <https://doi.org/10.1128/microbiolspec.UTI-0005-2012>.
- (2) Rasko, D. A.; Sperandio, V. Anti-Virulence Strategies to Combat Bacteria-Mediated Disease. *Nat Rev Drug Discov* **2010**, *9* (2), 117–128. <https://doi.org/10.1038/nrd3013>.
- (3) Newman, D. J.; Cragg, G. M. Natural Products as Sources of New Drugs over the Last 25 Years. *Journal of Natural Products*. 2007, pp 461–477. <https://doi.org/10.1021/np068054v>.
- (4) Salam, A. M.; Quave, C. L. Opportunities for Plant Natural Products in Infection Control. *Current Opinion in Microbiology*. 2018. <https://doi.org/10.1016/j.mib.2018.08.004>.
- (5) Froquet, R.; Lelong, E.; Marchetti, A.; Cosson, P. *Dictyostelium discoideum*: A Model Host to Measure Bacterial Virulence. *Nat Protoc* **2009**, *4* (1), 25–30. <https://doi.org/10.1038/nprot.2008.212>.
- (6) Dunn, J. D.; Bosmani, C.; Barisch, C.; Raykov, L.; Lefrançois, L. H.; Cardenal-Muñoz, E.; López-Jiménez, A. T.; Soldati, T. Eat Prey, Live: *Dictyostelium discoideum* as a Model for Cell-Autonomous Defenses. *Frontiers in Immunology*. 2018. <https://doi.org/10.3389/fimmu.2017.01906>.
- (7) Escoll, P.; Rolando, M.; Gomez-Valero, L.; Buchrieser, C. From Amoeba to Macrophages: Exploring the Molecular Mechanisms of *Legionella pneumophila* Infection in Both Hosts. *Curr Top Microbiol Immunol* **2013**, *376*, 1–34. <https://doi.org/10.1007/82-2013-351>.
- (8) Pukatzki, S.; Kessin, R. H.; Mekalanos, J. J. The Human Pathogen *Pseudomonas aeruginosa* Utilizes Conserved Virulence Pathways to Infect the Social Amoeba *Dictyostelium discoideum*. *Proc Natl Acad Sci U S A* **2002**, *99* (5), 3159–3164. <https://doi.org/10.1073/pnas.052704399>.
- (9) Cosson, P.; Zulianello, L.; Join-Lambert, O.; Faurisson, F.; Gebbie, L.; Benghezal, M.; Van Delden, C.; Kocjancic Curty, L.; Köhler, T. *Pseudomonas aeruginosa* Virulence

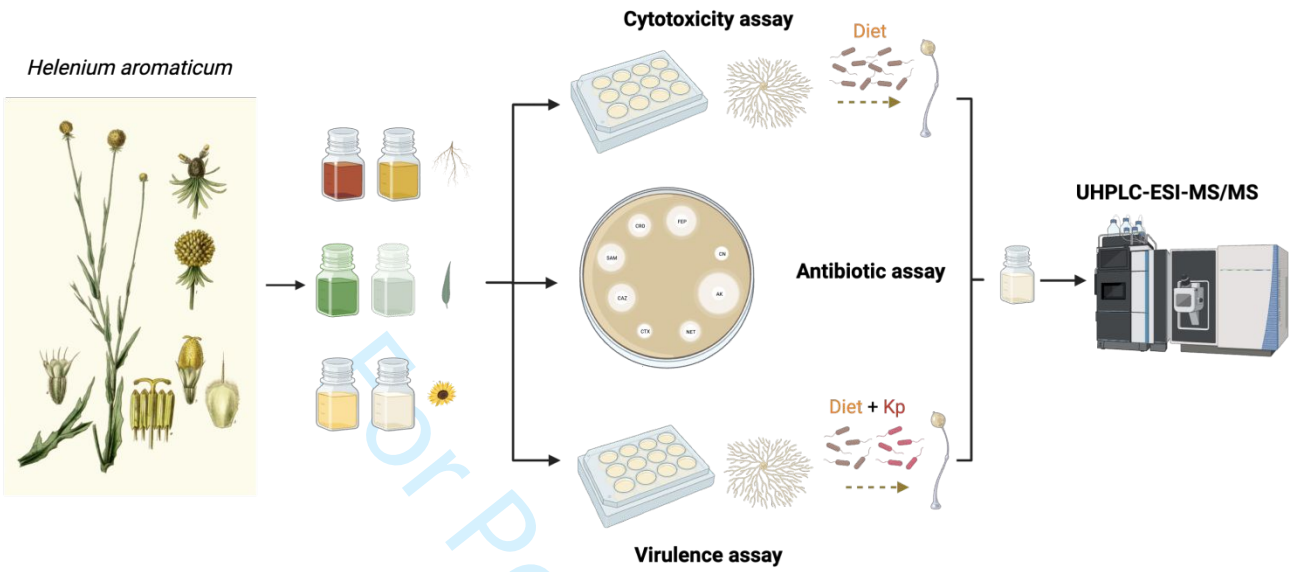
- 1
2
3 Analyzed in a *Dictyostelium discoideum* Host System. *J Bacteriol* **2002**, *184* (11), 3027–
4 3033.
5
6
7
8 (10) Bravo-Toncio, C.; Álvarez, J. A.; Campos, F.; Ortíz-Severín, J.; Varas, M.; Cabrera, R.;
9 Lagos, C. F.; Chávez, F. P. *Dictyostelium discoideum* as a Surrogate Host–Microbe
10 Model for Antivirulence Screening in *Pseudomonas aeruginosa* PAO1. *Int J Antimicrob*
11 *Agents* **2016**, 1–7. <https://doi.org/10.1016/j.ijantimicag.2016.02.005>.
12
13
14
15 (11) Marcoleta, A. E.; Varas, M. A.; Ortiz-Severín, J.; Vásquez, L.; Berríos-Pastén, C.; Sabag,
16 A. V.; Chávez, F. P.; Allende, M. L.; Santiviago, C. A.; Monasterio, O.; Lagos, R.
17 Evaluating Different Virulence Traits of *Klebsiella pneumoniae* Using *Dictyostelium*
18 *discoideum* and Zebrafish Larvae as Host Models. *Front Cell Infect Microbiol* **2018**, *8*
19 (February), 1–20. <https://doi.org/10.3389/fcimb.2018.00030>.
20
21
22
23
24 (12) Ilacqua, A. N.; Shettler, J. A.; Wernke, K. M.; Skalla, J. K.; McQuade, K. J. Theaflavins
25 from Black Tea Affect Growth, Development, and Motility in *Dictyostelium discoideum*.
26 *Biochem Biophys Res Commun* **2017**, *491* (2). <https://doi.org/10.1016/j.bbrc.2017.07.058>.
27
28
29
30 (13) McQuade, K. J.; Nakajima, A.; Ilacqua, A. N.; Shimada, N.; Sawai, S. The Green Tea
31 Catechin Epigallocatechin Gallate (EGCG) Blocks Cell Motility, Chemotaxis and
32 Development in *Dictyostelium discoideum*. *PLoS One* **2013**, *8* (3).
33 <https://doi.org/10.1371/journal.pone.0059275>.
34
35
36
37
38 (14) Hwang, J.-Y.; Kim, J.-H. Effect of Monoterpenes on Growth of Cellular Slime Mold,
39 *Dictyostelium discoideum* Ax-2. *Journal of Plant Biology* **2002**, *45* (4).
40 <https://doi.org/10.1007/bf03030361>.
41
42
43
44 (15) Jodynis-Liebert, J.; Murias, M.; Błozzyk, E. Effect of Sesquiterpene Lactones on
45 Antioxidant Enzymes and Some Drug- Metabolizing Enzymes in Rat Liver and Kidney.
46 *Planta Med* **2000**, *66* (3). <https://doi.org/10.1055/s-2000-8566>.
47
48
49
50 (16) Romo, J.; Joseph-Nathan, P.; Díaz, F. A. The Constituents of *Helenium aromaticum*
51 (Hook) Bailey. *Tetrahedron* **1964**, *20* (1). [https://doi.org/10.1016/s0040-4020\(01\)98399-1](https://doi.org/10.1016/s0040-4020(01)98399-1).
52
53
54
55
56
57
58
59
60

- 1
2
3
4 (17) Schmeda-Hirschmann, G.; Loyola, J. I.; Sierra, J.; Retamal, R.; Rodriguez, J. Hypotensive
5 Effect and Enzyme Inhibition Activity of Mapuche Medicinal Plant Extracts.
6 *Phytotherapy Research* **1992**, *6* (4). <https://doi.org/10.1002/ptr.2650060404>.
7
8
9 (18) Heilmann, J.; Wasescha, M. R.; Schmidt, T. J. The Influence of Glutathione and Cysteine
10 Levels on the Cytotoxicity of Helenanolide Type Sesquiterpene Lactones against KB
11 Cells. *Bioorg Med Chem* **2001**, *9* (8). [https://doi.org/10.1016/S0968-0896\(01\)00131-6](https://doi.org/10.1016/S0968-0896(01)00131-6).
12
13
14 (19) Drogosz, J.; Janecka, A. Helenalin - A Sesquiterpene Lactone with Multidirectional
15 Activity. *Curr Drug Targets* **2018**, *20* (4).
16 <https://doi.org/10.2174/1389450119666181012125230>.
17
18
19 (20) Adeosun, I. J.; Baloyi, I.; Aljoundi, A. K.; Salifu, E. Y.; Ibrahim, M. A.; Cosa, S.
20 Molecular Modelling of SdiA Protein by Selected Flavonoid and Terpenes Compounds to
21 Attenuate Virulence in *Klebsiella pneumoniae*. *J Biomol Struct Dyn* **2022**.
22 <https://doi.org/10.1080/07391102.2022.2148753>.
23
24
25 (21) Asensio, C.; Pérez-Díaz, J. C.; Martínez, M. C.; Baquero, F. A New Family of Low
26 Molecular Weight Antibiotics from Enterobacteria. *Biochem Biophys Res Commun* **1976**,
27 *69* (1), 7–14. [https://doi.org/10.1016/S0006-291X\(76\)80264-1](https://doi.org/10.1016/S0006-291X(76)80264-1).
28
29
30 (22) P Fey, A. K. P. G. K. P. R. C. Protocols for Growth and Development of *Dictyostelium*
31 *discoideum*. *Nat. Protoc.* **2007**, *2* (6), 1307–1316. <https://doi.org/10.1038/nprot.2007.178>.
32
33
34 (23) Basu, S.; Fey, P.; Pandit, Y.; Dodson, R.; Kibbe, W. A.; Chisholm, R. L. DictyBase 2013:
35 Integrating Multiple Dictyostelid Species. *Nucleic Acids Res* **2013**, *41* (D1).
36
37
38
39
40
41
42
43
44
45
46
47

48 Table of Content Graphic

49
50
51
52
53
54
55
56
57
58
59
60

1
2
3
4
5
6
7
8
9
10
11
12
13
14
15
16
17
18
19
20
21
22
23
24
25
26
27
28
29
30
31
32
33
34
35
36
37
38
39
40
41
42
43
44
45
46
47
48
49
50
51
52
53
54
55
56
57
58
59
60





Sociedad de Microbiología de Chile

Efectos de la mutación de la polifosfato quinasa sobre la patogenicidad, la biopelícula y la formación de cápsulas en *Klebsiella pneumoniae* hipervirulenta: un estudio proteómico global

Effects of Polyphosphate Kinase Mutation on Pathogenicity, Biofilm, and Capsule Formation in Hypervirulent *Klebsiella pneumoniae*: A Global Proteomic Study

Comunicación oral

Interacciones Patógeno-Hospedero

Diego Rojas Muñoz¹, Andrés Marcoleta¹, Matias Gálvez¹, Macarena Váras¹, Mauricio Díaz¹, Pablo Saldivia^{2, 3}, Jorge Vielma¹, Mauricio Hernández², Yunn Hwen Gan⁴, Yahua Chen⁴, Nicolas Guilliani¹, Francisco Chavez¹.

(1) Universidad de Chile, Departamento de Biología, Facultad de Ciencias, Las Palmeras 3425, Ñuñoa, Santiago, Chile.

(2) Instituto MELISA, División Biotecnología, Dalcahue 1120, suite 103, San Pedro de la Paz, Chile.

(3) Universidad de Concepción, Departamento de Biología, Facultad de Ciencias Biológicas,, Edmundo Larenas, 234, Concepción, Chile.

(4) National University of Singapore, Department of Biochemistry, Yong Loo Lin, School of Medicine, 21 Lower Kent Ridge Road, Singapore, Singapore.

drojasm@ug.uchile.cl

Infections caused by *Klebsiellapneumoniae* have become a serious threat to human health due to the development of hypervirulent and multidrug-resistant strains, causing hospital outbreaks and severe conditions that are difficult to treat with the available chemotherapy. Interference with bacterial virulence and cell-to-cell signaling pathways is attractive since it imposes less selective pressure for developing bacterial resistance than traditional strategies to kill pathogens or prevent their growth. In this

context, the inorganic polyphosphates (polyP) metabolism has gained considerable interest as a novel therapeutic target due to its pleiotropic role in regulating various virulence factors in several bacterial pathogens. To get into more detail about molecular processes involved in mutants in polyP metabolism, global proteomic profiling of $\Delta ppk1$, Δppx and double mutants was performed using non-isotopic LC-MS/MS spectrometry. The results revealed that the $\Delta ppk1$ mutant had a differential expression of proteins (DEP) involved in capsule synthesis (Wzi - Ugd), biofilm formation (MrkC-D-H), synthesis of the colibactin genotoxin precursor (ClbB), as well as proteins associated with related the synthesis and modification of lipid A (LpxC - PagP). These proteomic findings corroborate the phenotypic observations and indicate that the Ppk1 mutation is associated with impaired biofilm and capsule formation and attenuated virulence in hypervirulent *K. pneumoniae* using the social amoeba *D. discoideum* as a host-pathogen interaction model. Our results confirm that inorganic polyphosphate (polyP) metabolism, particularly the enzyme responsible for its synthesis, Ppk1, is a promising target for designing novel antivirulence drugs.

Keywords

(1) Polyphosphate, (2) Hypervirulent Klebsiella, (3) Proteomics, (4) *D. discoideum*, (5) Antivirulence.

Funding:

Fundación Maria Ghilardi

FONDECYT F. Chávez 1211852

FONDECYT A. Marcoleta 1221193

FONDEQUIP Lionheart EQM180216

Acknowledgement:

To the Maria Ghilardi Foundation for financing my doctoral studies.

To Professor Francisco Chaves and Nicolas Guiliani for receiving me in their laboratories



Biología molecular y celular de mutantes del metabolismo de polifosfatos de *Klebsiella pneumoniae* hipervirulenta

Molecular and cellular biology of polyphosphate metabolism mutants of hypervirulent *Klebsiella pneumoniae*

Poster

Interacciones Patógeno-Hospedero

Diego Rojas Muñoz¹, Mauricio Díaz¹, Matias Gálvez¹, Andrés Marcoleta¹, Macarena Varas¹, Nicolas Guilliani¹, Francisco Chavez¹.

(1) Universidad de Chile, Departamento de Biología, Facultad de Ciencias, Las Palmeras 3425, Ñuñoa, Santiago, Chile.

drojasm@ug.uchile.cl

Infections caused by *Klebsiella pneumoniae* have become a serious threat to human health due to the development of hypervirulent and multidrug-resistant strains causing hospital outbreaks and severe conditions that are difficult to treat with the available chemotherapy. However, the relation between antibiotic resistance and virulence is a complex issue that requires further study. In this context, understanding bacterial pathogenesis and virulence factors can guide the path to developing new strategies to combat infections. Interference with bacterial virulence and cell-to-cell signaling pathways is attractive since it imposes less selective pressure for developing bacterial resistance than traditional strategies to kill pathogens or prevent their growth. The inorganic polyphosphates (polyP) metabolism has gained considerable interest as a novel therapeutic target due to its pleiotropic role in regulating various virulence factors in several bacterial pathogens. However, polyP metabolism in *Klebsiella pneumoniae* remains poorly understood. Here, we study the molecular and cellular biology of polyP metabolism mutants we have constructed by homology

recombination in the hypervirulent *K. pneumoniae* SGH10. We found that polyP synthesis is essential for virulence in *K. pneumoniae*, as revealed by the deletion in the polyP synthesis gene (*ppk1*) that affects bacterial virulence and biofilm formation. To get into more details about molecular processes involved in these polyP mutant phenotypes, global proteomic profiling of *ppk1*, *ppx* and double mutants was performed using non-isotopic LC-MS/MS spectrometry. We found many known differentially expressed virulence factors in our polyP mutants that may explain the differential phenotypes between polyP synthesis (*ppk1*) and polyP degradation (*ppx*) mutants. Our results confirm that polyP metabolism, particularly the enzyme responsible for their synthesis, *ppk1*, is a good target for designing new antivirulence drugs.

Financiamiento:

Este proyecto se financia con el FONDECYT regular 1211852.

El financiamiento personal es gracias a la beca Maria Ghilardi.